Experimental and Numerical Study into the Performance Assessment of Stand-alone Screens in Steam Assisted Gravity Drainage Operations

by

Chenxi Wang

A thesis submitted in partial fulfillment of the requirements for the degree of

Doctor of Philosophy

in

Petroleum Engineering

Department of Civil and Environmental Engineering

University of Alberta

Abstract

Sand production is a significant issue for weakly consolidated and unconsolidated formations. Sanding can erode the wellbore and surface facilities and plug the wellbore. In SAGD operations, wellbores are typically completed by stand-alone screens such as slotted liners (SL), wire-wrapped screens (WWS), and punched screens (PS). These screens have different characteristics, including open-flow-area (OFA), aperture geometry, etc. Thus, they perform differently under the same operational condition and need to be appropriately designed to optimize their performance.

Past experimental studies have guided sand control testing and design but suffer deficiencies in testing analysis. For instance, the existing testing design ignores some influential factors, including particle size distribution (PSD), slot density, fluid properties, and fluid phase change. Therefore, existing performance analyses are not solid and comprehensive. This research aims to analyze and compare the stand-alone screens' performance comprehensively through experimental and numerical study. The design criteria for each screen will also be generated and presented in this thesis. The comprehensive performance comparison results will create the optimal screen selection protocol for SAGD operators.

The stand-alone screen performance is analyzed using a large-scale sand control testing facility. The testing procedure incorporates several key factors, including PSD, slot density, aperture size, fluid properties, and fluid-phase change. Sand production and retained permeability are the two main indicators to characterize the stand-alone screens' sanding and flow performance. Three representative oil sands with different PSDs from the McMurray Formation are used in this experimental study. The testing results are used to generate the design criteria for these three PSDs. The design criteria are presented graphically by the "Traffic Light System (TLS)." Proposed design criteria are given by two conditions: normal SAGD condition and aggressive SAGD condition. Also, empirical correlations are built using dimensionless factors to predict the safe design window mathematically by curve fitting. Moreover, numerical models using Computational Fluid Dynamics (CFD) are built to characterize the formation damage caused by fines migration and flow convergence during the testing. The numerical models simulate the flow condition without fines migration. The pressure data obtained in the near-screen zone are used to calculate the formation damage due to the flow convergence. The formation damage due to the fines

migration can be calculated by deducting the formation damage due to the flow convergence from the total amount of formation damage.

The sand production results show that fluid-phase change due to water and gas breakthrough causes more sand production. Particularly, massive sand production is observed under the gas associated flow condition. The retained permeability results indicate that higher OFA of the screen and lower fines concentration of the PSD lead to a better flow performance. The design criteria obtained based on the sand production and retained permeability results are presented graphically by the "TLS." The TLS simply uses the three colour codes to illustrate the design criteria, in which red means unacceptable design, yellow means marginal design, and green means acceptable design. Also, empirical correlations using dimensionless factors are formulated to obtain a safe aperture design window mathematically. The simulation results show that the WWS has linear flow streamlines, creating negligible pressure drop by the flow convergence. However, due to the low slot density nature, the SL and PS show highly converged flow streamlines. The formation damage calculation results indicate that most of the formation damage created by the WWS is due to the fines migration. For the SL and PS, both fines migration and flow convergence play roles in the total formation damage. However, in the dirty formation, fines migration is the dominant parameter in the formation damage. Regarding the screen selection protocol, the WWS is recommended to be used in DC-I formation for its superior flow performance. SL and PS shall be implemented in DC-II and DC-III due to their low cost and comparable performance with the WWS.

This thesis compares the performance of three stand-alone screens comprehensively by using experimental and numerical methods. The graphical and mathematical design criteria are created for each screen under SAGD conditions. The comprehensive performance comparison leads to the optimal screen selection protocol that can be used by SAGD operators in the screen selection and design.

Dedication

I dedicated this thesis to my mother, Mrs. Ruoping Gao, and my father, Mr. Jiawei Wang. Ph. D. study is like sailing in the ocean. I would not have reached the island without the unconditional support and love from my parents. My father's hardworking and persistent character encourages me to keep fighting and be strong.

Acknowledgements

I want to thank my dearest parents for their forever support and love. Family's love makes me strong in every period of my life. Words cannot describe how thankful I am to my parents.

I would like to express my sincere gratitude and deep love to my fiancé, Dan Li. It is our destiny that we met here at the University of Alberta. Her love and dedication make me faithful during my Ph.D. life.

I would like to show my deepest thanks to my supervisor Dr. Alireza Nouri. I appreciate that he gave me a chance to pursue my academic dream four years ago. His patient guidance and strict supervision facilitate me to be a good researcher. I will forever remember the lessons he has taught me and realize my dream of being a good researcher in my future life.

I acknowledge all my colleagues and friends for their support and help during my Ph.D. study.

I would like to thank all my committee members for providing valuable suggestions to improve my research work.

Table of Contents

List of Tables

List of Figures

Nomenclature

DC-I	Class I Oil Sand for Devon Pike I
DC-II	Class II Oil Sand for Devon Pike I
DC-III	Class III Oil Sand for Devon Pike I
DC-IV	Class IV Oil Sand for Devon Pike I
D	Diameter of Particle Size
D_{10}	Sieve opening size that retains 10% of the particles in a sample
D_{50}	Sieve opening size that retains 50% of the particles in a sample (Median size on the PSD curve)
D_{90}	Sieve opening size that retains 90% of the particles in a sample
A	Area
m	weight
k_{abs}	Absolute Permeability
k_{rw}	Relative Permeability
k_{ret}	Retained Permeability
δk	Absolute Uncertainty of Permeability
L	Length
ΔP	Pressure Drop
δp	Absolute Uncertainty of Pressure Drop
S_{or}	Residual Oil Saturation
q	Flow Rate
μ	Viscosity
P_{sand}	Produced Sand
W_{ub}	Upper Bound of the Aperture Size

W_{lb}	LowerBound of the Aperture Size
δW	Absolute Uncertainty of Produced Sand
P_{sand}	Produced Sand
γ	Dimensionless Parameter
ρ	Density
τ'	Effective Shear Strength
C_o	Cohesion
σ_a'	Effective Axial Stress
φ	Friction Angle
δ	Dimensionless Parameter
θ	Fines Concentration

Abbreviations

CRD   Collaborative Research and Development

DAQ   Data acquisition

SOP   Standard Operating Procedure

NSERC   Natural Sciences and Engineering Research Council of Canada

OFA   Open-flow Area

PPE   Personal Protective Equipment

PSD   Particle Size Distribution

RP   Retained Permeability

CSS   Cyclic Steam Stimulation

SAGD   Steam Assisted Gravity Drainage

SC   Sorting Coefficient

UC   Uniformity Coefficient

SCT   Scaled Completion Test

SOP   Standard Operating Procedure

SPC   Slot Per Column (number of slots in one column of 7" liner)

SRT   Sand Retention Test

TLS   Traffic Light System

SL   Slotted Liner

WWS   Wire-wrapped

PS   Punched Screen

CFD   Computational Fluid Dynamics

TDS   Total Dissolved Solids

CSC   Critical Salt Concentration

LPSA   Laser-particle Size Analysis

DIA   Dynamic Image Analysis

XRD   X-ray Powder Diffraction

MAE   Mean Absolute Error

SI Metric Conversion Factors

1 cp = 10^{-3} Pa·s

1 inch = 2.54 cm

1 ft = 0.3048 m

1 pound = 453.592 gram

1 psi = 6894.76 pa

Chapter 1: Introduction

1.1 Background

Alberta's oil sands are known as the third-largest proven heavy oil reserves in the world (Lunn, 2013; Wilson, 2013). There are two major technologies to exploit the rich oil sands in Canada: surface mining and in-situ recovery methods. The in-situ recovery is achieved by the SAGD process, which relies on the hot steam injection and gravity drainage (Butler, 1985).

Sand production is a common issue in weakly consolidated and unconsolidated oil sands during SAGD operation. Besides, most oil-bearing sands and sandstones contain clay and fine particles. Fines migration in porous media has contributed to drastic permeability reductions around production wells in oil reservoirs (Sharma and Yortsos, 1986; Sarkar and Sharma, 1990; Ohen and Civan, 1991; Denney, 1998; Al-Awad et al., 1999; Bybee, 2002; Qiu et al., 2008; Bedrikovetsky et al., 2011; Zeinijahromi et al., 2011; Musharova et al., 2012; Karazincir et al., 2017; You and Bedrikovetsky, 2018).

Different sand control devices have been developed to prevent sand production or limit sanding within an acceptable level while optimizing the near-wellbore reservoir performance and deliverability. These methods include gravel packs, expandable screens, and standalone screens, among others. SAGD wells are completed by stand-alone screens such as SL, WWS, and PS. The aim is to support the wellbores and restrict sand production in SAGD operations. Sub-optimal sand control selection and design would cause costly problems such as wellbore plugging, pump failure, and wellbore collapse in severe cases. Thus, proper selection of screen type is one of the most significant challenges for the operators to optimize their production and maximize profit (Tausch and Corley, 1958; Carlson et al., 1992; Denney, 2008; Bennion et al., 2009; Xie, 2015; Mahmoudi et al., 2016; Wang et al., 2020a).

Experimental and numerical studies have assessed the stand-alone screens' performance. Sand control testing is standard in the screen design and performance assessment in the industry (Romanova et al., 2014, 2017; Spronk et al., 2015; Fattahpour et al., 2018). In sand control testing, sand production and pressure data are the two direct measurements in the performance analysis. In general, a higher amount of produced sand and pressure drop signifies lower screen performance.

1.2 Problem Statement

A literature review indicates a few shortcomings in existing experimental and numerical studies in the SAGD context. These are limited real-time sand production and flow performance measurements as two critical factors in evaluating sand control performance. The systematic guideline for selecting the most appropriate sand control screen is not available for the project at hand.

Real-time sand production measurement is a crucial factor in sanding performance analysis. It allows for capturing the impact of fluid velocity, water cut, and fluid phase-change. However, in previous experimental studies, real-time sand production for the scaled sand control testing has not been achieved. Sanding in the past research has been measured only at the end of testing.

Retained permeability is an indicator of the sand control devices' flow performance and can be directly calculated for single-phase flow conditions by Darcy's Law. However, past research is limited in the flow performance analysis using the retained permeability for multi-phase flow conditions. Retained permeability value in existing sand control testing cannot be calculated from differential pressure readings under multi-phase testing conditions. Hence, past research works only use total pressure drop or productivity index in the near-screen zone as indicators of the flow performance. However, these data analysis methods cannot quantify the formation damage caused by the fines migration and pore plugging. Moreover, although the experimental SRT can be an excellent way to assess stand-alone screens' flow performance, it only provides a total formation damage in the near-screen zone without differentiating the formation damage caused by the fines migration and the flow convergence. Thus, the formation damage in the near-screen zone is not adequately characterized and understood.

The screen design criteria are either biased or missing in the literature due to current experimental studies' insufficiency. Also, the screen selection protocol is ad-hoc. No scientific guide has been created for SAGD operations.

1.3 Research Objectives

This research aims at characterizing the sanding and flow performance of stand-alone screens quantitatively through the experimental pre-packed SRT method. Based on the testing results, the design criteria of each stand-alone screens are presented graphically. Also, empirical correlations with dimensionless parameters are formulated to predict the safe aperture design window.

Moreover, this research aims at characterizing the formation damage due to the screen implementation by coupling the experimental SRT and the numerical CFD simulation. Finally, this research aims at establishing an optimal screen selection protocol for SAGD production wells based on the performance assessment and comparison.

1.4 Research Hypothesis

This section contains some expected results from the testing. Sand production is expected to increase exponentially with the aperture size. Also, the phase transition (water and gas breakthrough) is expected to cause more sand production. Notably, a significant amount of sand production is anticipated when the gas breakthrough occurs. Regarding stand-alone screens' flow performance, the higher flow rates and increase of water cut are expected to cause more considerable fines migration and more severe plugging.

Concerning the performance comparison of these stand-alone screens, the WWS is expected to have the highest sanding level and the lowest plugging for the same aperture size. The SL is anticipated to produce the least amount of sand production while suffering the most from the formation damage. The performance of the punched screen is expected to lie in between the WWS and SL.

Regarding the formation damage, for the WWS, it is expected that most of the formation damage is due to the fines migration. Negligible damage is created due to the flow convergence. However, due to the low slot density properties, the SL and PS are expected to show a higher pressure drop in the near-screen zone due to the higher flow convergence level. Thus, both fines migration and flow convergence are critical in the formation damage. While in the dirty formations, the fines migration is believed to be the dominant parameter.

Based on the performance comparison results, the WWS is expected to be suitable in formations with higher plugging potentials. The SL and PS are expected to be implemented in formations with a limited amount of plugging materials (fine particles) due to the comparable performance.

1.5 Research Methodology

This research uses experimental and numerical tools in the screen performance analyses. A large-scale sand control testing facility is used to characterize the sanding and flow performance. Synthetic sand-pack samples and flat-screen coupons with various specifications (slot density and

aperture size) are used in this scaled testing facility. The testing procedure is also designed to incorporate more influential factors and be realistic to the field conditions. Sand production, differential pressures, and fines production are measured during the tests. Retained permeability data are calculated by coupling the pressure readings with the sand-pack sample's relative permeability values.

Numerical modelling using Computational Fluid dynamics (CFD) is built to obtain the pressure drop in the near-screen zone. The CFD model uses a similar geometry with the physical testing model. Single-phase (water) flow condition without fines migration is employed in the numerical modelling. Pressure drops are used to assess the formation damage due to the flow convergence.

1.6 Significance of the Work

Canada produces about 3.74 million barrels of oil per day. About 2.16 million barrels are the total bitumen production, and 1.24 million barrels are bitumen produced from oil sands using in-situ production technology (CAPP, 2018). Canada is a world leader in the thermal exploitation of oil sands and is recognized as a safe, sustainable leader combined with highly educated and experienced engineers. The research in this proposal will advance our existing knowledge, which will result in increased wellbore productivity, higher reservoir recovery, the advancement of testing methods, and lower production costs.

The real-time sand production measurement allows analyzing the impact of fluid velocity, fluid-phase change, etc. The novel idea of coupling sand control testing with relative permeability values enables the characterization of formation damage for different screen types under multi-phase testing conditions. The testing design and results lead to more reliable and robust screen design criteria for the SAGD production wells. The comprehensive and quantitative screen performance comparison yields a scientific screen selection protocol for SAGD operators.

1.7 Thesis Structure

The flow of this thesis is presented below.

Chapter 1 briefly introduces the research background, problem statement, research methodology, and objective.

Chapter 2 gives a detailed and broad literature review on subjects related to this research, including SAGD, stand-alone screens, sand control testing, relative permeability, and CFD.

Chapter 3 describes the experimental facility, testing materials, testing procedure, and testing matrix.

Chapter 4 presents the testing results in sand production, retained permeability, fines production, and fines concentration.

Chapter 5 shows the graphical design criteria for each stand-alone screen (Traffic Light System)

Chapter 6 introduces mathematical models for predicting the safe aperture window based on the testing results.

Chapter 7 presents the numerical modelling procedure and simulation results.

Chapter 8 compares the performance between the slotted liner, wire-wrapped screen, and punched screen. The optimal screen selection protocol is also provided in this chapter.

Chapter 9 concludes the whole thesis work and contributions. Also, future work is presented in this chapter.

Chapter 2: Literature Review

2.1 Introduction

Canadian oil sands are the third-largest oil reserves in the world-wide oil reserves. The estimated cumulative oil reserves in Canada are around 170 billion barrels (AER, 2018). Most of these oil resources are in bitumen form. (CAPP, 2018). Most of these bitumen resources locate in the Peace River, Cold Lake, and Athabasca in Alberta, Canada. The McMurray Formation is the oil-bearing formation of the Athabasca oil resources. The vast and recoverable oil resources give a promising future to the Canadian economy. There are currently two main methods to exploit these oil sand reserves: open-pit mining and thermal in-situ operation (Gate et al., 2007; Han et al., 2007).

Open-pit mining, also known as surface mining, is only used in the bitumen exploitation of shallow formations, which make up less than 20% of the total Alberta oil sands (AER, 2018). This direct mining method also brings environmental issues such as landscape disruption, tailing disposal, etc. (Butler, 1985).

The thermal in-situ methods used in Alberta are cyclic steam stimulation (CSS) and SAGD. Both cases involve the injection of hot steam into the formation to reduce the bitumen's viscosity (Zhang et al., 2007). In the CSS process, three operation stages are repeated: 1. steam injection, 2. soaking the reservoir, and 3. oil production (Bybee, 2003). The CSS has a relatively low oil recovery of 25% (Jimenez, 2008). A large amount of fresh water is required to produce an equivalent amount of oil. Also, high injection pressure and cyclic thermal stresses could lead to wellbore failure (Al-bahlani and Babadagly, 2008).

SAGD is a more efficient and economical method, in which the oil recovery is around 50% (Handfield et al., 2009; Dang et al., 2010; Medina, 2010; Irani et al., 2013). Roger Butlers first invented the idea of SAGD during the 1970s. Nowadays, SAGD has been widely used in bitumen exploitation in Canada (Gates et al., 2007; Wang et al., 2020a). In the SAGD process, a pair of horizontal wells are drilled. The well length ranges from 500 to 1200 meters, and the two horizontal wells maintain a vertical distance of around 5 meters (Butler and Stephens, 1981; Nasr et al., 1998). The upper well is designed for steam injection, and the lower one is used for oil production. The injected steam forms a steam-saturated zone called a steam chamber inside the formation. The continuous steam injection allows progressive contact between the bitumen and the hot steam on the steam chamber interface. The temperature inside the steam chamber is around 250 ℃. The hot

steam transfers heat to the bitumen reducing the oil viscosity to 8 to 12 cp (Devere-Bennett, 2015). The melted bitumen associated with the steam condensate flow along the steam chamber's edge toward the liquid pool around the production well due to gravity (Butler, 2001; Gates et al., 2005). The configuration of SAGD wells and the steam chamber is shown schematically in Fig. 1.
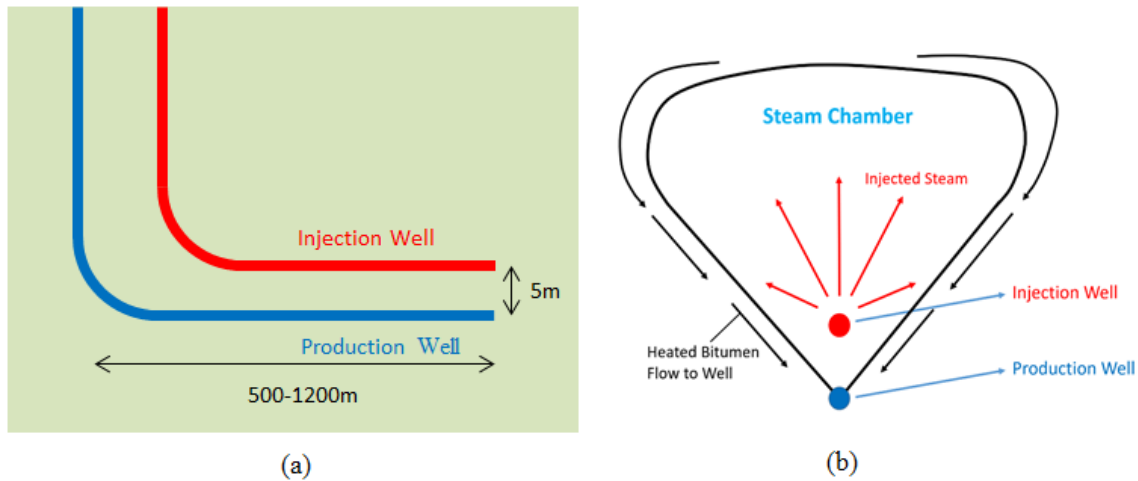
Figure 2. 1 Schematic configuration of SAGD well pair (a) and steam chamber (b) (modified from Butler, 1985)

2.2 Sand Production in SAGD

Sand production is a common issue encountered in the oil and gas industry. It is a process that solid particles are produced associated with reservoir fluids into the production well. Around 70% of the world's oil reserves suffer sand production issues (Fjar et al., 2008). The produced sand can erode and damage pipelines, down-hole pumps, and facilities. Also, it can increase the cost of remediation and sand disposal.

The mechanism for sand production is simply illustrated in Figure 2.2. The sand particles are produced when the hydrodynamic drag force created by the fluids overcomes the resisting force (Islam and George, 1989). The resisting force is a function of the stress condition and degree of cementation. However, it has been well known that the sand particles could not be dragged out of an intact rock by fluids even if the sandstone is weakly-consolidated. The sandstone rock needs to be degraded so that sand production can occur (Fjar et al., 2008). There are two mechanisms for sandstone degradation: shear and tensile failure. Shear failure occurs with low well-bore pressure, and tensile failure is usually due to the ultra-high pressure gradient (Morita et al., 1989).

$$F_h = \int_A P\,\overrightarrow{dA}$$
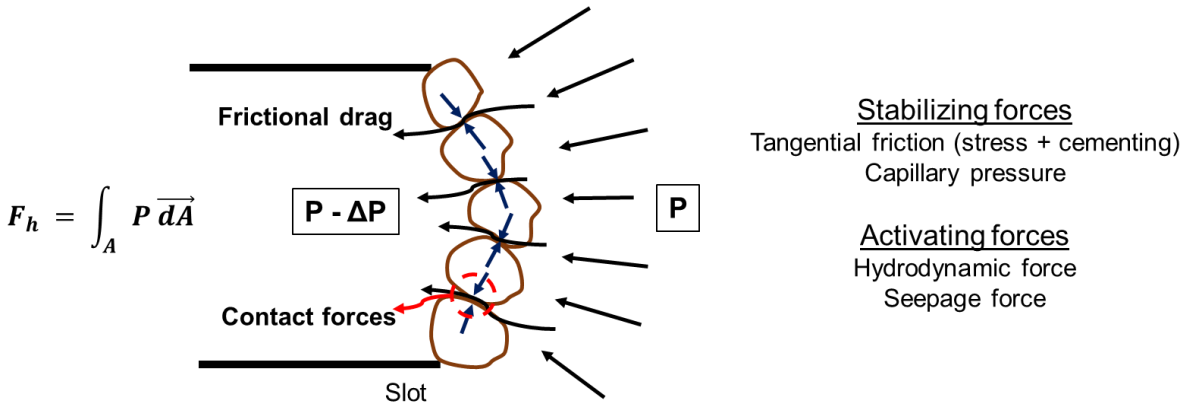
Figure 2. 2 Sand Production Mechanism

Mahmoudi (2017) categorized three sanding types in SAGD operations: (1) initial sand production, (2) transient sand production, and (3) continuous sand production. The initial sand production refers to the occasion that sand production ceases and becomes flow rate independent after a burst of sand production. In transient sand production, the amount of sand production is flow rate dependent. The amount of sand production increase with the increase of flow rate, but the sanding rate gradually reduces to zero after the flow stabilization. Continuous sand production is the case that sand is continuously produced, where no sand bridges can form.

In the field, the sand production process is susceptible to a few conditions: (1) natural unconsolidated formation, (2) water breakthrough scenarios, (3) production ramp-up, and (4) reservoir depletion (Morita and Boyd, 1991; Wu et al., 2006; Joseph et al., 2011). Oil sand is one of the typical unconsolidated formations. The primary bonding force existing in the oil sand reservoirs is the bitumen itself. This unconsolidated nature makes oil sand formations vulnerable to sand production (Penberthy and Shaughnessy, 1992). Due to the steam injection, the bitumen as the bonding material melts, causing the loss of the oil sands' cohesion, which makes sand production easier. Moreover, the horizontal SAGD wells have the undesirable capability to transport the produced sand to the surface. The produced sand may accumulate inside the well-bore and eventually plug the well-bore. Therefore, the sand control device is a must to control sand production in SAGD production wells.

2.3 Sand Control Methods

Various sand control techniques have been developed and applied in the oil and gas industry. Among them, drawdown control, chemical consolidation, and mechanical sand control are the three main methods to prevent sand production.

2.3.1 Production Drawdown Control

As stated in the previous section, the mechanism of sand production is that the hydrodynamic drag force overcomes the resisting force. Thus, sand production can be controlled by reducing the amount of drag force. Past field experience proved that sand production is limited when the production rate is below a certain level (Abass et al., 2002). In the drawdown control, the production rate is restricted below the critical flow rate to limit sand production. This technique is suitable for weakly to intermediately consolidated sandstones (Papamichos and Malmanger, 1999). However, due to the unconsolidated nature of oil sands, it is not feasible in SAGD operations.

2.3.2 Chemical Consolidation

Other than controlling the hydrodynamic drag force, enhancing the resisting force is another option to control sand production. The chemical consolidation method increases the bonding strength of the formation sand grains by injecting resin or other chemicals (Larsen et al., 2006). The resin cement and consolidates the sand grains, therefore, enhancing the rock strength. This method is successfully implemented in conventional oil reservoirs (Haavind et al., 2008). However, it is still a challenge for placing resin in the horizontal SAGD wells (Wan, 2011).

2.3.3 Mechanical Methods

Sand control devices, including stand-alone screens and gravel packing, are also commonly employed in the well completion job to control the sand production mechanically. These devices act like a filter retaining the sand particles while allowing liquid production. In the gravel packing method, gravels are injected into the annular gap between the stand-alone screen and open-hole or casing to prevent sand production. This method is widely used in conventional wells and offshore operations. However, due to the poor transportability, implementing gravels into a 1000-meter-long horizontal SAGD well is not economical doable.

Stand-alone screens, including the SL, WWS, and PS, due to their high mechanical strength properties and economy are widely used in SAGD operations for years. The stand-alone screens have a couple of functions: (1) controlling the sand production, (2) maintaining the wellbore

integrity, and (3) allowing desirable liquid production. In the next section, details of these stand-alone screens are given in terms of design, geometry, properties, and sand control and failure mechanism.

2.3.3.1 Slotted Liner

The SL is a hollow cylinder pipe with narrow slots. A rotating saw cuts the slots. The pipe used for the SL is usually carbon steel with standard grades. The SL is easy to install and can maintain strong mechanical integrity against compression, tension, and bending (Bennett et al., 2000; Yi, 2002; Furui et al., 2007; Xie et al., 2008; Martins et al., 2009; Van Vliet and Hughes, 2015). The slots can be manufactured in three different geometries: straight cut slots, keystone cut slots, and seamed slots. Figure 2.3 shows a real SL and different slot geometries. The straight cut slots have the same slot width along with the slot. The slot widths along the keystone cut slots and seamed slots are changing. The inner slot width is larger than the outer slot width in these two slot geometries, which reduces the chance of slots plugging by providing larger space for particles to flow through (Bennion et al., 2009). Also, the slots on the SL can have different patterns. Figure 2.4 presents four typical designs for the SL. The staggered pattern is preferred as it provides the most pipe strength (Ott and Woods, 2003).
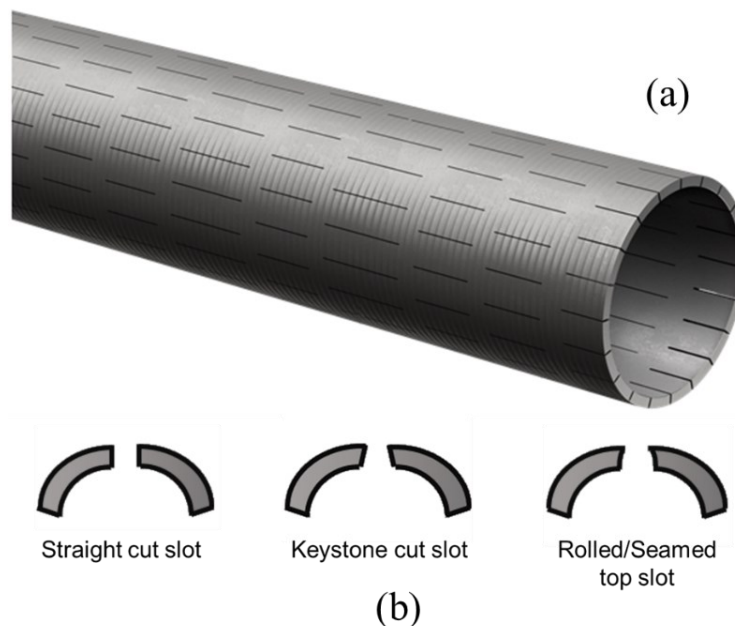
Figure 2. 3 (a) the slotted liner (RGL Reservoir Management Inc., 2018), and (b) schematic of the slot geometries (modified from Bennion et al., 2009)
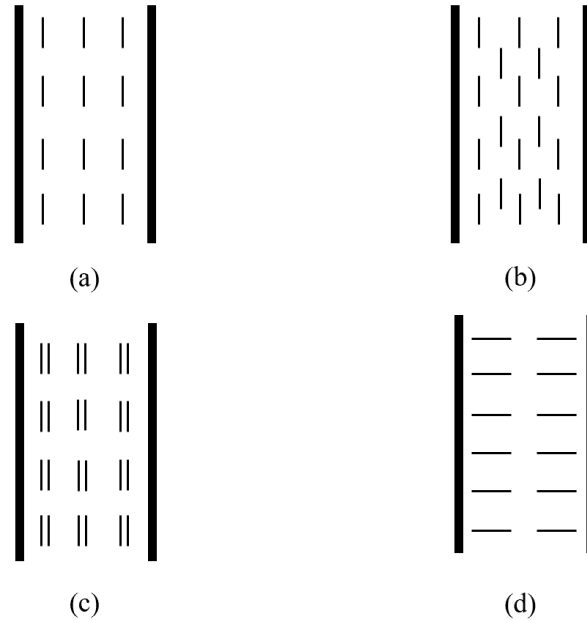
Figure 2. 4 Slots patterns in the slotted liner (a) line slots, (b) staggered slots, (c) gang slots, and (d) horizontal slots

In the industry, the slot size is referred to by the "gauge" terminology (Suman et al., 1985). One "gauge" equals 0.001 inches. Thus, a 10-gauge slot width means the slot size of 0.010 inches. Due to manufacture limitation and integrity concern, the commercial slot sizes range from 10 to 90 gauges (Petrowiki, 2017). The SL also has a different slot density design, indicated by slots per foot (SPF) or slots per column (SPC). The slot density describes the number of slots on a one-single column of the liner. The slot size associated with the slot density yields the open flow area (OFA) of the SL. OFA is the area that allows liquid production. The SL provides a limited OFA between 1 to 3% (Matanovic et al., 2012).

It has been reported that plugging is one reason causing SL failure (Bennion et al., 2009; Romanova and Ma, 2013). In SAGD wells completed by the SL, 90% of the slots may get fully plugged after years-operation (Romanova et al., 2014). The plugged slots result in higher resistance to the flow and increased pressure drawdown. The slots plugging mechanism includes fines migration, scaling, fouling, and corrosion (Bennion et al., 2009). The carbonate steel used in the SL, although cheap, makes it vulnerable to corrosion.

2.3.3.2 Wire-wrapped Screen

The WWS is another type of stand-alone screens that have been widely employed in SAGD production wells. In the WWS, a continuous trapezoidal or triangular wire is wrapped onto a supporting base pipe. Figure 2.5 shows the structure of the WWS.
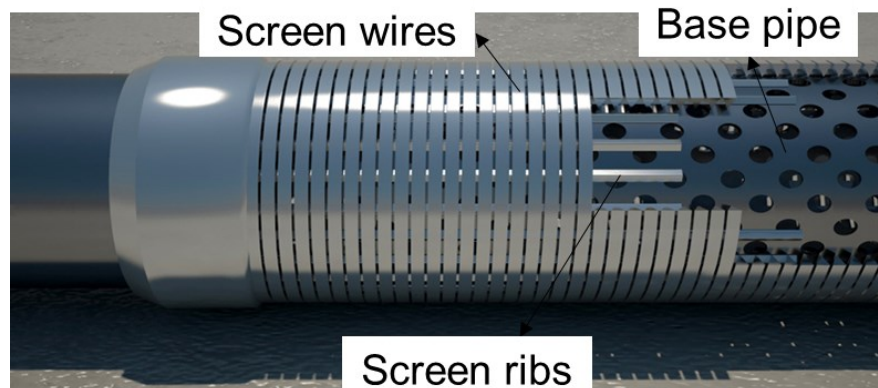
Figure 2. 5 Structure of the wire-wrapped screen

The wires are made of stainless steel to prevent corrosion. Usually, the AISI 304L or 316L steel are used for the wires (Romanova et al., 2014; Van Vliet and Hughes, 2015). The base pipe is perforated to reduce pressure loss and allow liquid production. The perforation sizes range from 0.375 to 1 inch in diameter. The diamond pattern is usually applied to provide a robust mechanical property of the base pipe (Van Vliet and Hughes, 2015). The minimum commercial aperture size of the WWS is 0.005 inches.

The WWS can provide a higher OFA ranging from 6 to 18% (Romanova et al., 2014). Such high OFA in the WWS offers higher resistance to the aperture plugging than the SL. Also, high OFA nature yields low-pressure drawdown and productivity impairment. However, the stainless steel and different manufacturing design make the WWS more expensive than the SL. Moreover, the mechanical strength of the WWS is weaker than the SL. It is vulnerable to compression, tension, and bending. In the SAGD operation, due to the in-situ stresses plus the induced thermal stresses, the stand-alone screens are bearing cyclic loads. The weak mechanical strength of the WWS may go through structural deformation resulting in the closure or expansion of apertures (Xie et al., 2008; Malbrel et al., 1999). The expansion or closure of the aperture could cause severe sanding or flow performance issues. Thus, the aperture sizes should not change more than +0.001/-0.002 inch under the thermal condition of quality control (Xie et al., 2008).

2.3.3.3 Punched Screen

The SL and WWS are the two traditional screens used in the SAGD production wells. The PS as a new type of stand-alone screen is recently designed and employed in thermal operations. The strong mechanical properties, intermediate OFA, and higher resistance to corrosion and erosion make it more popular and attention in the SAGD wells. Figure 2.6 shows the PS view and its schematic aperture geometry. The PS consists of a perforated supporting base pipe and a stainless-steel punched jacket. The punched jacket is welded onto the base pipe. Like the WWS, the stainless-steel jacket provides strong corrosion resistance, and the base pipe ensures mechanical integrity. The aperture size of the PS can be manufactured between 0.010 to 0.039 inches (Driscoll, 1986; Roscoe, 1990). The OFA of the PS is from 3 to 8 %. The intermediate OFA, strong mechanical properties, and high corrosion resistance make the PS gain more and more popularity and attention in the SAGD (Spronk et al., 2015) and other thermal operations (Naganathan et al., 2006).
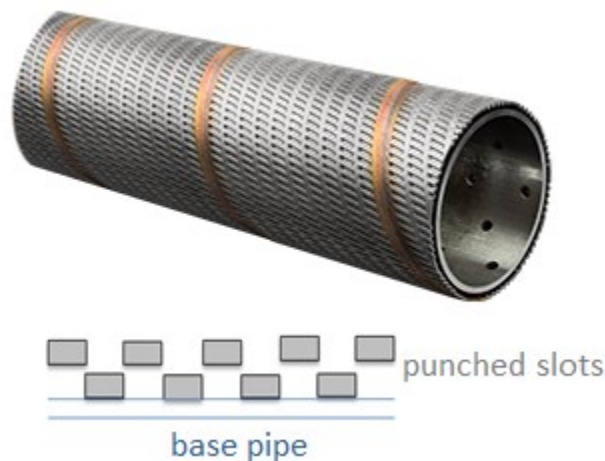
Figure 2. 6 Configuration (RGL Reservoir Management Inc., 2018) and schematic of slot geometry of PS

In summary, plenty of sand control methods are applied in the oil and gas industry to prevent sand production. However, stand-alone screens are widely employed in the SAGD operations due to the special operational conditions, including the unconsolidated nature of the oil sands, thermal conditions, and long horizontal wells.

2.4 Formation Damage in SAGD

Other than sand production, formation damage is another critical problem in the oil and gas industry. Fines migration is one of the reasons causing the near-wellbore formation damage,

particularly in the sandstone reservoirs (Muecke, 1979; Gray and Rex, 1996). Fines are small particles with a size of fewer than 44 μ m. Lots of studies have been done to investigate the fines migration process in the porous media (Barkman and Davidson, 1972; Abrams, 1977; Ives, 1987; Sharma and Yortsos, 1986; Ohen and Civan, 1991; Van Oort et al., 1993; Faure et al., 1997; Denney, 1998; Bedrikovetsky et al., 2002; Civan, 2007; Qiu et al., 2008; Bedrikovetsky, 2011; Zeinijahromi et al., 2011; Musharova et al., 2012; Sacramento et al., 2015; Rosenbrand et al., 2015; Karazincir et al., 2017; Yang et al., 2018; You et al., 2018, 2019). However, in this section, the literature review focuses on the fines migration related to the SAGD.

Valdes (2006) concluded three stages of fines migration that cause the pore plugging, namely, (1) fines generation, (2) fines mobilization and migration, and (3) fines entrapment. Generally, fine particles are attached to the grain surface by the gravitational and Van der Wallace forces. The repulsive electrical double layer force plus the drag force detaches the fine particles. The detached fine particles start to migrate due to the hydrodynamic drag force and can be entrapped in the pore throats. There are different fines entrapment mechanisms in the porous media, including straining in thin pores, gravity segregation, and bridging, as shown in Figure 2.7 (Russell et al., 2018). The clustering of the fine particles in the pore throat blocks the flow paths, therefore, reduce the permeability and cause the formation damage. These processes are affected by the fines size, mineralogy, pore structure, saturation fluids, salinity, and pH. Details of these influential factors are given below.

2.4.1 Impact of pore structure and fines size

Sand particles form a skeleton to bear the load in the oil sands. However, fine particles are not parts of this structure and can be mobilized and transported by fluids. During the fines migration, they tend to orient their longest dimension along the flow direction (Khilar and Fogler, 1998). Thus, the particle size referred to in the fines migration is the dimension normal to the longest dimension (Mahmoudi, 2017). Barkman and Davidson (1972) and Abrams (1977) conducted experiments. They found that: (1) particles equal or greater than one-third of the pore throat size bridge at the pore throat, (2) particles with a size between one-third and one-seventh of the pore throat size strains at the pore throat, and (3) particles smaller than one-seventh of the pore throat size can pass through the pore throat and only cause minor impairments.
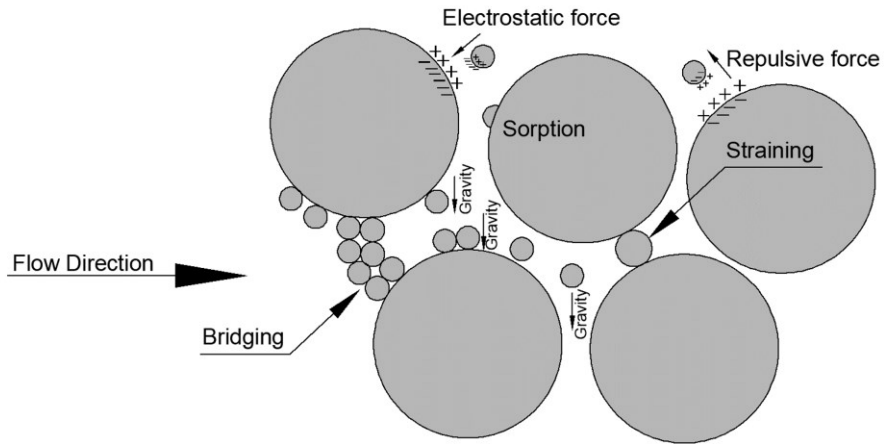
Figure 2. 7 Different mechanisms of fines entrapment in porous media

2.4.2 Impact of fluid properties and clay mineralogy

A few researchers have conducted experiments to investigate the impact of salinity and pH on the fines migration (Kotylar et al., 1996; Khilar and Fogler, 1984). Khilar and Fogler (1984) found a critical salt concentration (CSC) for the fine particles release and mobilization. They found that if the injecting brine's salinity is below the CSC level, there is a significant permeability reduction due to the fines migration. The CSC level depends on the type and valency of the ions of the fluids. However, the CSC only exists for the monovalent cations (Na^+, K^+, and Li^+). Bivalent or trivalent cations (such as Ca^{2+}, Mg^{2+}, and Ba^{2+}) and anions have a negligible impact on the fines migration. Also, different monovalent cations have other effects on fines migration (Khilar and Fogler, 1984). The mechanism that salinity affects the fines migration is that it affects the zeta potential of the particles. The particles' zeta potential impacts the magnitude of the repulsive electrical double-layer force (Khilar and Fogler, 1984; Sokolov and Tchistiakov, 1999; Rodriguez and Araujo, 2006; Russell et al., 2017, 2018). A higher level of the repulsive electrical double-layer force can enhance the release of the fines.

Besides the salinity, pH also affects the fines migration in the porous media. Several researchers have shown the clay release is mitigated at low pH (Mungan, 1965; Simon et al., 1976; Leone and Scott, 1988; Valdya and Fogler, 1992).

Clay mineralogy is another crucial factor in pore plugging. The pore plugging mechanism for the kaolinite and illite is due to fines migration. However, swellable clay, like montmorillonite, can

swell with water contact. After swelling, the clay reduces the pore throat size and cause formation damage (Aksu et al., 2015; Liu et al., 2017).

2.4.3 Salinity data of SAGD wells in the McMurray Formations

Since the fluid chemical properties play a critical role in the fines migration, it is essential to know the composition of the produced and formation water of the McMurray Formations. In SAGD operations, hot steam is injected into the formation to heat the reservoirs. The steam condensate mixes with the formation water. With the contact of the formation, the steam condensate desorbs salt and minerals from the formation and changes the salinity.

Cowie et al. (2015) conducted a hydrochemical analysis of 258 water samples of the McMurray Formation and mapped the total dissolved solids (TDS). Figure 2.8 shows the TDS mapping results in the McMurray Formation. It is found that the TDS of the formation water has a considerable variation ranging from 200 mg/L to 28000 mg/L. Birks et al. (2017) plotted a Piper diagram for the primary ions existing in different formations in the Athabasca oil sand area, as shown in Figure 2.9. This plot presents the chemical compositions of the produced water. It is demonstrated that Na^+ and K^+ are the dominant cations and Cl^- is the anion. Other studies regarding the hydrochemical analysis of the produced water are also presented in Table 1. The TDS of the produced water varies from 1000 to 7000 ppm. The pH of the produced water is between 7 and 9.
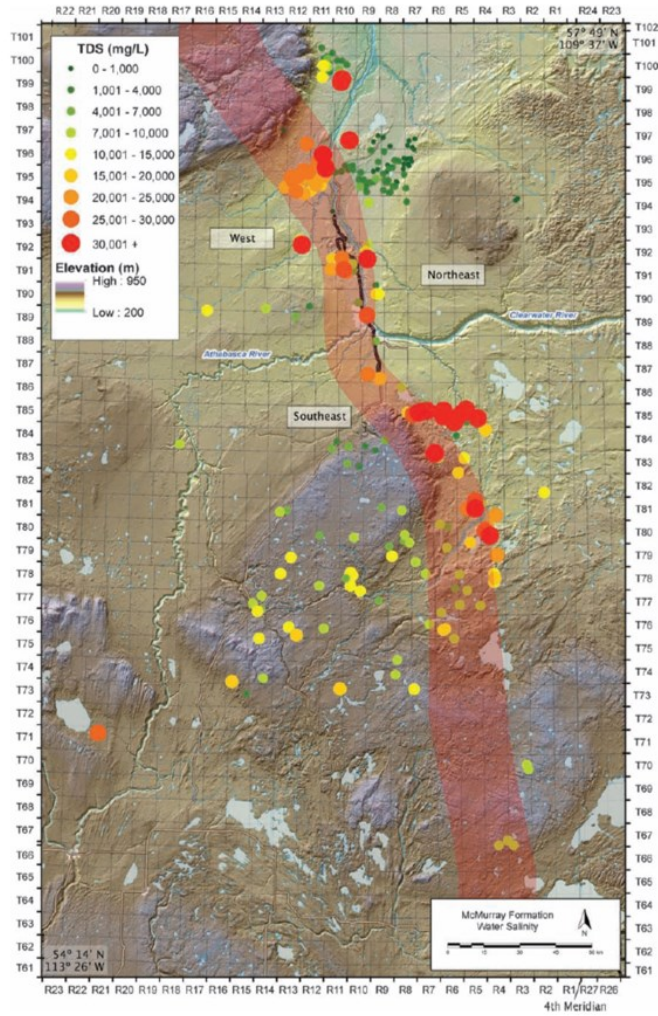
Figure 2. 8 TDS map of the McMurray Formation waters (Cowie et al., 2015)
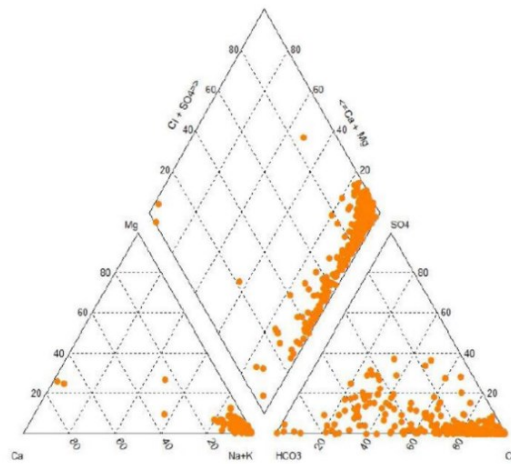
Figure 2. 9 Piper plot of water samples of the McMurray Formation (Birks et al., 2017)

Table 1 A summary of the hydrochemical analysis of produced water

Chemical Properties	Pedenaud et al. (2005)	Peterson (2007)	Pedenaud and Michaud (2009)	Pedenaud and Michaud (2009); Pedenaud et al. (2005)	Pedenaud and Michaud (2009)	Goodman et al. (2010)	Bhattacharjee (2010)	Peterson and Grade (2011)	Minnich et al. (2012)	Minnich et al. (2012)	Surmont Oil Sand Project (2018)
Calcium (Ca) (ppm)	23.2	20	2.7	3.9	22	1-52	7	2.5	10	2	NM
Magnesium (Mg) (ppm)	13.1	10	6.1	0.3	11	1.6-14	NM	0.05-0.15	3	1	NM
Barium (Ba) (ppm)	2	NM	0	0.2	0	NM	0.8	NM	NM	NM	NM
Sodium (Na) (ppm)	1615.9	1004	2200	706	780	130-3000	314	221	1310	321	NM
Iron (Fe$_2$) (ppm)	0	NM	1.9	0.7	0.3	NM	NM	<0.05	NM	NM	NM
Potassium (k) (ppm)	68	NM	62	28.7	13	14-240	NM	11.9	21	18	NM
Total Cations (ppm)	1722.3	NM	22.73	740	826	NM	NM	NM	NM	NM	NM
Sulfate (SO$_4$) (ppm)	2	70	56	1	58	NM	107	12	41	2	NM
Chloride (Cl) (ppm)	1395	1310	1697	930	962	48-4800	200	292	2060	260	650
Carbonate (CO$_3$) (ppm)	0	2	108	1	0	NM	150	NM	21	18	NM
Bicarbonate (HCO$_3$) (ppm)	2130	429	2677	332	489	NM	NM	NM	493	406	NM
Ammonia (NH$_3$) (ppm)	NM	NM	NM	NM	NM	11-64	NM	NM	NM	NM	NM
Ammonium (NH$_4$) (ppm)	NM	NM	NM	NM	NM	NM	NM	NM	46	66	NM
Total Anions (ppm)	3527	NM	4538	1264	1509	NM	NM	NM	NM	NM	NM
Silica (SiO$_2$) (ppm)	260	NM	260	260	250	11-260	NM	102	170	255	190
Alkalinity (as CaCO$_3$) (ppm)	NM	NM	NM	NM	NM	140-1400	NM	120	NM	NM	250
Salinity (ppm)	NM	NM	NM	NM	NM	NM	NM	NM	NM	NM	NM
NaCl (ppm)	NM	NM	NM	NM	NM	NM	NM	NM	3400	400	NM
Hardness (as CaCO$_3$) (ppm)	112	NM	32	11	100.9	NM	22	NM	NM	NM	10
Total Solid (TS) (ppm)	NM	NM	NM	NM	NM	NM	275-400	NM	5700	2800	NM
Total Dissolved Solid (TDS) (ppm)	5249.3	3040	6951	2370	2585	NM	1005	NM	NM	NM	1800
Suspended Solid (SS) (ppm)	164	<25	NM	NM	NM	NM	NM	NM	NM	NM	NM
Total Organic Carbon (TOC) (ppm)	NM	200	NM	NM	NM	170-430	NM	232	588	596	500
Oil (ppm)	NM	20	NM	NM	NM	NM	NM	29.1	NM	NM	65
pH (at 25°C)	7.9	7.9	7.9	8	7.7	7.3-8.8	8.5	7.1	NM	NM	7.5
Density (g/cm^3)	1.0032	NM	NM	1.001	NM	NM	1.005	NM	NM	NM	NM

NM: Not mentioned

2.5 Stand-alone Screens' Design

Proper designed stand-alone screens can control not only the sand production but also maintain desirable reservoir deliverability. The design process of stand-alone screens includes a few influential factors such as PSD, formation mineralogy, fluid properties, operational conditions, etc. (Guo et al., 2018, 2020; Wang et al., 2020a). The PSD controls the porosity, permeability, and mechanical properties (tensile and shear strength, stiffness) of the formation sands (Miura et al., 1997). Thus, the formation sand characterization is a must to achieve the optimal screen design.

2.5.1 Particle Size Distribution of the McMurray Formation

Dry sieve analysis is a typical and traditional laboratory testing method to measure the PSD of the formation sands. As shown in Figure 2.10, a series of sieves with standard mesh sizes are piled up. The opening sizes of these sieves gradually narrow from top to bottom. By shaking the sieves mechanically, the sand particles start falling through the sieves. After the sieve shaking process, the weight of the sand captured in each sieve is measured. The PSD curve can be plotted between the cumulative weight percentage and the sieve opening size on the semi-log coordinates. Figure 2.11 shows an example of the PSD curve obtained by the sieve analysis. From the PSD curve, the median size of the sand particles is at the 50% cumulative weight point, indicated by D_{50}. D_{10} means that the sieve size at which 10% of the sample's mass consists of particles with a diameter larger than this value. The same concept applies to other points. One drawback of the dry sieve analysis is that the fines content measurement is affected due to the adhesion of fine particles to the grain surface, leading to a biased result (Ballard and Beare, 2006).

Figure 2. 10 Dry Sieve Analysis Facility
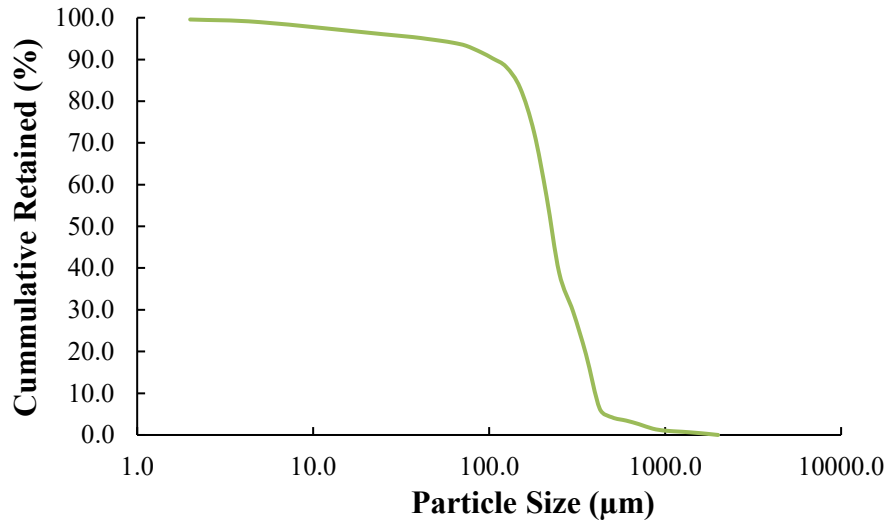
Figure 2. 11 PSD curve from dry sieve analysis

Laser-particle size analysis (LPSA) is another method to determine the PSD. LPSA can measure particles with sizes ranging from nanometers to millimeters. LPSA determines the PSD by measuring the scattered light intensity. Smaller particles can scatter the light at large angles, and larger particles scatter at small angles. By measuring the scattered angle and intensity, the PSD of the sample is determined. Although the LPSA can accurately determine the fines content accurately, the results are sometimes sensitive to the samples' dispersion. Also, the repeatability test is inconvenient in this application (Chanpura et al., 2012b). Ballard and Beare (2012) claimed that the PSD measurements could display deviations between these two methods. However, the difference shall decrease significantly if the sample is clean.

Another more advanced PSD measurement is dynamic image analysis (DIA). The DIA analyzes the image of each particle and generates the overall PSD curve. It gives more details about the particle dimensions.

2.5.2 Clay Mineralogy of the McMurray Formation

The clay mineralogy of the oil sands in the McMurray Formation includes mainly kaolinite and illite. Devere-Bennett (2015) conducted an X-ray powder diffraction (XRD) analysis on one oil sand sample and found a compositional percentage of 23.3%, 64.5%, and 11.3% for illite, kaolinite, and smectite. Also, there is some minor trace of chlorite in the sample. However, due to the thermal condition in the SAGD operations, the thermal diagenesis of kaolinite to smectite can happen (Imasuen et al., 1989; Romanova et al., 2015).

2.5.3 Sand Control Testing

Sand control testing has been commonly used in the industry to optimize screen design. There are two sand control testing: slurry and pre-packed sand retention tests (SRT). In the sand control testing, the sanding and flow performance is characterized and used for the optimal screen design.

2.5.3.1 Slurry SRT

In the slurry SRT, a sand sample is first dispersed in the viscous fluid (water and polymer), forming a sand slurry. Next, the sand slurry is diluted with brine to a concentration of less than 1% of volume (Chanpura et al., 2012a; Sanyal et al., 2012; Dong et al., 2014, Changyin et al., 2016; Wu et al., 2016). The diluted sand slurry is injected into a testing cell, as shown in Figure 2.12. A sand control screen coupon is placed at the bottom of the testing cell. During the testing, a sand-pack is gradually built-up on the screen coupon. The sand accumulative above the screen increases the pressure drop, which is considered the plugging measurement (Markestad et al., 1996; Gillespie et al., 2000; Underdown, 2001; Williams et al., 2006). Also, the amount of the produced sand is measured to characterize the sanding performance.

The slurry SRT is designed to emulate the initial period of the production stage, in which there is an annular gap between the formation of sand face and the sand control devices. The gap fills with a low concentration of sand slurries. It is believed that the slurry SRT is a useful application for conventional wells instead of thermal operations (Markestad et al., 1996; Gillespie et al., 2000; Williams et al., 2006).
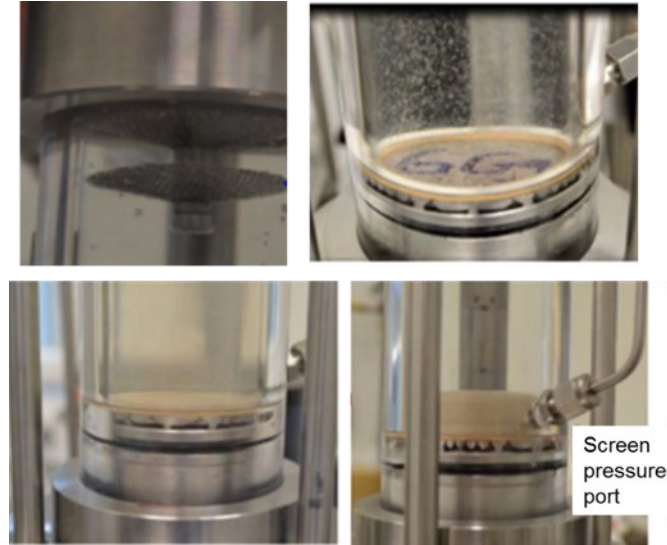
Figure 2. 12 Slurry SRT Cell (Wu et al., 2006)
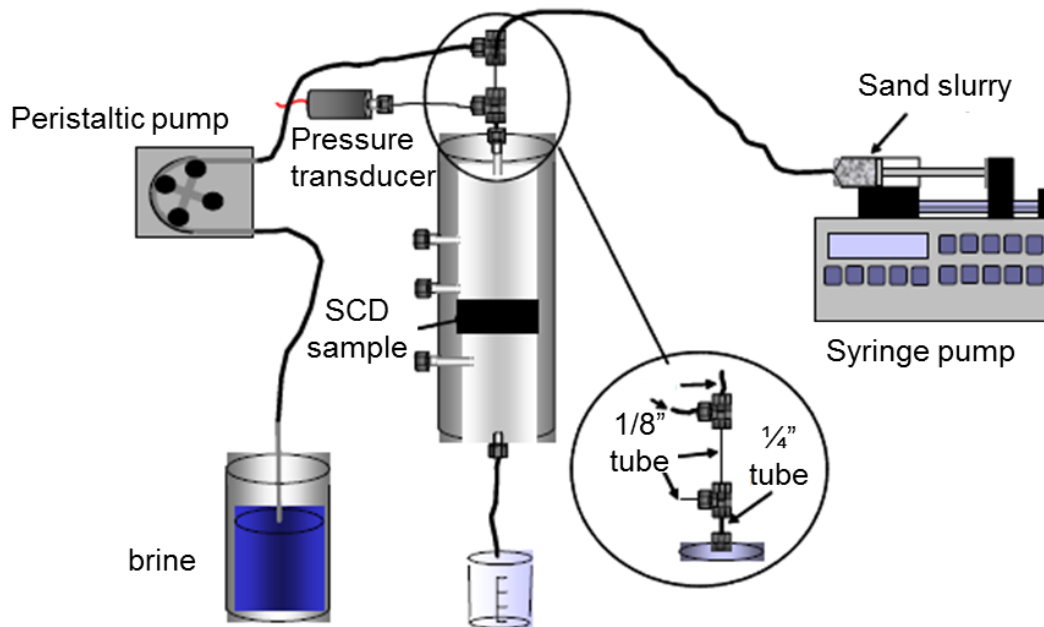
Figure 2. 13 Schematic of Slurry SRT modified after Ballard and Beare (2003)

2.5.3.2 Pre-packed SRT

For the pre-packed SRT, a sand sample is directly packed into a testing cell, forming a sand-pack sample sitting on the screen coupon. Fluids are injected from the top of the sand-pack towards the coupon. Like the slurry SRT, sand production and pressure drops are recorded during the pre-packed SRT to analyze the sanding and flow performance of the screen. This testing procedure

mimics the scenario in which the wellbore is collapsed. The formation sands fill the annular gap between the sand face and the sand control screen, forming a high-porosity zone (Guo, 2018). Figure 2.14 presents the schematic concept of pre-packed SRT. In the SAGD condition, the formation oil sands are bonded by the viscous bitumen. However, during the pre-heat stage, the bitumen is melted due to the steam injection. The unconsolidated formation sands, therefore, collapse and accumulate around the stand-alone screens. Figure 2.15 shows the downhole condition of the SAGD wells, in which the collapsed formation sands form a high-porosity zone around the stand-alone screens.   Thus, the pre-packed SRT has been justified for properly emulating the SAGD conditions (Chanpura et al., 2011; Mahmoudi, 2016; Guo, 2018).
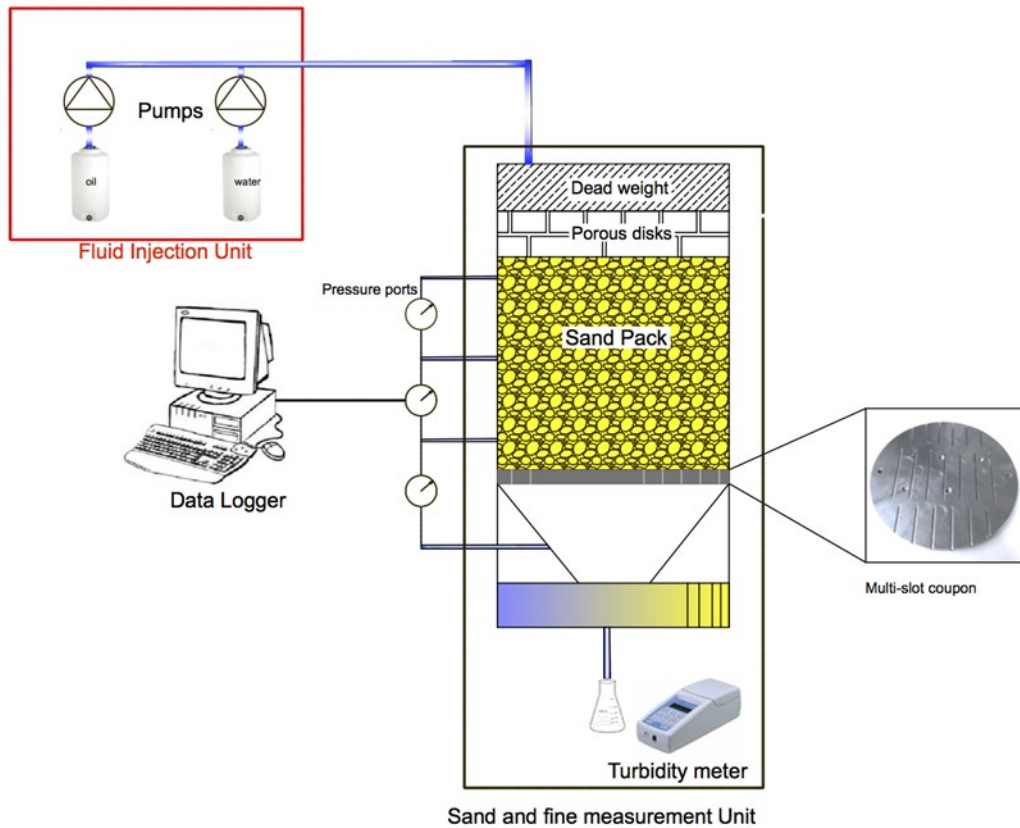
Figure 2. 14 Pre-packed SRT, after Montero Pallares et al. (2018)
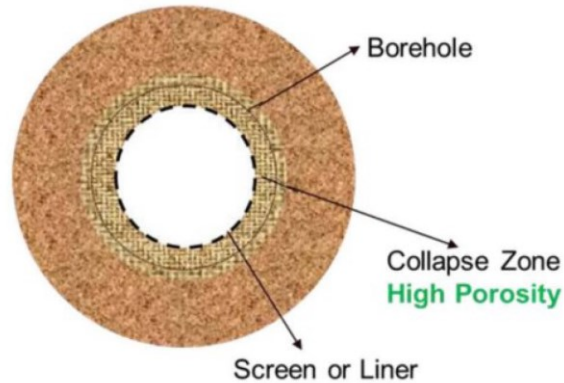
Figure 2. 15 Schematic of the downhole condition of SAGD wells after formation collapse

The pre-packed SRT facility can be customized in different ways based on testing purposes. The difference in the testing design and procedures stems from the screen type, number of fluid phases, stress level, and flow geometry. There are three major categories of the pre-packed SRT, namely, conventional pre-packed SRT, tri-axial pre-packed SRT, and full-scale pre-packed SRT.

Conventional Pre-packed SRT

As shown in Figure 2.14, the conventional pre-packed SRT allows various injection fluids, including single-phase or multi-phase. Also, the flow geometry is linear as the fluids are injected normal to the screen coupon. However, it can only bear minor axial stress. Moreover, the axial and horizontal stresses are not independent. This type of pre-packed SRT has been used for analyzing the screen performance and optimizing the screen aperture design by several researchers due to its convenience and economy (Bennion et al., 2009; Romanova et al., 2015; Mahmoudi, 2016; Ma et al., 2018, 2019a, 2019b; Wang et al., 2020a, 2020b, 2020c).

Tri-axial Pre-packed SRT

The tri-axial pre-packed SRT improves the conventional one by allowing a higher stress level. Figure 2.16 presents the schematic concept of this SRT setup. In this setup, the axial load is applied by a loading frame, and the horizontal stress is generated by the hydraulic oil connected to the piston pump. In such a way, one can control the horizontal and normal stress independently.

The SAGD wells usually bear loads due to in-situ stresses and thermal stresses (Fattahpour et al., 2016; Roostaei et al., 2018). This facility allows assessing the stand-alone screens' performance

under various stress conditions. Guo (2018) and Wang et al. (2018) conducted experiments analyzing the performance of the SL under different stress conditions.
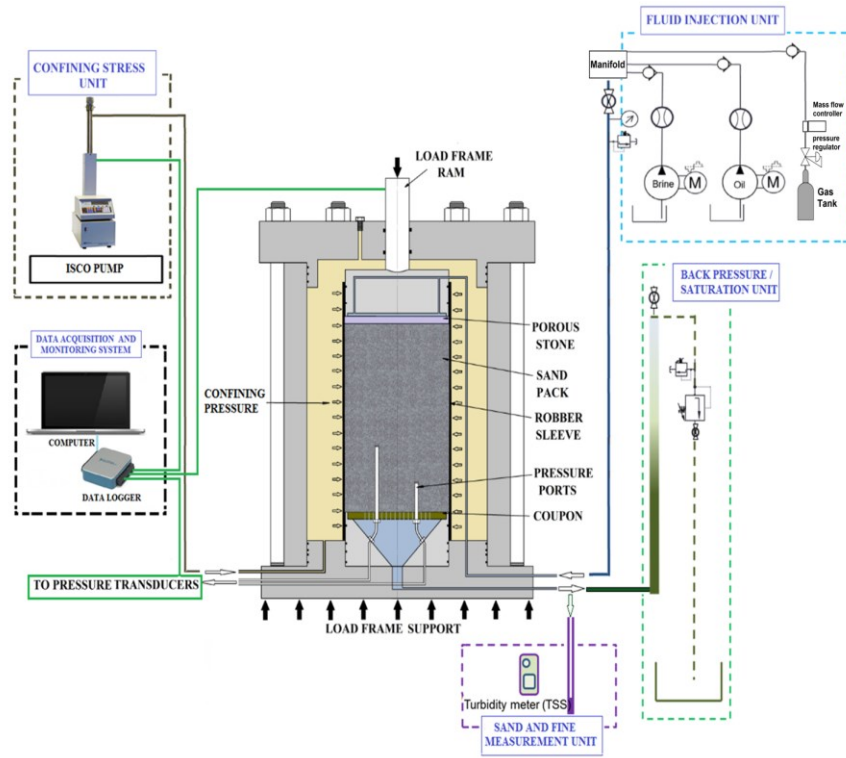
Figure 2. 16 Schematic of Tri-axial Pre-packed SRT

Full-scale Pre-packed SRT

The main criticism of the conventional and tri-axial SRT is the linear flow geometry. In both cases, the fluids are injected perpendicular towards the screen coupons. However, in the real SAGD downhole condition, the actual flow geometry is radial. The full-scale pre-packed SRT allows investigating the screen performance under radial flow conditions by implementing an entire cylindrical liner inside the testing cell. Figure 2.17 presents the schematic view of this setup. Few researchers conducted experiments using this facility (Chenault, 1938; Jin et al., 2012; Anderson, 2017; Haftani et al., 2020). Although this full-scale setup represents a more realistic downhole condition, the heavy-duty and costly nature limits the application.
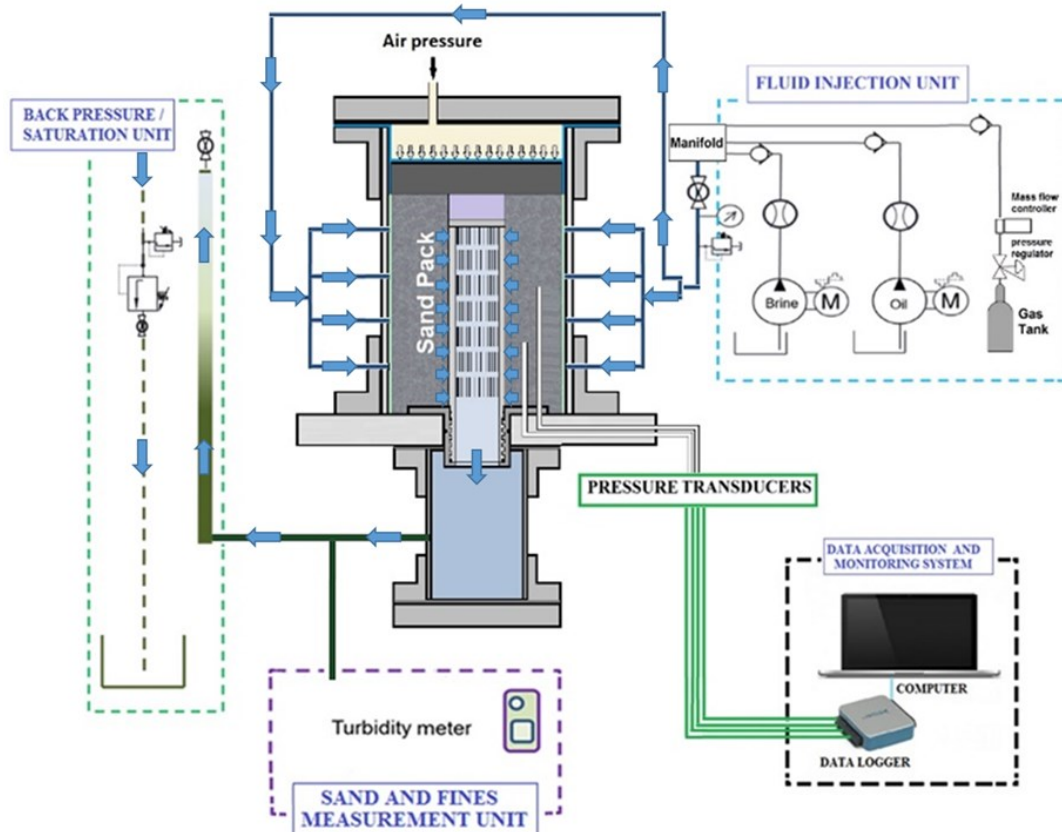
Figure 2. 17 Schematic of the Full-scale Pre-packed SRT

2.5.4 Design Criteria of Stand-alone Screens

Generally, adequately designed stand-alone screens should meet the following objectives: (1) maintain the wellbore integrity from geological stresses, (2) control the sand production to a limited level, and (3) ensure the reservoir deliverability, in other words, providing a desirable flow performance. Thus, sanding and flow performance are the two main parameters in the design criteria. The aperture size design is the primary objective, which plays a critical role in sanding and flow performance. Smaller aperture size could reduce the sand production but increase the plugging tendency, and vice versa. Therefore, the aperture size of the stand-alone screens must be designed to optimize both the sanding and flow performance.

2.5.4.1 General Design Criteria of Sand Control Devices

The experimental method is mainly used in creating the design criteria for sand control devices. Although some numerical studies also attempted to generate the proper aperture size, the missing

of several physical components, demanding computing time, and lack of validation makes them unsuitable for design purposes.

Coberly (1937) first investigated the bridging mechanism for the SL by conducting a series of tests with a single-slot coupon. He found a stable sand arch (bridge) would form if the slot size were smaller than two times D_{10} (D_{10} represents the sieve opening size that can retain 10% of the sample mass). Thus, he claimed that the slot size should not be larger than 2 D_{10} to form a stable sand bridge to prevent sand production. Coberly's design criteria have been adopted by the industry for years and proven to be valid. Suman (1985) also conducted experiments with synthetic grains and proposed that the safe slot size should be equal to or smaller than D_{10} of the formation PSD. Both of them used one single point of the whole PSD to create the design criteria.

Markestad et al. (1996) conducted an experimental study for the design criteria of the WWS. They found that the whole PSD data shall be included in the design criteria assessment instead of only one single point through their testing. Also, they provided a slot size window for given PSDs. The sand retention capability determined the upper bound of the window, and the lower bound controlled the flow performance (plugging). They defined four slot sizes to characterize the slot size window: (1) the largest slot size (d_{++}) where severe sand production happened, (2) the largest slot size (d_{+}) where sand production did not occur, (3) the smallest size (d_{--}) where severe plugging occurred, and (4) the smallest size (d_{-}) where no plugging occurred. Thus, the optimal slot size window was between d_{+} and d_{-}. Although they only qualitatively described the "severe sanding and flow performance," they included sand production and plugging into the design criteria assessment.

2.5.4.2 Design Criteria of Sand Control Devices in SAGD Operations

As mentioned before, the sand production issue in the horizontal wells needs special attention due to the poor transportability of the sand particles. Several experimental studies using the pre-packed SRT have been done to assess stand-alone screens' design criteria in SAGD operations.

Bennion et al. (2009) conducted a small-scale pre-packed SRT with a single-slot coupon to analyze the performance of the SL in SAGD wells. In their testing procedure, different fluid phases were established, including single-phase (oil), two-phase (oil and brine), and three-phase (oil, brine, and gas). The amount of sand production and pressure drops in the near-screen zone were used to characterize the sanding and flow performance of the SL coupon. Based on their testing results,

the rolled-top slot geometry showed a better performance in preventing plugging. Also, it was found that the clay materials play an essential role in the formation damage. Following Bennion et al. (2009), other researchers used similar experiment procedures and set up in the screen design work. Romanova et al. (2014), O'Hara (2015), and Spronk et al. (2015) compared the performance between the WWS, SL, and PS for the same formation sand. Devere-Bennet (2015) also employed the multi-phase pre-packed SRT and found out the optimal slot size for some PSDs in the McMurray Formation. In this study, acceptable sanding performance was achieved if the amount of the produced sand is below the threshold value. Regarding the plugging indicator, a rigid pressure differential was used to judge the flow performance of the screens. For example, if the pressure drop reading in the near-screen zone went above five psi, it was deemed an undesirable flow performance.

Various influential factors were included in the above-mentioned testing design, such as fluid velocity, fluid-phase change, PSD, clay mineralogy, and slot size. However, the slot density and stress conditions are excluded from the testing design. Also, using a severe pressure drop as the flow performance indicator is qualitative and subjective.

Mahmoudi (2016) employed a large-scale pre-packed SRT to investigate the impact of slot density and generated design criteria of the SL for two formation sands in the McMurray Formations. He used a multi-slots coupon in the testing in his study, and the testing fluid is brine only. He used a retained permeability concept proposed by Hodge et al. (2002) to characterize the flow performance of the SL instead of the rigid pressure differential. The retained permeability (RP) is defined as the screen permeability over the initial sand-pack permeability. Ideally, the retained permeability should equal one if there is no formation damage. However, due to the fines migration and screen itself, the retained permeability is usually less than one. Hodge et al. (2002) recommended using 50% as the retained permeability threshold value. In other words, if the retained permeability value falls below 50%, the flow performance is considered unacceptable. They also normalized the sand production with the surface area of the screen and proposed using 0.12 lb/ft^2 as the sand production threshold.

Guo (2018) modified Mahmoudi's testing facility and investigated the impact of stress conditions on the performance of the SL. She used the tri-axial pre-packed SRT facility with a multi-slot coupon in the study. Also, the testing fluid was brine only, and retained permeability was used as

the flow performance indicator. She found that the stress could help form a stable sand bridge and prevent sand production, resulting in a wider slot size design.

Table 2-1 summarized the literature work regarding the sand control testing in assessing the performance of the stand-alone screens.

Table 2.1 Review of Existing Work on Sand Control Testing

Author	Year	Experiment Design						Fluids and rates		
		SCD type	Core Diameter cm	Core Length, cm	Number of phases	Constant Drawdown or rate	Stress applied, psi	pH	Salinity, ppm	Equivalent SAGD flow rate, bbl/d
Markestad et al.	1996	WWS	19.05	57.15	One: Brine	Constant rate	None	N/M	Seawater: 35,000-40,000	N/M
Tiffin	1998	GP	2.54-3.81	5.08	One: Brine	Applied pressure surges at 50 psi increments reaching 1000 psi	Axial: N/M Confining: N/M	N/M	N/M	First phase: 36-832 N/A
Hodge	2002	GP	1.5748	1.27	One: Oil	Constant drawdown 200 psi	Confining increases in 200 psi increments	N/A	N/A	N/M
Ballard and Beare	2003	PS	N/M	N/M	One: Methanol	Constant rate	Axial 10	N/A	N/A	88,000
Williams et al.	2006	GP PS ES	N/M	N/M	One: Brine	Constant rate	None	N/M	2,000	100cc/hr
Constien and Skidmore	2006	WWS PS	Variable	Variable	One: Oil	Constant drawdown 200 psi	None	N/A	N/A	Variable
Bennion et al.	2007	SL-SC SL-RT	5	20	Three: Brine, Oil, Nitrogen	Constant rate	Axial: 500	N/M	N/M	Oil: 1141-4565 Water: 2282-9130
Bennion et al.	2009	SL-SC SL-RT	7	20	Three: Brine, Oil, Nitrogen	Constant rate	Up to 5,000 psi	Varied	N/M	Steam:944-2,831 Water: 1,510-6,038 Oil: 755-3,019

Chanpura et al.	2011	WWS PS	3.81	N/M	One: Oil	Constant drawdown 200 psi	None	N/A	N/A	Variable
Agunloye, and Utunedi	2014	WWS	N/M	N/M	One: Brine	Constant drawdown	Cyclic Brine test: 700 Constant Drawdown: Variable	N/M	N/M	N/A
Romanova et al.	2014	WWS SL-SC SL-RT	6.36	N/M	Three: Brine, Oil, Nitrogen	Constant rate	N/M	N/M	1,000	Steam:944-2,831 Water: 1,510-6,038 Oil: 755-3,019

		Experiment Design						Fluids and rates		
Author	Year	SCD type	Core Diameter cm	Core Length, cm	Number of phases	Constant Drawdown or rate	Stress applied, psi	pH	Salinity, ppm	Equivalent SAGD flow rate, bbl/d
Devere-Bennett	2015	WWS SL-RT SL-SC	5	20	3	Constant rate	Axial 500	Used formation water	Used formation water Salinity: N/M	WWS_Water: 515-6,871 WWS_Oil: 172-3,436 SL_Oil: 288-4,565 SL_Water: 685-9,130
O'Hara	2015	PPS WWS SL PS	4.42	1.3	One: oil	Constant drawdown 200 psi	None	N/M	N/A	Oil: 540
O'Hara	2015	SL-RT WWS PS	6.35	20	Three: Brine, Oil, Nitrogen	Constant rate	Axial: 500	N/M	1,000	WWS_Water: 1718-6871 WWS_Oil: 859-3436 SL_Oil: 1141-4565 SL_Water: 2283-9130
Mahmoudi et al.	2016	SL-Seamed	17	34.29	One: Brine	Constant rate	Axial: 2	6.8,7.9,8.8	0-7,000-14,000	800-40,000
Anderson	2017	WWS SL-RT PPS	30	100	Two: Oil & Brine	Constant rate	Axial: 35 psi	6-8	1,000	Oil: 1,490-11,921 Water: 4,470-13,411

2.5.4.3 Retained Permeability Characterization under Multi-phase Testing Conditions

Although the retained permeability is a quantitative way to characterize the flow performance as it presents the formation damage directly by describing the permeability reduction, it has only been used in the single-phase testing condition.

Wang et al. (2020b) proposed a methodology to obtain the retained permeability under the multi-phase testing condition. In this methodology, first, the relative permeability data of the sand-pack samples are measured by the Penn State steady-state method (Honarpour and Mahmood, 1998). The Penn State steady-state method is employed in the relative permeability determination because

(1) the Penn State apparatus has similar characteristics with the pre-packed SRT facility, (2) capillary end effects can be avoided in both apparatuses, and (3) low fluid flow rates can be applied to prevent core damage (Firoozabadi and Aziz, 1986; Rose, 1987). Figure 2.18 shows the schematic of the Penn State experimental setup in measuring the relative permeability of core samples. Second, the saturation data associated with the relative permeability data are obtained by the external method. The external technique relies on the mass balance concept. The mass difference between inlet and outlet is the mass accumulated in the sand-pack, which yields the average saturation (Honarpour and Mahmood, 1998). Finally, the measured relative permeability data are coupled with pressure differential readings recorded during the pre-packed SRT to calculate the retained permeability using the partial Darcy's equation. Notably, in Wang et al. (2020b)'s work, the saturation history in the relative permeability measurement was kept the same as the one in the pre-packed SRT testing to avoid the capillary hysteresis effect.

Montero Pallares et al. (2020) conducted a multi-phase testing study assessing the performance of the WWS. They applied such methodology and successfully obtained the retained permeability at the residual oil saturation condition in their work. In such a way, they quantitatively analyzed the flow performance of the WWS by describing the permeability reduction directly.
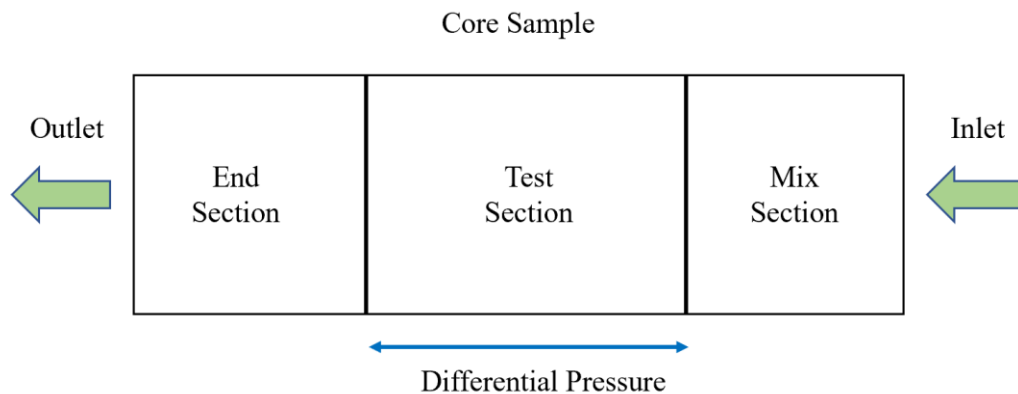
Figure 2. 18 Schematic of Penn State Relative Permeability Measurement Facility

2.5.4.4 Summary of Existing Design Criteria of Stand-alone Screens for SAGD Production Wells
This section summarizes the current design criteria for all three stand-alone screens in the SAGD operations.

Slotted Liner

(1) Coberly (1937): two times D_{10} of the formation PSD (2 D_{10}).

(2) Fermaniuk (2013) proposed an ad-hoc criterion: The safe slot size window should be between 2 times D_{70} and 3.5 times D_{50} (2 D_{70} < Slot Size < 3.5 D_{50}).

(3) Mahmoudi (2016) presented graphical design criteria for two specific formation sands in the McMurray Formation.

(4) Wang et al. (2020a) presented graphical design criteria for one formation sands in the McMurray Formation.

Wire-wrapped Screen

(1) Coberly (1937): two times D_{10} of the formation PSD.

(2) Suman (1985): D_{10} of the formation PSD.

(3) Gillespie et al. (2000): smaller than two times D_{50} when the formation sand is uniform.

(4) Weatherford Criteria: D_{25} of formation sand (D_{25}).

(5) Industrial Rule-of-thumb Criteria: 0.004" smaller than the equivalent slot size of the SL.

Punched Screen

As far as the author's knowledge, there is no literature work regarding the design criteria of the PS for SAGD wells, perhaps due to the recent application of the PS in SAGD operations. Thus, the only available criteria would be Coberly's criteria.

2.6 Inflow Performance of Stand-alone Screens

Although the experimental sand control testing has been generally accepted and used to assess the performance of sand control devices, the formation damage formed by the flow convergence is not fully described and understood as the experimentally physical model only yields an overall formation damage. Several researchers have attempted to build numerical models using computational fluid dynamics (CFD) to understand the fluid dynamics and pressure drop in the near-screen zone (Kaiser et al., 2002). Sivagnanam et al. (2017) built a CFD model on understanding the fluid dynamics around the SL under the steam break-through condition in SAGD. In their model, a full-scale liner was used, and the injection fluid was steam. Mahmoudi et al. (2017) created a CFD model to assess the inflow performance of the SL coupon. The geometry of the numerical model was generated based on the experimental setup (pre-packed SRT). They compared the pressure drop in the near-screen zone with the one from the testing. Velayati et al.

(2018, 2019) analyzed the impact of slot density on the flow convergence magnitude by using a CFD model. They found that under low flow rates conditions, the flow convergence effect was negligible.

Previous numerical models focus on the inflow performance of the SL only. No model has been done to assess the performance of the WWS and PS. Also, there is no study combining experimental work and numerical work characterizing the formation damage in the near-screen zone.

2.7 Summary

This chapter, first, provided a detailed overview of the SAGD operations and related sand production issues. Different sand control techniques were presented. The mechanism of each sand control methods and its pros and cons were also described. Due to the robust mechanical property, easy implementation, and economy, stand-alone screens are commonly used in the SAGD production wells.

Next, different types of sand control testing facilities were introduced to assess the sanding and flow performance of the stand-alone screens. Pre-packed SRT is the most common one used for SAGD purposes as it can emulate the collapsed wellbore condition.

Subsequently, the design criteria of the stand-alone screen were discussed. The safe aperture window aims to provide a good sanding performance and a desirable flow performance.

Other than the experimentally physical model, the numerical model using CFD was also describe in assessing the formation damage in the screen vicinity.

Chapter 3: Experimental Set-up, Design, and Procedure

3.1 Introduction

A large-scale pre-packed SRT facility is used in this study to assess the performance of stand-alone screens. Screen coupons are used in this facility. This facility allows including necessary influential factors into the performance assessment, such as aperture size, slot density, fluid property, phase change, and flow rate. The experimental procedure is designed based on SAGD operational conditions.

The following sections provide the details regarding the testing facility, testing matrix, testing design, and procedures.

3.2 Experimental Set-up

Figure 3.1 shows the schematic view of the larger-scale pre-packed SRT facility, and Figure 3.2 presents the laboratory view of the experimental set-up. This facility consists of five major components, including (1) fluid injection units, (2) data acquisition system, (3) SRT cell and accessories, (4) sand-trap and fines measurements, and (5) back-pressure column.
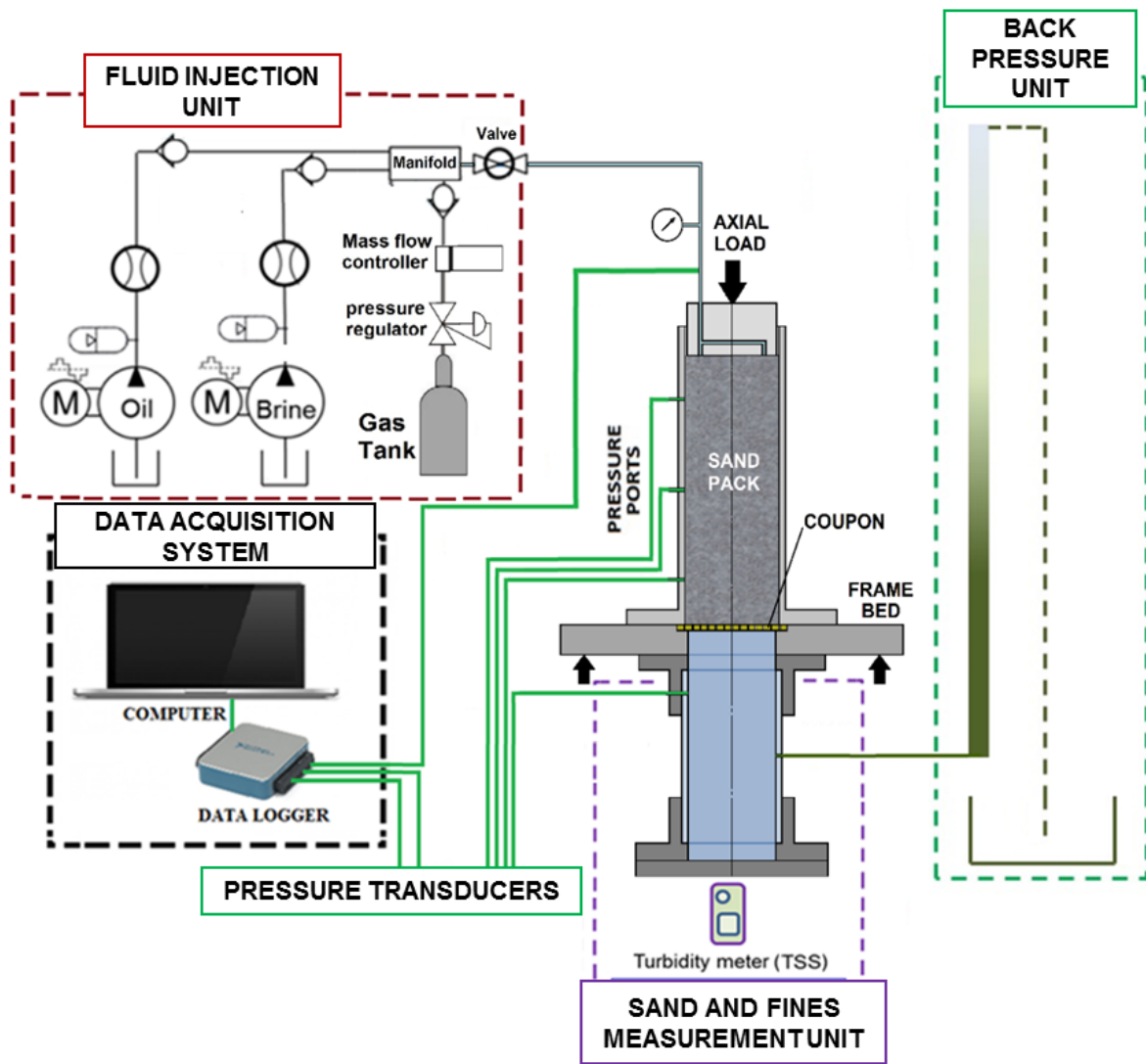
Figure 3. 1 Schematic of the experimental setup
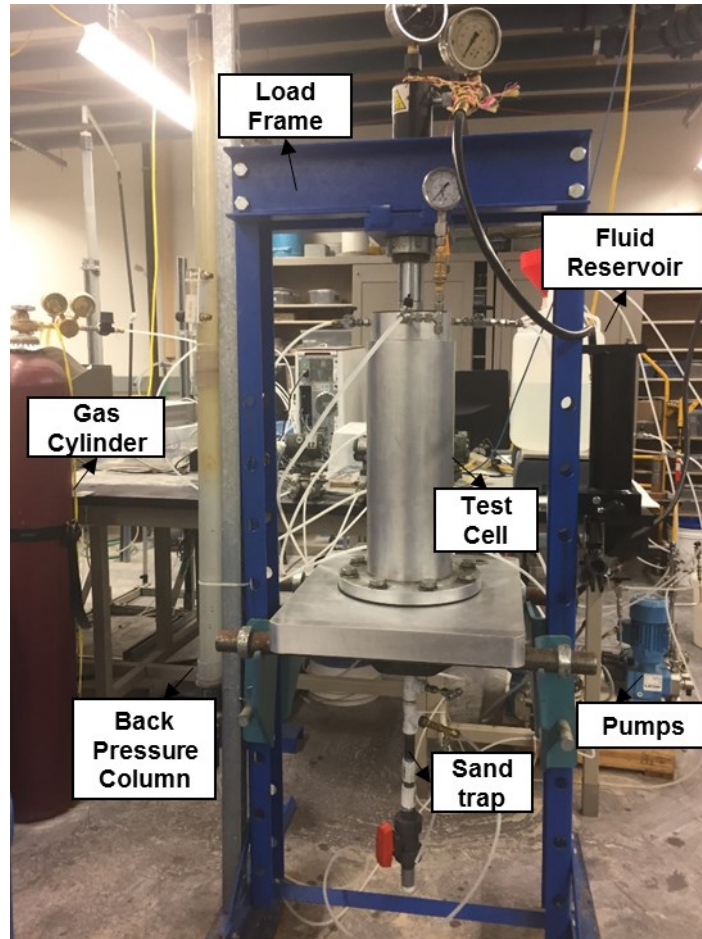
Figure 3. 2 Laboratory view of the testing facility

3.2.1 Fluid Injection Units

Two hydraulically-actuated diaphragm triplex metering pumps (LEWA ecodos® ESC 0006-13) are used for the brine and oil injection. Each pump can deliver a flow rate of 18 litres per hour at 50 psi. The pumps are connected to a variable frequency drive to control the flow rate output. The triplex design helps to damp the pressure pulse during the injection. The ramp-up rate of the pumps is 1000 cc/hr. Two barrels with 40 litres capacity are used as the brine and oil reservoirs. Two weight balances (ULINE Deluxe Counting Scale H-5822, ±1g accuracy) are used to measure the weight loss of the two reservoirs. The weight loss is converted to the injection flow rates.

The nitrogen cylinder achieves gas injection. The nitrogen cylinder fills with higher pressure nitrogen. A pressure regulator and a gas rotameter are connected to the gas cylinder to control the gas injection rate. The gas rotameter is manufactured by OMEGA with a 3% full-scale accuracy.

3.2.2 Data Acquisition System

Pressure transducers (DPharp EJX110A) manufactured by Yokogawa are used to measure the pressure differential. The pressure transducer range is 0-15 psi, and the accuracy is $\pm$ 0.00375 psi. A data acquisition system (National Instruments Data Acquisition System Model USB-6002) is connected to the pressure transducers to record the real-time pressure differential values during the tests.

3.2.3 SRT Cell and Accessories

The SRT cell is a hollow cylinder made of aluminum, which can stand up to 200 psi bursting pressure at room temperature. The cell height is 18.5 inches, and the inner diameter is 6.75 inches. There are three ports along the wall of the cell. These ports are connected to the pressure transducers to record the pressure differential during the tests. The ports locate 2 inches, 7 inches, and12 inches from the bottom of the cell. Figure 3.3 schematically shows the locations of the ports along with the cell. The cell sits on a thick metal plate. There is a hole in the center of the metal plate designed for holding the screen coupons. The Viton gasket is used to provide a good seal between the SRT cell and the base plate.

The sand-pack sample is held by this SRT cell. After preparing the sand-pack sample, a top platen is placed on top. The top platen has two functions: (1) allow multi-phase fluids injection, and (2) transmit stress from the loading frame to the sand pack. There are three flowlines connected to the platen for the brine, oil, and gas injection. The loading frame can apply a force output of up to 8 metric tons. The hydraulic oil inside a hand-pump generates the loads. The pressure gauge is connected to the hydraulic system to control the load output.
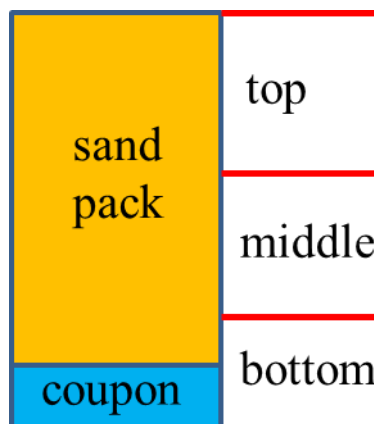
Figure 3. 3 Location of the ports along with the SRT cell

3.2.4 Sand-trap and Fines Measurements

A sand-trap is installed below the screen coupon to collect the produced sand particles. The sand trap consists of a cone, a channeling pipe, and a removable sand collector. The produced sand falls into the collector due to the gravity effect. The sand collector is connected to the channeling pipe with a ball valve. When collecting the produced sand, the ball valve is closed first. Then, the sand collector is removed from the sand trap. Such design allows measuring the amount of sand production for each flow stage. The amount of the produced sand is measured by a weight scale (American Weigh ZEO-50). The accuracy of the weight scale is 0.001grams.

Also, there is a port on the wall of the cone of the sand-trap. This port is connected to a metering valve used to collect fluid samples for the fines measurements. The fines concentration of the produced liquid is obtained by measuring the turbidity of the fluid samples. A turbidimeter (HACH 2100P) with 2% full-scale accuracy is used to measure the liquid samples' turbidity.

3.2.5 Back-pressure Unit

A back-pressure column provides the back-pressure in the tests. The back-pressure column is 7 feet in height, giving around three psi back-pressure. Also, the back-pressure column is used for saturating the sand-pack sample.

3.2.5 Screen Coupons

The pre-packed SRT facility uses a screen coupon in the testing. The screen coupon is a flat coupon, which is directly cut from an actual screen liner. Figure 3.4 shows how the slotted liner coupon is obtained from the actual slotted liner.

In this thesis, three different screen coupons are used in the experimental study, including slotted liner coupon, wire-wrapped screen coupon, and punched screen coupon. The slot configuration of the slotted liner coupon is seamed. Figures 3.5 to 3.7 present the three different screen coupons and their design parameters.
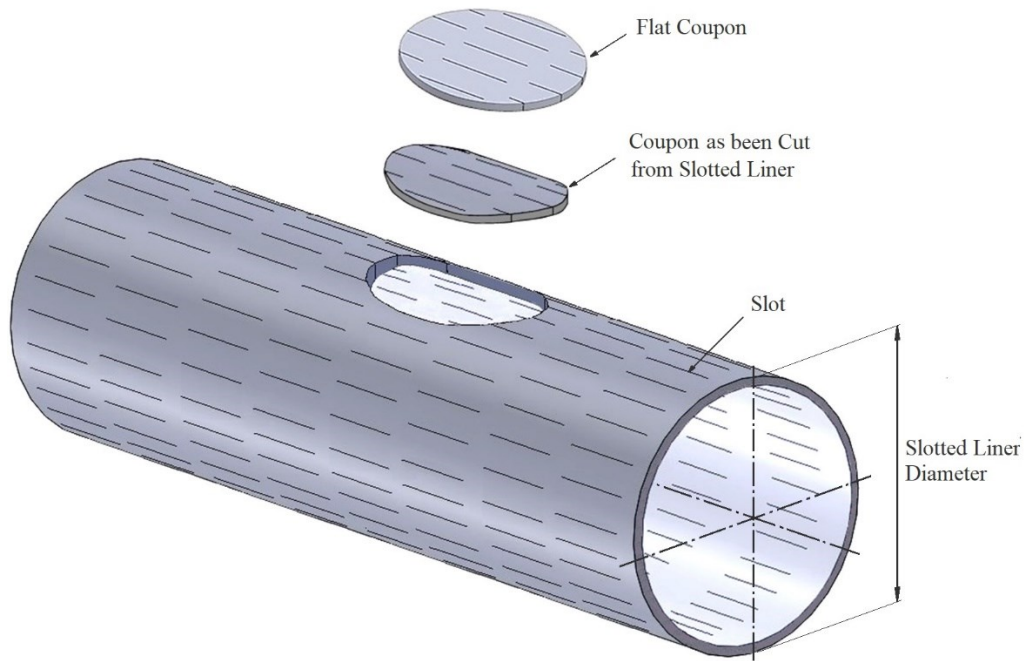
Figure 3. 4 Schematic of screen coupon creation
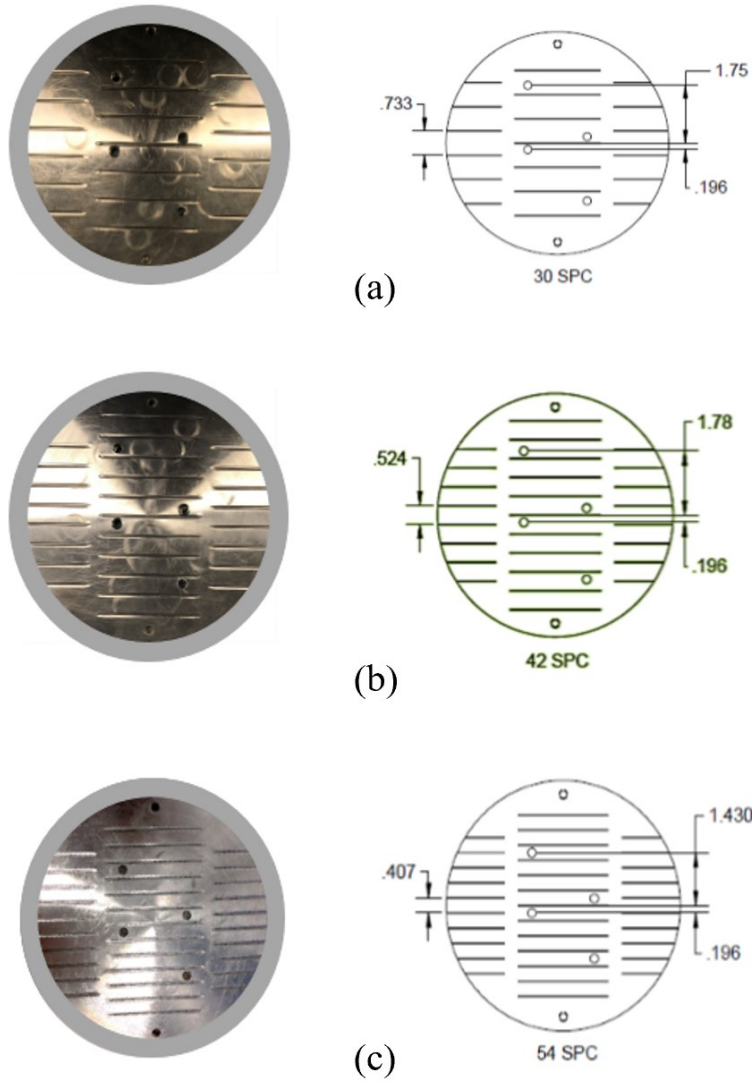
Figure 3. 5 Slotted liner coupons and their design parameters, (a) SPC 30, (b) SPC 42, and (c) SPC 54
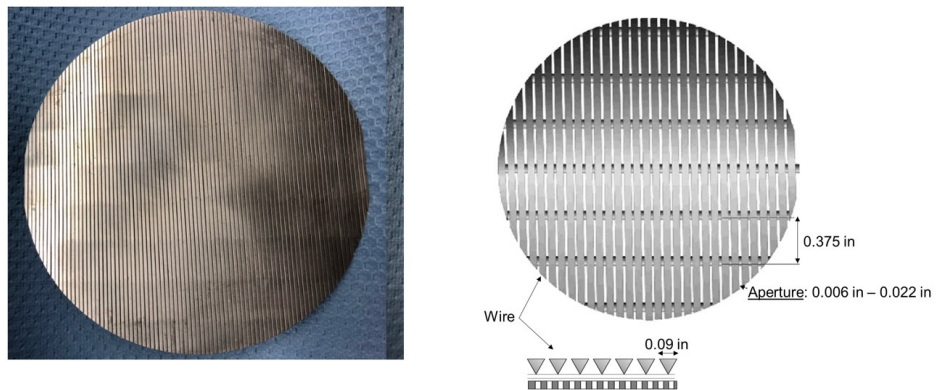
Figure 3. 6 The wire-wrapped screen and its design parameters
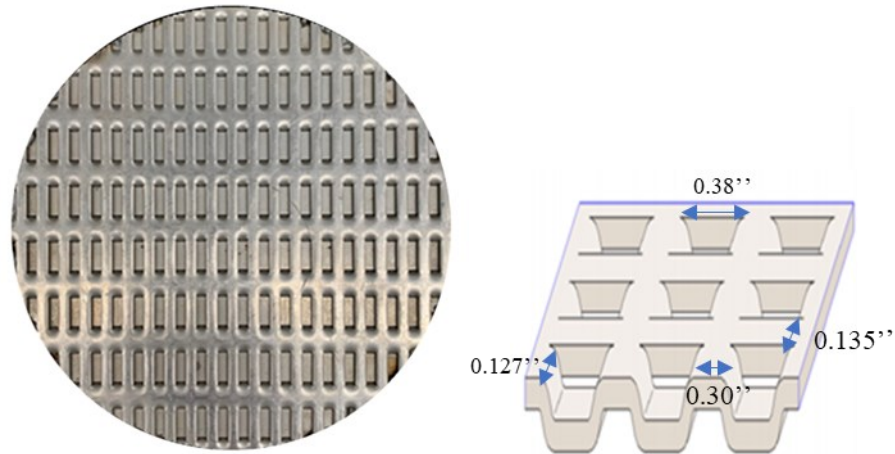
Figure 3. 7 Punched screen and its design parameters

3.3 Testing Procedure

This section introduces the testing procedure details, including sample preparation, SRT cell assembly, sand-pack packing, flow testing, and post-mortem testing.

3.3.1 Fluid Sample Preparation

For the brine preparation, 40 grams of sodium chloride (NaCl) is added to one hundred liters of de-ionized water to achieve a salinity of 400 ppm. Then, the brine is mixed uniformly by a mechanical mixer. It has been shown in the previous section that salinity plays a critical role in the fines migration process. A 400-ppm salinity of NaCl is the minimum values reported in the SAGD produced water, which can create a worst-case scenario of the fines migration (Minnich et al., 2013).

Next, the pH of the brine sample is adjusted to 7.9 by adding pH chemical boosters. Sodium carbonate (Na_2CO_3) and sodium bisulfate ($NaHSO_4$) are used to increase and decrease pH.

Regarding oil preparation, 50 liters of mineral oil is prepared. The mineral oil has a viscosity of 8 cp at laboratory temperature (20 ℃). The viscosity emulates the actual bitumen viscosity at SAGD downhole condition. It is reported that under the thermal SAGD condition, the bitumen viscosity is reduced to around ten cp.

The pressure of the nitrogen cylinder is checked to ensure a continuous injection of the gas during the test. A minimum requirement of 100 psi is needed for the nitrogen cylinder.

3.3.2 SRT Facility Assembly

The screen coupon is mounted to the coupon holder on the thick metal plate. Then, the SRT cell and sand-trap are installed and fastened by bolts and nuts. Plastic tubes are connected between the transducers and the pressure ports on the SRT cells.

3.3.3 Sand-pack Sample Preparation

Synthetic sand-pack samples are used in the testing, which is obtained by mixing several commercial sands with different PSDs. The use of synthetic sand-pack samples ensures the economy and repeatability of the samples. The synthetic sand-pack samples share similar PSD data with the real formation sands. Also, they have identical mineralogy, mechanical properties, and shape factor compared to the formation sands. Abram and Cain (2014) categorized the PSDs of the McMurray Formation into four main groups, namely, DC-I, DC-II, DC-III, and DC-IV. This thesis employs three dominant PSDs (DC-I, II, and III) in the testing. DC-I is deemed a fine to very fine sand, and DC-II and III are fine and medium-coarse sand, respectively. Table 3.1 shows the details of the PSD characteristics of the three formation sands. Figure 3.8 shows the PSD matching results between the actual formation sands and the synthetic sand-pack samples.

Table 3. 1 PSD Characteristics of the McMurray Formation Sands

Type of sand	D90	D70	D50	D10	% fines	Uniformity Coefficient	Sorting Coefficient
DC-I	25	80	135	232	14.5	5.9	9.3
DC-II	76	118	175	260	7.4	2.7	3.4
DC-III	110	187	215	341	5.4	2.4	3.1

Uniformity Coefficient (UC=D40/D90), Sorting Coefficient (SC=D10/D90)
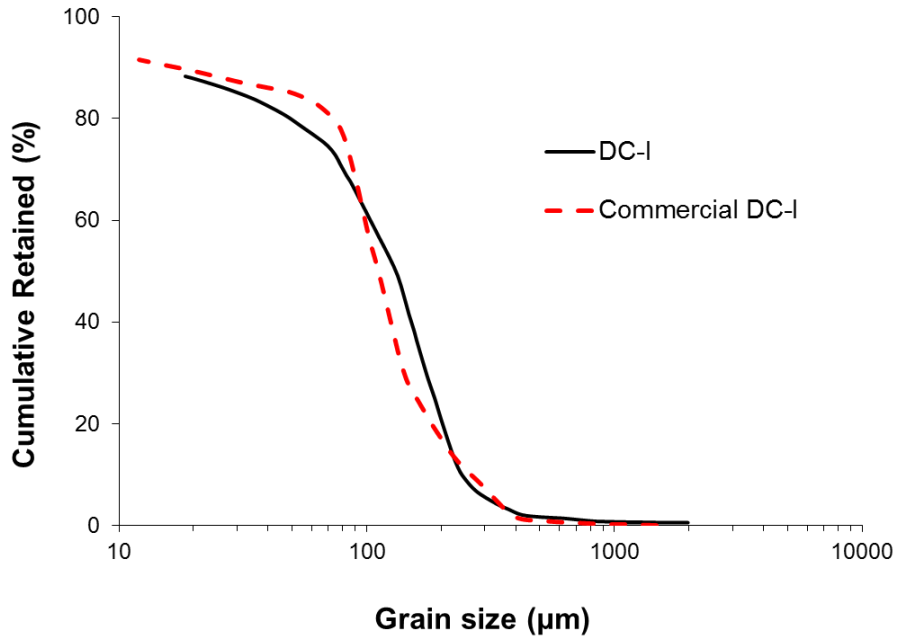
(a)
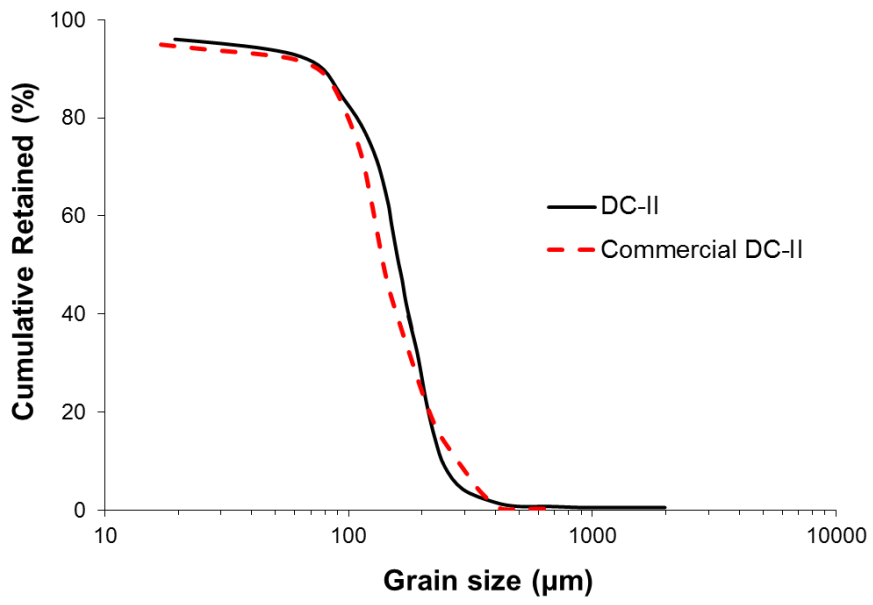
(b)
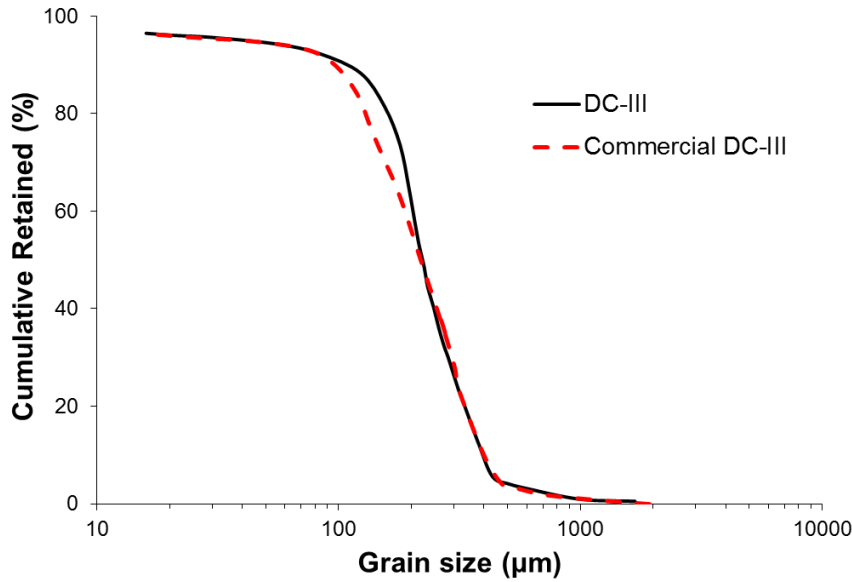
(c)

Figure 3. 8 PSD matching results between the real formation sands and the synthetic sand-pack samples (a) DC-I, (b) DC-II, and (c) DC-III

Twelve kilograms of sand-pack sample is needed for each test. A mixer achieves the mixing of the synthetic sand-pack samples to ensure a uniform mixer. After mixing the sample, ten weight percent (wt%) of brine is added to the sample and mixed again in the mixer. Then, the sand sample is ready to pack. A layer-by-layer moist tamping method is used to pack the sand samples. According to Ladd (1978) and Bradshaw and Baxter (2007), the moist tamping method can ensure uniform sand-pack samples. In the test, each layer contains 1 kilogram of sand. The height of each layer is pre-calculated to have a porosity of around 35%.

3.3.4 Saturation and Fluid Injection

After SRT cell assembly and sand-pack sample preparation, it is ready for the flowing test. Figure 3.9 presents the procedure for the flowing test.

First, the sand-pack sample is saturated by injecting brine from the bottom of the sample towards the top. The saturation rate is 500 cc/hr to avoid damage to the sand-pack sample. During the saturation, 60 psi of axial stress is applied on top of the platen by the loading frame. The platen transmits the load to the sand-pack sample. The axial stress helps to prevent the fluidization of the sand-pack sample during the saturation process. Also, the low amount of axial stress ensures the

worst-case scenario in sand production. The saturation process is considered finishing after the brine flowing from the ports in the platen continuously.

Second, after sample saturation, the absolute permeability of the sand-pack sample is measured by flowing brine from the top of the sample towards the bottom. Also, a flow rate of 1000 cc/hr is used to minimize the fines migration. Permeability data along the sand-pack sample are used to verify the uniformity of the sand-pack. The sand-pack is considered a failure if the permeability variations exceed 5%. After sample saturation and permeability measurement, a drainage process is initiated by injecting oil into the sand-pack sample displacing the brine inside the sample. The oil injection rate is 1250 cc/hr, and the displacement takes around two hours. The oil displacement procedure is to mimic the initial saturation condition of the reservoir (Bennion et al., 2009). After the oil displacement, the sand-pack sample is ready for the multi-phase fluid injection test.

The multi-phase fluid injection test includes three different flow conditions, such as single-phase flow (oil), two-phase flow (brine and oil), and three-phase flow (brine, oil, and nitrogen). Also, different flow rates are employed for each flow condition. The flowing testing design includes several influential factors into the performance assessment of the stand-alone screens, including fluid velocity, fluid-phase transition, and water cut.

Each flow stage needs to reach a steady-state condition before entering the next flow stage. Also, each flow stage must ensure the amount of fluid injection is more than one pore volume. The duration of each flow stage varies depending on the flow rate and flow condition. Figure 3.9 also shows the time duration and pore volume of the injected fluids for each flow stage.
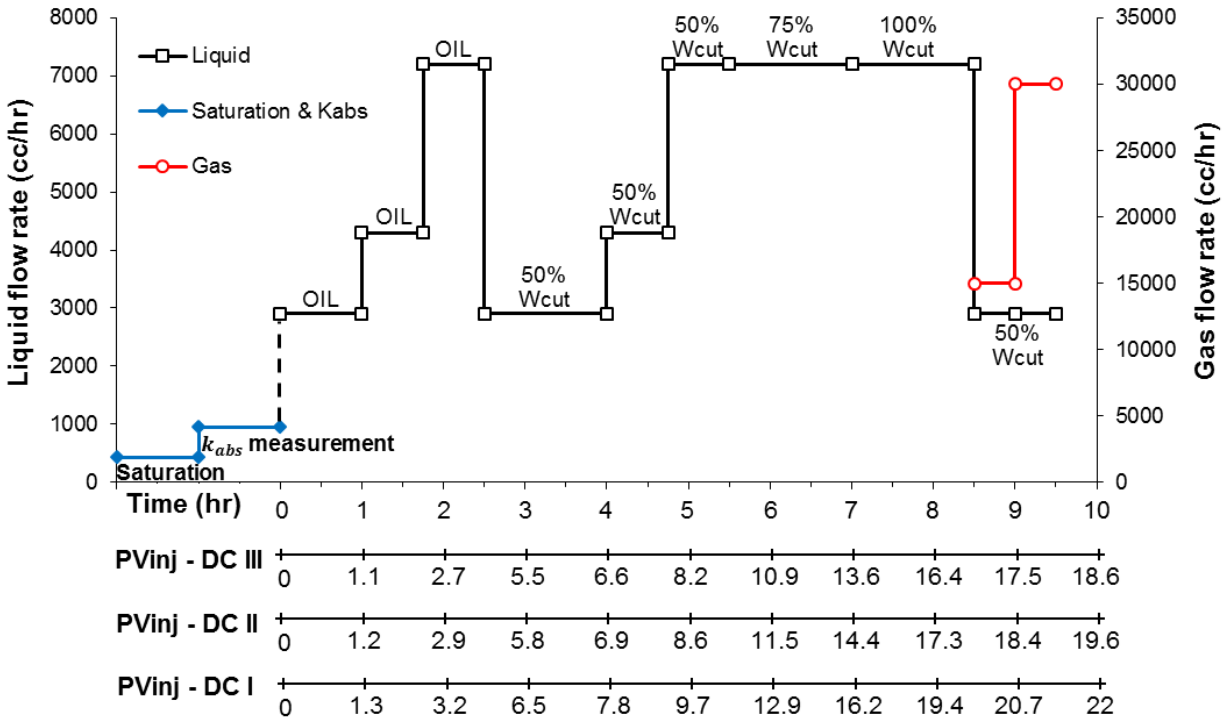
Figure 3. 9 Flowing test design and procedure

The multi-phase flowing test starts with three steps of the single-phase flow of oil, designed to emulate the early stages of the SAGD operation. In the early stage, the bitumen is melted and flow towards the production well. Next, two-phase brine and oil flow follow the single-phase oil flow stages. Five steps with varying water cut and flow rates are established during these two-phase flow stages. This two-phase flow design emulates that water and bitumen are produced together due to the steam condensation over time. AER (2018) reported that the water cut of 90% in the produced liquid. Thus, in the flowing test design, a 100% water cut is employed at the last two-phase flow stage. The saturation condition of this stage is the residual oil saturation condition. The establish of the 100% water cut flow stage also ensures a worst-case scenario in terms of sand production and fines migration (Gabriel and Inamdar, 1983; Mahmoudi, 2017). Finally, another two stages of the three-phase flow condition are designed to emulate the potential steam breakthrough scenario in the SAGD production well. Previous researchers have attempted to implement the three-phase injection to simulate the steam breakthrough phenomenon (Bennion et al., 2009; Romanova et al., 2014; Devere-Beneet 2015; O'Hara, 2015). However, the exact flux rate during the steam breakthrough is not known. Montero et al. (2018) proposed that the high

mobility nature of the steam can restrict the liquid flow rates. Thus, low fluid flow rates are used during the three-phase injection stages.

The flow rates used in the testing procedure are determined based on the SAGD production rates. The typical production rate of SAGD wells is between 800 bbl/day to 7000 bbl/day of liquids production (AER, 2018). In the flow rate design, an average value of 4000 bbl/day is used. Also, a typical stand-alone screen used in SAGD is 600 meters long and 7 inches in diameter. Thus, the liquid production rate normalized by the surface area of the screen liner is around 7400 cc/hr/ft^2. The area of the screen coupon is 0.196 ft^2. Thus, the basic flow rate scale-down by the coupon area is 1450 cc/hr. However, this basic flow rate does not account for the slots plugging or non-uniform distribution of the fluid. It has been reported that up to 90% of the slots in the SL were plugged due to fines migration, corrosion, scaling, and asphaltene precipitation (Romanova and Ma, 2013). The plugged slots cannot contribute to flow anymore, increasing the effective fluid velocity for the remaining slots. Also, the non-uniform distribution is another factor causing the increase of fluid rate in certain areas. Due to the reservoir heterogeneity and excursion of the wellbore trajectory, a non-uniform flow pattern is expected for the long horizontal SAGD wells. Beshry et al. (2006) and Stone and Bailey (2014) claimed that some parts of the well might experience two times the normal flow rates. Besides, Beshry et al. (2006) proposed that the majority of the flow may enter from the top of the production well due to the gravity and temperature differential effect. Therefore, the final flow rates used in the testing procedure are obtained by applying three different effective flow percentages (50%, 30%, and 20%) to this basic flow rate to account for the increase of flow velocity due to the aperture partially plugging and non-uniform flow distribution along the well.

3.3.5 Post-mortem Test

After running the test, a core sample is taken to investigate the concentration of the fines, along with the sample. The core sample is taken in the center of the sand-pack by using an aluminum pipe. The diameter of the core sample is 2.5 inches. Figure 3.10 shows a picture of the core sample taken from one of the tests. Three representative parts (top, middle, and bottom) in the core sample shown in Figure 3. 10 are used in the following wet sieving analysis to assess the fines migration process. First, in the wet sieving analysis, all three samples are put into an oven and dried for 24 hours at a 140 ℃ temperature. This procedure is to evaporate all the oil or water on the sand grains. After liquid evaporation, the weight of the sand samples is measured (m_1). Next, the samples are

crushed and put into a beaker. Then, one liter of water is added to the beaker and stirred by a mixer to make a sand slurry. Subsequently, the sand slurry samples are washed by water through a sieve with an opening size of 44 microns. The sieve retains all the particles larger than 44 microns and discharges the fines (smaller than 44 microns). Finally, the sands retained on the sieve are dried in the oven again at 100 ℃ for 12 hours. Then, the weight of the dry sample is measured again (m_2). The fines concentration in the core samples is calculated based on the weight difference. Equation (1) shows the calculation for the fines concentration in the core samples.
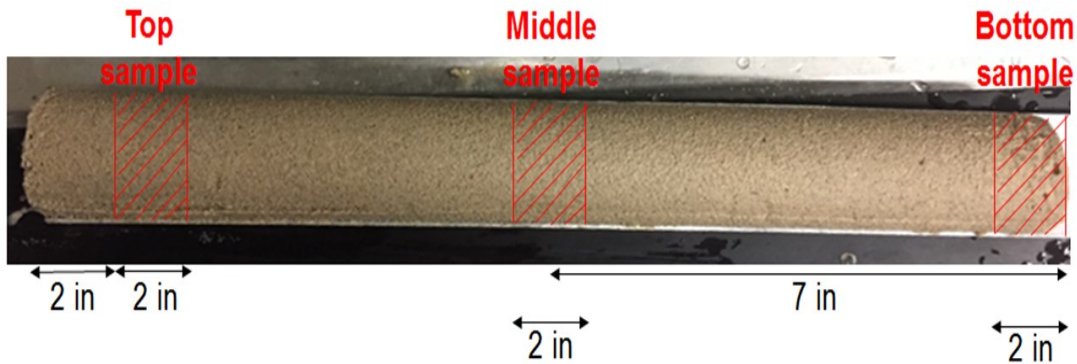
Figure 3. 10 Core sample taken after the test

$$fines\ concentration = \frac{m_1 - m_2}{m_1} \times 100\% \qquad\qquad Eq.(3.1)$$

3.4 Screen Coupon Matrix

Tables 3.2 to 3.4 lists the screen coupons and their characteristics used in the experimental study. Different aperture sizes are employed for each PSD to assess the impact of the aperture size on the screen performance and create the design criteria for stand-alone screens.

Table 3. 2 Screen Coupon Matrix of Slotted Liner

	DC-I			DC-II			DC-III		
SPC	30	42	54	30	42	54	30	42	54
Aperture Size (inches)	0.010	0.010	0.010	0.010	0.010	0.010	0.010	0.010	0.010
	0.014	0.014	0.014	0.014	0.014	0.014	0.014	0.014	0.014
	-	-	0.016	-	-	0.016	-	-	0.016
	0.018	0.018	-	0.018	0.018	-	0.018	0.018	-
	-	-	-	-	-	-	0.022	-	0.022

Table 3. 3 OFA of the Slotted Liner Coupons

Slotted Liner	SPC	OFA (%)	SPC	OFA (%)	SPC	OFA (%)
	30		42		54	
Aperture (inches)	0.010	1.2	0.010	1.7	0.010	2.1
	0.014	1.7	0.014	2.4	0.014	3
	-	-	-	-	0.016	3.5
	0.018	2.2	0.018	3	-	-
	0.022	2.7	-	-	0.022	4.7

Table 3. 4 Screen Coupon Matrix of Wire-wrapped Screen and Punched Screen

PSD	DC-I				DC-II		DC-II	
Screen Coupon	WWS	OFA (%)	PS	OFA (%)	WWS	PS	WWS	PS
Aperture Size (inches)	0.006	6	0.010	3.7	0.006	0.010	0.006	0.010
	0.010	10	0.014	5.2	0.010	0.014	0.010	0.014
	0.014	14	0.019	8	0.014	0.019	0.014	0.019
	0.018	18	-	-	0.018	-	0.018	-
	-	-	-	-	-	-	0.022	-

3.5 Experimental Error and Uncertainty Analysis

The testing measurements and data analyses contain errors due to instrumental errors. This section introduces the error analyses for the testing measurements during the pre-packed SRT, including the amount of sand production, retained permeability calculation, and fines concentration.

In the sand production data analysis, the amount of the produced sand is measured by a weight scale in grams. The accuracy of the scale (δW_b) is ±0.001 grams. Next, the weight in gram is converted to pound (lb). Then, the amount of the produced sand is normalized by the area of the coupon (lb/ft^2). Equation 3.2 shows the error calculation for the reported cumulative sand production (δW_s) after the unit conversion and normalization. c is constant.

$$\delta W_s = c \cdot \delta W_b \qquad\qquad Eq.\,(3.2)$$

The retained permeability (k_{ret}) calculation uses Darcy's Law. The error sources are from the flow rate and pressure differential measurements. The accuracy of the graduate cylinder used in the flow rate measurement is two ccs, and the accuracy of the pressure transducers is 0.00375 psi. The retained permeability calculation relies on two absolute permeability measurements, one at the

initial condition ($k_{abs,initial}$), the other at the final condition ($k_{abs,final}$). Equations 3.3 and 3.4 are used to calculate the errors in the retained permeability results.

$$\delta k_{abs} = |k_{abs}| \cdot \sqrt{\left(\frac{\delta q}{q_w}\right)^2 + \left(\frac{\delta p}{\Delta P}\right)^2} \qquad\qquad Eq.\,(3.3)$$

$$\delta k_{ret} = |k_{ret}| \cdot \sqrt{\left(\frac{\delta k_{abs,initial}}{k_{abs,initial}}\right)^2 + \left(\frac{\delta k_{abs,final}}{k_{abs,final}}\right)^2} \qquad\qquad Eq.\,(3.4)$$

Regarding the error analysis for the concentration of the fines (C_{fine}) in the post-mortem testing, Equation 3.5 is used to obtain the errors and uncertainties. m_{fine} is the weight of fines in the sample and m_{total} is the total weight of the sample.

$$\Delta C_{fine} = \left|\frac{m_{fine}}{m_{total}}\right| \sqrt{\left(\frac{\Delta m_{fine}}{m_{fine}}\right)^2 + \left(\frac{\Delta m_{total}}{m_{total}}\right)^2} \qquad\qquad Eq.\,(3.5)$$

3.6 Assumptions and Limitations

This section lists and summarizes a few assumptions and limitations in the pre-packed SRT experimental study.

(1) The temperature effect is not included in the testing procedure. The pre-packed SRT facility is not able to employ high temperatures during the test. However, in the real SAGD downhole condition, the temperature is around 250 degrees Celsius. The high temperature could lead to bitumen viscosity reduction, rock properties variation, thermal expansion of the formation, and mineralogy metamorphism.

(2) Screen damage due to corrosion and erosion is not emulated during the pre-packed SRT testing. Due to sour gases, such as CO_2 and H_2S and saline water, the screen is prone to corrosion in the reservoir. Also, after the sand erosion for long periods, mechanical integrity may fail.

(3) Limited stress levels can be employed in the pre-packed SRT facility. In the pre-packed SRT, a 60 psi axial stress is applied. However, due to thermal expansion and in-situ stresses, the screen in the downhole may bear higher stress levels. Also, the pre-packed SRT facility

is a uni-axial strain testing facility, which does not independently control the in-situ stress condition. The horizontal stress to the sample is generated as a result of the axial stress.

(4) The flow geometry is linear in the pre-packed SRT facility. However, in the actual SAGD production well, the flow geometry is radial. The effect of the flow geometry on the screen performance is not assessed in this facility.

(5) Testing materials used in the experiments may not be representative. Although mineral oil has the same viscosity as bitumen at downhole conditions, the chemical components and properties are different. Also, in SAGD produced liquid, the water-in-oil emulsion is the dominant fluid type (Noik et al., 2005). While in the laboratory testing, water and oil are two separate phases. The emulsion is not created during the test. Second, the brine used in the testing only contains NaCl. Other chemicals, such as Magnesium (Mg^{2+}), Calcium (Ca^{2+}), Barium (Ba^{2+}), carbonate (CO_3^{2-}), bicarbonate (HCO_3^-), and sulfate (SO_4^{2-}), are not used in the brine. Third, the fine particles used in the sand-pack sample is kaolinite only. Smectite is not included in the sample. However, it is reported that the McMurray Formation contains a certain amount of smectite in the fine particles. The smectite is swelling clay. It swells with the contact of water and can cause pore plugging. The impact of the clay mineralogy is not included in the testing procedure.

3.7 Summary

This chapter introduces the pre-packed SRT testing facility, testing materials, testing procedure and design, and testing matrix. The pre-packed SRT facility utilizes screen coupons in the testing for convenience. The synthetic sand-pack sample is also employed to ensure economy and consistency. The testing procedure is designed to include several key factors into the screen performance assessment, including PSD, aperture size, slot density, fluid velocity, fluid-phase change, and multiphase flow. The incorporation of these influential factors ensures a comprehensive and reliable performance analysis of the stand-alone screens. Post-mortem tests and data analysis techniques are also introduced to analyze the sanding and flow performance of the stand-alone screens.

Chapter 4: Testing Results: Sand Production, Retained Permeability, and Fines Production

4.1 Introduction

The main function of the stand-alone screens is to control the amount of sand production and allow a desirable level of liquid production. Thus, sanding and flow performance are the two major indicators to characterize the performance of the stand-alone screens. The cumulative sand production amount describes the sanding performance, and the retained permeability quantifies the flow performance. Also, the stand-alone screens are designed to allow as much fines production as possible to reduce the formation damage level due to the fines migration and pore plugging. Therefore, the production of the fines is another performance indicator of the stand-alone screens. In this chapter, the testing results in terms of sand production, retained permeability, and fines production for all three stand-alone screens are presented to characterize the screen performance.

4.2 Sand Production

The amount of sand production of each flow stage is captured and measured during the testing procedure. The cumulative sand production is reported in this section for the SL, WWS, and PS. Hodge et al. (2002) proposed two threshold values for sanding performance. The optimal sanding level is considered below 0.12 lb/ft^2, and the maximum acceptable sand production amount is 0.15 lb/ft^2. Hodge et al. (2002) proposed the sanding criteria also aligned with the rule-of-thumb criteria proposed by Chanpura et al. (2011). Chanpura et al. (2011) suggested that the amount of cumulative sand production should be less than 1% of the stand-alone screens' volume over the entire SAGD well life. Considering an 7-inches-diameter screen, 1% of the screen volume corresponds to a normalized cumulative sand production of 0.15 lb/ft^2.

4.2.1 Sand Production Results of the Slotted Liner

Figures 4.1 to 4.3 present the cumulative sand production results of the SL with different slot sizes and slot density for DC-I, II, and III, respectively.

The testing results show that minimal sand production is observed during the single-oil phase flow stages (Stages 1 to 3). Although the oil flow rate reaches the maximum in Stage 3, which exhibits a strong drag force on the sand grains, a limited amount of sand production is measured. This is due to the strong capillary bonding force existing inside the sand-pack at the irreducible water saturation condition. The drag force is not strong enough to overcome the resisting force to cause

sand production. The strong capillary bonding force holds the sand grains together and prevents sand production. However, the amount of sand production increases after the first stage of the two-phase flow (water and oil) due to the reduction of the capillary bonding force. The drag force overcomes the capillary resisting force and causes more sand production.

Further, the rise of fluid velocity and water cut (Stages 5 to 8) causes more sand production due to increased drag force and decreased capillary bonding force. However, for the slot size of 0.010'', there is negligible sand production in stages 1 to 8 in all three PSDs. This is attributed to the strong sand bridges formed on the narrow slot opening. Even though the drag force can overcome the capillary resisting force, it cannot overcome the resisting force created by the sand bridge. Thus, a negligible amount of sand production is found for the slot size of 0.010''.

Another notable finding is substantial sand production is observed after the gas breakthrough (Stage 9 and 10). This phenomenon can be attributed to the increase of the actual velocity of the liquid phases due to the three-phase flow condition. When three fluids are flowing in the porous channel, the actual velocity of each fluid is enhanced compared to the single-phase flow condition. Hence, the rise of the actual velocity exhibits a stronger drag force on the sand particles and causes more sand production.

Other than the rise of the fluid velocity, due to the relative permeability, the three-phase flow condition also exhibits a higher pressure gradient on the sand grains, which facilitates the sand production. Besides, the pore pressure inside the sand-pack sample increases due to the high pressure gradient. Since the total amount of load is fixed, the increase of pore pressure leads to a reduction of the effective stress. The effective stress reduction decreases the friction resisting force between the sand grains and increases sand production. Notably, for larger slot sizes, like 0.018'' and 0.022'', the impact of the gas breakthrough on the sand production is more evident as the sand bridge formed on the larger slot size is weaker than those formed on narrower slot sizes.

The testing results also indicate the slot size plays a dominant role in sand production. The increase of slot size could yield more substantial sand production, with the rest parameters the same. Regarding the impact of slot density, the results show that higher slot density produces more sand production for the same slot size. The SL coupon with higher slot density (e.g., SPC 54) has a higher open-flow-area, which provides more space for sand production. However, the impact of slot density is less critical than the slot size.

Moreover, for the same slot size and slot density, formation sand with coarser PSD, like DC-III, produces less sand production compared to finer PSDs (DC-I and II). This is because the sand bridge formed with larger sand particles is stronger than the one formed with smaller sand grains. For example, the slot size 0.018'' in DC-I reaches the minimum sanding limit on stage 5, while in DC-II and DC-III, the slot size 0.018'' shows excellent sanding performance until the gas breakthrough.
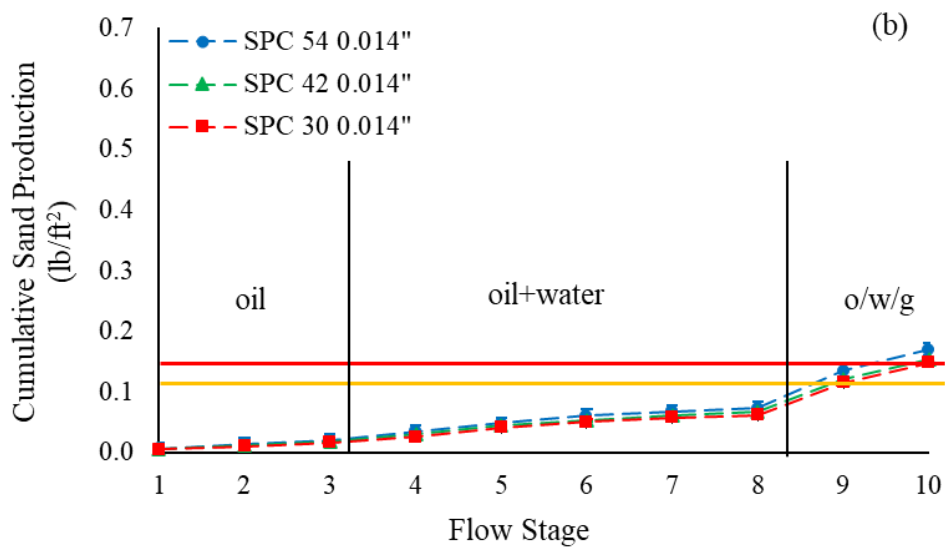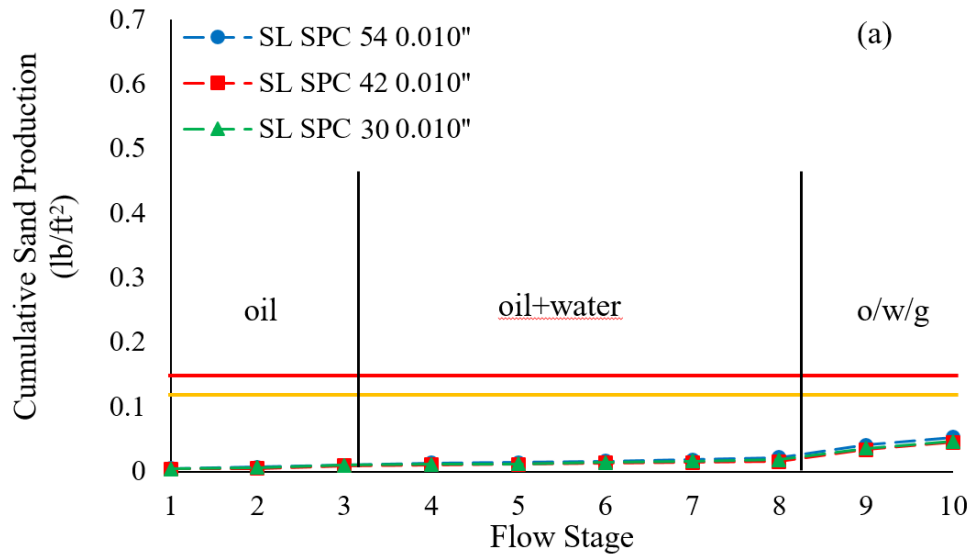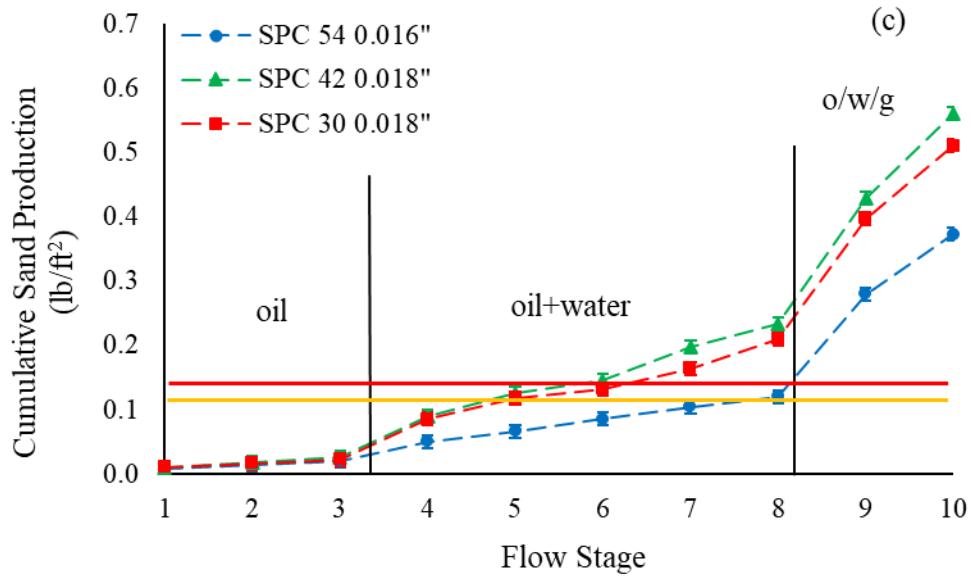
Figure 4. 1 Cumulative sand production results of slotted liner for DC-I, (a) slot size of 0.010'', (b) slot size of 0.014'', and (c) slot size of 0.018'' (0.016'')
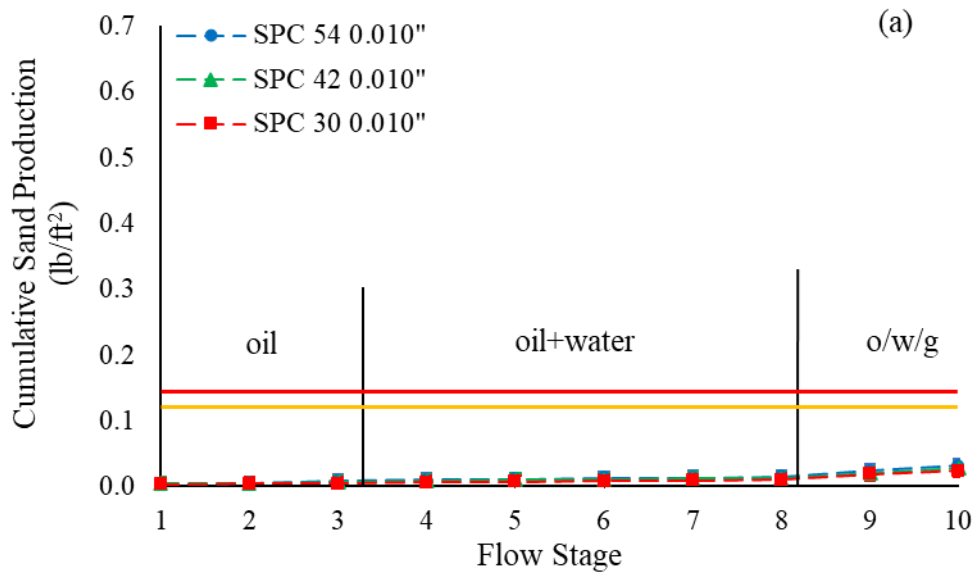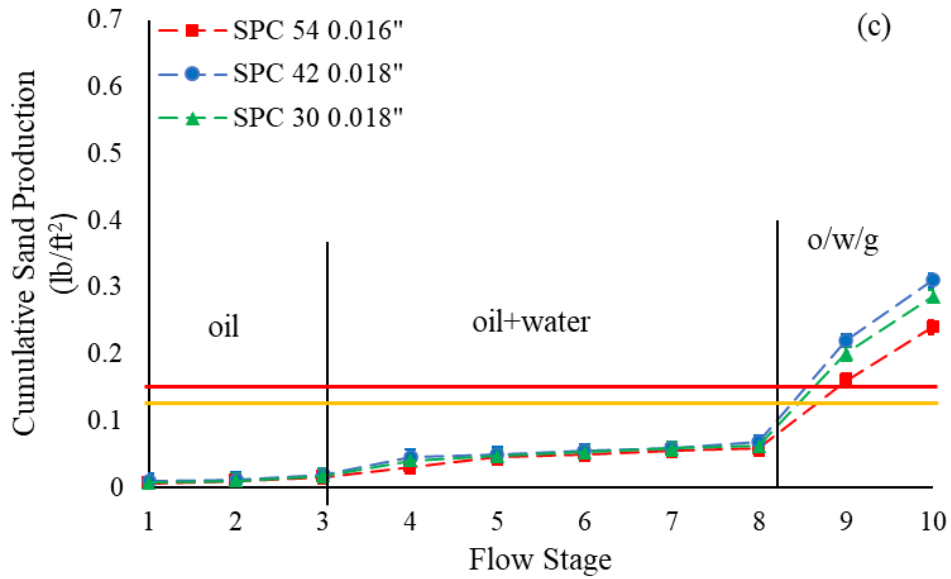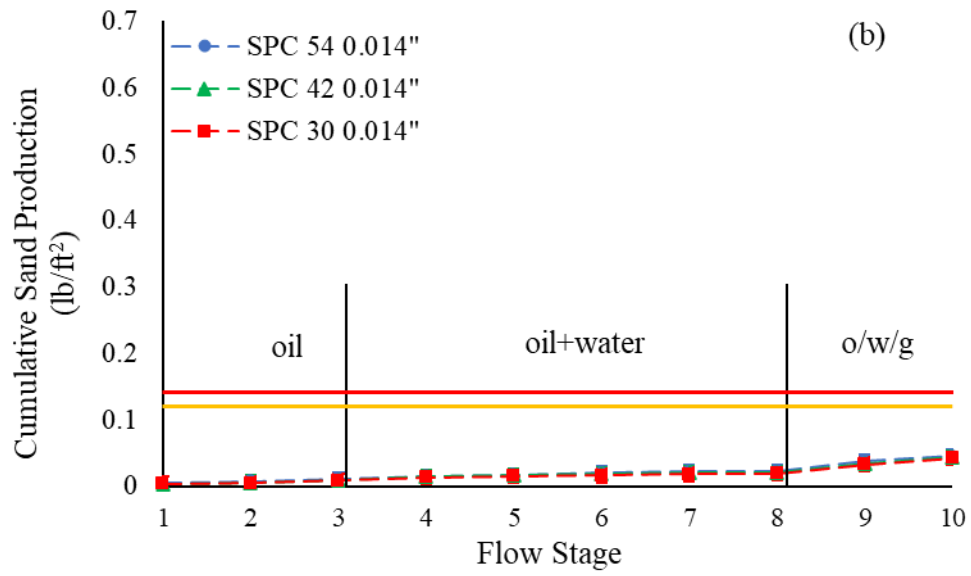
Figure 4. 2 Cumulative sand production results of slotted liner for DC-II, (a) slot size of 0.010'', (b) slot size of 0.014'', and (c) slot size of 0.018'' (0.016'')

58
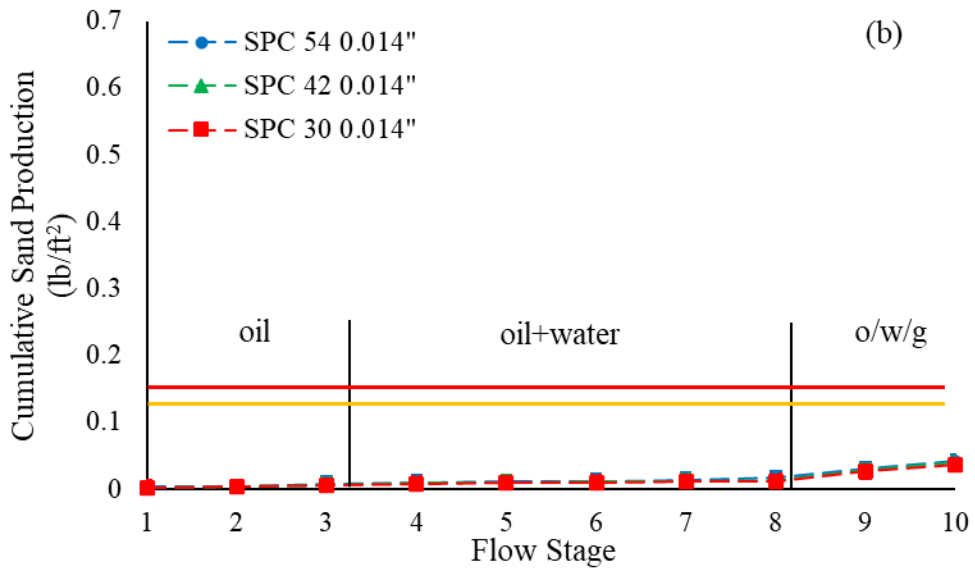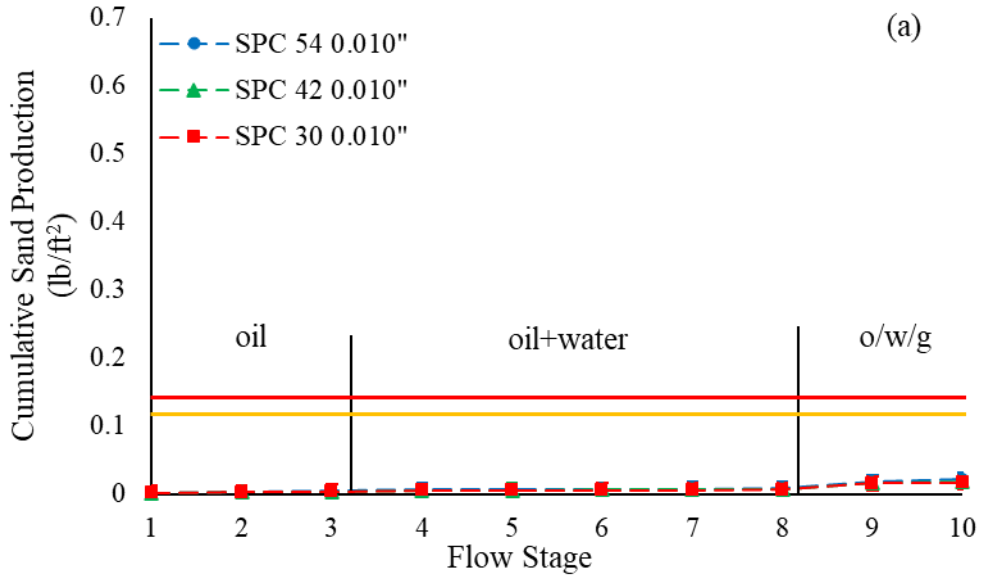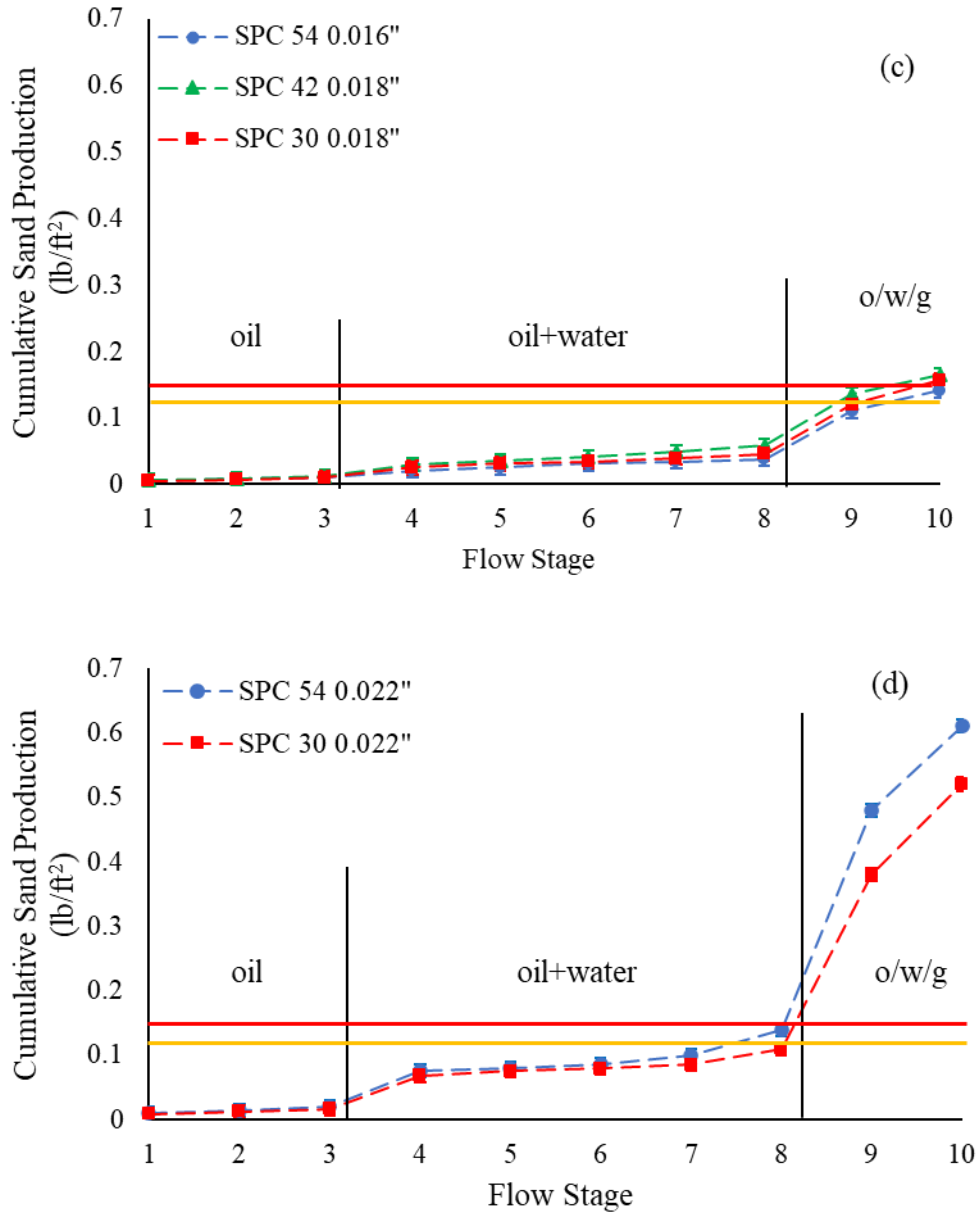
Figure 4. 3 Cumulative sand production results of slotted liner for DC-III, (a) slot size of 0.010'', (b) slot size of 0.014'', (c) slot size of 0.018'' (0.016''), and (d) slot size of 0.022.''

4.2.2 Sand Production Results of the Wire-Wrapped Screen

Figures 4.4 show the cumulative sand production results of the WWS with different aperture sizes for DC-I, II, and III, respectively.

Like the testing results of the SL, the WWS shows negligible sand production during single-phase (oil) flow stages. For the aperture size 0.006'', the initial sanding mode is observed in all three PSDs. No further sand production is obtained after the water breakthrough indicating a stable sand

59

arch. The rest aperture sizes exhibit transient sand production behavior. The amount of sand production increases with increased flow rate and water cut. Moreover, the transient behavior intensity increases with aperture size and a decrease in the grain size.
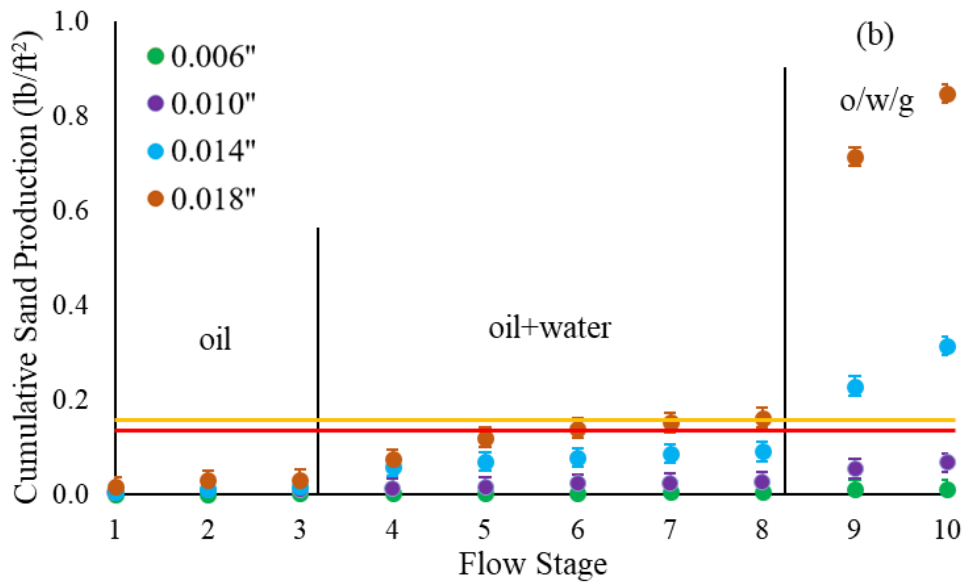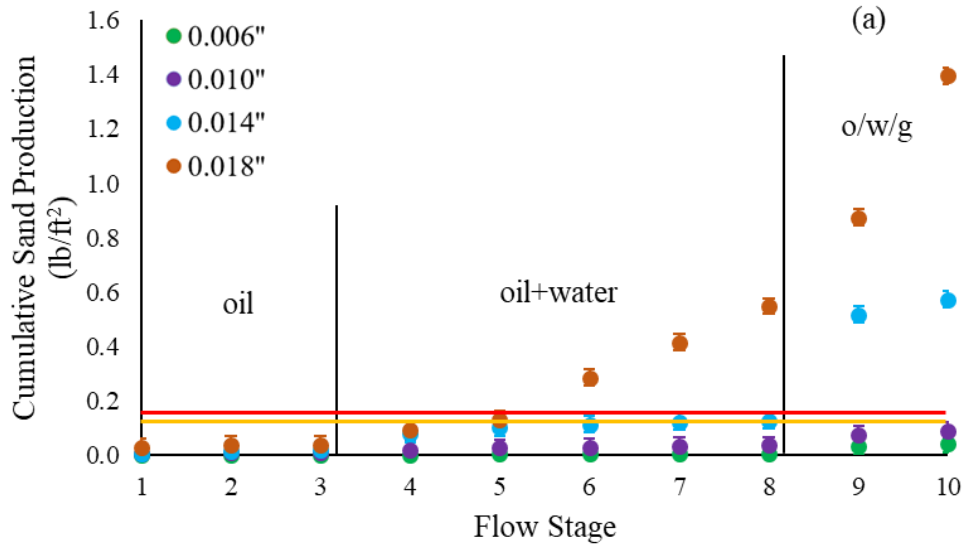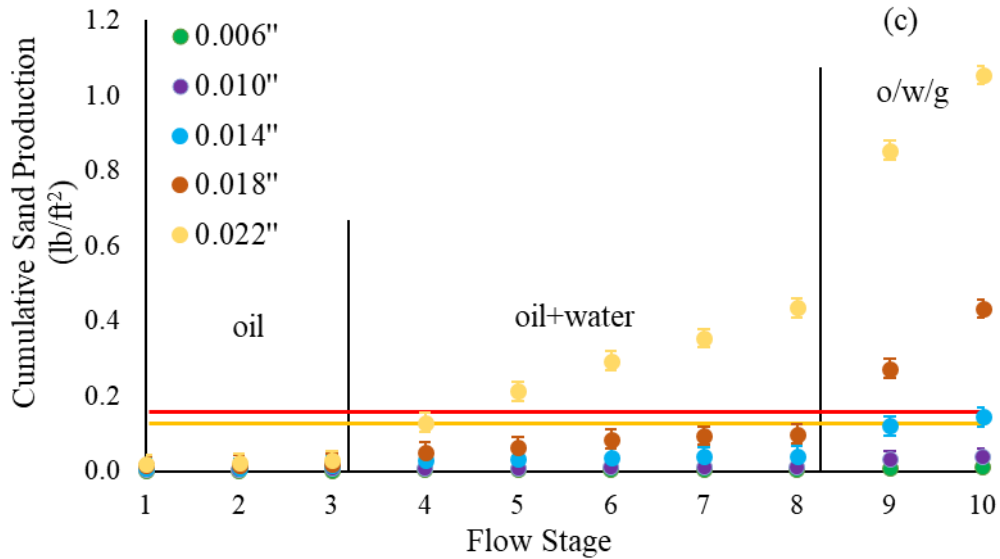
Figure 4. 4 Cumulative sand production results of the wire-wrapped screen (a) DC-I, (b) DC-II, and (c) DC-III

4.2.3 Sand Production Results of the Punched Screen

Figures 4.5 present the cumulative sand production results of the PS with different aperture sizes for DC-I, II, and III, respectively.

The testing results of the PS show a similar trend compared to the SL and WWS, as explained in the above paragraphs. Notably, it is found that for DC-I, the aperture size of 0.019'' could not provide desirable sand control performance. The amount of cumulative sand production exceeds the sanding limit during the liquid flow stage. The aperture size 0.014'' shows good sanding performance during the liquid flow stage. However, the cumulative sand production exceeds the limit (0.15) during the three-phase flow condition. The aperture size of 0.010'' can provide excellent sand retention capability, although the final cumulative sand production is at the margin of the sanding limit (0.12).

For DC-II and III, all aperture sizes (0.010'', 0.014'', and 0.019'') can provide an excellent sanding performance during liquid flow stages (Stages 1-8). However, when it comes to three-phase flow, the PS with 0.019'' aperture size shows less sand retention capability. The cumulative amount of sand production is over the sanding limit (0.15), which means this aperture size could not provide desirable sanding performance during the three-phase flow condition.
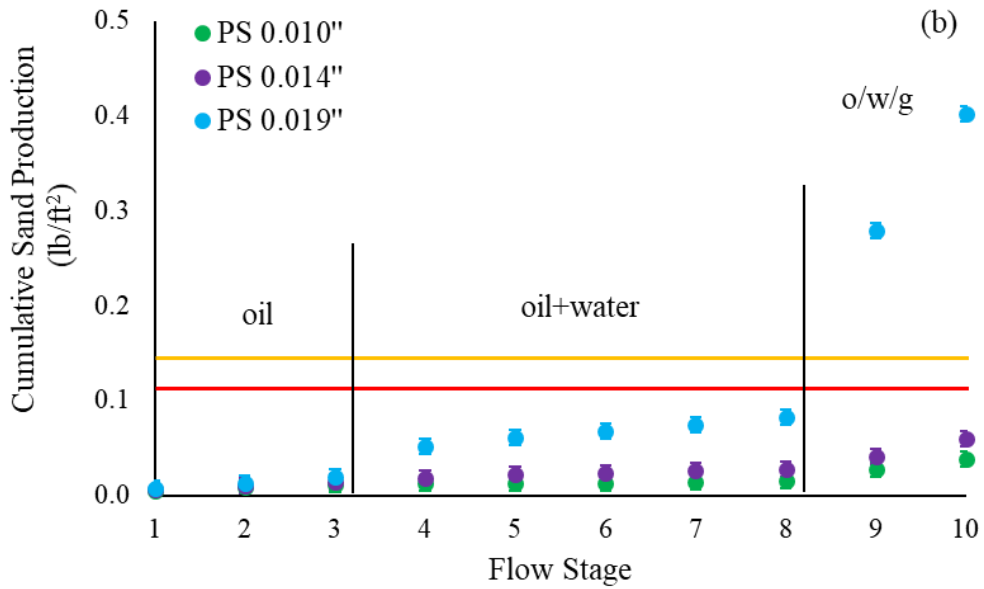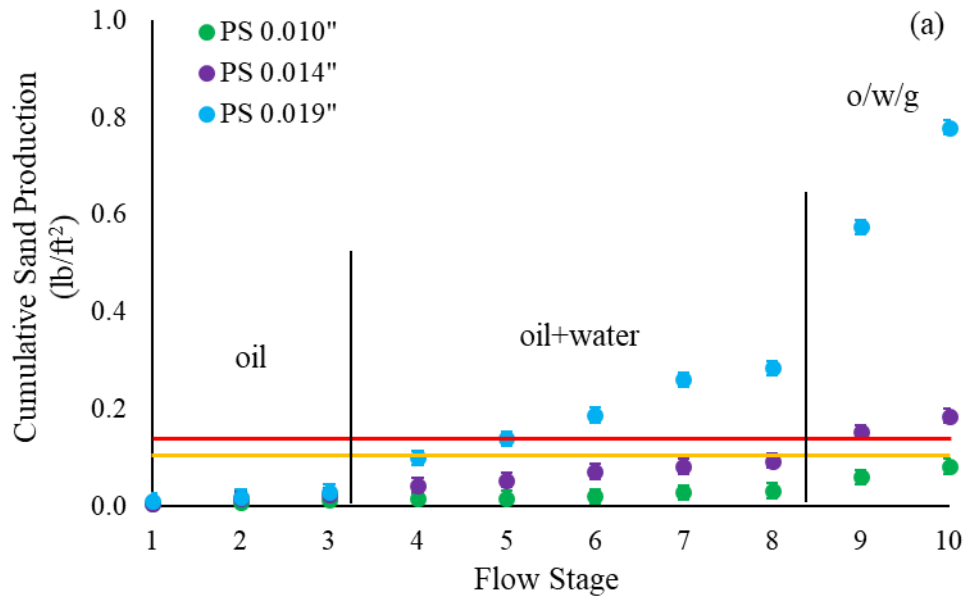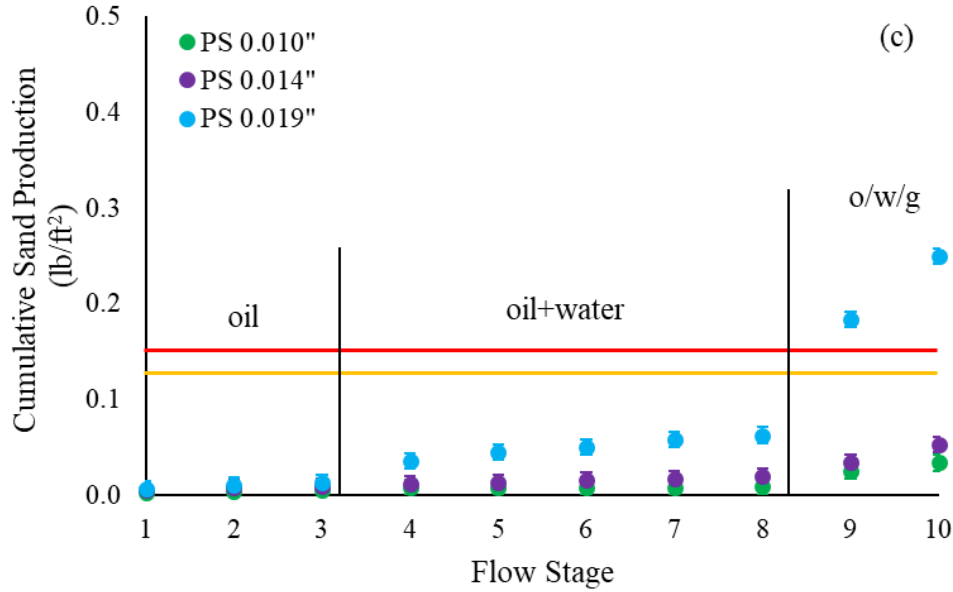
Figure 4. 5 Cumulative sand production results of punched screen (a) DC-I, (b) DC-II, and (c) DC-III

4.3 Retained Permeability

Researchers have widely used retained permeability to characterize the flow performance of stand-alone screens. It is defined as the screen permeability over the initial permeability. The screen permeability includes the near-screen zone plus the screen itself. Ideally, the retained permeability will be equal to one if there is no formation damage. However, due to the fines migration and pore plugging, the retained permeability in the near-screen zone is less than one. The lower the retained permeability value is, the more flow performance is impaired. Figure 4.6 shows the schematic of the three sections of the pressure measurement of the pre-packed SRT. The sand-pack is divided into three sections: the top section, middle section, and bottom section. In the testing, the fine particles migrate from the top of the sand pack towards the screen coupons. In the 2-inches bottom section, the fine particles are captured and plugged in the bottom area, which increases the pressure difference in the 2-inches zone. Equations 4.1 and 4.2 are used to calculate the retained permeability for the single-phase (brine) testing condition, where q_w is the water flow rate, μ_w is the water viscosity, A is the cross-section area of the sand-pack sample, ΔP_b is the pressure difference in the bottom section, and k_b is the screen permeability. The initial permeability of the sand-pack is obtained at the beginning of the testing using a low flow rate to minimize the impact of fines migration.

63

$$k_b = \frac{q_w \cdot \mu_w \cdot L_b}{\Delta P_b \cdot A} \qquad\qquad Eq.\,(4.1)$$

$$k_{ret} = \frac{k_b}{k_{initial}} \qquad\qquad Eq.\,(4.2)$$

Regarding the multi-phase testing condition of the pre-packed SRT in this thesis, the retained permeability is obtained at the 100% WC flow stage (Stage 8). The saturation condition of this stage is the residual oil condition. Equations 4.3 and 4.4 are used to calculate the retained permeability at the residual oil saturation condition.

$$k_{abs,b} = \frac{q_w \cdot \mu_w \cdot L_b}{\Delta P_b \cdot A \cdot k_{rw,@Sor}} \qquad\qquad Eq.\,(4.3)$$

$$k_{ret} = \frac{k_{abs,bottom}}{k_{initial}} \qquad\qquad Eq.\,(4.4)$$

The relative permeability of water for DC-I, II, and III samples are measured using the Penn-state steady-state method. Figure 4.7 shows the testing procedure of the relative permeability measurement. First, the sample is saturated with brine with high salinity (10000ppm) to minimize the fines migration process. Second, oil is injected to displace the water in the sample. Next, the two-phase injection starts with increasing water cut. Last, brine alone is injected to achieve the residual oil saturation condition. The saturation history is kept the same as the pre-packed SRT testing to avoid the capillary hysteresis effect on the relative permeability.
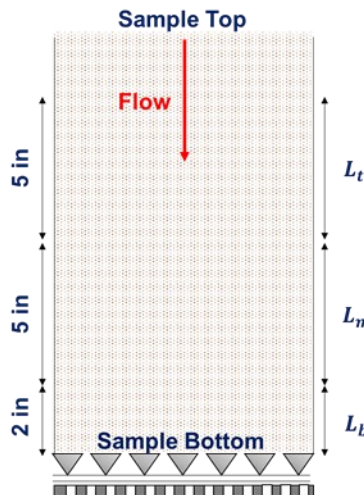
Figure 4. 6 Schematic of pressure measurements sections.
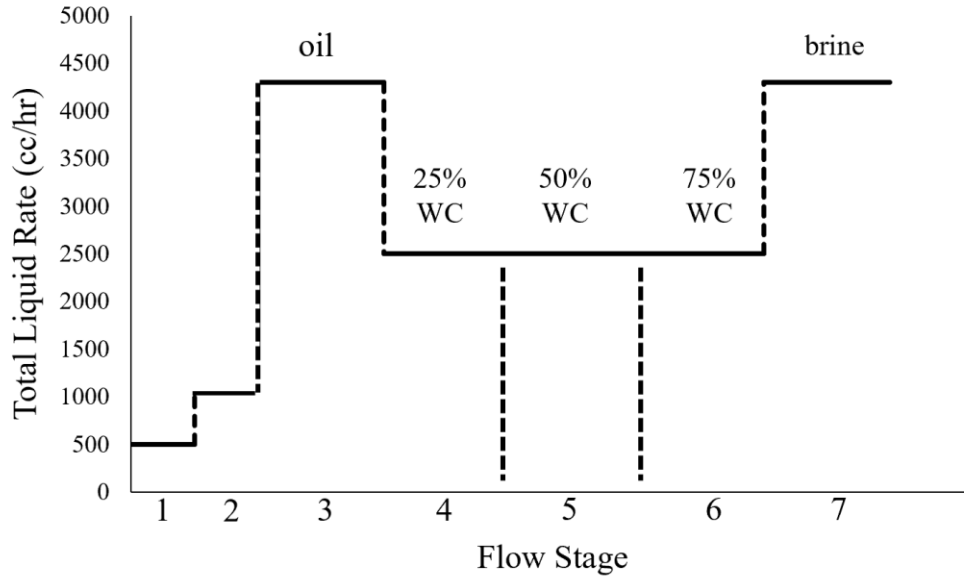
Figure 4. 7 Testing procedure of the relative permeability measurement

Table 4.1 shows the initial permeability and relative permeability of water for DC-I, II, and III samples.

Table 4. 1 Absolute permeability and relative permeability of water at residual oil saturation condition

Sand	k_{abs} (md)	k_{rw} at S_{or}
DC-I	950	0.48
DC-II	1800	0.52
DC-III	2400	0.54

In this thesis, the retained permeability is only obtained at the last two-phase flow stage. After three-phase (brine, oil, and gas) injection, the retained permeability is not assessed as the relative permeability measurement under the three-phase testing condition is complicated. Besides, assessing the flow performance under liquid flow condition represents the actual SAGD condition as the steam breakthrough scenario only occurs at specific locations.

Regarding the flow performance criteria, 70% of the retained permeability is considered an optimal flow performance, and 50% is the minimum limit. If the retained permeability falls below 50%, the flow performance of the stand-alone screens is deemed unacceptable.

4.3.1 Retained Permeability Results of the Slotted Liner

Figure 4.8 presents the retained permeability data of the slotted liner coupons for different PSDs.

Based on the retained permeability results, it is found that the retained permeability increases with the increase of slot size and slot density. This is due to the increase of the OFA, which allows more fine particles production. Thus, fewer fine particles accumulate in the near-screen zone and cause pore plugging. Also, with the increase of slot density, the flow streamline is less converged than the flow regime with a lower slot density. The reduced flow convergence effect also decreases the pressure drop in the near-screen zone, leading to increased retained permeability.

Due to the low OFA characteristics of the SL, it could not provide optimal flow performance in DC-I and II. All the testing results in DC-I and DC-II fall below 70% (Fig 4.8a and 4.8b). Notably, the slot size of 0.010'' could not even reach the minimum flow performance criteria in DC-I. This is due to DC-I is the dirtiest formation type in the McMurray Formation, which contains the highest number of fine particles. Thus, in this scenario, the SL is vulnerable to the formation damage due to the pore plugging. When it comes to DC-II and III, the formations are getting cleaner, and fines concentration is decreasing. Although the SL could not provide an optimal screen performance in DC-II, it can still meet the minimum flow performance requirement. In DC-III, due to the least fines concentration, the SL shows satisfactory flow performance with larger slot sizes, like 0.018'' and 0.022'' (Fig 4.8c).

(a)

(b)
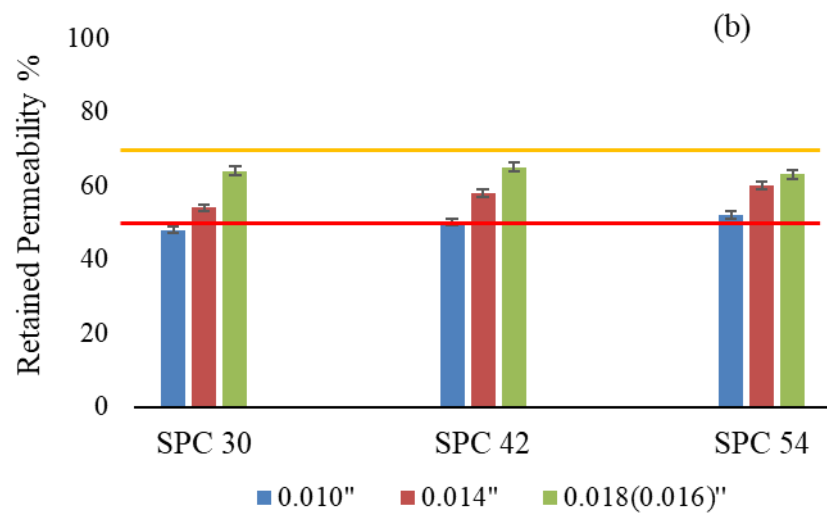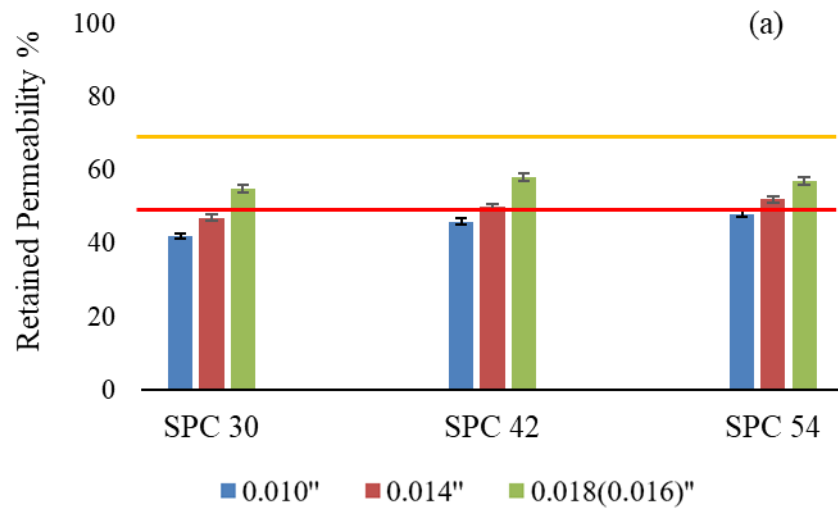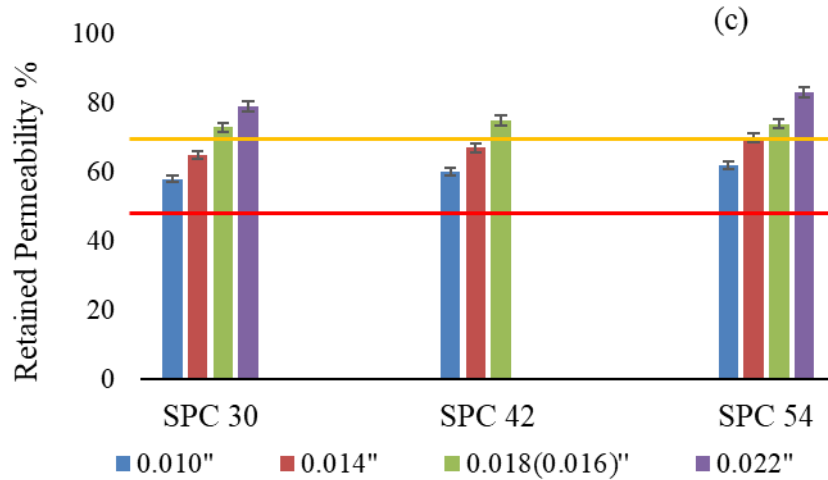
Figure 4. 8 Retained permeability data of slotted liner (a) DC-I, (b) DC-II, and (c) DC-III

4.3.2 Retained Permeability Results of the Wire-wrapped Screen

Figure 4.8 presents the retained permeability data of the WWS coupons for different PSDs.

A similar trend is found in the WWS that the retained permeability increases with the aperture size. In the WWS, the aperture (slot) density is constant, and the aperture size determines the OFA. Due to the high aperture numbers, the WWS has the highest OFA than other screen types, ensuring superior flow performance by providing more space for the fines production. As per Figure 4.9, even the smallest aperture size (0.006'') can still reach the minimum limit of the flow performance in DC-I. Also, aperture sizes of 0.014'' and 0.018'' yield a desirable flow performance in DC-I. In clean formations, like DC-II and III, all the aperture sizes could maintain the retained permeability above the acceptable limit (70%), except for the 0.006''.
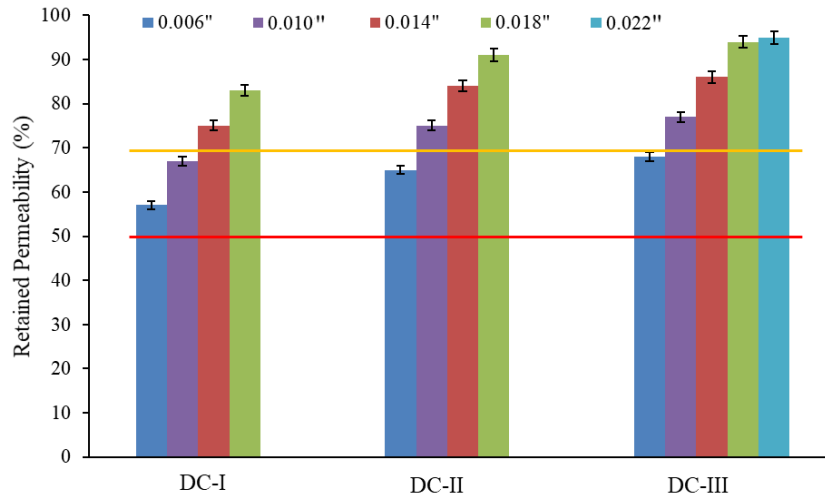
Figure 4. 9 Retained permeability data of wire-wrapped screen

4.3.2 Retained Permeability Results of the Punched Screen

Figure 4.10 shows the retained permeability data for the PS.

The retained permeability results of the PS also show an ascending trend with the increase of aperture size. Although the OFA of the PS is around twice as the SL's, the optimal flow performance is not achieved in DC-I. The testing result of 0.010'' almost meets the minimum requirement. While in the clean formations, the 0.019'' yields a desirable flow performance in DC-II and retained permeability results of 0.014'' and 0.019'' are above the upper limit of the flow performance criteria in DC-III (Fig 4.10).
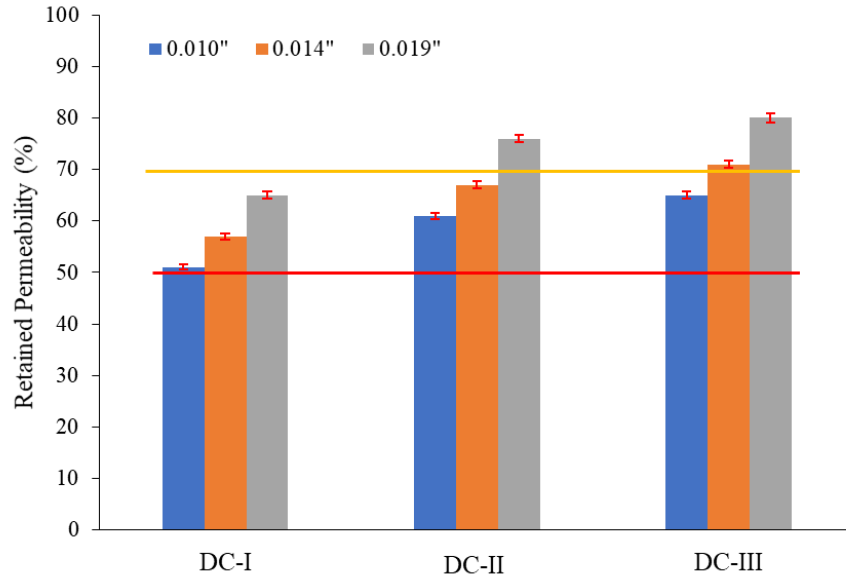
Figure 4. 10 Retained permeability data of punched screen

4.4 Fines Production

Fines migration and pore plugging are the main reasons causing the formation damage. Thus, the optimal stand-alone screen design aims to allow as more fines release as possible from the reservoir to reduce the level of pore plugging. During the testing, the amount of the fines in the discharged liquid is measured by a turbidity meter to quantify the fines production. Also, post-mortem tests of wet sieve analysis are applied to assess fines concentration along the core sample extracted after the test. The variation of the fines concentration along the core sample indicates the fines migration process.

Similar result patterns are observed for all stand-alone screens. The results of the SL are discussed as an example.

4.4.1 Fines Production Results of the Slotted Liner
Figure 4.11 through 13 present the cumulative fines production results for the SL.

It is found that there is negligible fines production during the single-phase (oil) flow stages. This is due to the water-wet characteristic of the fine particles. During the mixing process, the fine particles are coated on the sand grain surface by capillary force. When the non-wetting phase fluid (oil) flows in the sand-pack sample, the shear stress cannot overcome the capillary bonding force; hence, fine particles are not mobilized. However, fine particles start to migrate and get produced

after water breakthrough (Stage 3) as the wetting-phase fluid (brine) flows. The drag force created by the flowing brine mobilizes the fine particles and causes fines migration. With the increase of flow rate (Stage 3 to 4), further fines production is observed due to the rise of the drag force. Also, when the water cut increases from 50% to 100% (Stages 4 to 6) while the total liquid flux maintains the same level, more fines are produced. This is attributed to the increase of the contact area between the wetting-phase fluid and fine particles. Thus, more fines are exposed to the flowing brine and get migrated.

Regarding the impact of slot size, slot density, and PSD, it is observed that more fines are produced with the increase of slot size and slot density as more open space is created for fines to be discharged out of the sand-pack. Also, for the same slot size and density, DC-I produces more fines than DC-II and III because it contains the highest amount of the fine particles.
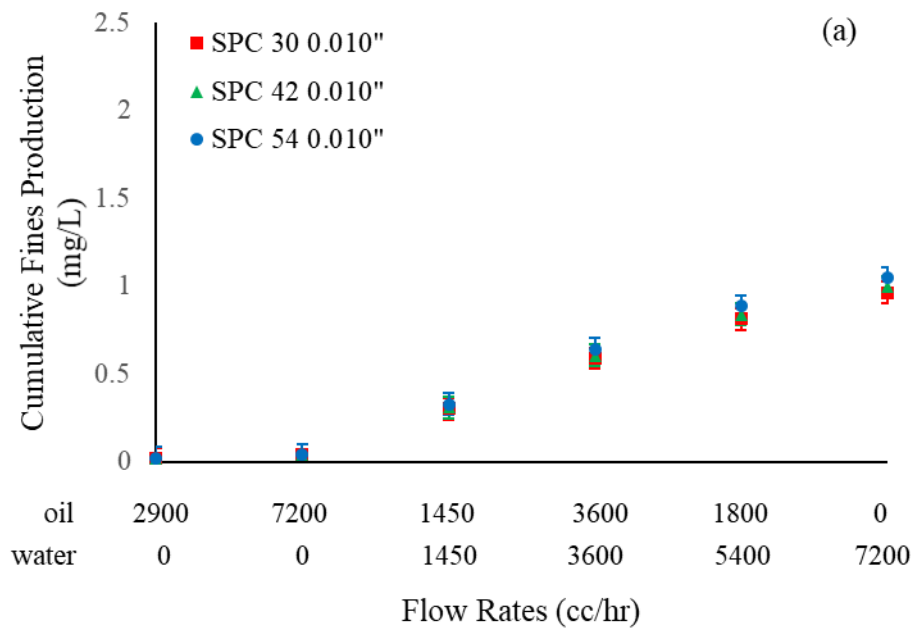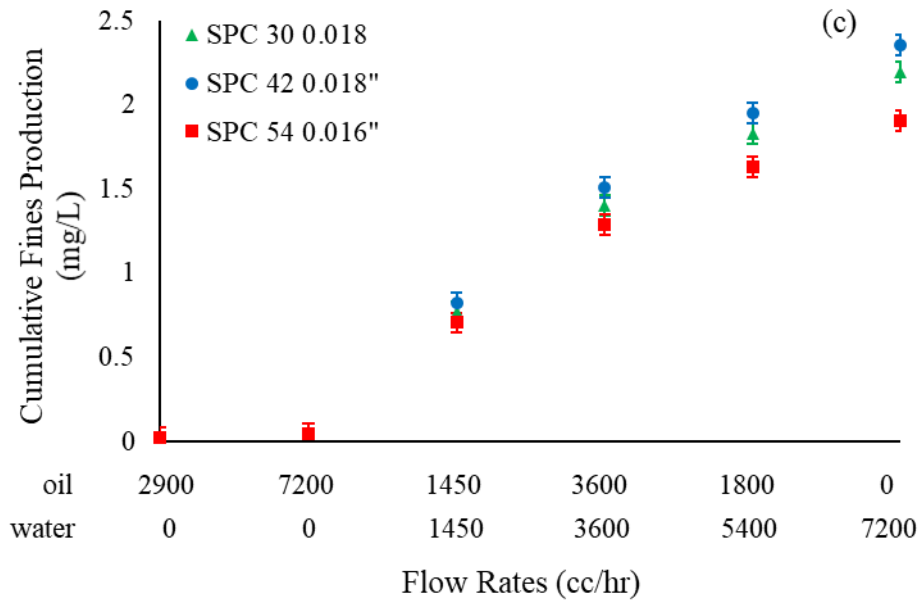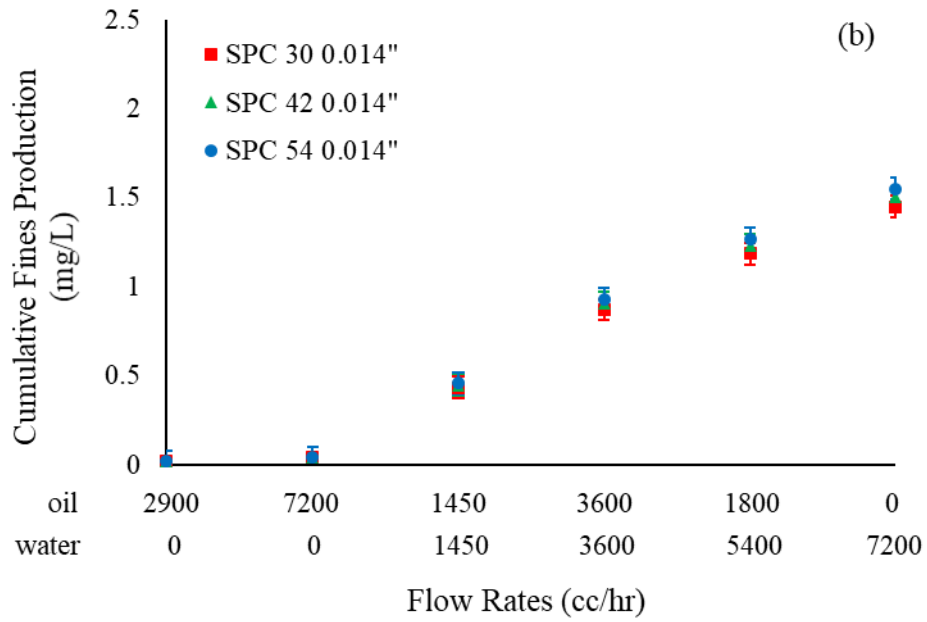
Figure 4. 11 Cumulative fines production of slotted liner for DC-I, (a) 0.010'', (b) 0.014'', and (c) 0.018'' (0.016'')

(a)

(b)
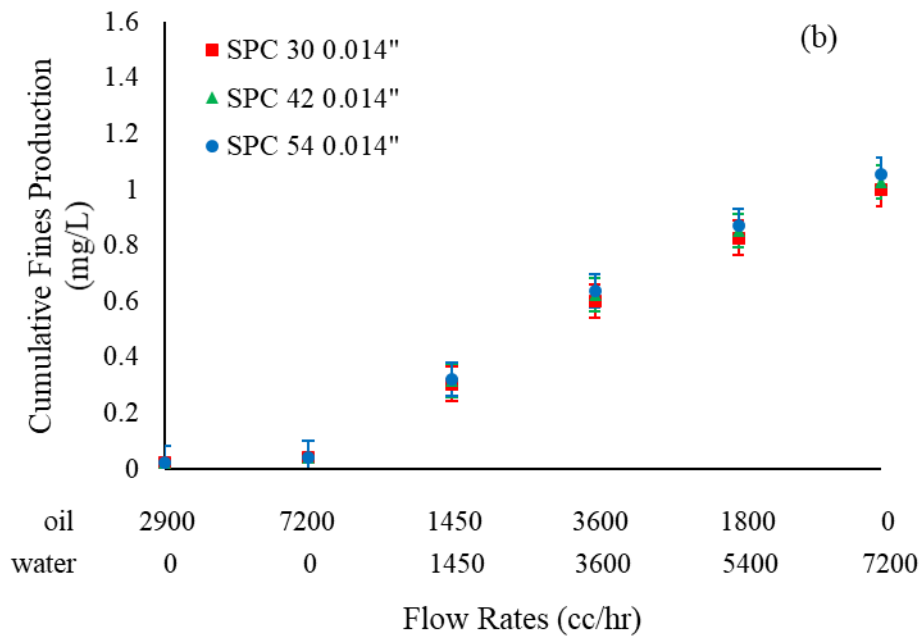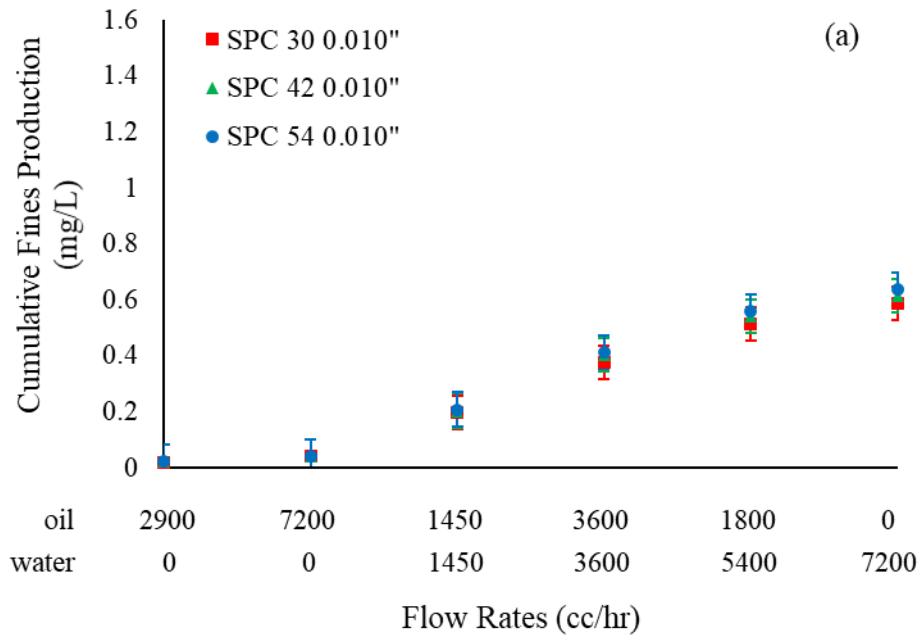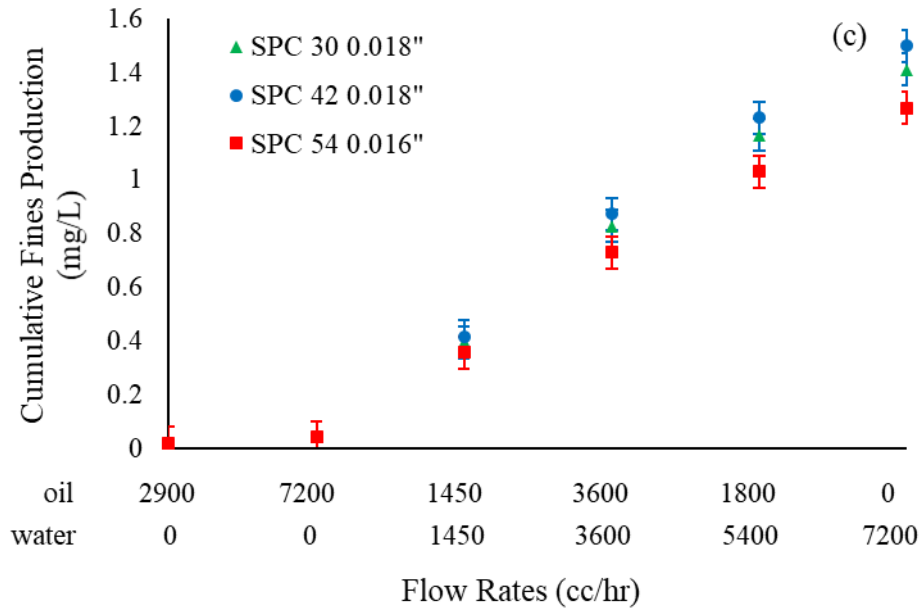
Figure 4. 12 Cumulative fines production of slotted liner for DC-II, (a) 0.010'', (b) 0.014'', and (c) 0.018'' (0.016'')
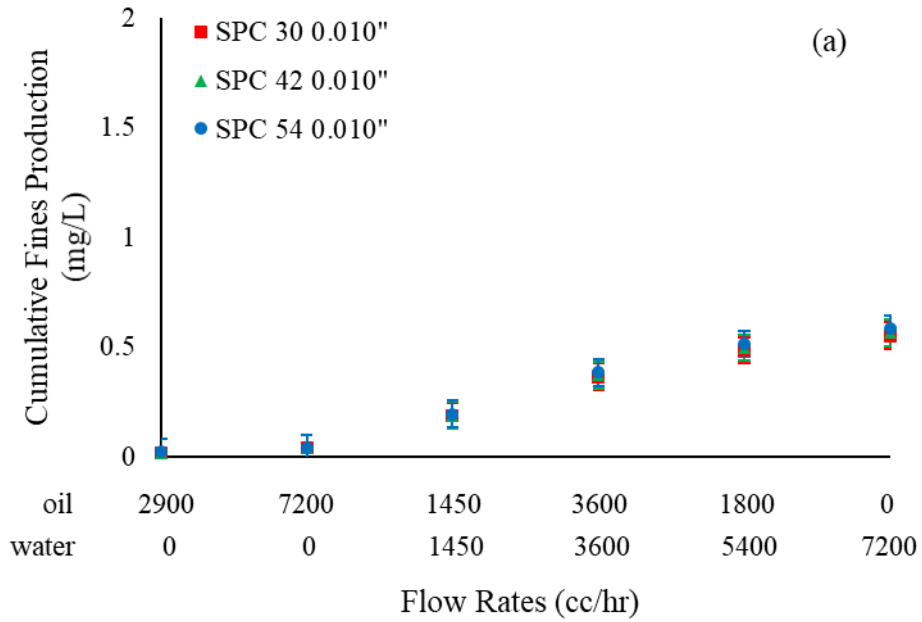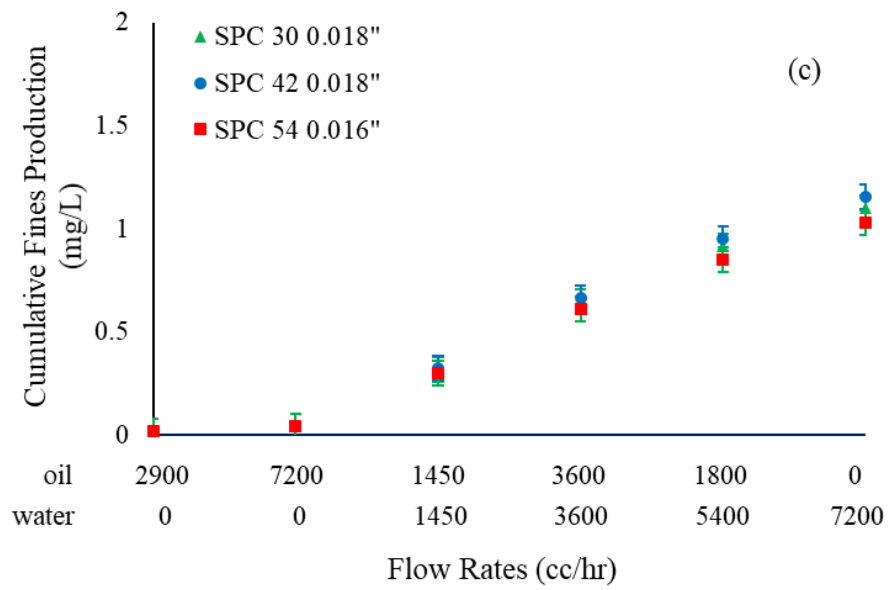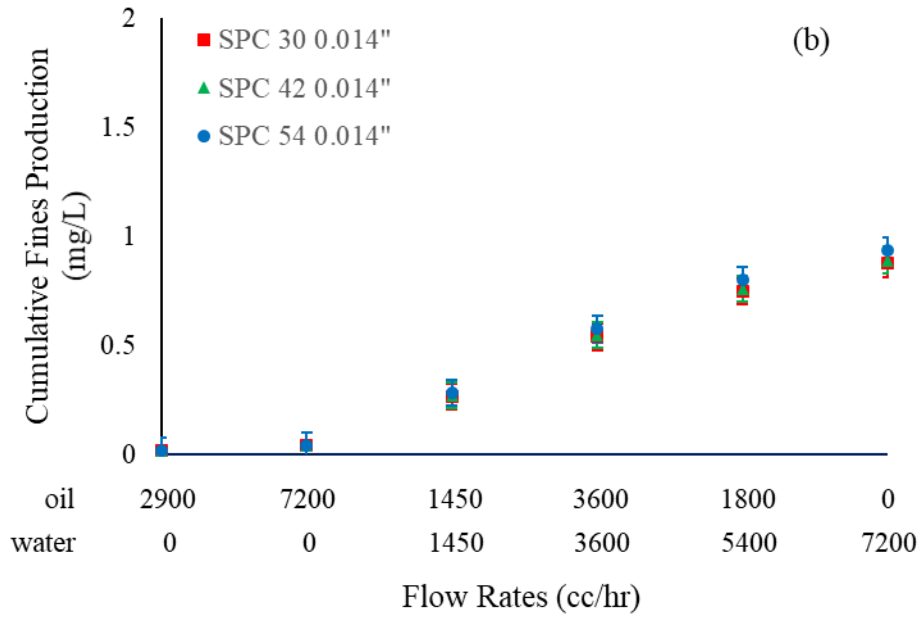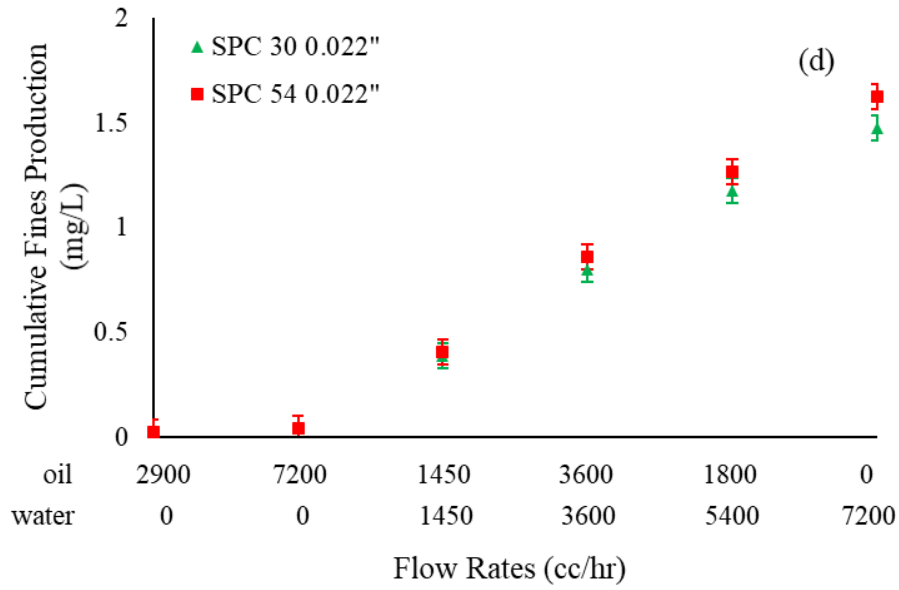
Figure 4. 13 Cumulative fines production of slotted liner for DC-III, (a) 0.010'', (b) 0.014'', (c) 0.018'' (0.016''), and (d) 0.022''

Figure 4.14 to 16 show the fines concentration results from the post-mortem wet-sieving analysis.

The fines concentration profile along the core sample indicates that the fines are migrating from the top of the sand-pack sample towards the bottom. The fines concentration in the top section shows a negative concentration change as there is not feed of fine particles. The fines concentration in the middle area nearly changes before and after the tests. This is due to the loss of the fines in the middle section is compensated by the fines gained from the top section. The middle section of the sand-pack sample acts as a transition zone for the fines migration. The bottom section, which represents the near-screen zone, is gaining fines. The fine particles are captured by the stand-alone screens and accumulated behind the screens. The fines accumulation verifies the reduction of the retained permeability in the near-screen zone.

Notably, the slot size only affects the fines concentration variation in the near-screen zone. A larger slot size shows fewer fines concentration. However, the top and middle sections are independent of the slot size as they are far away from the screen coupons. Also, when comparing Figure 4.14 (a) with 4.15 (a) and 4.16 (a), it is found that DC-I shows a higher level of fines migration. In DC-I, around 3% of the fines are migrated, while in DC-II and III are around 2.5% and 2.2%, respectively. This phenomenon also verifies the fines production results between DC-I, II, and III.
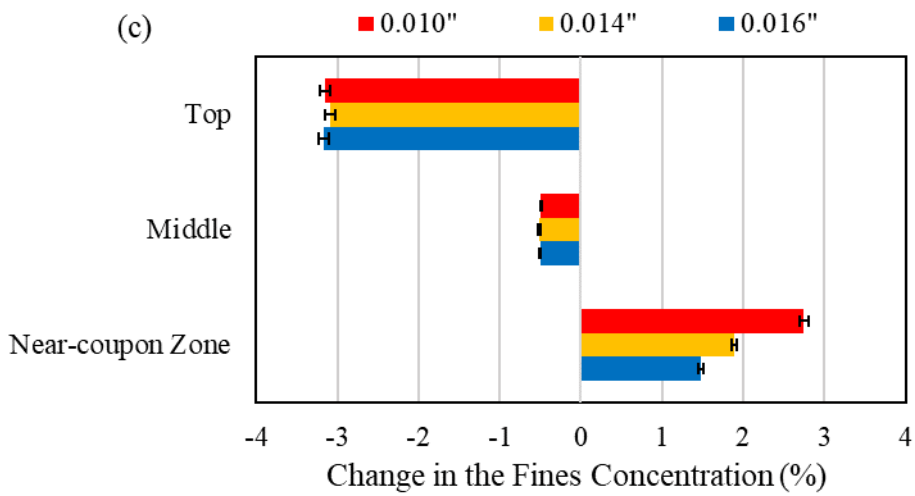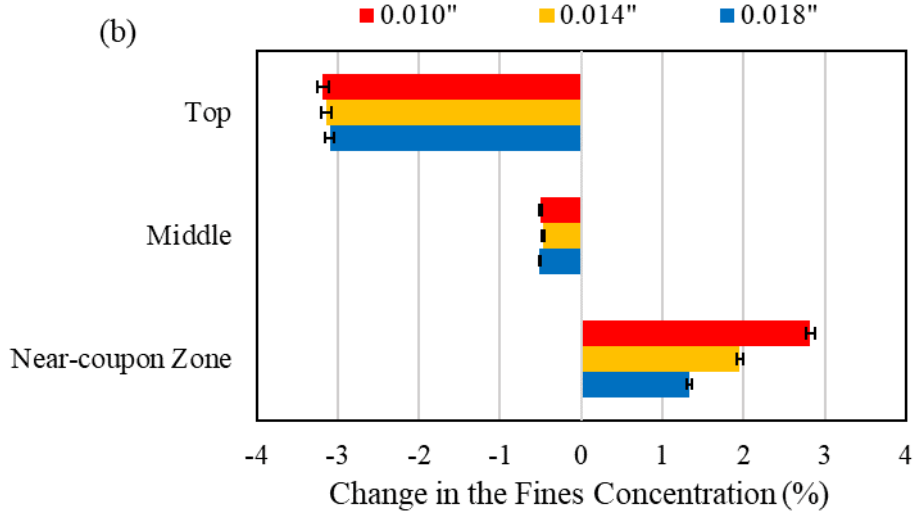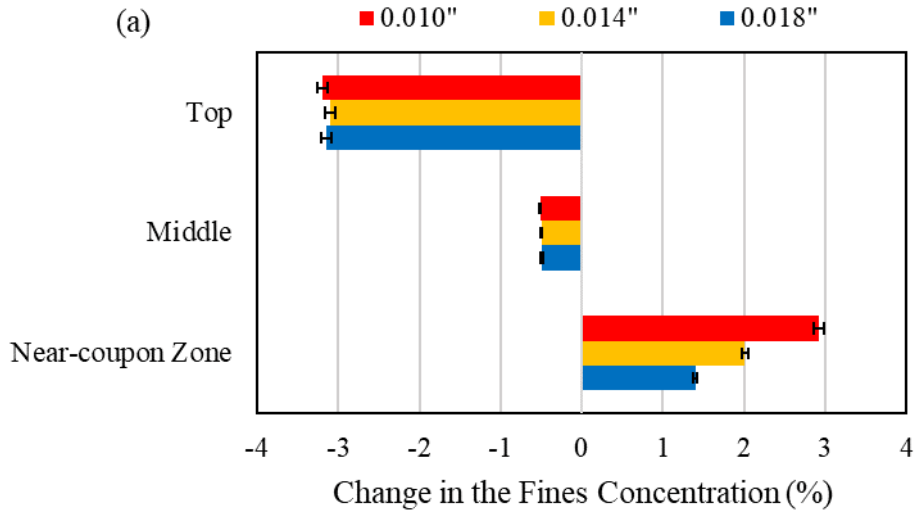
Figure 4. 14 Fines concentration results of slotted liner for DC-I, (a) SPC 30, (b) SPC 42, and (c) SPC 54
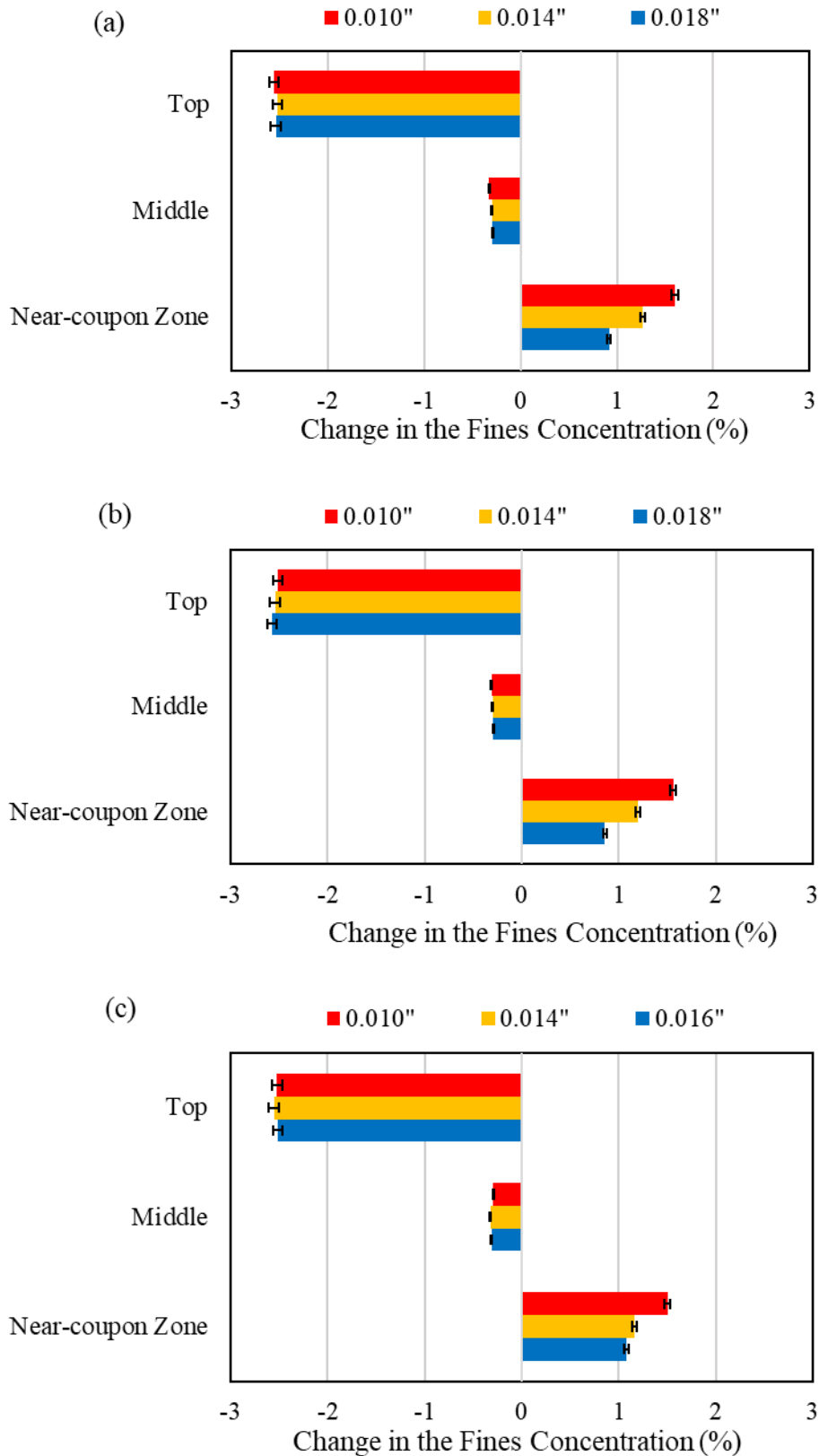
Figure 4. 15 Fines concentration results of slotted liner for DC-II, (a) SPC 30, (b) SPC 42, and (c) SPC 54
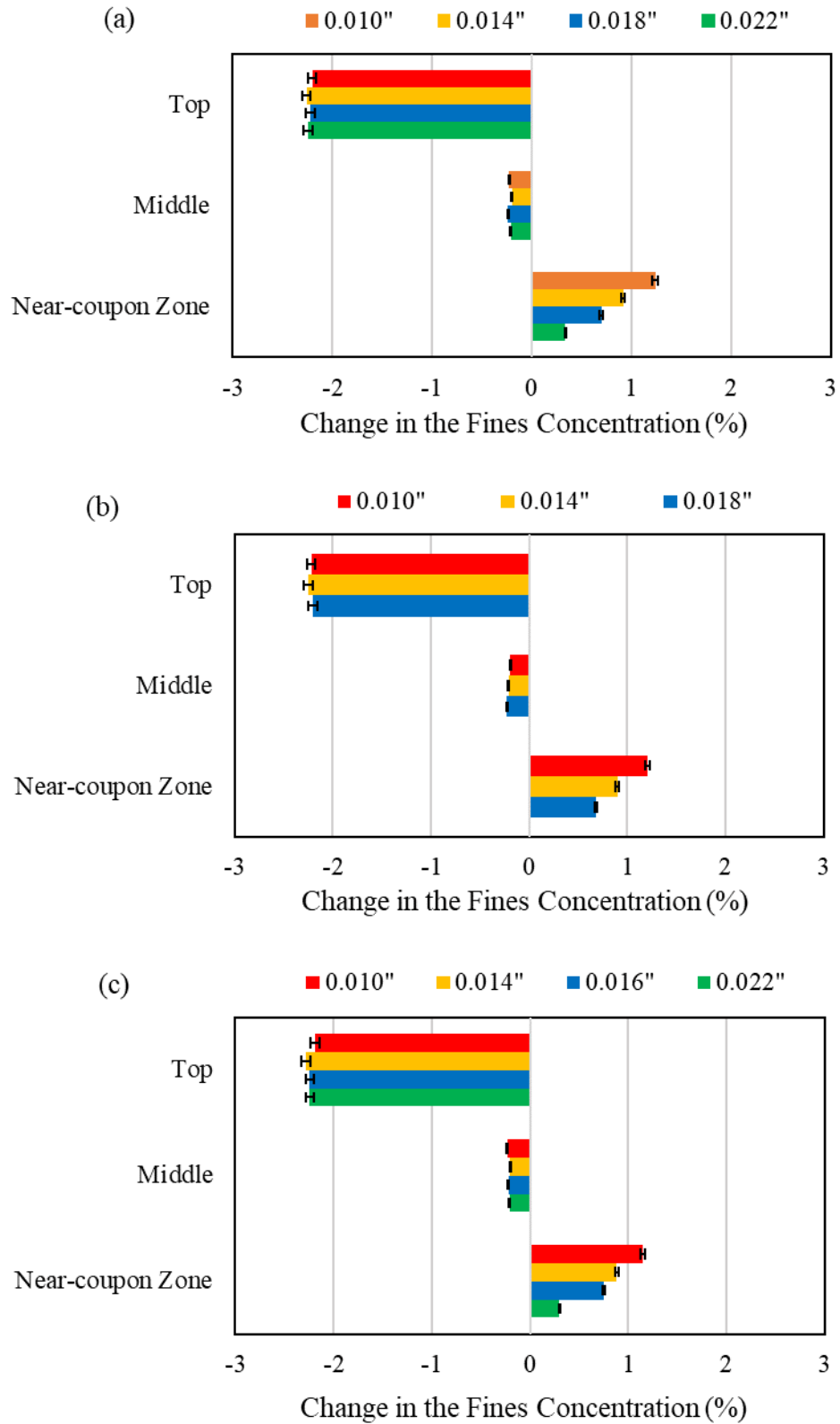
Figure 4. 16 Fines concentration results of slotted liner for DC-III, (a) SPC 30, (b) SPC 42, and (c) SPC 54

4.4.2 Fines Production Results of the Wire-wrapped Screen

Figures 4.17 and 4.18 show the cumulative fines production and fines concentration results for the WWS, respectively.
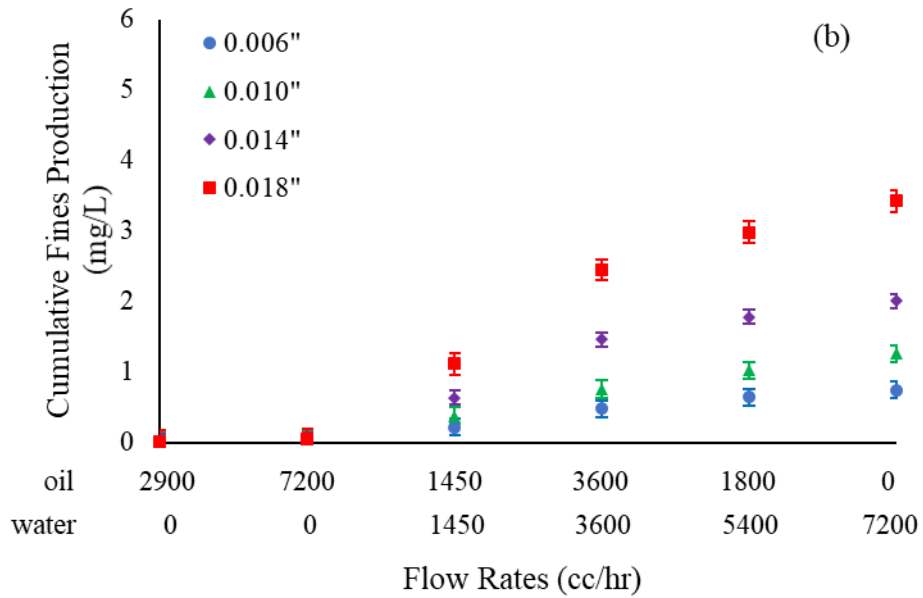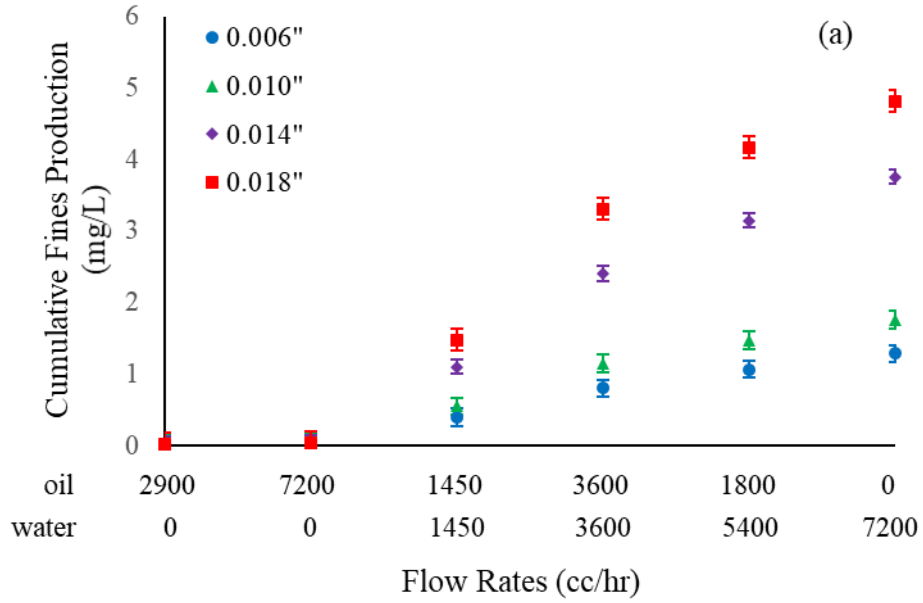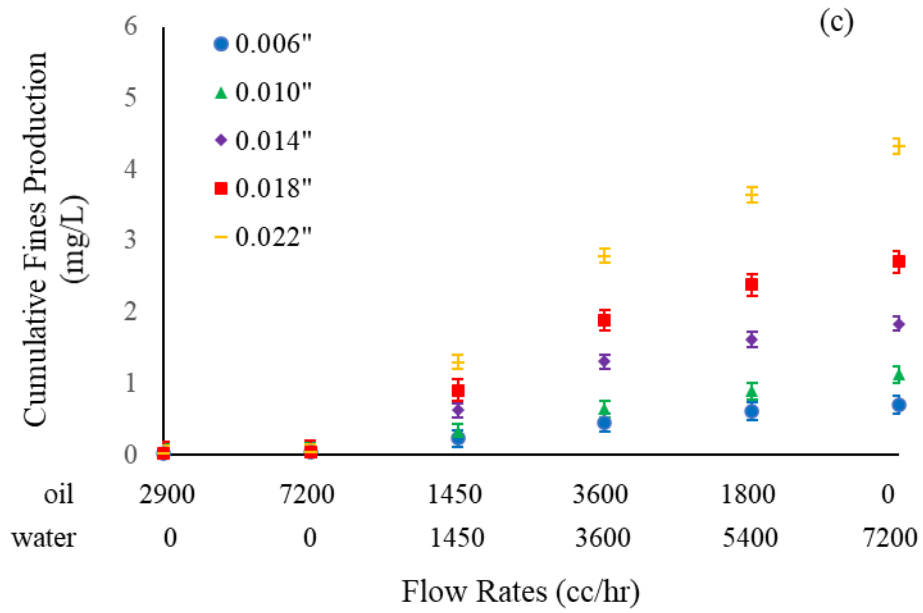
Figure 4. 17 Cumulative fines production of the wire-wrapped screen, (a) DC-I, (b) DC-II, and (c) DC-III
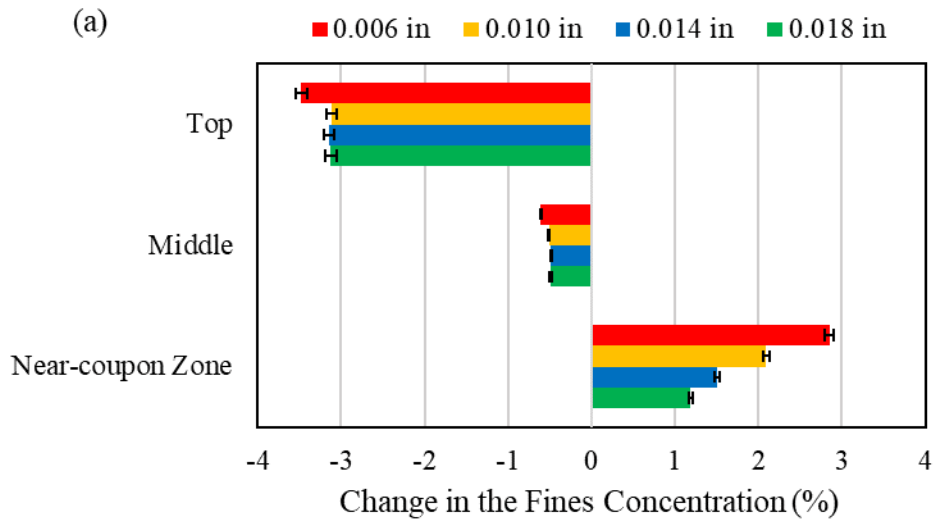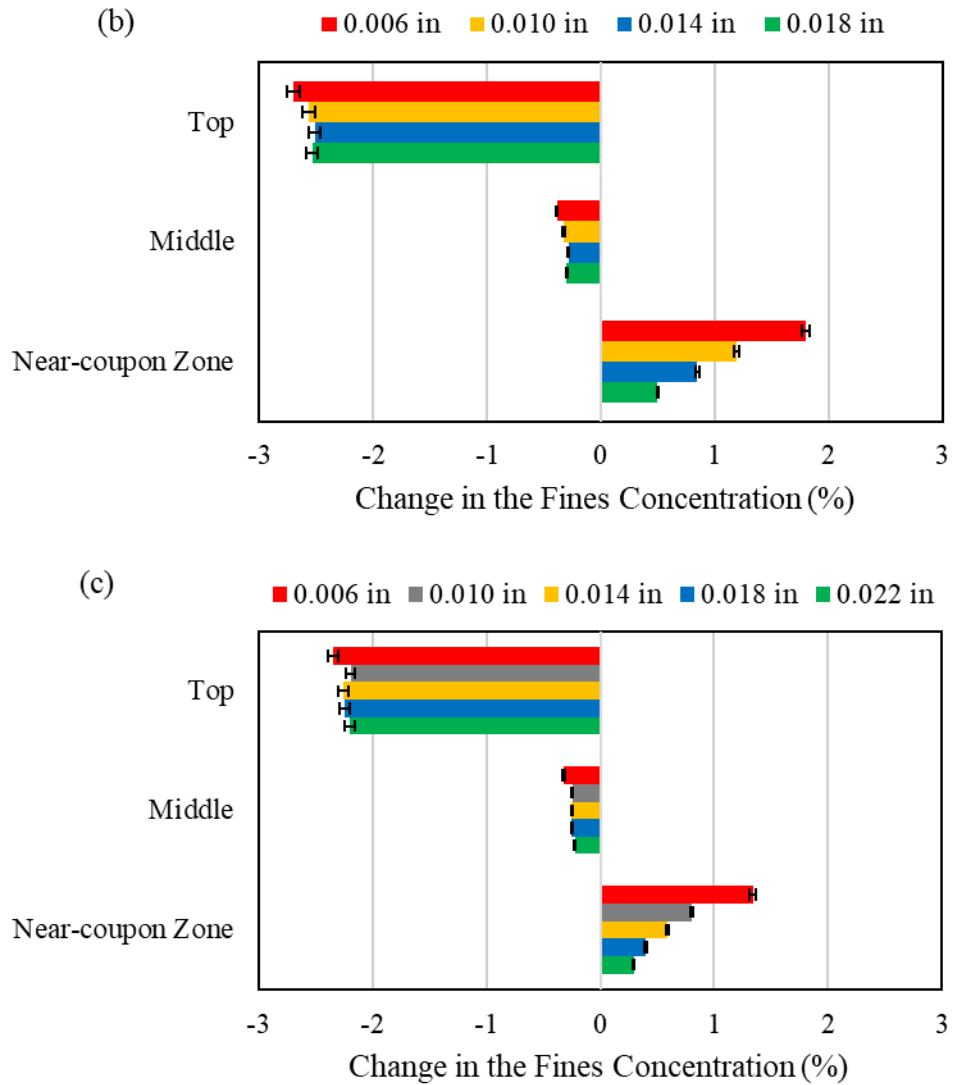
Figure 4. 18 Fines concentration results of the wire-wrapped screen, (a) DC-I, (b) DC-II, and (c) DC-III

4.4.3 Fines Production Results of the Punched Screen

Figures 4.19 and 4.20 illustrate the cumulative fines production and fines concentration results for the PS, respectively.
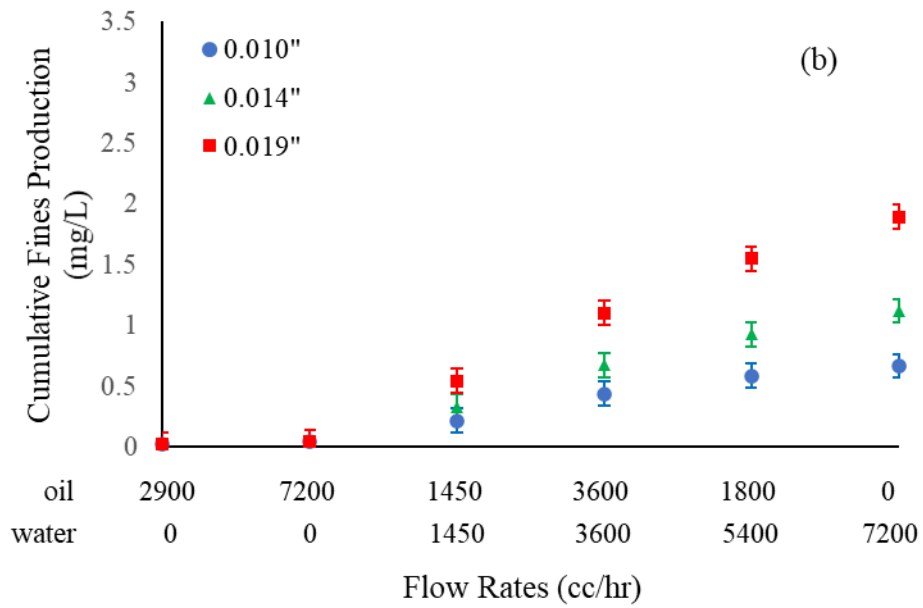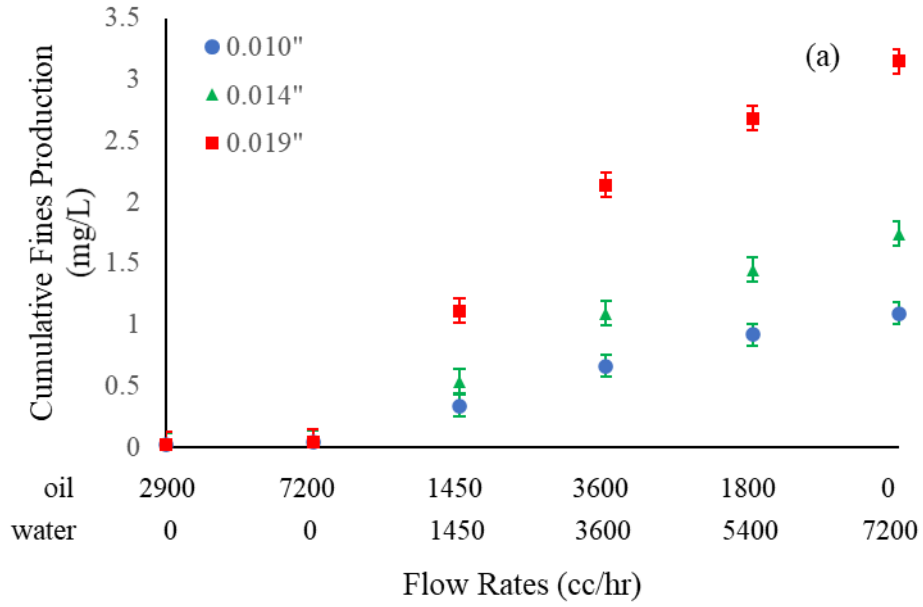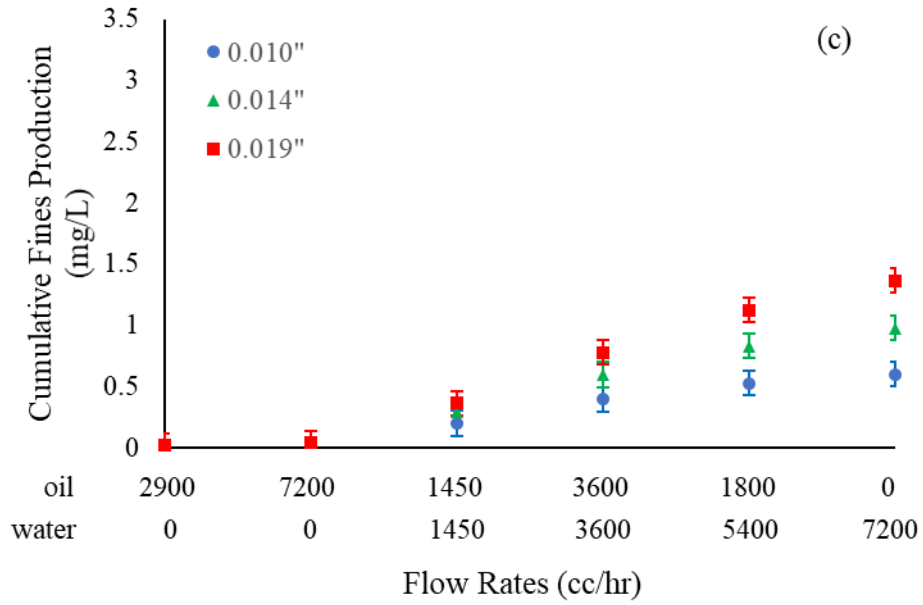
Figure 4. 19 Cumulative fines production of the punched screen, (a) DC-I, (b) DC-II, and (c) DC-III
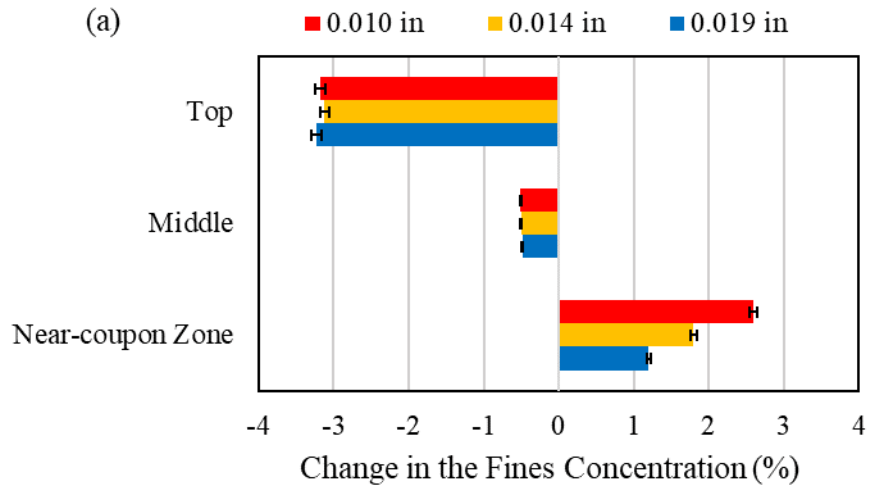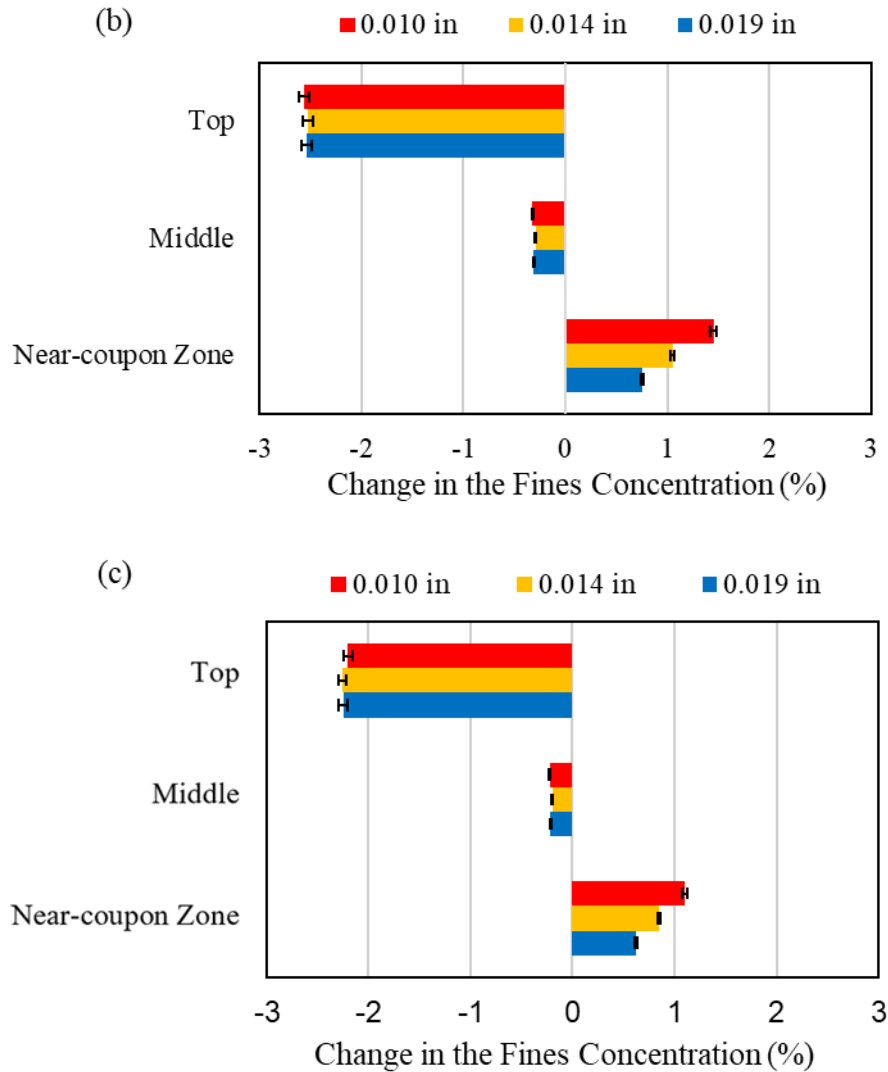
Figure 4. 20 Fines concentration results of the punched screen, (a) DC-I, (b) DC-II, and (c) DC-III

4.5 Conclusion

This chapter presents the experimental results of the pre-packed SRT, including sand production, retained permeability, fines production, and fines accumulation. Sand production and retained permeability are two main data to assess the stand-alone screens' sanding and flow performance.

Factors such as aperture size, slot density, fluid phase, fluid velocity, and PSD play a critical role in the testing results. As for aperture size and slot density increase, the amount of sand production increases. Also, the retained permeability and fines production increase, and fines concentration in the near-screen zone decreases. Substantial sand production is observed after water and gas breakthrough. The increase of fluid velocity and water cut cause further sand production due to

the rise of the drag force and reduction of the capillary bonding force. Also, fines migration is intensified, hence more fines production and pore plugging. Finally, it is found that dirty formation, like DC-I, has higher plugging potential due to the immense source of fine particles. Clean formations (DC-II and III) are less vulnerable to formation damage due to fines migration and pore plugging.

Chapter 5: Aperture Size Design Criteria of Stand-alone Screens (Traffic Light System)

5.1 Introduction

This chapter presents the aperture size design criteria of stand-alone screens. The design criteria are generated based on the sand production and retained permeability data described in the previous chapter. Also, the proposed design criteria use color codes (green, yellow, and red) to illustrate the safe aperture size window graphically. The safe aperture size window indicates the range of the aperture sizes that can control the sand production within an acceptable limit and maintain the flow performance at a desirable level.

5.2 Traffic Light System

The aperture size design criteria are generated based on the testing results: sand production and retained permeability. The design criteria are illustrated graphically using the "Traffic Light System" (TLS). In the TLS design criteria, the red, yellow, and green colours represent unacceptable, marginal, and acceptable performance, respectively. The aperture size design criteria in the TLS are based on sanding and flow performance. The sand production controls the upper limit of the aperture window, while the retained permeability dictates the lower limit of the aperture window. The definitions of colours are summarized in Table 5.1.

The green zone in the sanding performance represents the condition that the cumulative sand production is below 0.12 lb/ft^2, which indicates an optimal sand control performance. The yellow zone is the scenario when the cumulative sand production is between 0.12 to 0.15 lb/ft^2, which means an intermediate sanding performance. The red color indicates the cumulative sand production is beyond 0.15 lb/ft^2, which is not acceptable.

Like the sanding performance, the green zone in the flow performance denotes the optimal flow performance, where the retained permeability is above 70%. The yellow zone describes a mediocre flow performance, where the retained permeability is between 50% and 70%. The red zone indicates an undesirable flow performance, where severe formation damage happens, and the retained permeability drops below 50%.

Table 5. 1 Colour definition in TLS

Sand production performance

red	sand production > 0.15 lb/ft^2
yellow	$0.12 <$ sand production < 0.15 lb/ft^2
green	sand production < 0.12 lb/ft^2
Flow performance	
red	retained permeability < 0.5
yellow	$0.5 <$ retained permeability < 0.7
green	retained permeability > 0.7

In the TLS, the aperture size windows are plotted along a linear axis. Also, each PSDs' D-values are marked along the linear axis to indicate the PSD data of each formation sand. Figure 5.1 shows the linear axes of all three PSDs (DC-I, DC-II, and DC-III) used for building up the TLS.
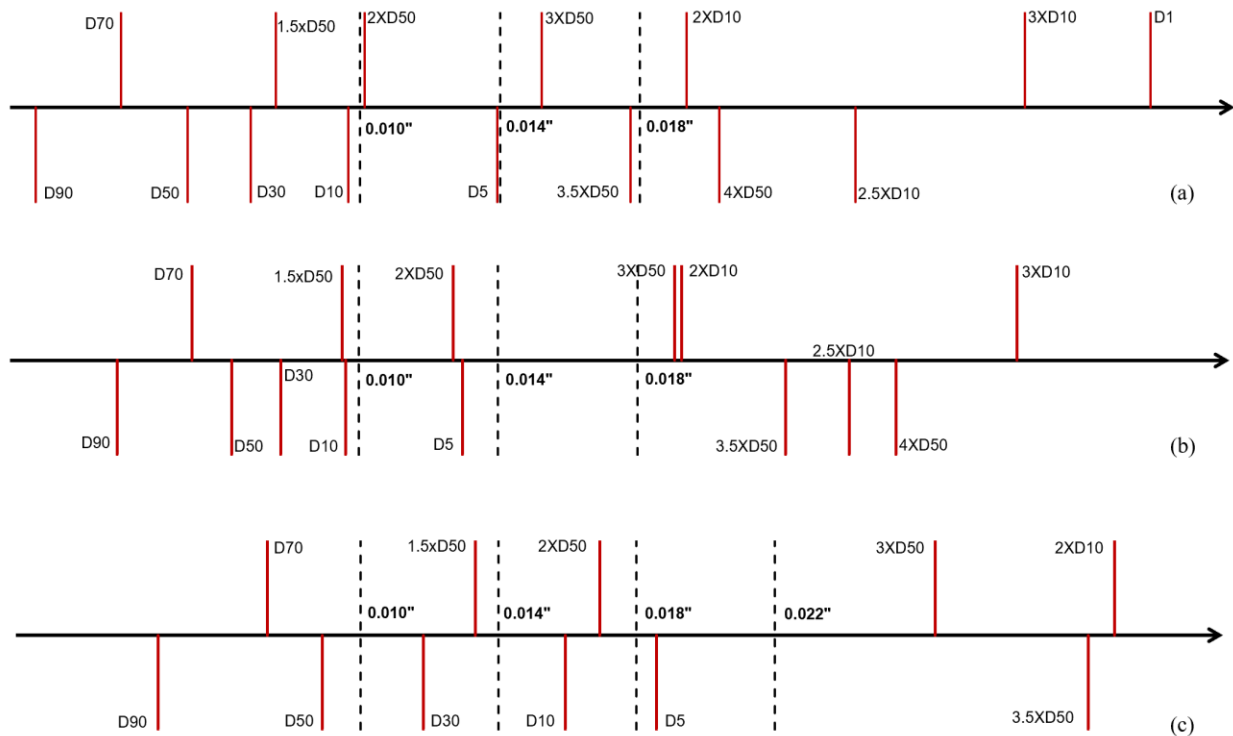
Figure 5. 1 Linear axes of the TLS for (a) DC-I, (b) DC-II, and (c) DC-III

In the TLS, two representative scenarios are considered: normal SAGD condition and aggressive SAGD condition. The normal condition includes only the liquid flow stages (Stages 1-8) since the

liquid production is the common production scenario throughout the whole SAGD well life. Nevertheless, few hot spots are identified in the steam chamber, leading to the steam breakthrough scenario. Thus, the aggressive SAGD condition includes gas flow stages (Stages 9-10) to account for the potential steam breakthrough scenario.

Figure 5.2 summarizes how to create the TLS based on the sand production and retained permeability results.

Step 1	• Plot the sand production data against aperture size. • Obtain an equation for sanding by curve fitting.
Step 2	• Plot the retained permeability data against aperture size. • Obtain an equation for retained permeability by curve fitting.
Step 3	• Find aperture sizes corresponding to the maximum allowable sand production and minimum allowable retained permeability. • Draw the TLS bars for sand production and retained permeability.
Step 4	• Combine the TLS bars to obtain the size selection criteria.

Figure 5. 2 TLS creation procedure

Figures 5.3 through 5.7 show an example of the creation of TLS. The example uses the testing results of the PS for DC-I at normal SAGD conditions. First, the final cumulative sand production and retained permeability results obtained from different tests are plotted against aperture sizes, as shown in Figures 5.3 and 5.4, respectively. Next, mathematical equations that correlate the sand production or retained permeability with the aperture size are obtained by curve fitting. These equations are used to find the aperture sizes corresponding to the acceptable boundaries for the sanding (0.12 and 0.15 lb/ft^2) and flow performance (50% and 70%). Once the appropriate aperture size is determined, the TLS bars are separately created for the sand production (Figure 5.5) and retained permeability (Figure 5.6). Finally, the sand production and retained permeability TLS

bars are combined to obtain the overall TLS showing the safe window for aperture size design, as shown in Figure 5.7.
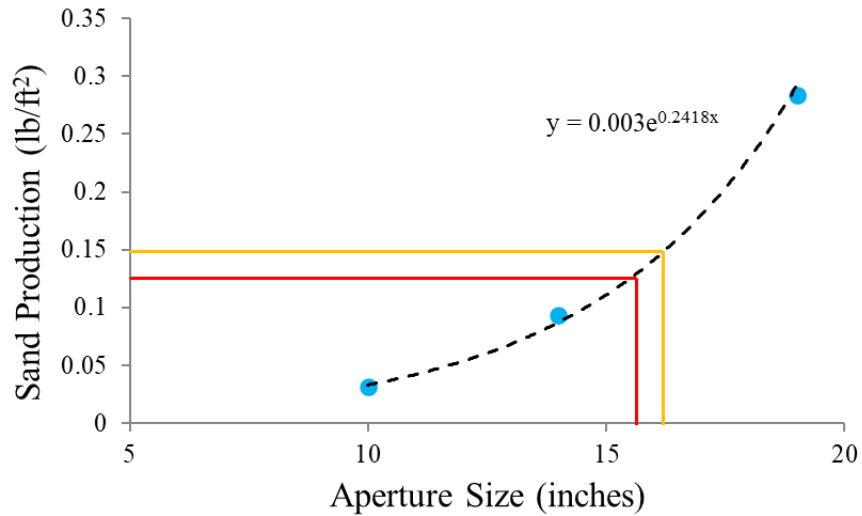
Figure 5. 3 Sand production data points versus aperture sizes (DC-I normal condition)
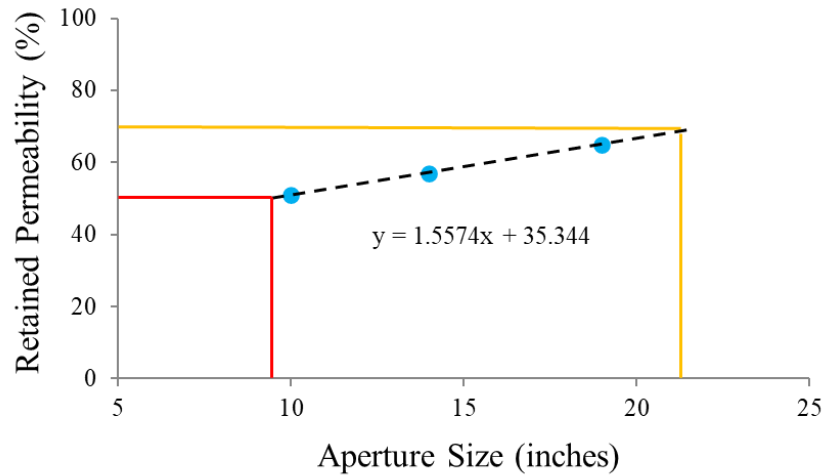
Figure 5. 4 Retained permeability data versus aperture sizes (DC-I normal condition)
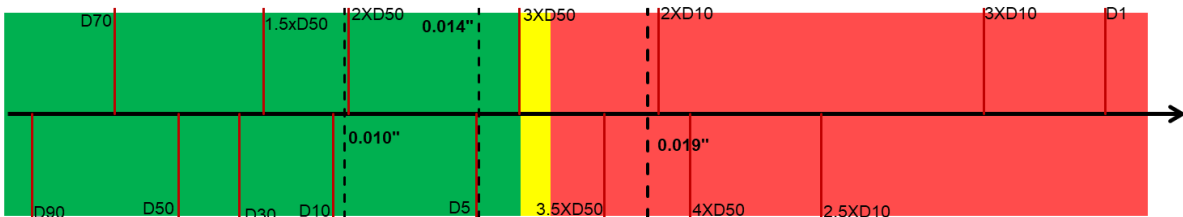
Figure 5. 5 Traffic light bar for sand production for DC-I (normal condition)
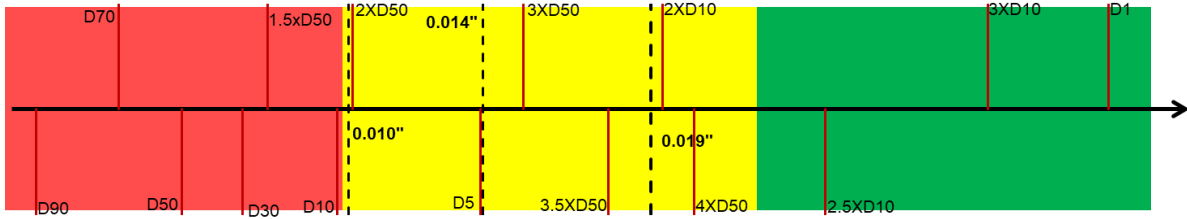
Figure 5. 6 Traffic light bar for retained permeability for DC-I (normal condition)
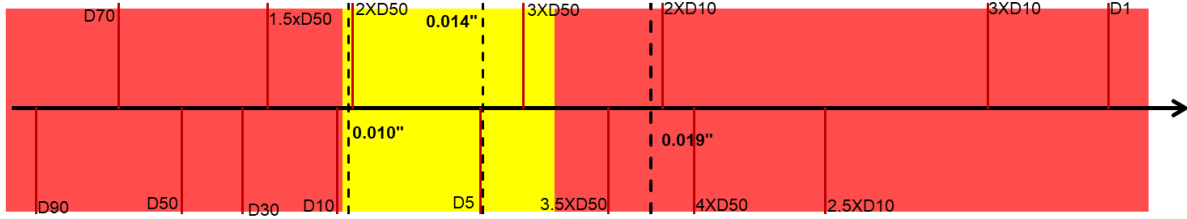
Figure 5. 7 Overall traffic light system of safe size window for DC-I (normal condition)

5.2.1 TLS of Slotted Liner

Figures 5.8 to 5.13 present the TLS results of the SL. The blue lines show the error due to the measurement uncertainties of the sand production and retained permeability data. Based on the TLS results, it is found that the safe slot size window gets wider from DC-I to DC-III. There are only some narrow yellow zones existing in DC-I (Figure 5.8). This is attributed to the undesirable flow performance of the SL due to the low OFA. DC-I contains the highest fines concentration compared to DC-II and III, making it more vulnerable to pore plugging. The low OFA characteristic of the SL restrains the fines production and causes lower retained permeability. Besides, the finer PSD characteristics make DC-I produce more sand production compared to DC-II and III with the same coupon specifications. Thus, the higher amount of sand production and lower retained permeability cause no optimal zone (green zone) in the DC-I. However, due to the limited amount of fines content in DC-II and III and coarser PSD characteristics, the SL can provide a desirable sanding and flow performance, resulting in green zones in DC-II and III. Particularly in DC-III (Figure 5.12), which is the coarsest sand and contains the least amount of fines concentration, the green zone becomes wider than DC-II (Figure 5.10). Another finding is with the increase of slot density, the yellow zones in DC-I become wider and shift to the left (Figure 5.8). Also, a similar phenomenon happens in DC-II and III (Figure 5.10 and 5.12). This is due to the increase of the open-flow-area, which leads to a higher amount of sand production and

91

retained permeability. Thus, both the upper and lower bound of the safe window shift to the left. Regarding the impact of the SAGD condition, the safe window shrinks with the presence of gas flow due to the massive sand production during the gas breakthrough (Figures 5.9, 5.11, and 5.13). Thus, in aggressive SAGD operational conditions, the upper bound of the safe window shifts towards the left, resulting in the design window becomes narrower compared to the normal SAGD condition. Notably, there is no safe window for SPC 30 in DC-I under aggressive SAGD conditions. Therefore, the SL is recommended to be implemented in clean formation to ensure a satisfying performance.

(a)

(b)

(c)
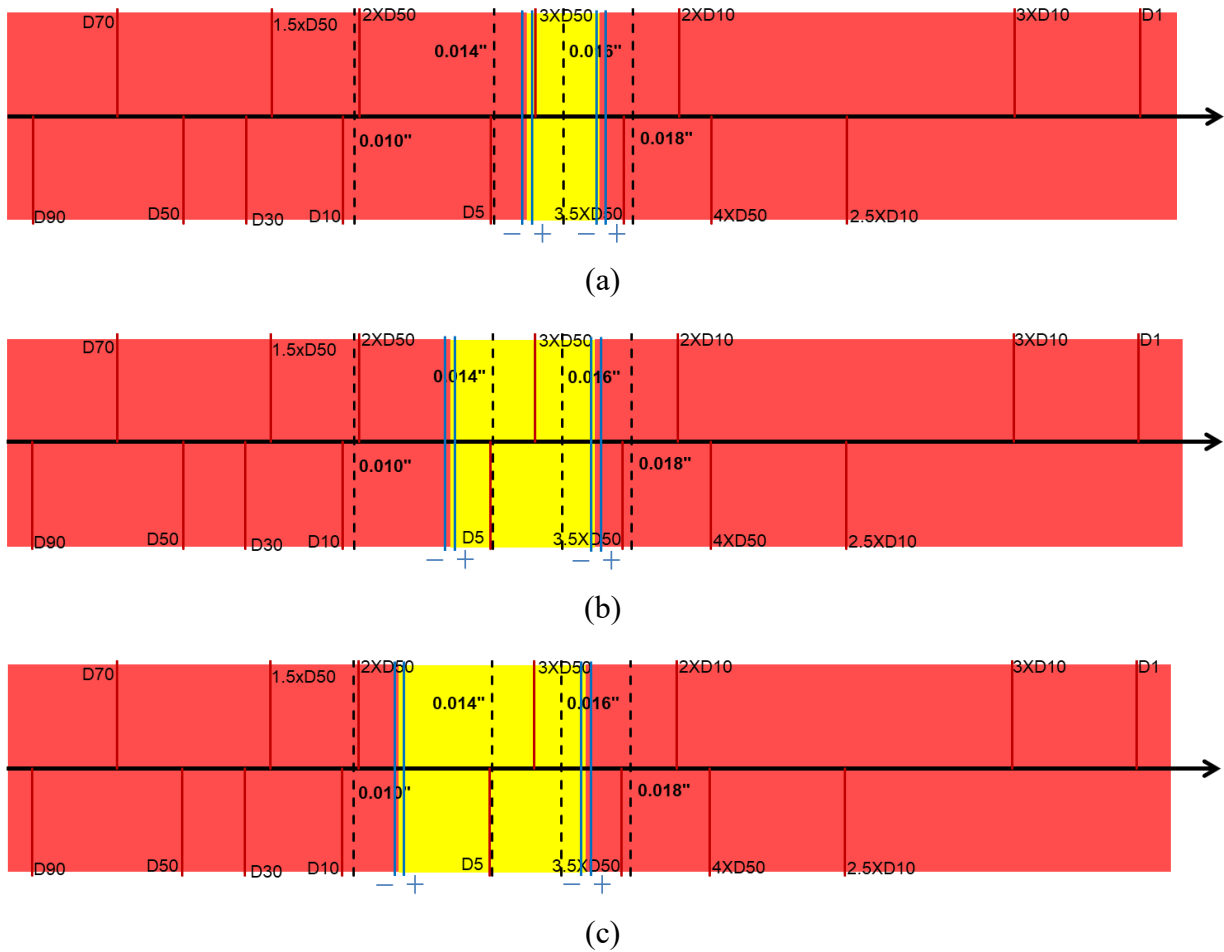
Figure 5. 8 TLS of DC-I in regular condition for (a) SPC 30, (b) SPC 42, and (c) SPC 54
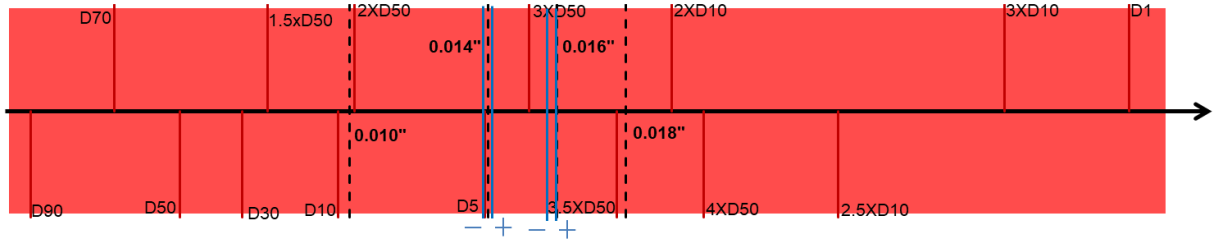
(a)
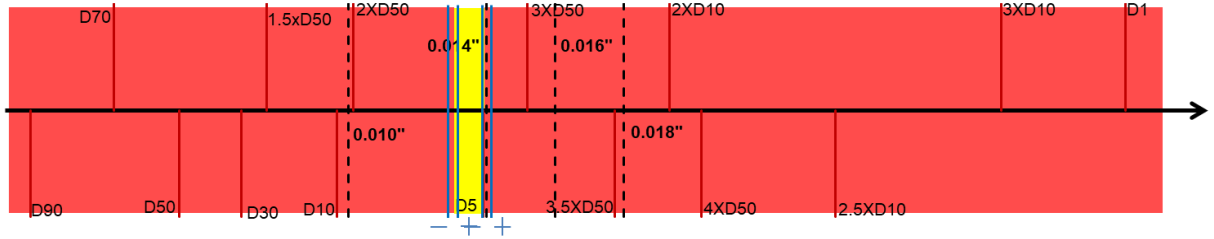
(b)
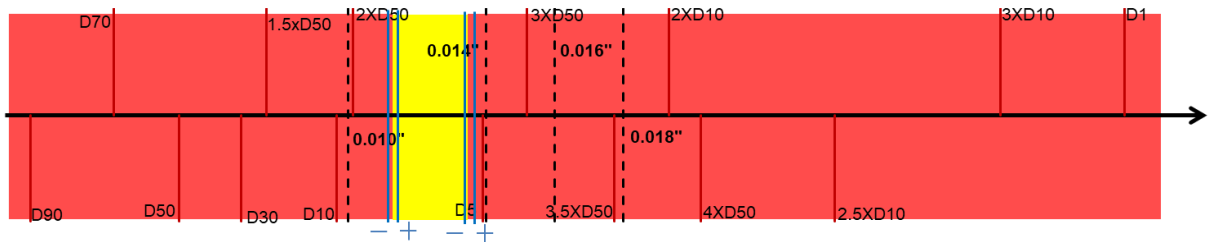
(c)

Figure 5. 9 TLS of DC-I in aggressive condition for (a) SPC 30, (b) SPC 42, and (c) SPC 54.
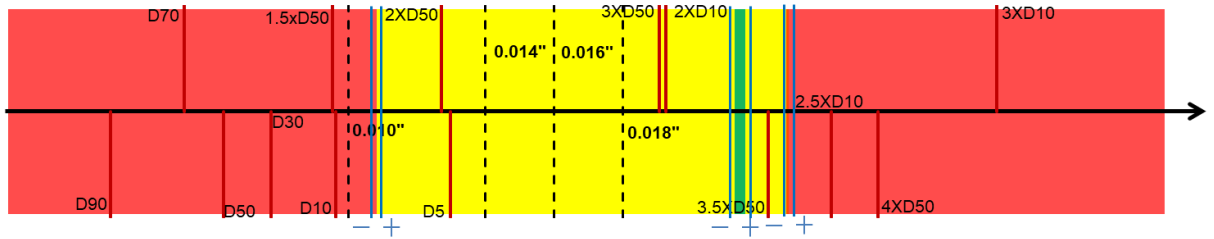
(a)
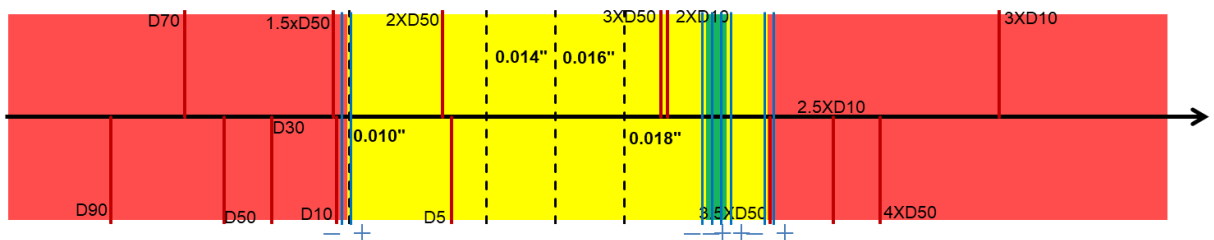
(b)
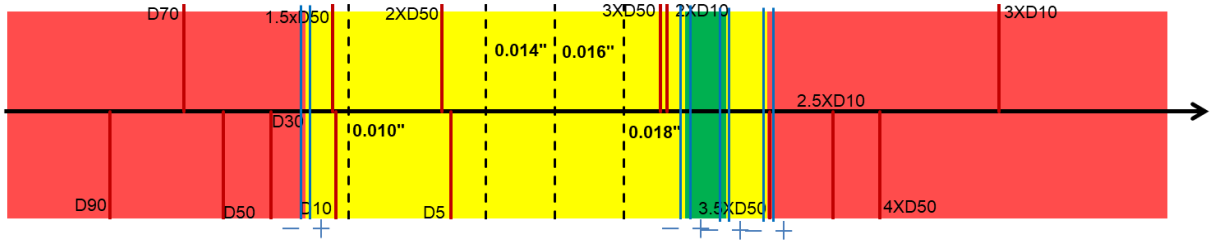
(c)

Figure 5. 10 TLS of DC-II in regular condition for (a) SPC 30, (b) SPC 42, and (c) SPC 54
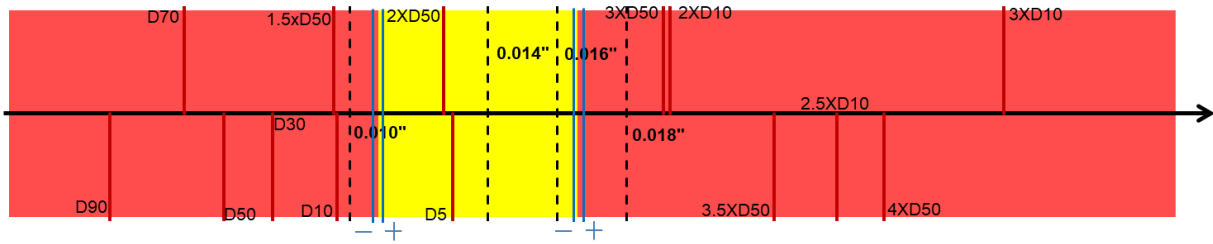
(a)
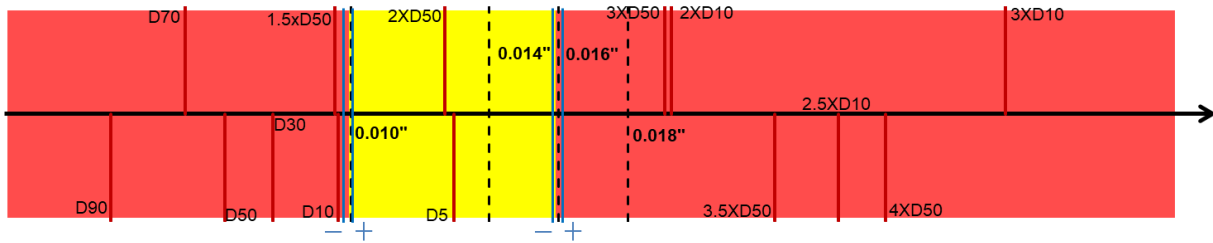
(b)
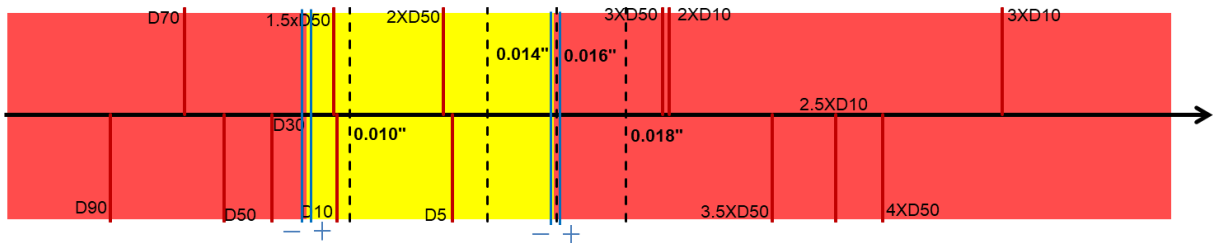
(c)

Figure 5. 11 TLS of DC-II in aggressive condition for (a) SPC 30, (b) SPC 42, and (c) SPC 54

(a)

(b)
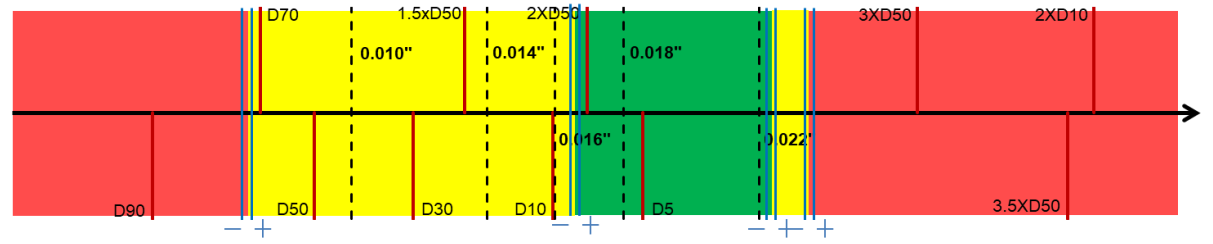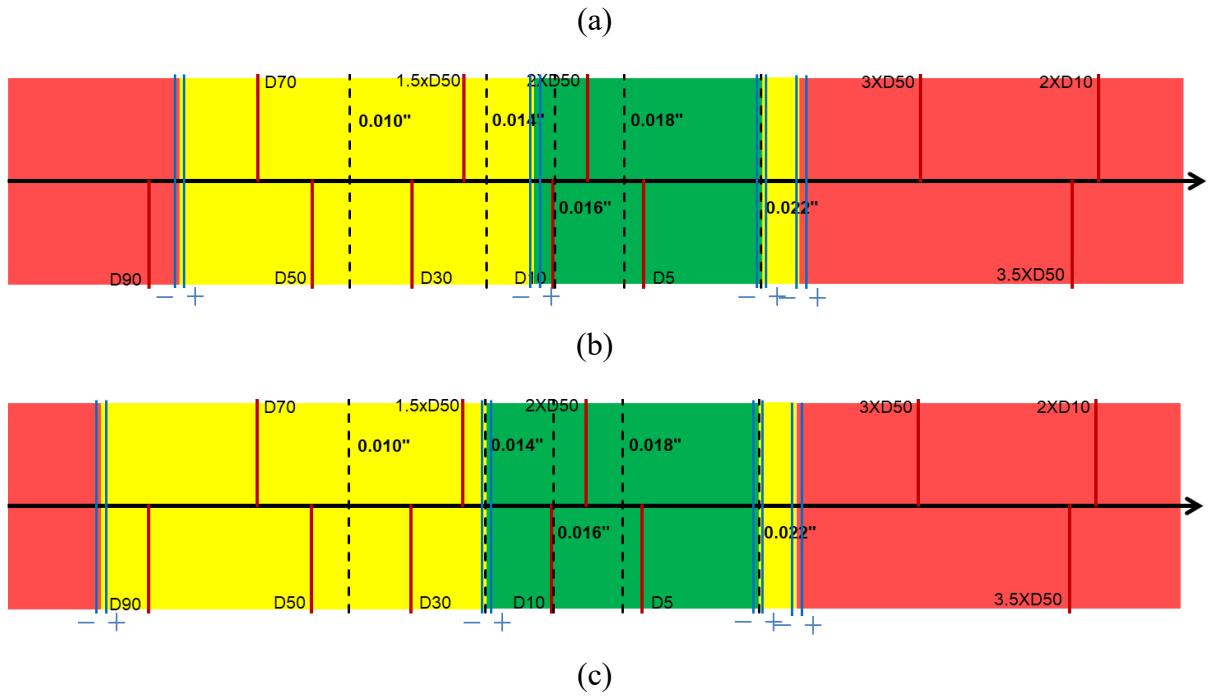
Figure 5. 12 TLS of DC-III in regular condition for (a) SPC 30, (b) SPC 42, and (c) SPC 54

(a)

(b)

(c)
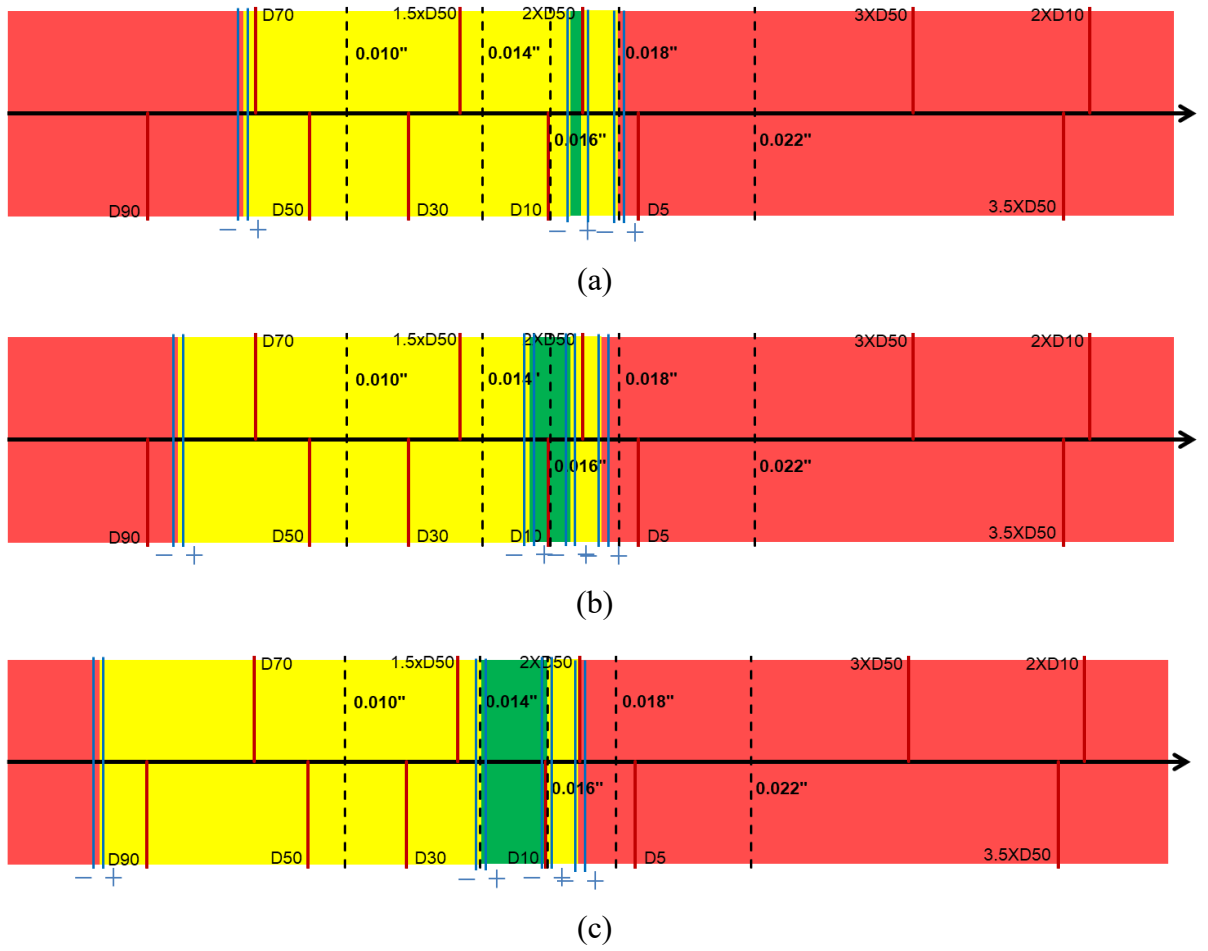
Figure 5. 13 TLS of DC-III in aggressive condition for (a) SPC 30, (b) SPC 42, and (c) SPC 54

5.2.2 TLS of Wire-wrapped Screen

Figures 5.14 through 5.16 show the TLS design criteria for the WWS for DC-I, II, and III, respectively. There are optimal aperture design windows in each formation sand. Even in DC-I, there is a 4-inch-wide green zone, which means the WWS can provide desirable performance for DC-I, even under the aggressive SAGD condition (Figure 5.14b). This the due to the high OFA nature of the WWS. The higher OFA design guarantees a satisfied retained permeability for the formations with a larger number of fine particles. Thus, the WWS is suitable for dirty formations to provide a desirable performance.
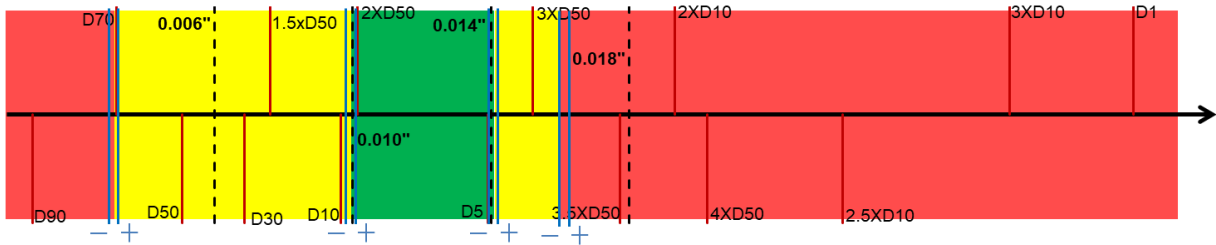
(a)
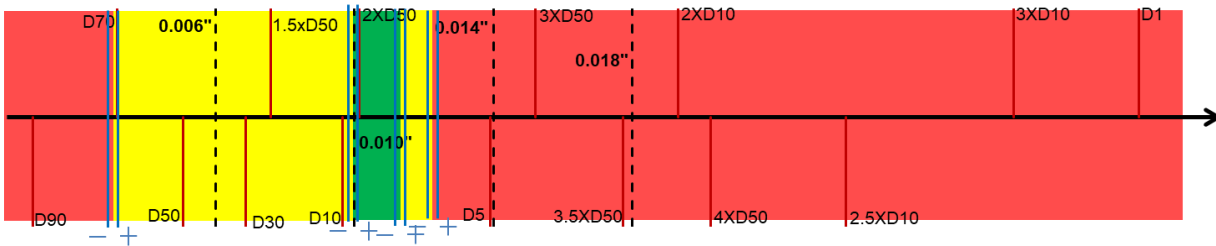
(b)

Figure 5. 14 TLS of DC-I of wire-wrapped screen (a) normal condition, (b) aggressive condition
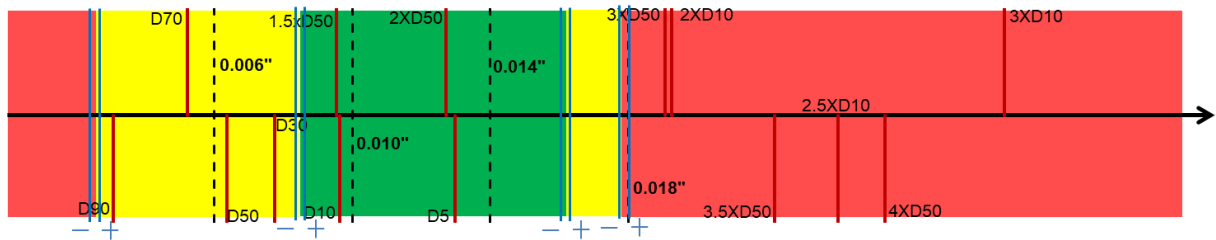
(a)
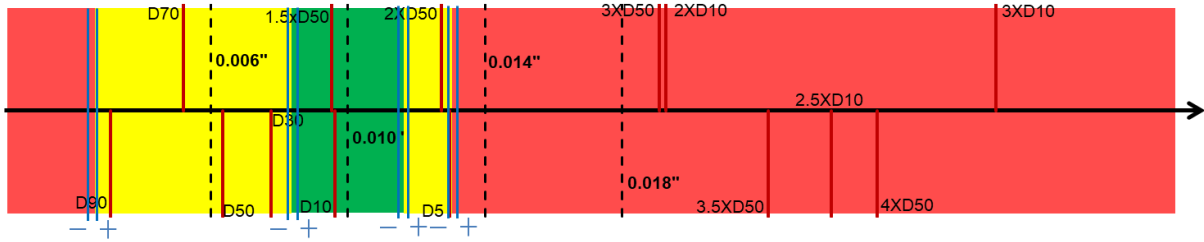
(b)

Figure 5. 15 TLS of DC-II of wire-wrapped screen (a) normal condition, (b) aggressive condition
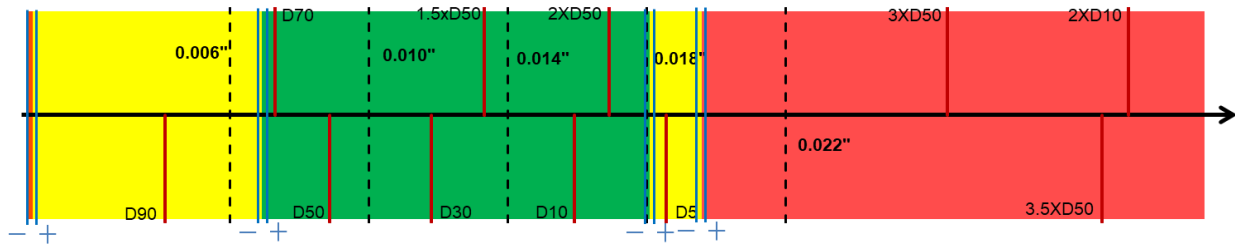
(a)
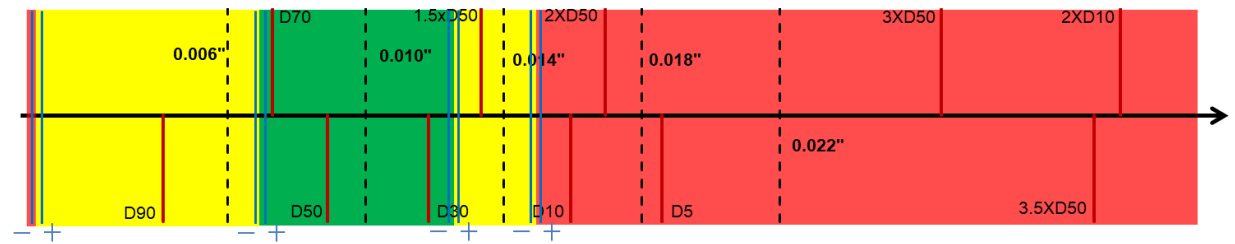
(b)

Figure 5. 16 TLS of DC-III of wire-wrapped screen (a) normal condition, (b) aggressive condition

5.2.3 TLS of Punched Screen

Figures 5.14 through 5.16 show the TLS design criteria for the WWS for DC-I, II, and III, respectively. Like the design criteria of the SL, there is no green zone in DC-I, indicating the PS is not capable of providing desirable performance for DC-I, either. However, there is still a yellow zone in DC-I under the aggressive SAGD condition compared to the SL (Figure 5.17b). This is due to the relatively larger OFA design of the PS. Although the OFA of the PS is not comparable to the WWS, it is still around two times the SL. Thus, precautions are needed to use the PS in dirty formations, like DC-I.
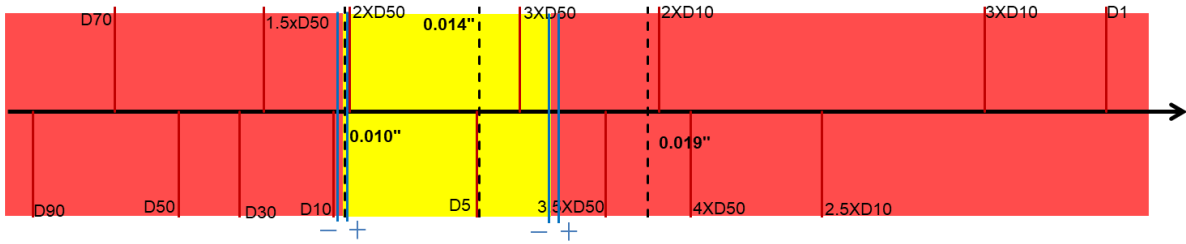
(a)
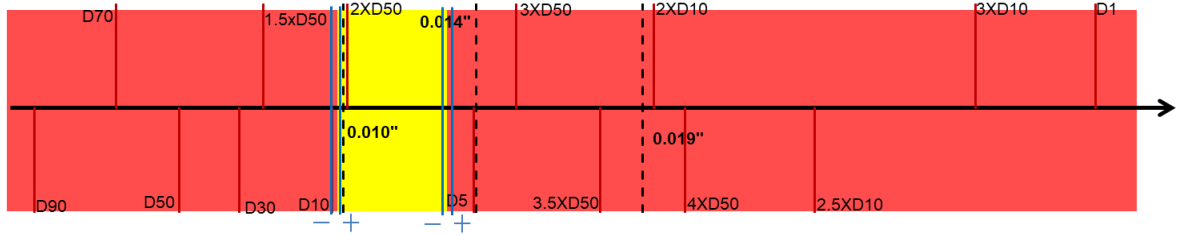
(b)

Figure 5. 17 TLS of DC-I of punched screen (a) normal condition, (b) aggressive condition
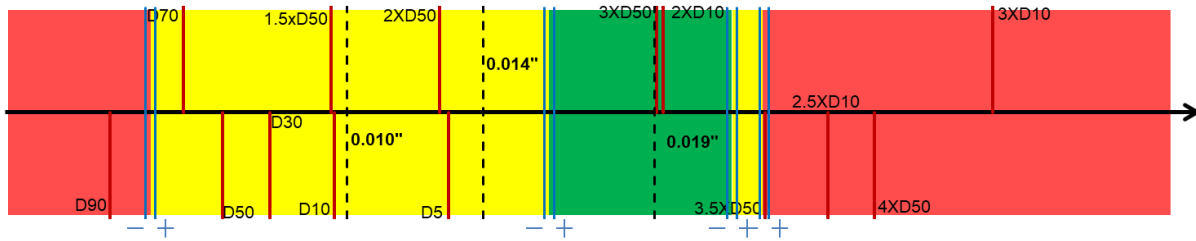
(a)
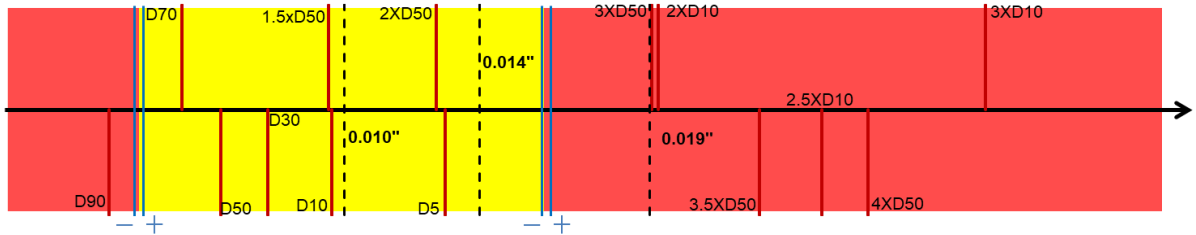
(b)

Figure 5. 18 TLS of DC-II of punched screen (a) normal condition, (b) aggressive condition

(a)

(b)
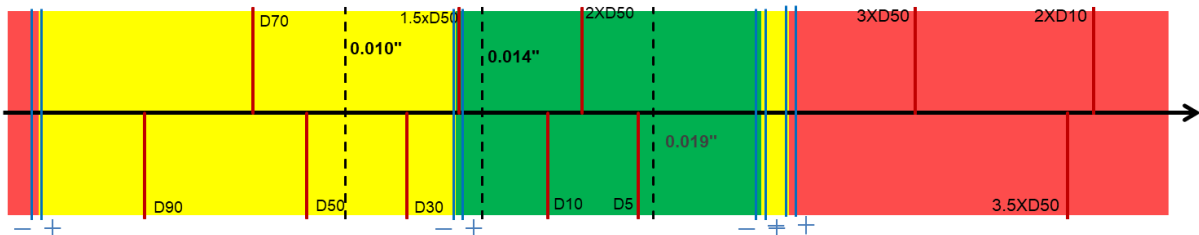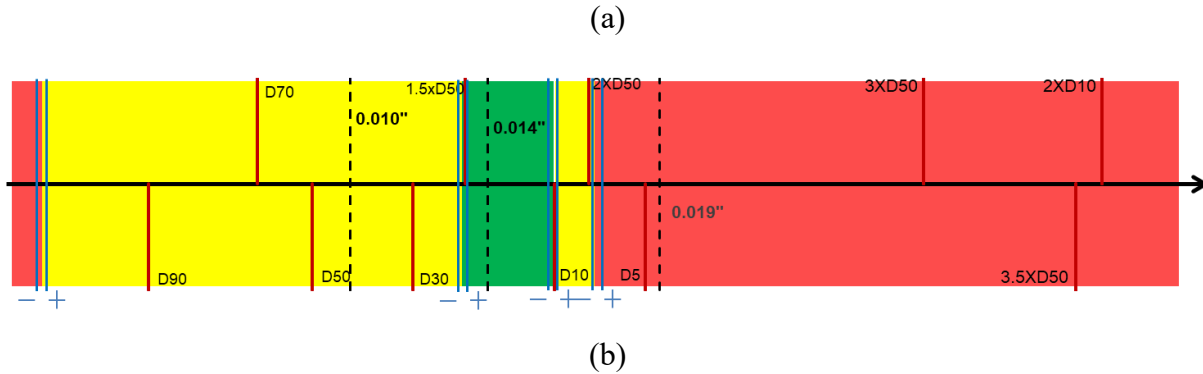
Figure 5. 19 TLS of DC-III of the punched screen (a) normal condition, (b) aggressive condition

5.3 Design Criteria Comparison

This section compares the proposed TLS design criteria with the existing literature criteria for the three PSDs.

5.3.1 Slotted Liner Design Criteria Comparison

Table 5.2 compares the existing design criteria in the literature and the proposed TLS design criteria of the SL.

Table 5. 2 Comparison of the slot size design criteria for slotted liner (all sizes are inches)

PSD	Coberly (1937)	Fermanuik (2013)	Mahmoudi (2017); Wang et al. (2020a)			TLS Criteria		
			SPC 30	SPC 42	SPC 54	SPC 30	SPC 42	SPC 54
DC-I	0.019	0.006-0.018	normal condition			normal condition		
			0.011-0.024	0.008-0.0215	0.007-0.021	0.015-0.017	0.013-0.017	0.0115-0.0165
			aggressive condition			aggressive condition		
			0.0175-0.022	0.014-0.021	0.012-0.020	-	0.013-0.014	0.0115-0.0135
DC-II	0.020	0.010-0.022	normal condition			normal condition		
			0.026	0.025	0.026	0.011-0.0215	0.010-0.022	0.009-0.022
			aggressive condition			aggressive condition		
			0.013-0.021	0.010-0.025	0.011-0.022	0.011-0.0165	0.010-0.016	0.009-0.016
DC-III	0.032	0.014-0.031	normal condition			normal condition		
			0.032	0.0315	0.031	0.006-0.0235	0.005-0.023	0.003-0.023
			aggressive condition			aggressive condition		
			0.026	0.030	0.030	0.006-0.018	0.005-0.0175	0.003-0.017

As per Coberly (1937), the slot size of 2×D10 could form a stable sand arch to prevent sand production for unconsolidated sands. Based on RGL Reservoir Management Inc.'s field

experience, Fermanuik (2013) suggested 2×D70 to 3.5×D50 as the safe design window. However, both criteria are based on one or two points on the PSD curve. Mahmoudi (2017) and Wang et al. (2020) proposed new design criteria for SAGD production wells by conducting single-phase SRT tests. Their criteria considered the PSD curve, slot density, and operational conditions.

Table 5.2 shows that the upper bounds of the design window obtained from the existing design criteria are similar to the same in the proposed criteria for the normal condition. However, for aggressive conditions, the upper bounds from the proposed criteria are much smaller than the same in the existing criteria. This is because, in the new design criteria, the impact of phase change, including water and steam breakthrough on the sand production, is considered. The multi-phase liquid-gas flow condition results in the production of more sand than the single-phase brine flow testing condition. Thus, the upper bound of the design window provides a narrower slot in the new design criteria.

A comparison of the lower bound of the slot size, governed by the plugging level, shows that the lower bounds obtained from the current laboratory testing (single-phase brine or multi-phase) have consistent results. However, the lower bound designed by Fermanuik (2013) seems unreasonable. For example, based on the testing results, the lower bound designed by Fermanuik (2013), which is 0.006'', may not be suitable for DC-I. This can be attributed to insufficient design criteria of 2 times D70 for the lower bound, which neglects the impact of fines content and PSD. The DC-I formation contains a large amount of fines contents, which make it susceptible to plugging. Based on the testing results, if the slot size of 0.006'' is used in DC-I, the retained permeability will be lower than 50%, leading to undesirable flow performance.

5.3.2 Wire-wrapped Screen Design Criteria Comparison

Table 5.3 shows the design criteria comparison of the WWS.

Table 5. 3 Comparison of the aperture size design criteria for the wire-wrapped screen (all sizes are inches)

PSD	Coberly (1937)	Rogers (1937)	Gillespie et al. (2000)	Rule of Thumb	TLS normal condition	TLS aggressive condition
DC-I	0.019	0.008	0.011	0.002-0.014	0.003-0.016	0.003-0.012
DC-II	0.020	0.009	0.014	0.006-0.018	0.002-0.017	0.002-0.013
DC-III	0.032	0.013	0.017	0.010-0.026	0.001-0.019	0.001-0.015

It is found that Coberly's criteria show a larger upper bound compared to other criteria, which may result in undesirable sand production. The rest of the design criteria are close and comparable. The

industrial ad-hoc design criteria seem to be aligned with the TLS criteria at normal SAGD conditions. However, at aggressive SAGD condition, the rule-of-thumb design criteria may not be suitable due to the massive sand production. Also, the lower bound in the proposed TLS criteria is smaller than the current criteria. This is due to the desirable flow performance of the WWS. Even though a narrow aperture size is selected, it can still maintain proper flow performance due to the high OFA characteristics.

5.3.3 Punched Screen Design Criteria Comparison

Table 5.4 shows the design criteria comparison of the PS. There are limited documents in the literature regarding the design criteria of the PS for SAGD purposes. Thus, the general design criteria from Coberly (1937) and Fermaniuk (2013) are used in the comparison.

Table 5. 4 Comparison of the aperture size design criteria for the punched screen (all sizes are inches)

PSD	Coberly (1937)	Fermaniuk (2013)	TLS	
			normal condition	aggressive condition
DC-I	0.019	0.006-0.018	0.009-0.016	0.009-0.013
DC-II	0.02	0.010-0.022	0.004-0.022	0.004-0.016
DC-III	0.032	0.014-0.031	0.003-0.025	0.003-0.017

The comparison results indicate that the upper bound, which is governed by the sanding performance in the proposed TLS design criteria for the PS, is similar to the existing ones under normal SAGD condition. However, the lower bound is smaller than Fermaniuk's criteria. This is due to PS has better flow performance than the SL. Thus, the lower bound can be selected relatively smaller than the SL. Moreover, the upper bound in the aggressive condition is smaller than the existing criteria due to the massive sand production during the steam breakthrough.

5.4 Conclusions

This chapter presents the graphical aperture size design criteria of stand-alone screens using the TLS method. The TLS design criteria are generated based on the testing results of the sand production and retained permeability. The sand production controls the upper bound of the design window, and the retained permeability governs the lower bound.

The design criteria results indicate that the safe design window is affected by the testing conditions. The three-phase testing condition (aggressive SAGD condition) introduces massive sand production, which shrinks the overall safe design window.

The WWS with higher OFA characteristics shows desirable performance in DC-I, while the PS and SL could not provide optimal performance. However, in clean formation, the performance of the PS and the SL is comparable to the WWS.

The design criteria comparison results show that the proposed TLS design criteria are generally aligned with existing design criteria under the normal SAGD condition. However, the upper bound of the TLS of the aggressive SAGD condition is narrower than the existing ones, which is due to the massive sand production observed during the testing.

Chapter 6: Empirical Correlations for Predicting the Safe Aperture Design Window

6.1 Introduction

The experimental pre-packed SRT provides a reliable way to design the safe aperture size. However, the testing process can be time-consuming and expensive. Thus, in this chapter, empirical formations using dimensionless parameters are proposed to formulate the safe aperture size window with influential factors mathematically. The empirical correlations are obtained by curve fitting with the testing data, including sand production and retained permeability. Proposed mathematical correlations can be used to predict the safe aperture size for other PSDs. Details about the empirical correlations build-up are presented in Appendix E.

6.2 Empirical Correlations for the Slotted Liner

6.2.1 Sand Production Correlation

Figure 6.1 compares the cumulative sand production between the pre-packed SRT testing and the proposed empirical correlation for all coupon specifications. In this figure, each group of data points belongs to one certain coupon specification. Also, for each coupon specification, each data point relates to one flow stage, as defined in Figure 3.9. The correlation results overall match against the testing data, indicating good curve fitting results. Equation 6.1 shows the sand production correlation for the SL after curve fitting. Notably, the gas velocity coefficient is immense, meaning the gas velocity plays a significant role in sand production. This agrees with the experiments' observation that massive sand production is observed during the gas breakthrough.
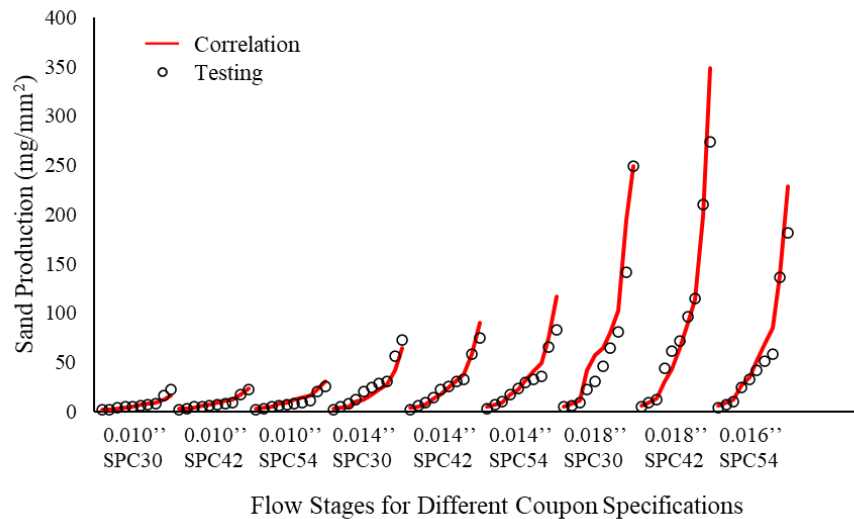
(a)
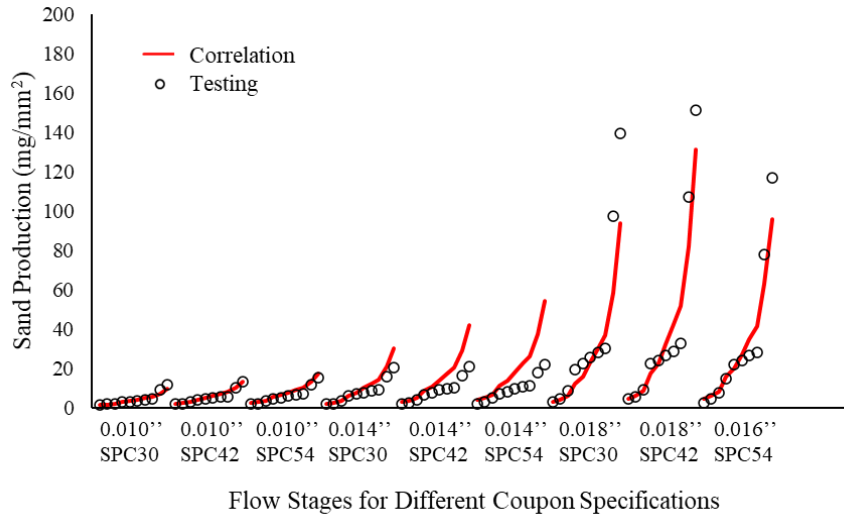
(b)
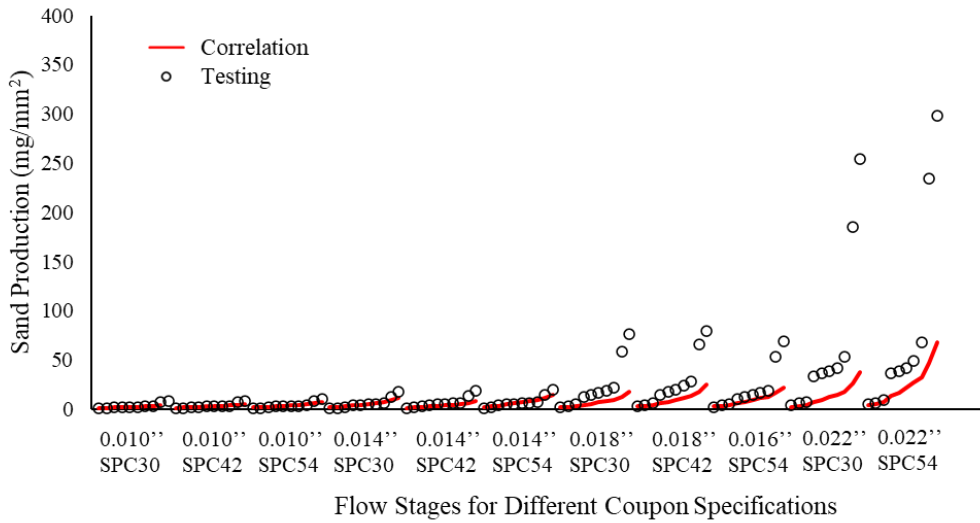
(c)

Figure 6. 1 Sand production comparison result between testing and correlation for slotted liner, (a) DC-I, (b) DC-II, and (c) DC-III

$$P_{sand} = 0.02 \cdot SPC \cdot (8.1x10^{15} \cdot \gamma_w + 5.1x10^{13} \cdot \gamma_o + 6.2x10^{18} \cdot \gamma_g)^{0.11 \cdot \delta} \qquad Eq.(6.1)$$

6.2.2 Retained Permeability Correlation

Figure 6.2 presents the curve fitting results between the retained permeability correlation and testing data for the three PSDs. The x-axis represents different coupon specifications, and the y-axis shows the corresponding retained permeability results, which are obtained at the 100% WC flow condition as described in Figure 4.8. The correlation results show a good agreement with the testing results. Equation 6.2 shows the final retained permeability correlation after the curve fitting process.
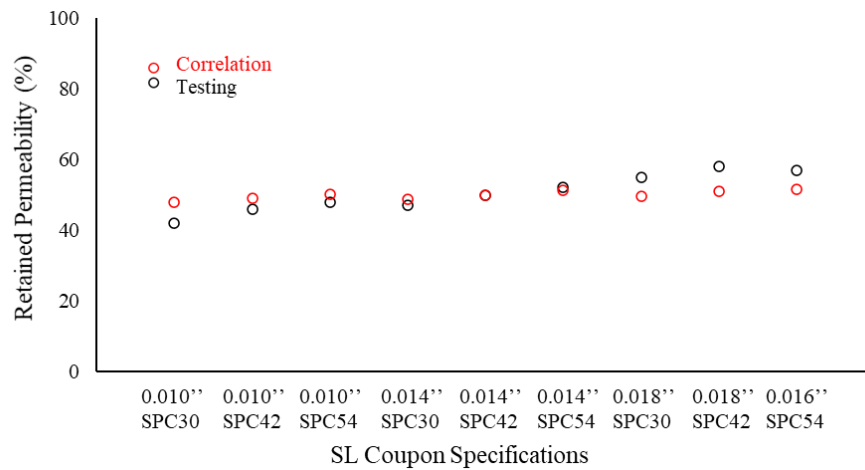
(a)
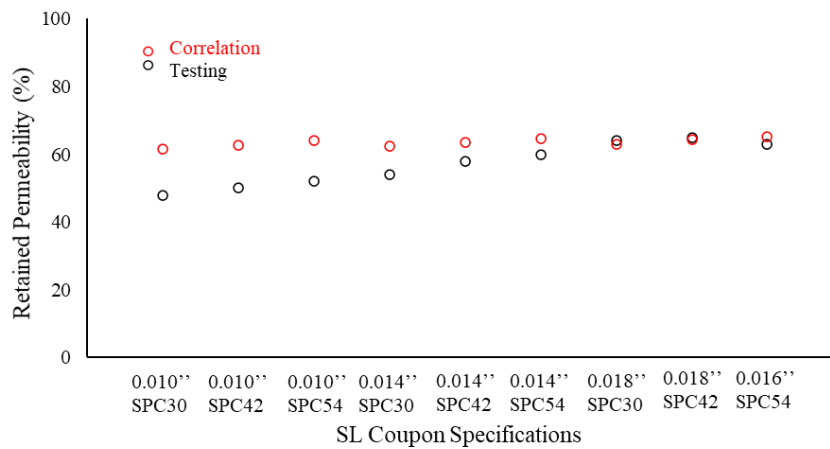
(b)
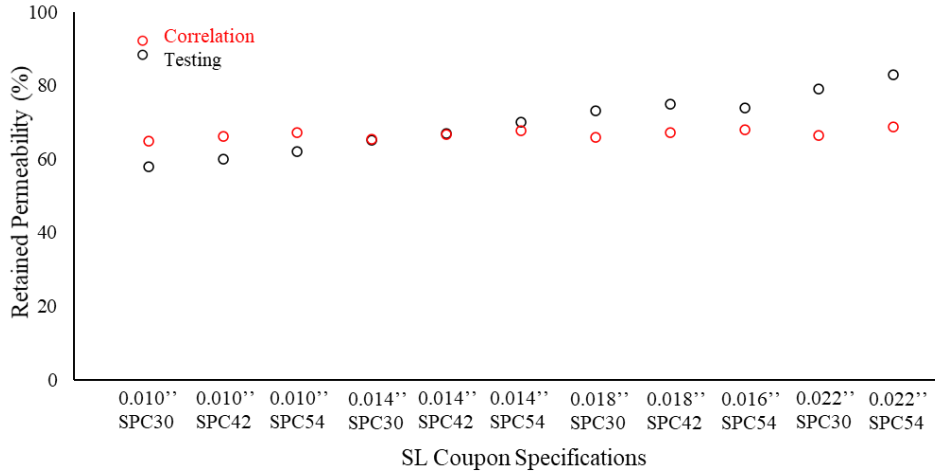
(c)

Figure 6. 2 Retained permeability comparison result between testing and correlation (a) DC-I, (b) DC-II, and (c) DC-III

$$k_{ret} = 71 + 0.1 \cdot SPC + 1.2 \cdot \delta - 2 \cdot \theta \qquad\qquad Eq.\,(6.2)$$

6.2.3 Correlations Validation

Two validation tests are conducted with the same testing procedure after obtaining the empirical correlations for the sand production and retained permeability. Figure 6.3 shows the PSD information about the two new formation sands used for the validation tests. Testing coupons used in New PSD-1 and 2 are SPC 42, 0.014'' and 0.018'', respectively.
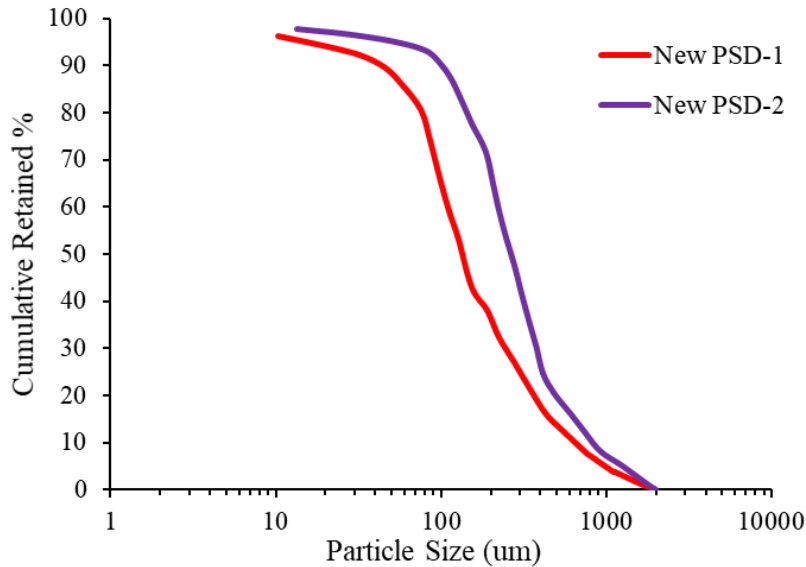
Figure 6. 3 Two new PSDs for validation tests

Figure 6.4 shows the validation results for the two new PSDs based on cumulative sanding. Each data point belongs to one flow stage in the testing. Table 6.2 presents the retained permeability validation results. The retained permeability results of the two new PSDs are also obtained at the 100% WC flow condition. It is found that the correlation results show good agreement with the experiment results, which means proposed correlations are validated.
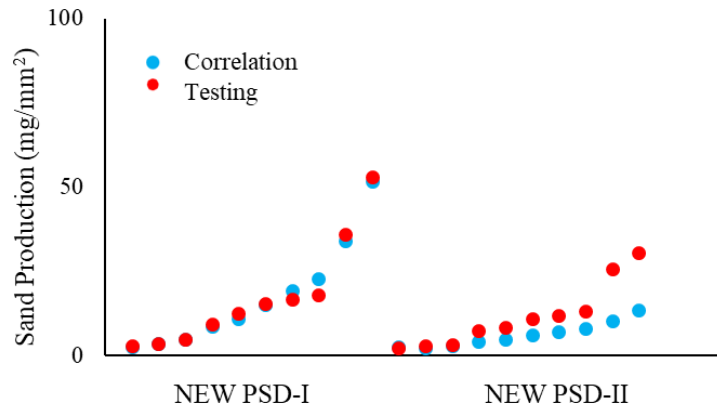
Figure 6. 4 Validation results of sand production for New PSD-1 and New PSD-2

Table 6. 1 Validation results of the retained permeability for New PSD-1 and New PSD-2

	predicted k_{ret} (%)	experimental k_{ret} (%)	Error (%)
New PSD-1	57	58	1
New PSD-2	68	76	8

6.2.4 Correlations for Slot Size Window

After model validation, proposed empirical correlations can be used to design the proper slot size window by setting limits to sand production and retained permeability. The sand production determines the upper bound of the window, and the retained permeability decides the lower bound. In the literature, sand production of 0.15 lb/ft^2 and retained permeability of 50% have been used as the stand-alone screen design criteria guideline (Hodge et al., 2002). Thus, by setting P_{sand}= 73 mg/mm^2 (0.15 lb/ft^2) in Equation 6.1 and k_{ret}=50% in Equation 6.2. Below, two equations (Equations 6.3 and 6.4) give the mathematical models for designing the optimal slot size window.

$$W_{ub} = \frac{74.6 \cdot D_{50}}{ln \, [SPC \cdot (8.1x10^{15} \cdot \gamma_w + 5.1x10^{13} \cdot \gamma_o + 6.2x10^{18} \cdot \gamma_g)]} \qquad Eq. (6.3)$$

$$W_{lb} = (1.67\theta - 0.08SPC - 17.5) \cdot D_{50} \qquad Eq. (6.4)$$

6.3 Empirical Correlations for the Wire-wrapped Screen

Similar to the correlation of the SL, this section introduces the empirical correlation for the WWS to predict the safe aperture window.

6.3.1 Sand Production Correlation

Figure 6.5 shows the curve fitting results of the sand production for the WWS. The corresponding correlation is given in Equation 6.5.
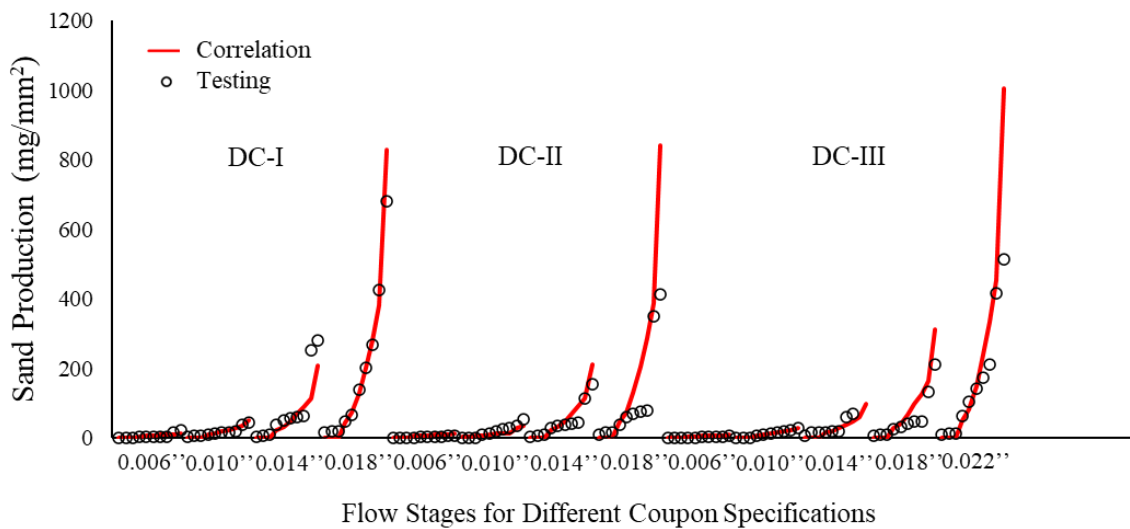
Figure 6. 5 Sand production comparison result between testing and correlation for the wire-wrapped screen

$$P_{sand} = 1.62 \cdot (3.9x10^{14} \cdot \gamma_w + 5.6x10^8 \cdot \gamma_o + 1.3x10^{17} \cdot \gamma_g)^{0.16 \cdot \delta} \qquad Eq. (6.5)$$

6.3.2 Retained Permeability Correlation

Figure 6.6 presents the curve fitting results of the retained permeability for the WWS. Equation 6.6 shows the retained permeability correlation obtained by the curve fitting process.
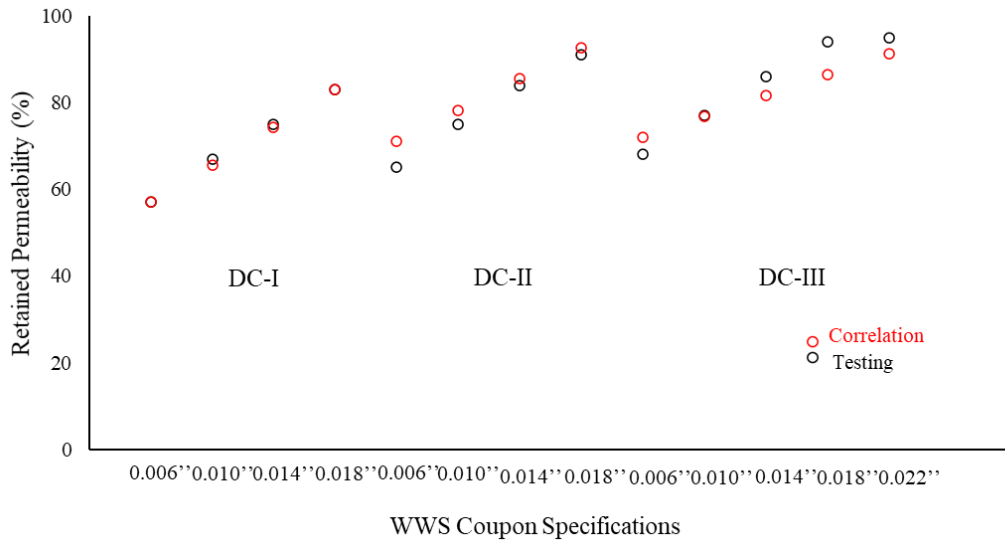
Figure 6. 6 Retained permeability comparison result between testing and correlation for the wire-wrapped screen

$$k_{ret} = 77 + 10.8 \cdot \delta - 2.3 \cdot \theta \qquad\qquad Eq.\,(6.6)$$

6.3.3 Correlations Validation

Figure 6.7 and Table 6.3 shows the validation results between the correlations and the experimental results, respectively. Testing coupons used in New PSD-1 and 2 are 0.014'' and 0.018''. The testing results are aligned with the correlation results indicating the correlations are validated.
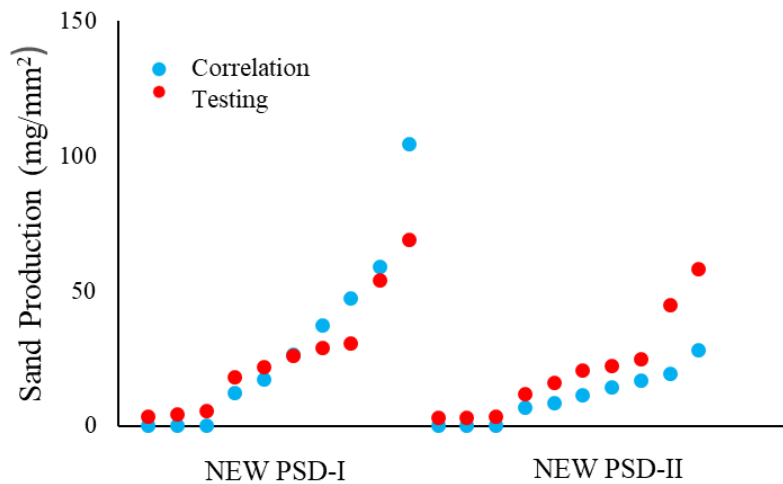
Figure 6. 7 Validation results of sand production for New PSD-1 and New PSD-2

109

Table 6. 2 Validation results of the retained permeability for New PSD-1 and New PSD-2

	predicted k_{ret} (%)	experimental k_{ret} (%)	Error (%)
New PSD-1	81	78	3
New PSD-2	85	90	5

6.3.4 Correlations for Aperture Window

Equation 6.7 and 6.8 show the upper and lower bounds of the safe aperture window obtained from the empirical correlations, respectively.

$$W_{ub} = \frac{23.8 \cdot D_{50}}{ln\,[(3.9x10^{14} \cdot \gamma_w + 5.6x10^8 \cdot \gamma_o + 1.3x10^{17} \cdot \gamma_g)]} \qquad Eq.\,(6.7)$$

$$W_{lb} = (0.38\theta - 3.85) \cdot D_{50} \qquad Eq.\,(6.8)$$

6.4 Empirical Correlations for the Punched Screen

This section introduces the empirical correlations for the PS.

6.4.1 Sand Production Correlation

Figure 6.8 shows the curve fitting results of the sand production for the PS. The corresponding correlation is given in Equation 6.9.
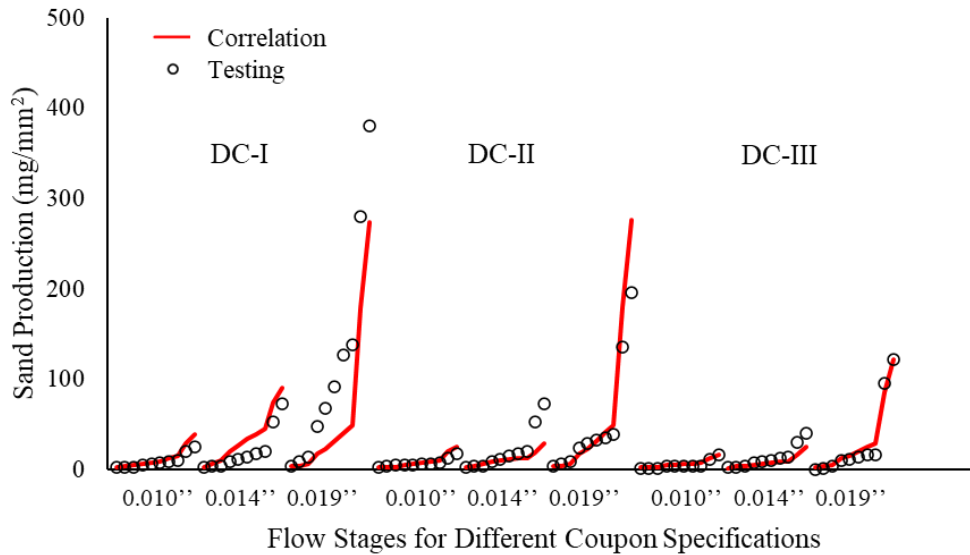
Figure 6. 8 Sand production comparison result between testing and correlation for the punched screen

$$P_{sand} = 1.77 \cdot (2.1x10^{15} \cdot \gamma_w + 4.2x10^{12} \cdot \gamma_o + 2.7x10^{19} \cdot \gamma_g)^{0.08 \cdot \delta} \qquad Eq.\,(6.9)$$

6.4.2 Retained Permeability Correlation

Figure 6.9 presents the curve fitting results of the retained permeability for the PS. Equation 6.10 shows the retained permeability correlation obtained by the curve fitting process.
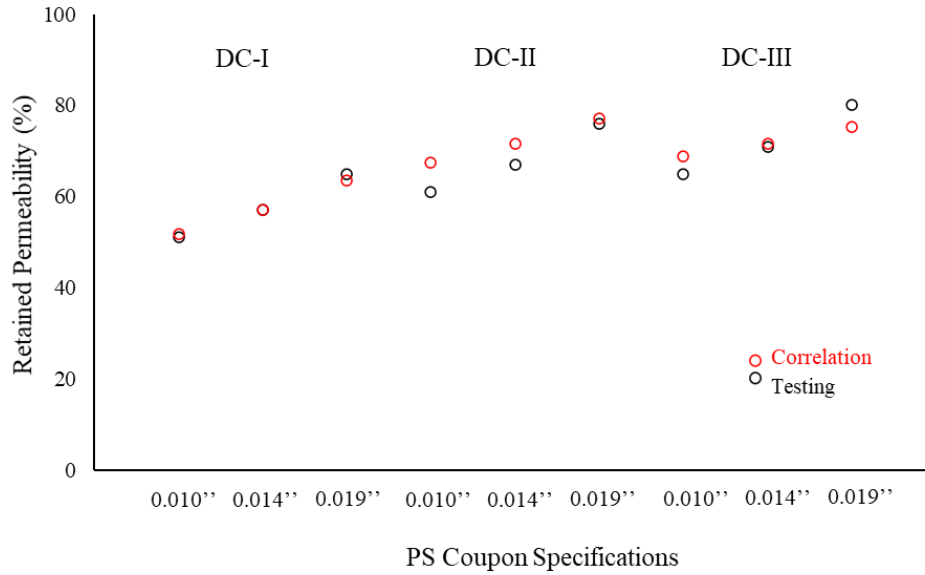
Figure 6. 9 Retained permeability comparison result between testing and correlation for the punched screen

$$k_{ret} = 75 + 6.5 \cdot \delta - 2.5 \cdot \theta \qquad\qquad Eq.\,(6.10)$$

6.4.3 Correlations Validation

Testing coupons used in validation tests for the New PSD-1 and 2 are 0.014'' and 0.019''.
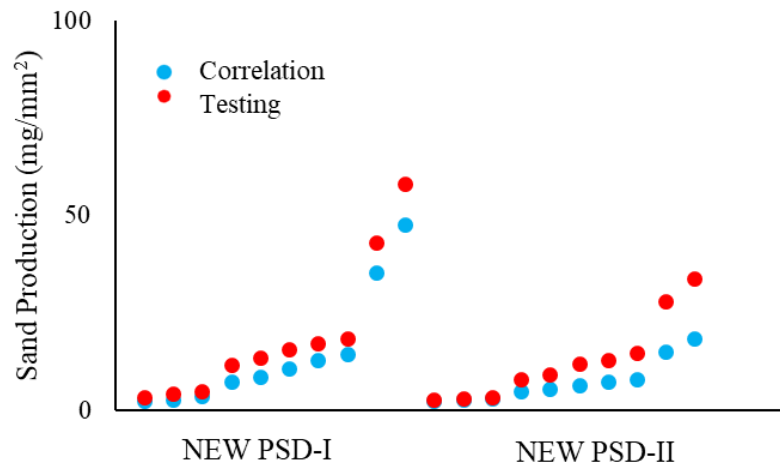
Figure 6. 10 Validation results of sand production for New PSD-1 and New PSD-2

Table 6. 3 Validation results of the retained permeability for New PSD-1 and New-PSD-2

	predicted k_{ret} (%)	experimental k_{ret} (%)	Error (%)
New PSD-1	65	64	1
New PSD-2	74	82	8

6.4.3 Correlations for Aperture Window

Equation 6.11 and 6.12 show the upper and lower bounds of the safe aperture window obtained from the empirical correlations, respectively.

$$W_{ub} = \frac{46.5 \cdot D_{50}}{ln\left[(2.1x10^{15} \cdot \gamma_w + 4.2x10^{12} \cdot \gamma_o + 2.7x10^{19} \cdot \gamma_g)\right]} \qquad Eq.(6.11)$$

$$W_{lb} = (0.21\theta - 2.5) \cdot D_{50} \qquad Eq.(6.12)$$

6.5 Conclusion

This chapter introduces empirical correlations with dimensionless parameters to predict the safe aperture window mathematically. The sand production controls the correlation corresponding to the upper bound of the safe aperture window, and the low bound corresponding correlation is governed by the retained permeability. The empirical correlations are obtained from testing results through the curve fitting process. After curve fitting, pre-packed SRT with another two PSDs are conducted to validate the proposed correlations. Next, after applying sanding and flow performance limits to proposed equations, the correlations corresponding to the safe aperture window are obtained. Finally, it shall mention the applicability of the empirical formulations. Since the pre-packed SRT testing procedure is designed for the SAGD production wells, proposed empirical correlations are oriented and validated specifically for the SAGD operation conditions.

Chapter 7: Formation Damage Characterization of Stand-alone Screens

7.1 Introduction

Retained permeability is used to characterize the level of the formation damage. The formation damage causes additional pressure drop compared to the no damage condition. Two factors are contributing to such additional pressure drop ($\Delta P_{formation\,damage}$), namely, flow convergence ($\Delta P_{flow\,convergence}$) and fines migration ($\Delta P_{fines\,migration}$). The total pressure drop (ΔP_{total}) can be obtained from ΔP_{linear} using the retained permeability values from the testing. The ΔP_{linear} is the theoretical single-phase pressure drop for linear flow without formation damage, obtained by Darcy's equation. Since the retained permeability only describes the ΔP_{total} , the $\Delta P_{flow\,convergence}$ and $\Delta P_{fines\,migration}$ cannot be characterized and assessed individually. Thus, single-phase flow numerical CFD models are conducted for each screen to characterize the $\Delta P_{flow\,convergence}$ as the numerical models are independent of the impact of fines migration. The $\Delta P_{flow\,convergence}$ can be obtained by comparing the pressure drop from the simulation ($\Delta P_{simulation}$) with ΔP_{linear}. The difference is the pressure drop due to the flow convergence. Then, the $\Delta P_{fines\,migration}$ can be obtained by subtracting the $\Delta P_{flow\,convergence}$ from the $\Delta P_{formation\,damage}$. The formation damage characterization procedure is briefly summarized as: (1) build CFD models for each screen, (2) calibrate CFD models with Darcy's Law and obtain the $\Delta P_{flow\,convergence}$ in the near-screen zone, (3) calculate the $\Delta P_{fines\,migration}$ by deducting the $\Delta P_{flow\,convergence}$ from the $\Delta P_{formation\,damage}$ obtained by the retained permeability. Details of the numerical CFD modelling and formation damage characterization are described in the following sections.

7.2 General CFD Model Description

This section describes the general information of numerical modelling. Commercial CFD software package CFX, ANSYS 2020R1, is used to build numerical models for the SL (SPC 54), WWS, and PS. The geometry of the CFD model is designed based on the experimental pre-packed SRT facility. The aperture size used in the CFD models is 0.014'' for all screens.

7.2.1 CFD Modelling

Figure 7.1 shows the numerical model for the SL. Figure 7.2 shows a zoomed view of the slots. The model consists of two domains: one is the porous media domain, the other one is the fluid domain. The fluid domain includes the slots part and the outlet part.
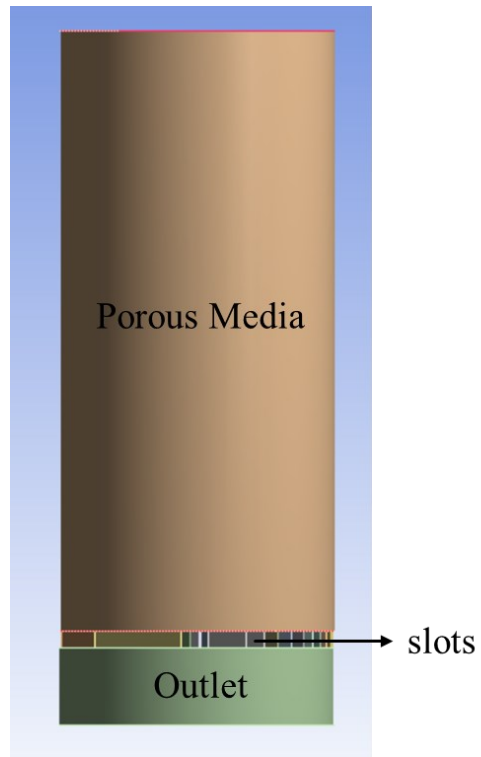
Figure 7. 1 Example of the CFD model
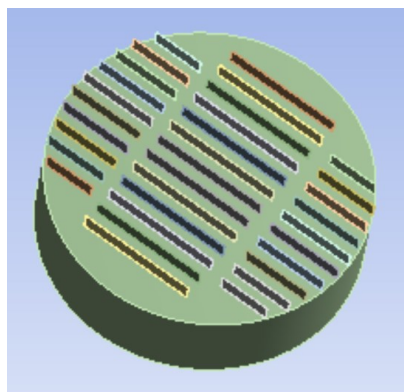
Figure 7. 2 Zoomed view of the slots

7.2.1.1 Theory

The mathematical governing equations to describe the fluid flow in the slots and pipe are shown in Equations 7.1 and 7.2. Equation 7.1 is the continuity equation (mass conservation), and Equation 7.2 is the momentum equation (Navier-Stokes Equation) for steady-state, incompressible fluid, laminar flow, and isothermal condition.

$$\frac{\partial \rho}{\partial t} + \nabla \cdot (\rho \vec{v}) = 0 \qquad\qquad Eq.\,(7.1)$$

$$\rho \frac{\partial \vec{v}}{\partial t} + \rho \vec{v} \cdot grad\,(\vec{v}) = div\,(\vec{T}) + \rho \vec{b} \qquad\qquad Eq.\,(7.2)$$

Darcy's Law governs the fluid flow in the porous media domain. Equation 7.3 shows Darcy's equation, where k is the permeability of the porous media domain.

$$\nabla P = -\frac{\mu}{k} \vec{v} \qquad\qquad Eq.\,(7.3)$$

7.2.1.2 Numerical Settings

Table 7.1 presents the numerical settings of the CFD simulation for all stand-alone screens with DC-III as an example, including boundary conditions, porosity, permeability, advection scheme, and convergence criteria.

Table 7. 1 General Numerical Settings

inlet boundary	7200 cc/hr
outlet boundary	0 kPa
fluid property	water
viscosity	1 cp
porosity	0.35
permeability	2.4 Darcy
advection	higher resolution
convergence criteria	RMS 1e-6

7.2.2 Details of CFD Modeling

In this section, details of the CFD models for each screen are presented, such as mesh size, local refinement, and mesh sensitivity analysis.

7.2.2.1 Slotted Liner Modeling

Meshing

Figure 7.3 presents the meshing results of the SL model. The general maximum mesh size is 0.0025 meters. Since the near-screen zone is the target area, where the fluid flow starts to converge, a local refinement is added to this section. The mesh size in the local refinement is 0.0022 meters at the interface between the cell and the slots. The locally refined mesh has a 1.2 growth rate towards the main body of the cell, which allows a smooth transition from the main cell to the slots. The influential length of the local refinement is 0.05 meters. Also, the slots with narrow features need local refinement to the mesh size. A mesh size of 0.0022 meters is applied to the slots. Figure 7.4 shows a zoomed view of the meshing results for the slots. Finally, the outlet section is locally refined as well due to the fluid direction change after the fluid exits from the slots to an open channel. Like the near-screen zone, the mesh size at the interface between the slots and the outlet is 0.0022 meters. The growth rate is 1.2, and the influential length is 0.02 meters.
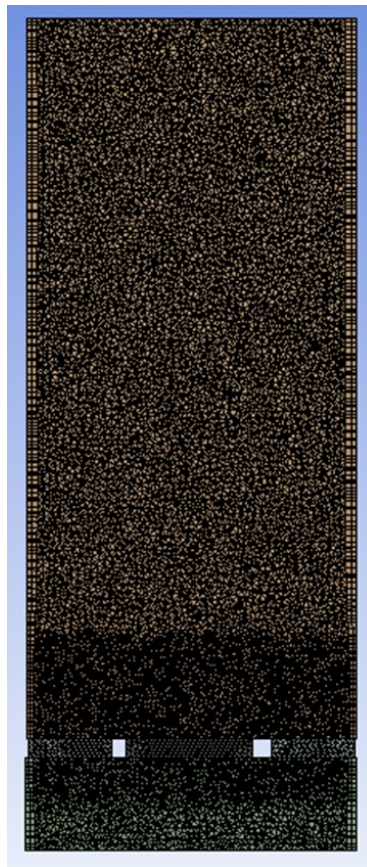
Figure 7. 3 Meshing results for the slotted liner model
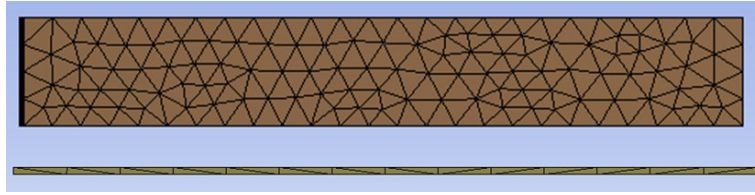
Figure 7. 4 Mesh refinement for the slots

Simplified Slotted Liner Model

The narrow characteristic and larger number of slots require extremely small mesh sizes for the accuracy of the numerical model, which tremendously increases the computational time. Since the objective of the CFD model is to understand the fluid dynamics in the near-screen zone, a simplified model is proposed, which focuses on the near-screen zone. Instead of having numerous narrow slots in the modelling, this simplified model uses surface slots on the outlet of the cell, as shown in Figure 7.5. The surface slots have the same feature in terms of slot size and slot density. The only difference is that the surface slots are 2D, while the real slots are one inch in height.
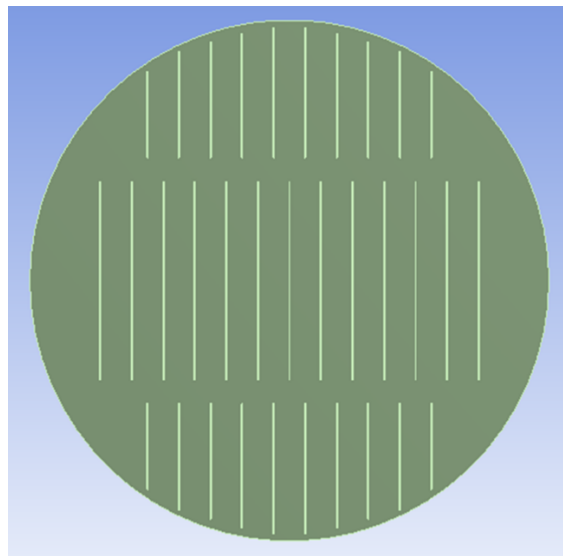
Figure 7. 5 Simplified Slotted Liner Model

A comparison study between the simplified model and the original model is done to prove the validity of the simplified model. In this comparison, both models have identical mesh size, local refinement, boundary conditions, and any other numerical settings. Velocity, pressure, and pressure gradient data are used to compare the two models. The data points are obtained from the line in the center of the model, as shown in Figure 7.6. Figures 7.7 through 7.9 present the

117

simulation results comparing velocity, pressure, and the pressure gradient between the two models, respectively. It can be found that the simulation results of the simplified model are in good agreement with the original model. Thus, it can replace the original model and be used in actual simulation to reduce unnecessary extensive computational time.
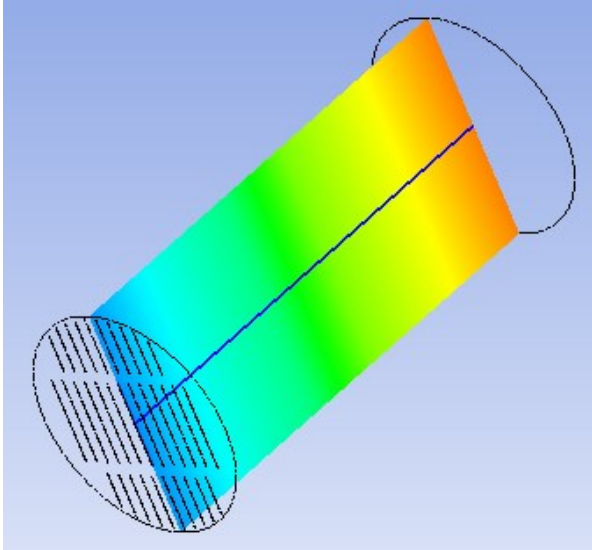
Figure 7. 6 Line location for the data points
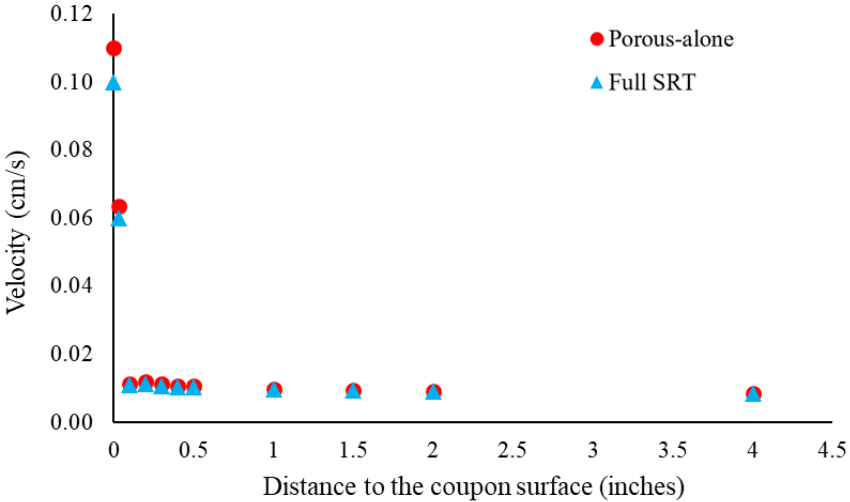
Figure 7. 7 Velocity data comparison results
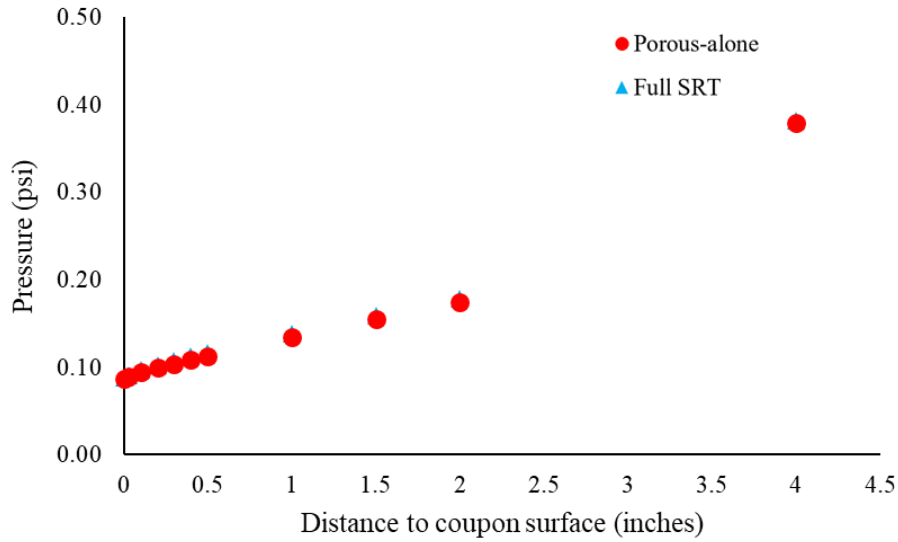
Figure 7. 8 Pressure data comparison results
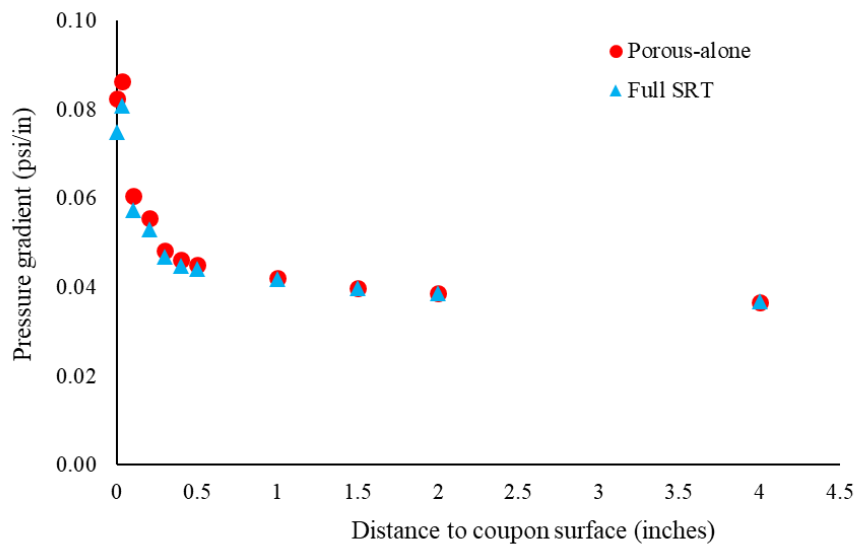
Figure 7. 9 Pressure gradient data comparison results

Mesh Sensitivity Analysis

A mesh dependent study is conducted to examine if the mesh size used in the simulation is in the asymptotic region. Velocity, pressure, and pressure gradient data in the same locations from six models with different mesh sizes are used to judge the grid independence. Table 7.2 shows the seven models with different mesh sizes. The statistical data of the mesh number are also provided.

Table 7. 2 Mesh sensitivity sizes of the slotted liner

Mesh Size (meter)	0.0021	0.0025	0.003	0.0036	0.0043	0.0051	0.006
Element Number	8932763	5303208	3105264	1807190	1069111	639637	392909

Figure 7.10 shows the velocity results at different vertical distances above the coupon. The data are extracted from the centerline, as shown in Figure 7.6. Figures 7.11 and 7.12 present the pressure drop of the near-screen zone (0-5.08 cm) and total pressure drop results of the mesh sensitivity analysis, respectively. It is clearly shown that grid independence is achieved with the last three consecutive mesh sizes. The mesh size of 0.0025 meters is used in the actual simulation.
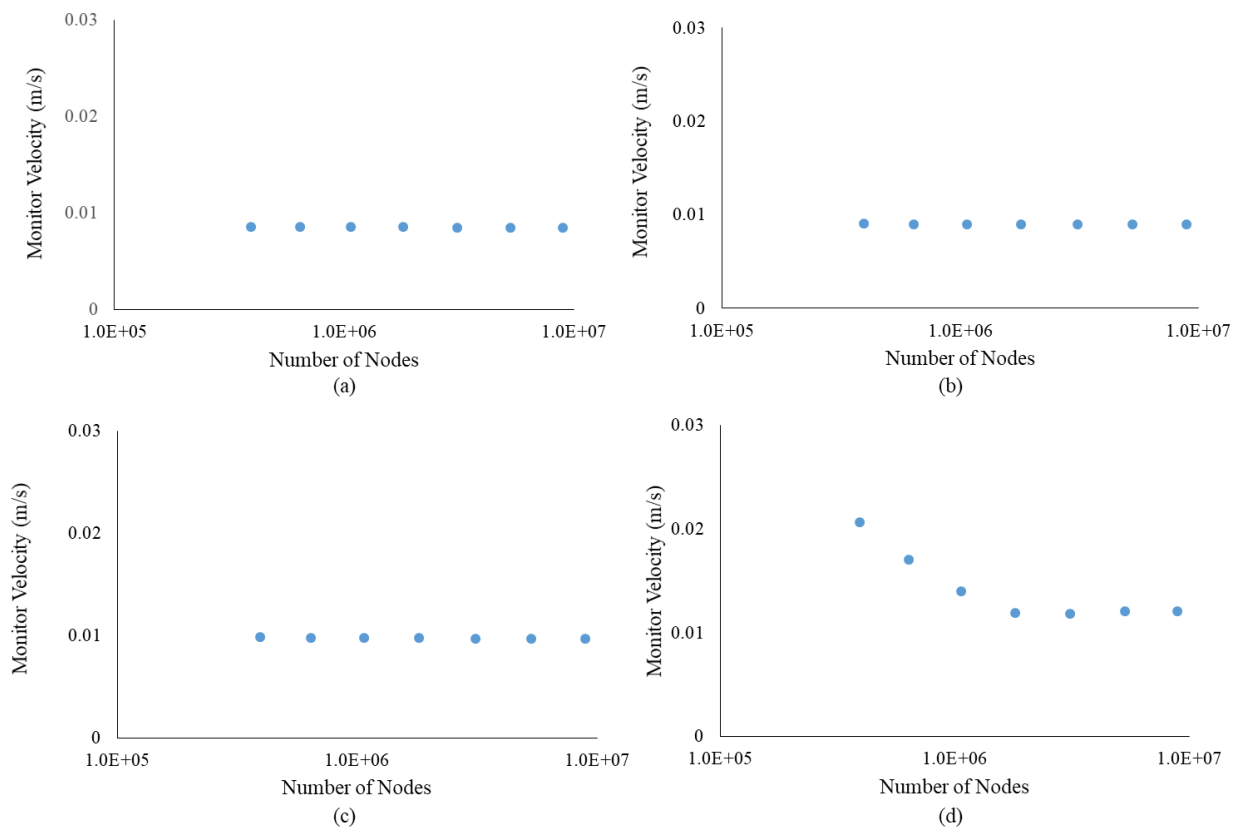
Figure 7. 10 Mesh sensitivity of Velocity data comparison of different vertical distance (a) 7.5'', (b) 2'', (c) 1'', and (d) 0.1'' for slotted liner

120
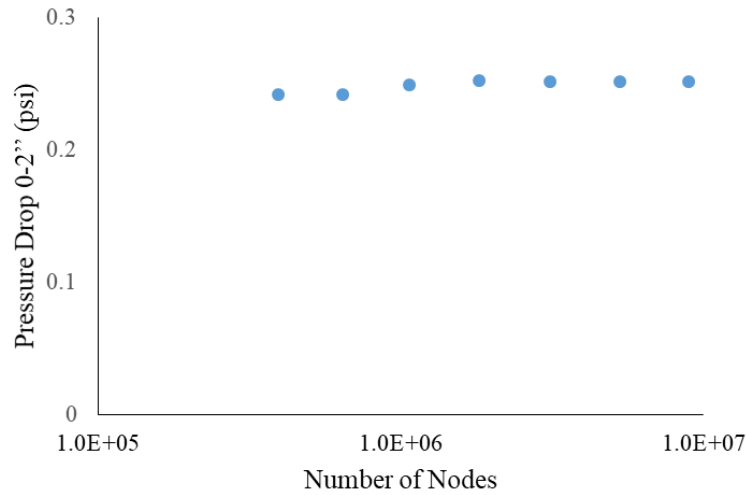
Figure 7. 11 Mesh sensitivity of pressure drop in near-screen zone data comparison for slotted liner
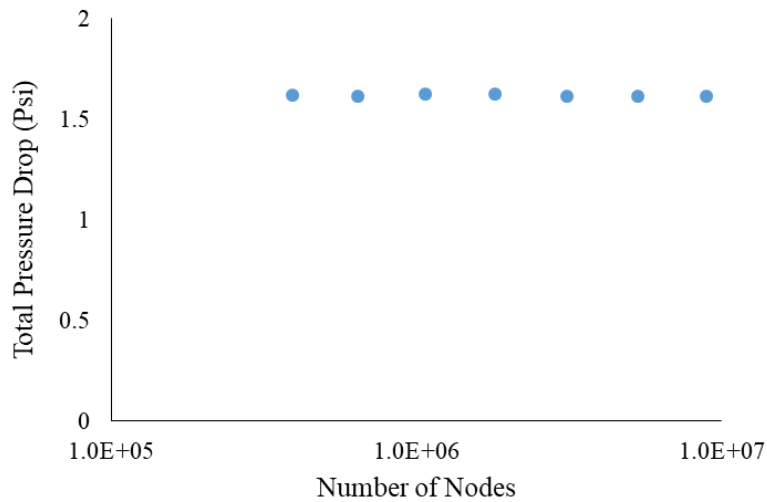
Figure 7. 12 Mesh sensitivity of total pressure drop data comparison for slotted liner

7.2.2.2 Wire-wrapped Screen Modeling

Like the simplified SL model, a simplified model is designed for the WWS. The WWS has more slots, which requires more unnecessary computational time. The simplified WWS could save significant computational time for this purpose. Figure 7.13 presents simplified WWS geometry. The 2D apertures are built on the surface of the outlet.
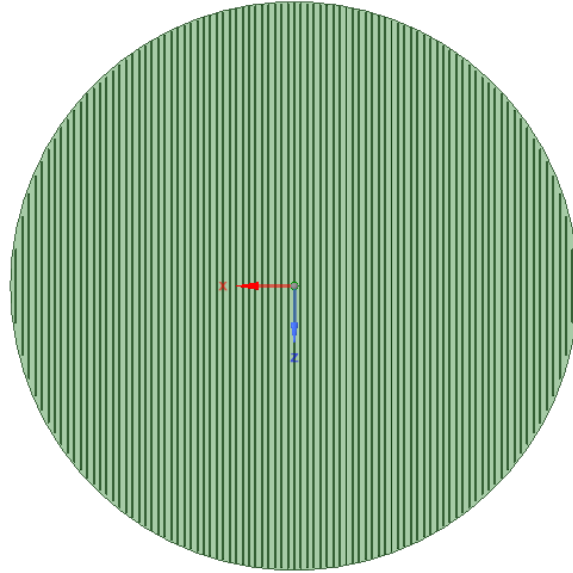
Figure 7. 13 Geometry of the simplified wire-wrapped screen model

Meshing

Figure 7.14 shows the meshing results of the model. The general maximum mesh size is 0.0025 meters. Local refinement is applied to the near-screen zone to capture the flow convergence phenomenon more accurately. The mesh size in the local refinement is 0.0022 meters at the outlet surface. The locally refined mesh has a 1.2 growth rate towards the main body of the cell, which allows a smooth transition from the main cell to the slots. The influential length of the local refinement is 0.05 meters.
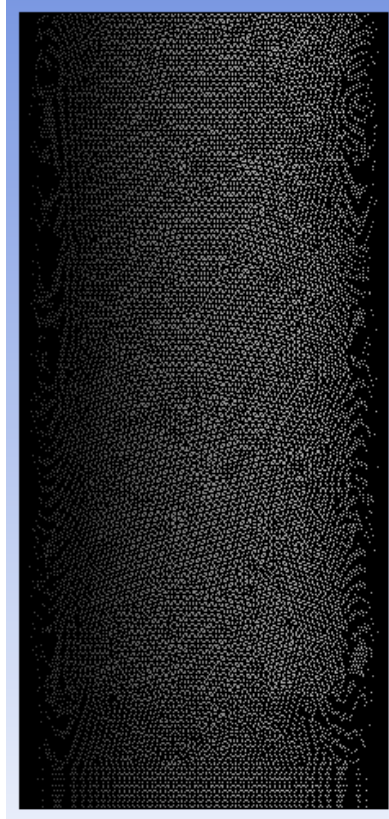
Figure 7. 14 Meshing results of the simplified wire-wrapped screen model

Mesh Sensitivity Analysis

Grid independence analysis is also done for the WWS model. Velocity, pressure, and pressure gradient data in the same locations from six models with different mesh sizes are used to judge the mesh sensitivity. Table 7.3 shows the seven models with varying sizes of mesh. The statistical data of the mesh number are also provided. Figures 7.15 through 7.17 demonstrates the mesh sensitivity analysis results. It is found that the asymptotic region is achieved within the three smallest mesh sizes. The mesh size of 0.0025 meters is used in the actual simulation.

Table 7. 3 Mesh sensitivity sizes of wire-wrapped screen

Mesh Size (meter)	0.0021	0.0025	0.003	0.0036	0.0043	0.0051	0.006
Element Number	8951579	5323520	3128122	1829464	1086819	659342	408947
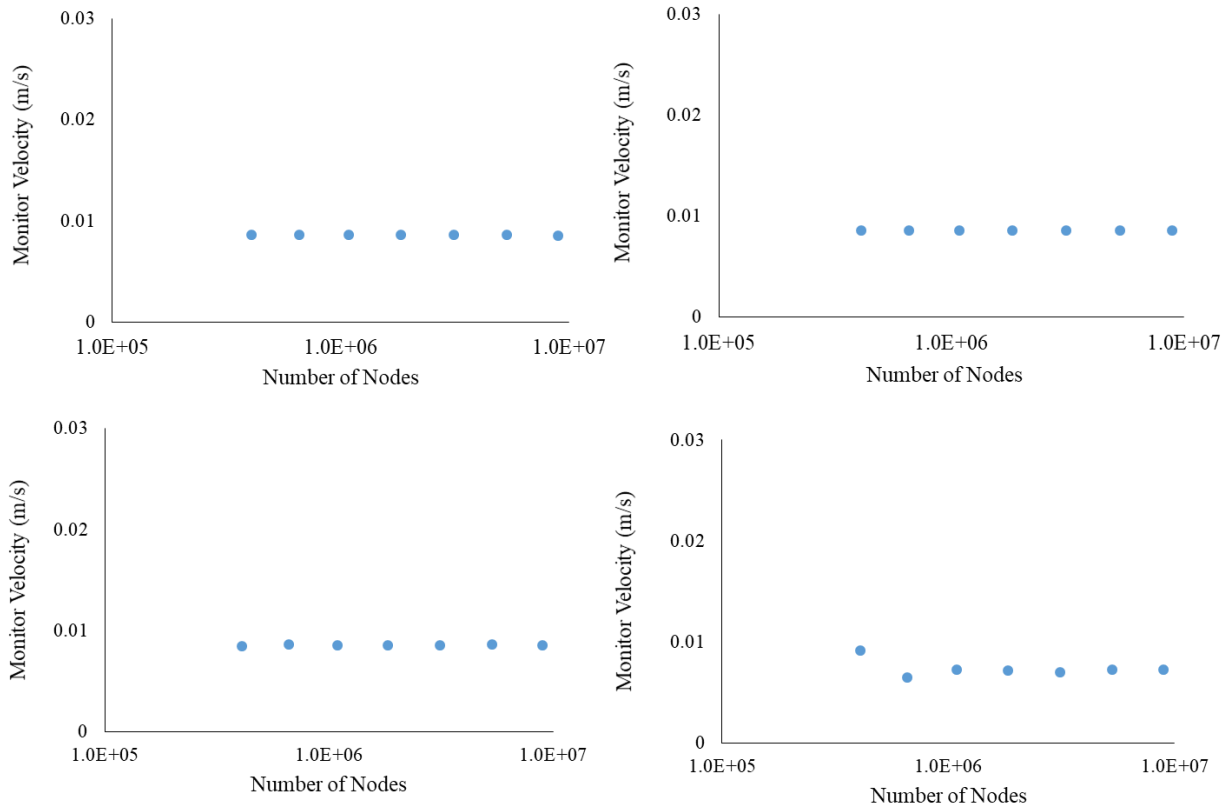
Figure 7. 15 Mesh sensitivity of Velocity data comparison of different vertical distance (a) 7.5'', (b) 2'', (c) 1'', and (d) 0.1'' for the wire-wrapped screen
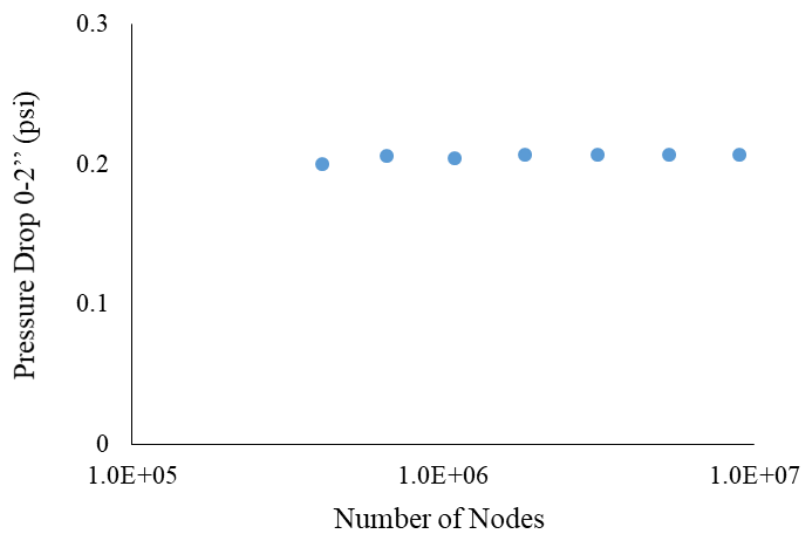
Figure 7. 16 Mesh sensitivity of pressure drop in near-screen zone data comparison for the wire-wrapped screen
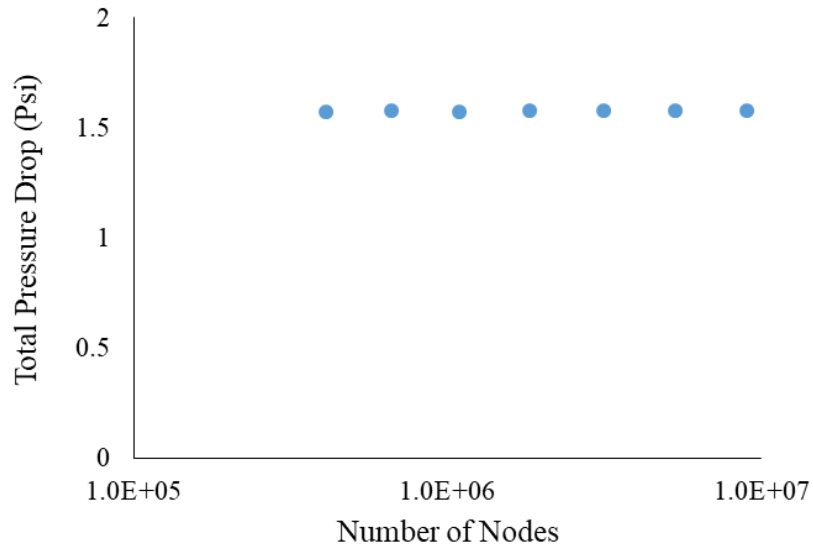
Figure 7. 17 Mesh sensitivity of total pressure drop data comparison for the wire-wrapped screen

7.2.2.3 Punched Screen Model

For the PS, the aperture openings are on the sides of each punched pit. Thus, the flow direction needs to turn around 90 degrees to exit from the aperture openings. Due to the unique geometry design in the PS, the simplified model cannot capture the flow direction change with 2D surface apertures. Hence, a full-scale model coupled with a porous media domain (cell) with a fluid domain (punched slots) is necessary. However, some simplifications can still be done to reduce unnecessary computational time. As shown in the experimental setup section, the pre-packed SRT cell and punched screen coupon are symmetric. Therefore, a quarter of the full-scale model can be built and used in the simulation. Figure 7.18 shows the geometry of the quarter PS model.
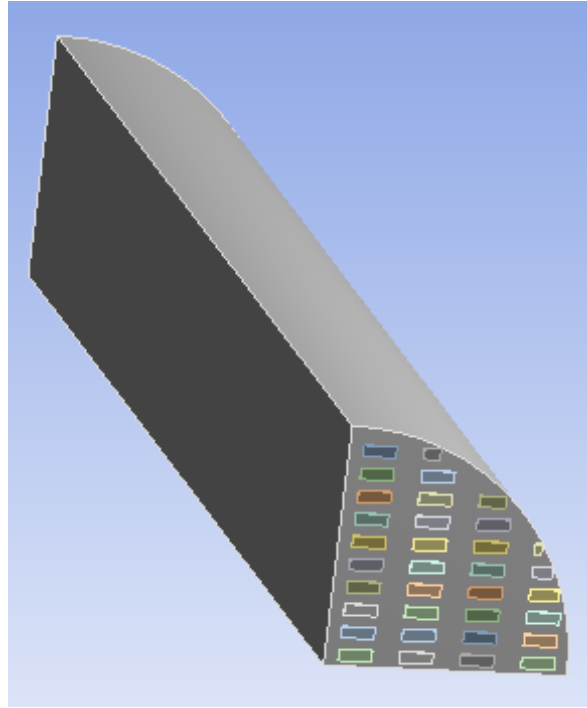
Figure 7. 18 Quarter punched screen model

Meshing

Figure 7.19 presents the meshing results of the PS model. The general maximum mesh size is 0.002 meters. The mesh size in the local refinement is 0.0015 meters at the interface between the cell and the punched slots. The locally refined mesh has a 1.2 growth rate and 0.05 meters influential length. Also, the punched slots with narrow features are further refined with a mesh size of 0.0015 meters.

(a)   (b)
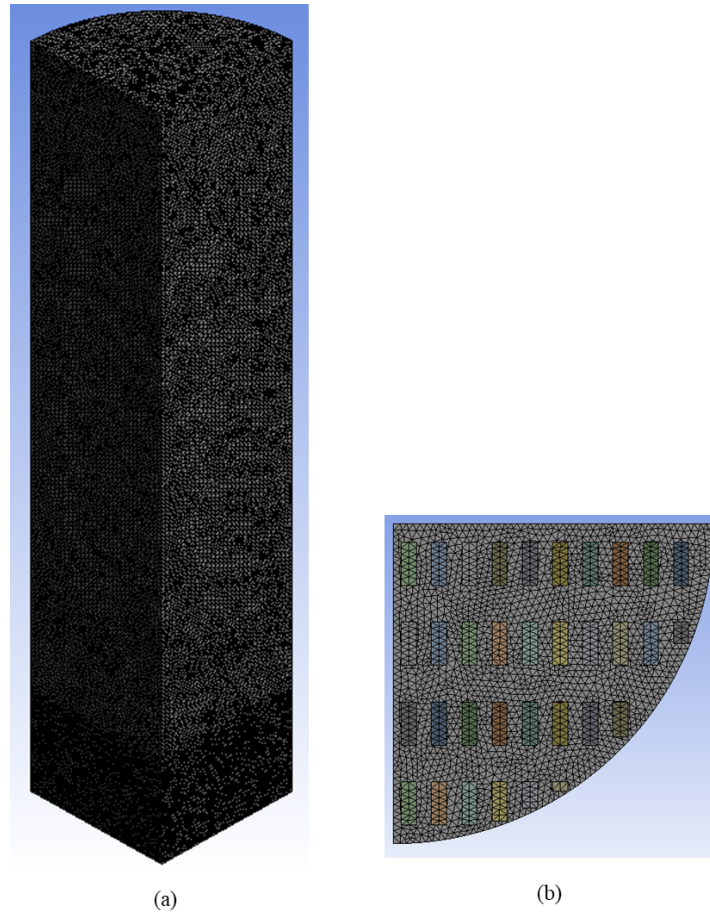
Figure 7. 19 Meshing results of (a) the punched screen model, and (b) punched slots

Mesh Sensitivity Analysis

Figure 7.20 presents the line location from where the data points are extracted. Table 7.6 presents different mesh sizes used in the mesh sensitivity analysis and Figures 7.21 through 23 show the results. From the results, it proves that grid independence is achieved within the three smallest meshes.

Table 7. 4 Mesh sensitivity sizes of punched screen

Mesh Size (meter)	0.0020	0.0024	0.0029	0.004	0.0048	0.0057
Element Number	2042956	1186557	697120	310438	151452	90517
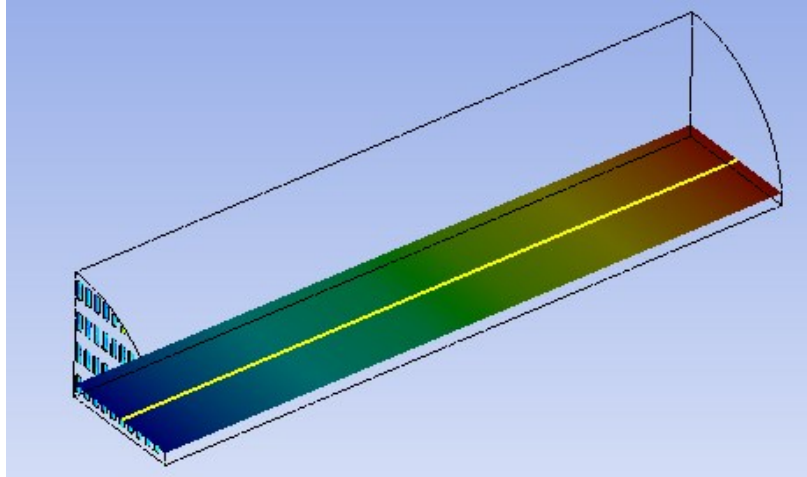
Figure 7. 20 Demonstration of line location of the data points
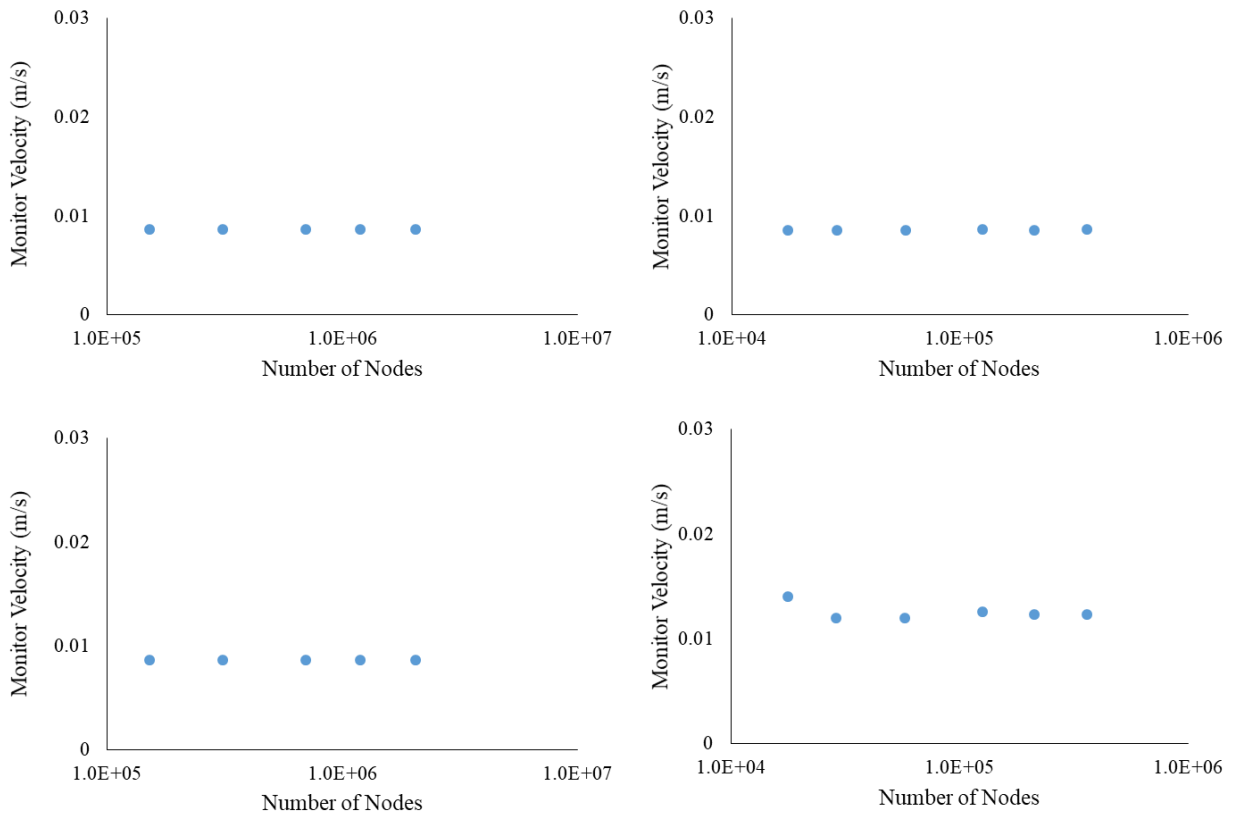
Figure 7. 21 Mesh sensitivity of Velocity data comparison of different vertical distance (a) 7.5'', (b) 2'', (c) 1'', and (d) 0.1'' for the punched screen
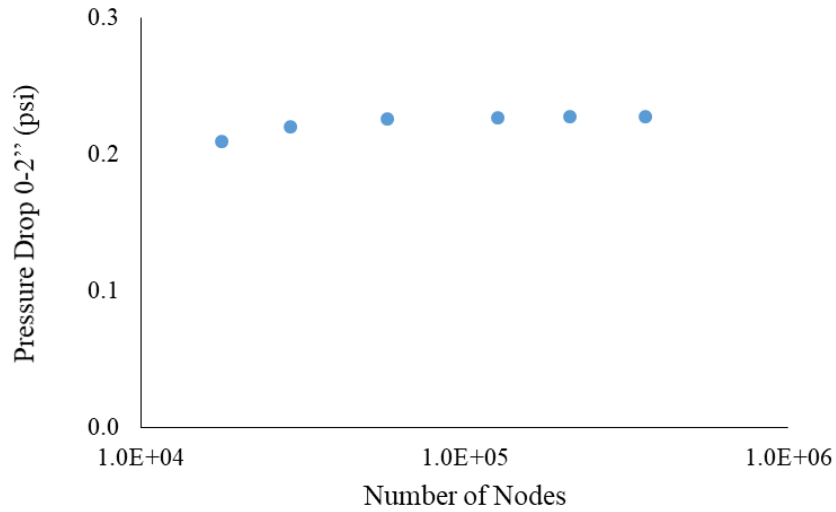
Figure 7. 22 Mesh sensitivity of pressure drop in near-screen zone data comparison for the punched screen
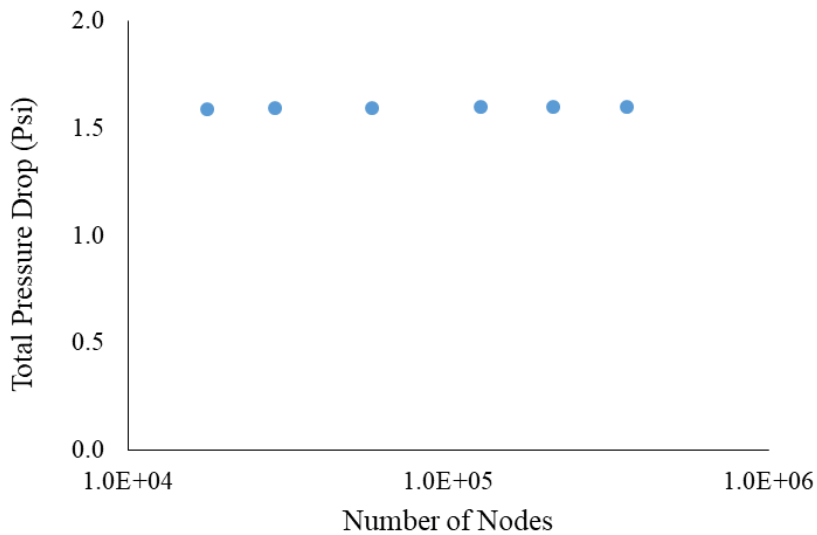
Figure 7. 23 Mesh sensitivity of total pressure drop data comparison for the punched screen

7.3 Model Calibration and Formation Damage (flow convergence) Characterization

This section introduces the simulation results to quantify the $\Delta P_{flow\ convergence}$. First, the numerical models are calibrated with Darcy's Law for the top and middle section with a 7200 cc/hr flow rate, which is consistent with the one used in the testing to calculate the retained permeability. Next, the pressure drop in the near-screen zone is obtained from the simulation results ($\Delta P_{simulation}$). Then, Equation 7.4 yields the $\Delta P_{flow\ convergence}$.

$$\Delta P_{flow\ convergence} = \Delta P_{simulation} - \Delta P_{linear} \qquad\qquad Eq.\,(7.4)$$

7.3.1 CFD Model Calibration

The numerical CFD models for different screens are calibrated by matching the differential pressure values in the top and middle sections of the model with pressure drop by the Darcy' Law (ΔP_{linear}). Table 7.5 shows an example of the calibration results for the SL with DC-III.

Table 7. 3 Model calibration with Darcy's Law

Calibration	ΔP_{top} (pa)	ΔP_{middle} (pa)
SL	1860	1860
ΔP_{linear}	1860	1860

7.3.2 Simulation Results and Formation Damage (flow convergence) Characterization

7.3.2.1 Slotted Liner

This section shows the simulation results for the SL regarding the flow streamlines, fluid velocity, and pressure. After model calibration, the pressure drop in the near-screen zone can be obtained from the simulation results to calculate the $\Delta P_{flow\ convergence}$ using Equation 7.4 abovementioned. The Figure 7.24 through 26 present the simulation results. It is found that the streamlines are converging when they approach the slots, resulting in the velocity increase (Figures 7.24 and 7.25). The converged flow streamlines and elevated fluid velocity cause the generation of the $\Delta P_{flow\ convergence}$. Table 7.4 shows the $\Delta P_{flow\ convergence}$ calculation results from Equation 7.4.

Table 7. 4 Flow Convergence Calculation for SL

$\Delta P_{simulation}$ (pa)	ΔP_{linear} (pa)	$\Delta P_{flow\ convergence}$ (pa)
2250	1860	390
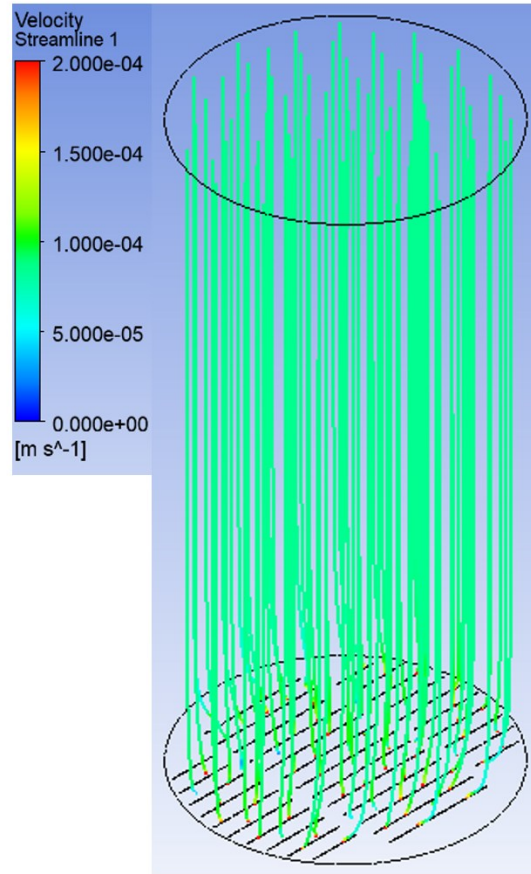
(a)
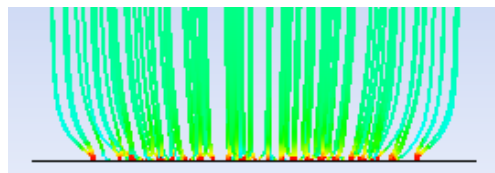
(b)

Figure 7. 24 Streamlines result of the (a) slotted liner, (b) zoomed-in view of the near-screen zone.
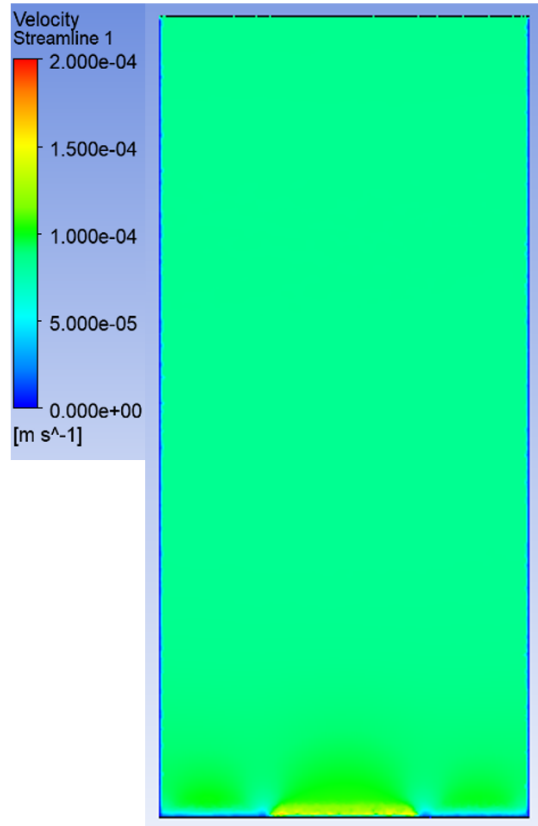
Figure 7. 25 Velocity profile of the slotted liner at the center plane.
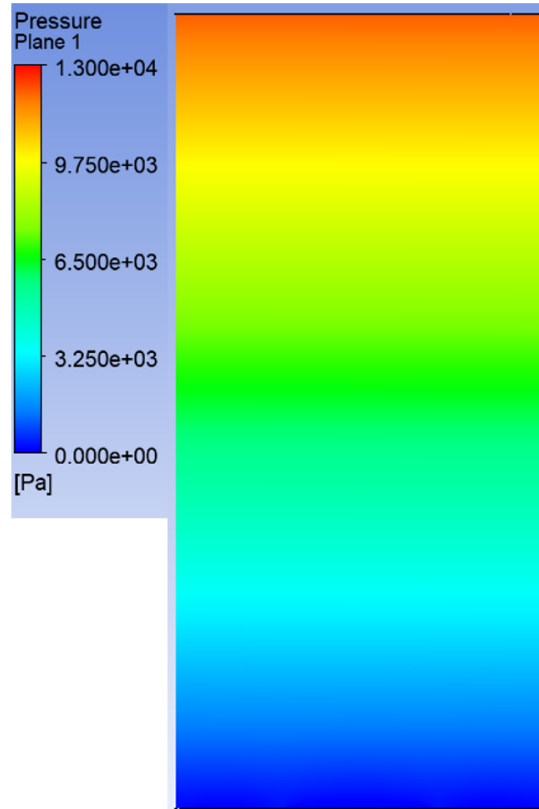
Figure 7. 26 Pressure profile of the slotted liner at the center plane.

7.3.2.2 Wire-wrapped Screen Results

Figures 7.27 through 7.29 show the streamline, velocity, and pressure data for the WWS, respectively. It is found that the flow streamlines are almost linear in the near-screen zone due to the high aperture density. Thus, the fluid velocity does not have an evident increase when approaching the WWS. Table 7.5 shows the $\Delta P_{flow\ convergence}$ calculation results.

Table 7. 5 Flow Convergence Calculation for WWS

$\Delta P_{simulation}$ (pa)	ΔP_{linear} (pa)	$\Delta P_{flow\ convergence}$ (pa)
1914	1860	54
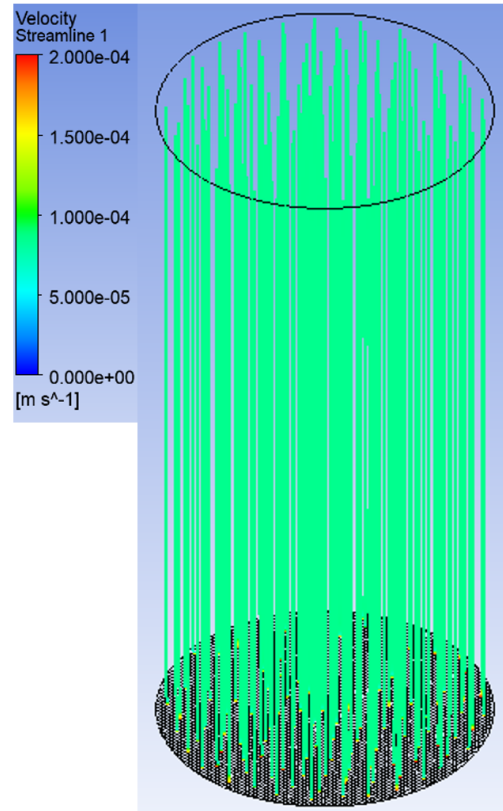
(a)

(b)

Figure 7. 27 Streamlines result of the (a) wire-wrapped screen, (b) zoomed-in view of the near-screen zone.
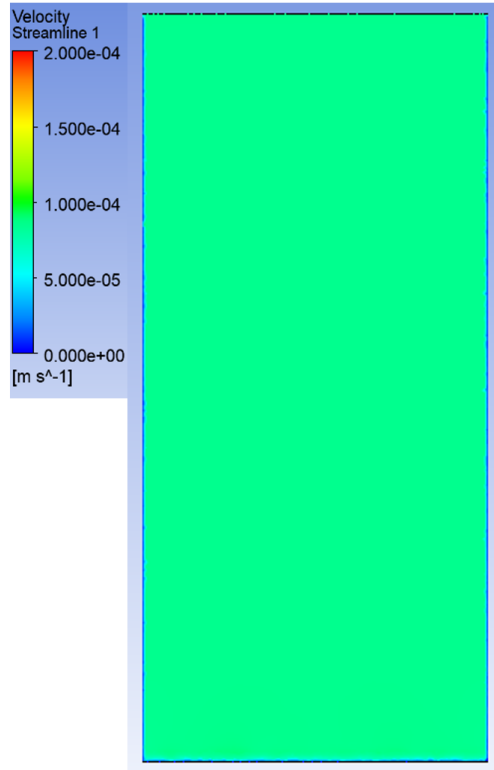
Figure 7. 28 Velocity profile of the wire-wrapped screen at the center plane

7.3.2.3 Punched Screen Results

The simulation results of the PS are shown in Figures 7.30 to 7.32. The location of the plane for the velocity and pressure profile is shown in Figure 7.20. It is found that the flow streamlines are redirected towards the punched slots on the sides of the punched pits. The flow direction change and the convergence effect increase the fluid velocity in the near-slot area, as shown in Figure 7.31. Table 7.6 shows the $\Delta P_{flow\ convergence}$ calculation results.

Table 7. 6 Flow Convergence Calculation for PS

$\Delta P_{simulation}$ (pa)	ΔP_{linear} (pa)	$\Delta P_{flow\ convergence}$ (pa)
2060	1860	200
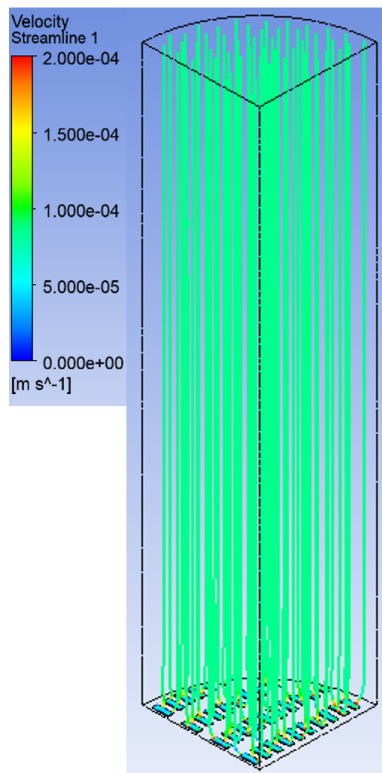
(a)
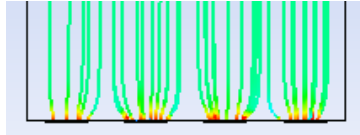
(b)

Figure 7. 30 Streamlines result of the (a) punched screen, (b) zoomed-in view of the near- screen zone
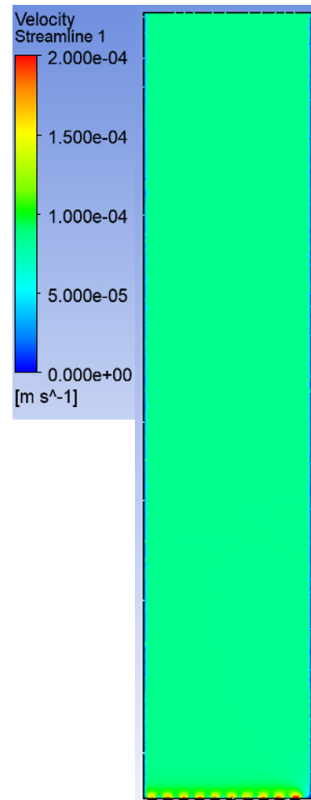
Figure 7. 31 Velocity profile of the punched screen
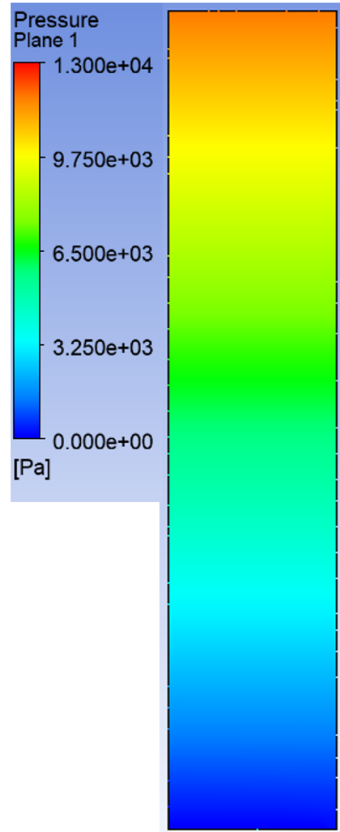
Figure 7. 32 Pressure profile of the punched screen

7.4 Formation Damage (fines migration) Characterization

After obtaining the $\Delta P_{flow\ convergence}$ from the simulation, the $\Delta P_{fines\ migraion}$ due to the fines migration can be calculated by Equations 7.5 through 7.7. Notably, the ΔP_{total} is not the direct pressure measurement in the testing as the testing condition is multi-phase flow. Instead, the pressure drop due to the formation damage (ΔP_{total}) is obtained through the retained permeability by Equation 7.7, as retained permeability objectively describes the level of the pressure build-up due to the fines migration and flow convergence, which is independent of the testing condition. The difference between ΔP_{total} and ΔP_{linear} is the additional pressure drop due to the formation damage ($\Delta P_{formation\ damage}$), as shown in Equation 7.5. The $\Delta P_{formation\ damage}$ equals to $\Delta P_{flow\ convergence}$ plus $\Delta P_{fines\ migraion}$. Table 7.8 summarizes the $\Delta P_{flow\ convergence}$ and $\Delta P_{fines\ migraion}$ results calculated based on the testing and the numerical results. The percentage of $\Delta P_{flow\ convergence}$ and $\Delta P_{fines\ migraion}$ contribute to the $\Delta P_{formation\ damage}$ are also given in the table.

$$\Delta P_{formation\ damage} = \Delta P_{total} - \Delta P_{linear} \qquad\qquad Eq.\,(7.5)$$

$$\Delta P_{fines\ migraion} = \Delta P_{formation\ damage} - \Delta P_{flow\ convergence} \qquad\qquad Eq.\,(7.6)$$

$$\Delta P_{total} = \Delta P_{linear}/k_{ret} \qquad\qquad Eq.\,(7.7)$$

The results indicate that most of the formation damage in the WWS is due to the fines migration. This is due to the linear flow streamline geometry. The $\Delta P_{flow\ convergence}$ due to the flow convergence is negligible. Regarding the SL and PS, due to the higher level of flow convergence, it is found that both flow convergence and fines migration play critical roles in the formation damage. However, in the dirty formation (DC-I), fines migration is the dominant factor that causes the formation damage. While in the clean formation (DC-III), both flow convergence and fines migration are contributing to the formation damage.

Table 7. 7 Formation Damage Calculation for stand-alone screens

	DC-III			DC-II			DC-I		
	SL	WWS	PS	SL	WWS	PS	SL	WWS	PS
ΔP_{total}	2696	2163	2620	4137	2955	3704	9015	6251	8225
k_{ret} %	69	86	71	60	84	67	52	75	57
ΔP_{linear}	1860	1860	1860	2482	2482	2482	4688	4688	4688
$\Delta P_{fines\ migration}$	446	249	560	1133	401	988	3342	1427	3095
$\Delta P_{flow\ convergence}$	390	54	200	522	72	234	985	136	442
$\Delta P_{fines\ migration}$ %	53	82	74	68	85	81	77	91	88
$\Delta P_{flow\ convergence}$ %	47	18	26	32	15	19	23	9	12

7.5 Conclusion

This chapter introduces the numerical model using CFD to characterize the formation damage of stand-alone screens for different formation sands. The CFD simulation allows streamline visualization, which helps understand the pressure build-up due to the flow convergence in the near-screen zone of each stand-alone screen. The results show that the streamline in the SL is converged due to the low slot density. Also, in the PS, the direction of the streamline has a sharp change close to the punched slots. However, the streamline in the WWS is almost linear, indicating there is negligible flow convergence, which also explains the lower pressure drop in the near-screen zone. The pressure results from the simulation models are combined with the experimental results to differentiate the formation damage. It is found that the formation damage in the WWS is mainly due to the fines migration. However, both flow convergence and fines migration contribute to the pressure build-up for the SL and PS.

Chapter 8: Comparison of Stand-alone Screens

8.1 Introduction

This chapter compares the performance analyses of stand-alone screens based on the experimental results. Sanding, retained permeability, fines production and concentration, and design criteria are used as the performance comparison indicator. The testing data of the aperture sizes within the safe aperture design window are used in the comparison study. Finally, based on the testing and simulation results, the screen selection protocol is proposed for SAGD operators choosing the optimal screen type.

8.2 Comparison Results

8.2.1 Sand Production Comparison

Figures 8.1 through 8.3 present the sand production comparison between the SL, WWS, and PS for DC-I, DC-II, and DC-III, respectively. The aperture sizes used in the comparison analysis are 0.010'' and 0.014'', obtained from the safe aperture window.

(a)
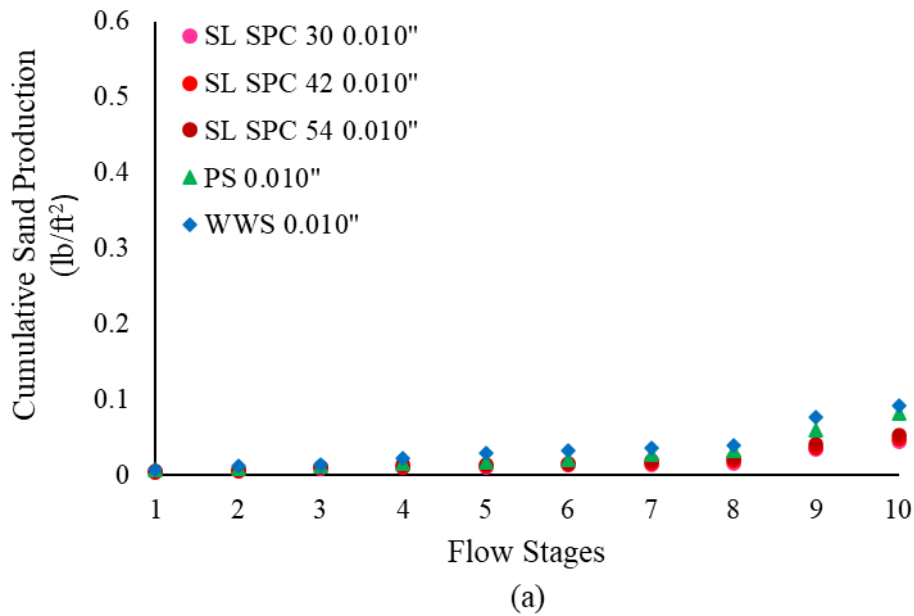
Figure 8. 1 Sand production comparison of DC-I, (a) 0.010'', (b) 0.014''
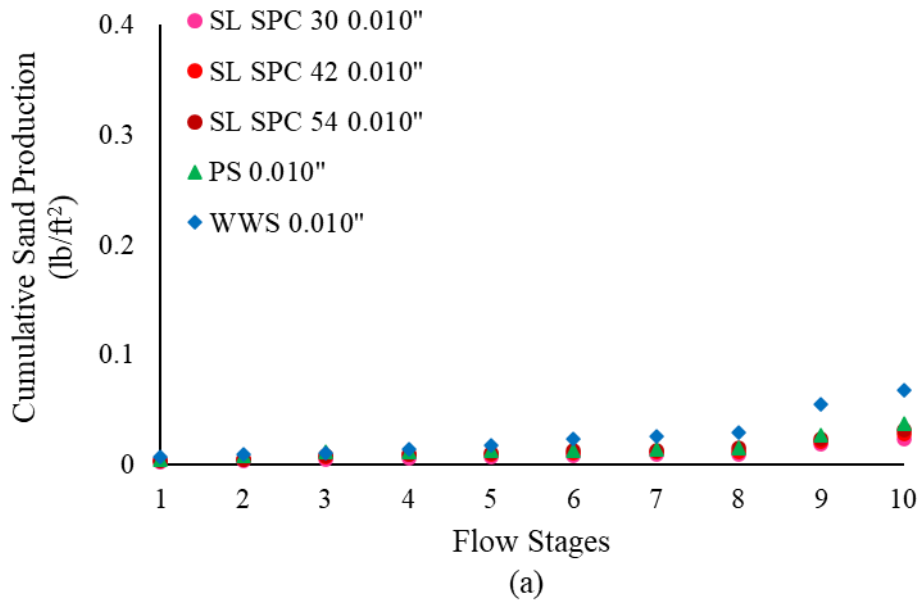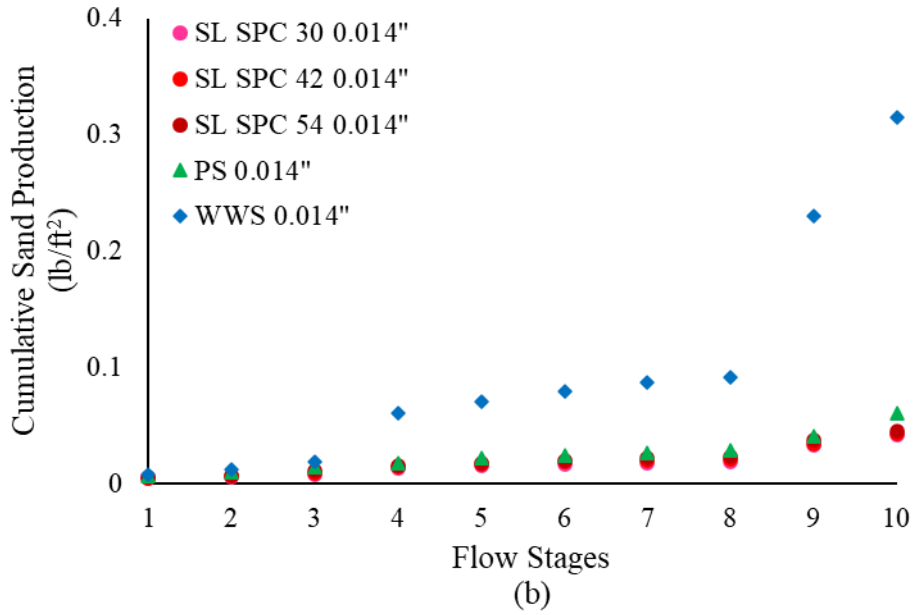
Figure 8. 2 Sand production comparison of DC-II, (a) 0.010'', (b) 0.014''
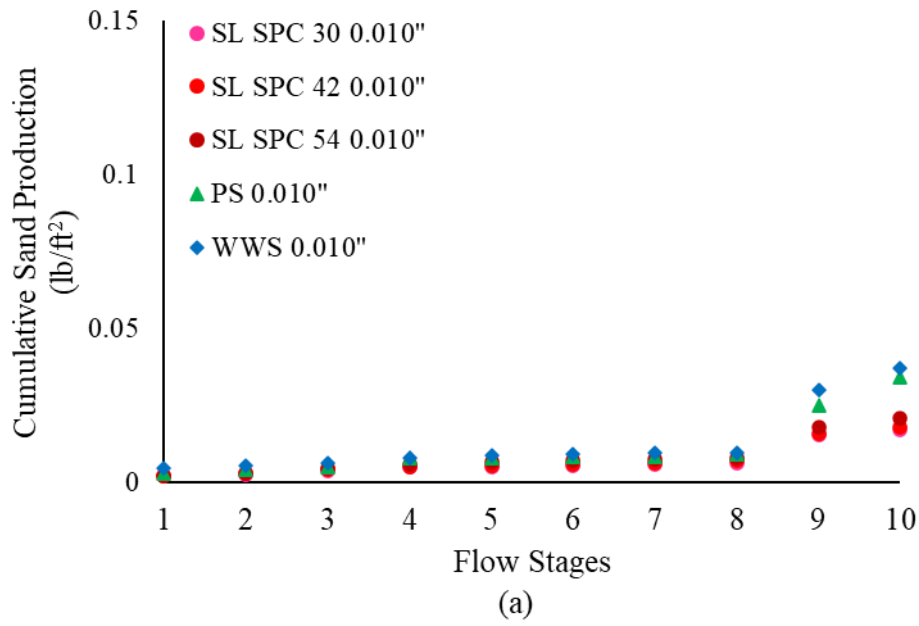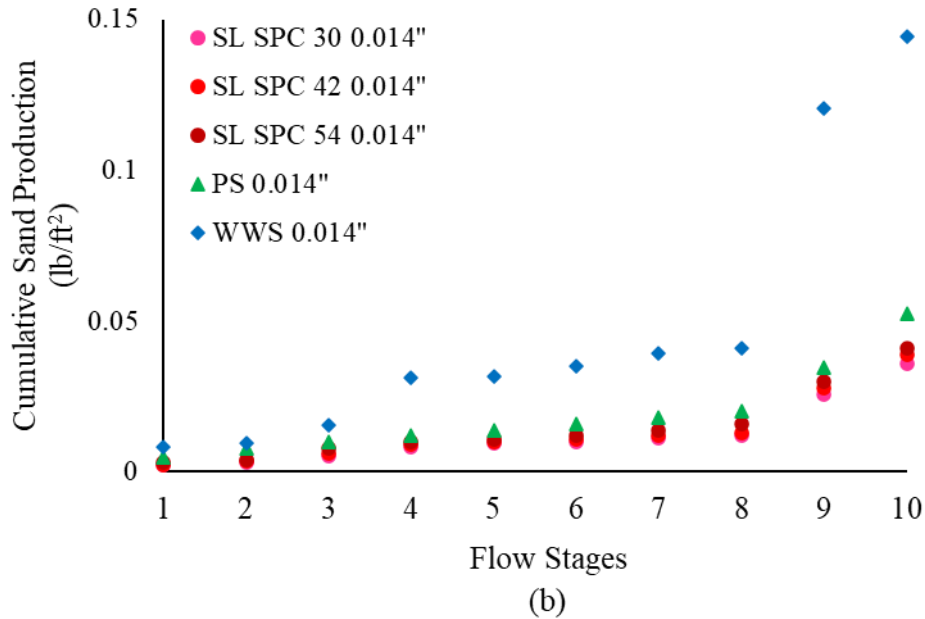
Figure 8. 3 Sand production comparison of DC-III, (a) 0.010'', (b) 0.014''

Based on the comparison of the results, generally, it is found that the WWS produces the most amount of sand production. The SL has the best sanding performance, and the amount of sand production for the PS is in the middle. Also, with the increase of slot density, the amount of sand production increases. This phenomenon is related to the OFA, as explained in the previous chapter. Thus, the WWS with the highest OFA characteristics produces the highest amount of sand production.

However, the difference in the amount of sand production is not evident for aperture size of 0.010'' for all three PSDs (Figures 8.1 (a), 8.2 (a), and 8.3 (a)). For DC-I, the WWS produces 12% more sand production than the PS, and PS produces sand around 60% more than the SL with SPC 54. SL with SPC 54 yields a 33% extra sand production compared to SPC 30. For DC-II, the WWS produces 80% more sand production than the PS. The SL with SPC 54 produces 19% less sand than the PS and 33% more sand than the SPC 30. For DC-III, the WWS has a 10% increase in sand production compared to the PS. The PS shows 60% more sand production than SL with SPC 54. The SL with SPC 30 produces 24% less sand than SPC 54. The slight variation of the cumulated sand production between these screens is due to the narrow aperture size characteristics. The aperture size of 0.010'' is narrow enough to retain the sand grains and provide excellent sanding performance for all the screens.

When it comes to the aperture size of 0.014'', the cumulative sand production gap gets wider between the WWS and the rest two screens. In DC-I, the WWS produces 200% more sand than the PS. The difference between PS and SL with SPC 54 is 10%, and the difference between SPC 54 and SPC 30 is 15% (Figure 8.1 (b)). In DC-II, the WWS shows 435% more sand production than the PS. The difference between PS and SL with SPC 54 and SPC 54 and SPC 30 is 33% and 7%, respectively (Figure 8.2 (b)). And in DC-III, the WWS produce 170% more sand than the PS. The PS has 29% more sand production than the SL with SPC 54, and SPC 54 has 14% more sand production than SPC 30 (Figure 8.3 (b)).

The significant increase in the sand production of the WWS compared to PS and the SL is due to the larger aperture size. The sand retention mechanism for the aperture of 0.014'' is sand bridging rather than size exclusion for aperture size of 0.010''. The ability to form a stable arch is the key to prevent sand production. A stable arch can only form on the slot after some initial sand production. Since the WWS has the greatest number of slots, the amount of the produced sand needed to form stable arches is more than the PS and SL. Moreover, another finding is that the sand production difference between the WWS and PS and SL increases after the gas breakthrough. This can be attributed to the weaker bridge stability of the WWS. The sand bridges on the slots undertake the in-situ stresses in the near-screen zone. In other words, the sand bridges share the total amount of in-situ stresses. Thus, the more sand bridges formed on the slots, the less in-situ stresses are taken for each sand bridge. The WWS with the greatest number of slots results in a low stress-taken sand bridge. The low in-situ stresses condition causes a weaker sand bridge that may be break easily. During gas breakthrough, the high-velocity fluid creates greater hydrodynamic drag force on the sand grains. The weaker sand bridges formed on the WWS are broken, which causes more sand production. While PS and SL have relatively lower slot density, the sand bridge formed on the slots is relatively stronger. Therefore, less sand production is observed after the gas breakthrough.

8.2.2 Retained Permeability Comparison

Figures 8.4 through 8.6 compare the retained permeability for DC-I, DC-II, and DC-III, respectively. The aperture sizes used in the comparison analysis are 0.010'' and 0.014'', obtained from the safe aperture window.
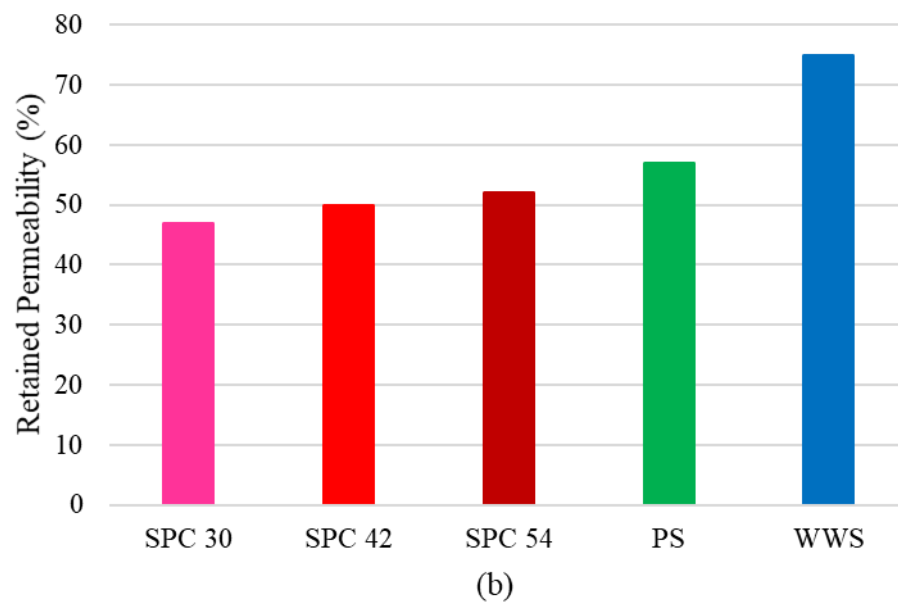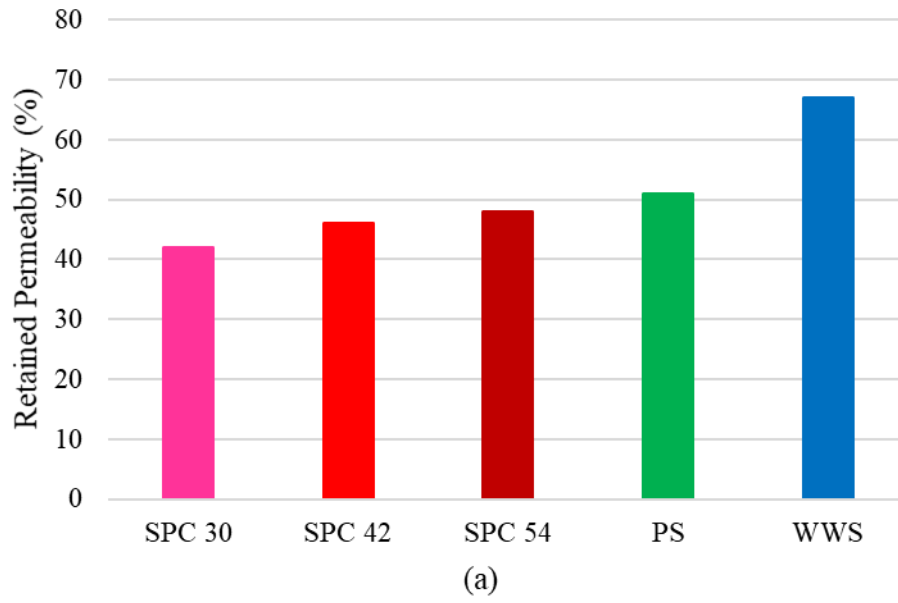
Figure 8. 4 Retained permeability comparison for DC-I, (a) 0.010'', (b) 0.014''
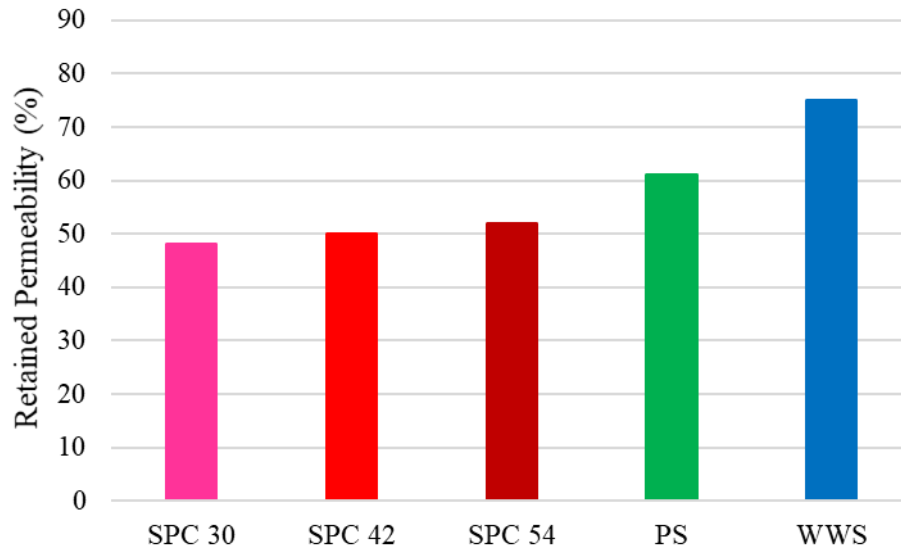
(a)
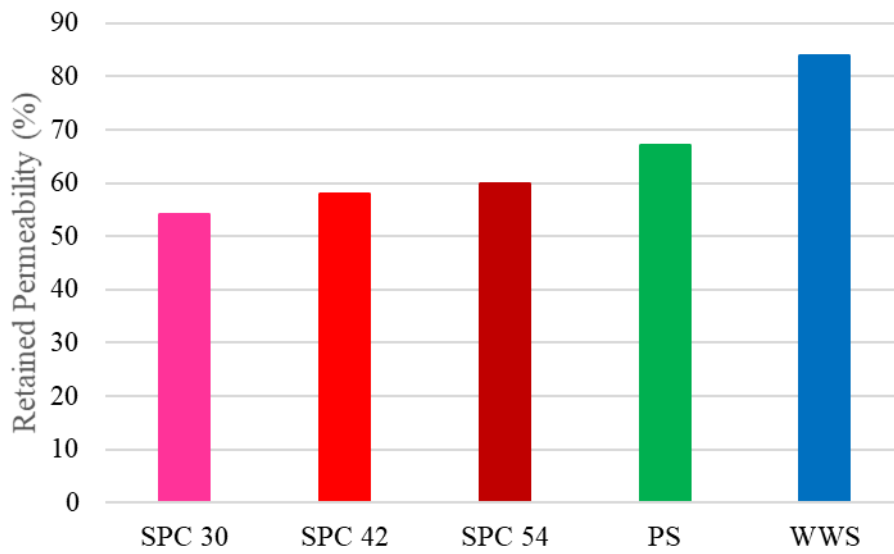
(b)

Figure 8. 5 Retained permeability comparison for DC-II, (a) 0.010'', (b) 0.014''
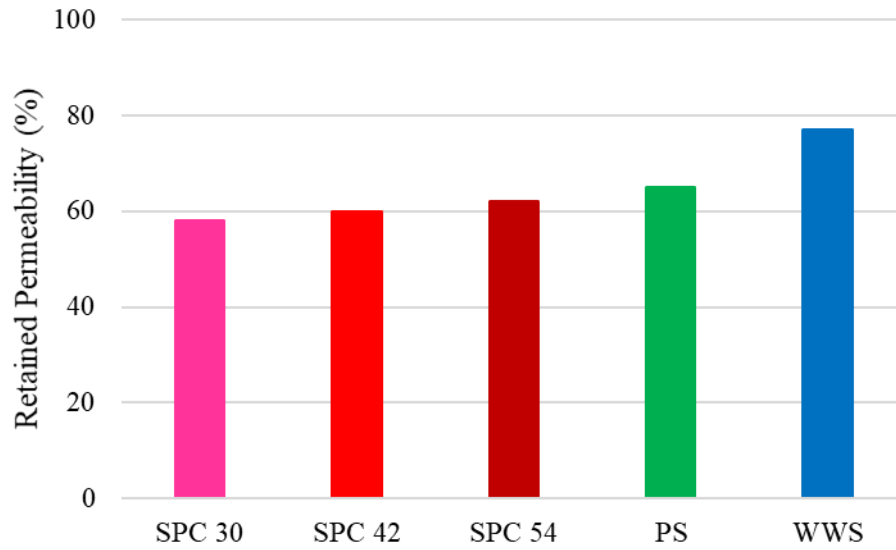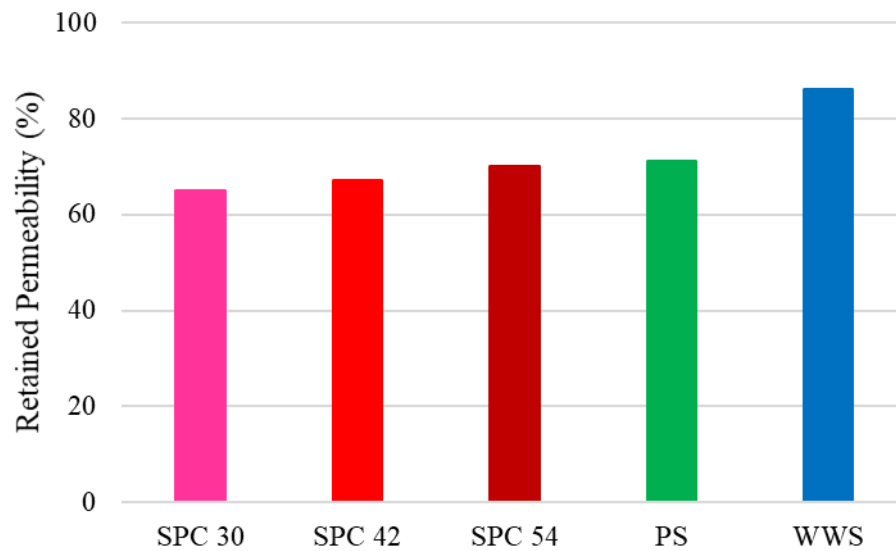
Figure 8. 6 Retained permeability comparison for DC-II, (a) 0.010'', (b) 0.014''

From the comparison of the results, it is found that generally, the WWS has the best flow performance indicated by the highest retained permeability values. The retained permeability values of the PS are slightly higher than the SL; the difference is close, though. The SL with higher slot density has higher retained permeability values than the low slot density.

In DC-I, the retained permeability of the WWS is 16% higher than the PS for aperture size of 0.010''. The PS has a 3% more retained permeability value than the SL with SPC 54. The retained permeability increases by 6%, with the slot density changing from SPC 30 to 54 (Figure 8.4 (a)). While for aperture size of 0.014'', the WWS has 18% higher retained permeability than the PS. The PS has a 5% more retained permeability value than the SL with SPC 54. The retained permeability increases by 5%, with the slot density changing from SPC 30 to 54 (Figure 8.4 (b)).

In DC-II, for the aperture size of 0.010''the retained permeability of the WWS is 14% higher than the PS. The SL with SPC has a 9% less retained permeability value than PS. The SL with SPC 54 has a 4 % higher retained permeability value than SPC 30 (Figure 8.5 (a)). While for aperture size of 0.014'', the WWS has 17% higher retained permeability than the PS. The PS has a 7% higher retained permeability than the SL with SPC 54. The retained permeability increases by 6%, with the slot density changing from SPC 30 to 54 (Figure 8.5 (b)).

In DC-III, the retained permeability of the WWS is 12% higher than the PS for aperture size of 0.010''. The PS has a 3% more retained permeability value than the SL with SPC 54. The retained permeability increases by 4% from SPC 30 to SPC 54 (Figure 8.6 (a)). While for aperture size of 0.014'', the PS has 15% less retained permeability than the WWS. The SL with SPC 54 has 1% less retained permeability value than the PS. The retained permeability decreases by 5%, with the slot density changing from SPC 54 to 30 (Figure 8.6 (b)).

The difference in the retained permeability can be attributed to the OFA of the stand-alone screens. The WWS with the highest OFA allows more fines production; therefore, fewer fines accumulation in the near-screen zone and formation damage. The PS and SL with low OFA produce fewer fines than the WWS, yielding lower retained permeability values.

8.2.3 Fines Production Comparison
Figures 8.7 through 8.9 compare the fines production for DC-I, DC-II, and DC-III, respectively. The fines production data are obtained from the turbidity measurements of the produced liquid. The aperture sizes used in the comparison analysis are 0.010'' and 0.014'', obtained from the safe aperture window.

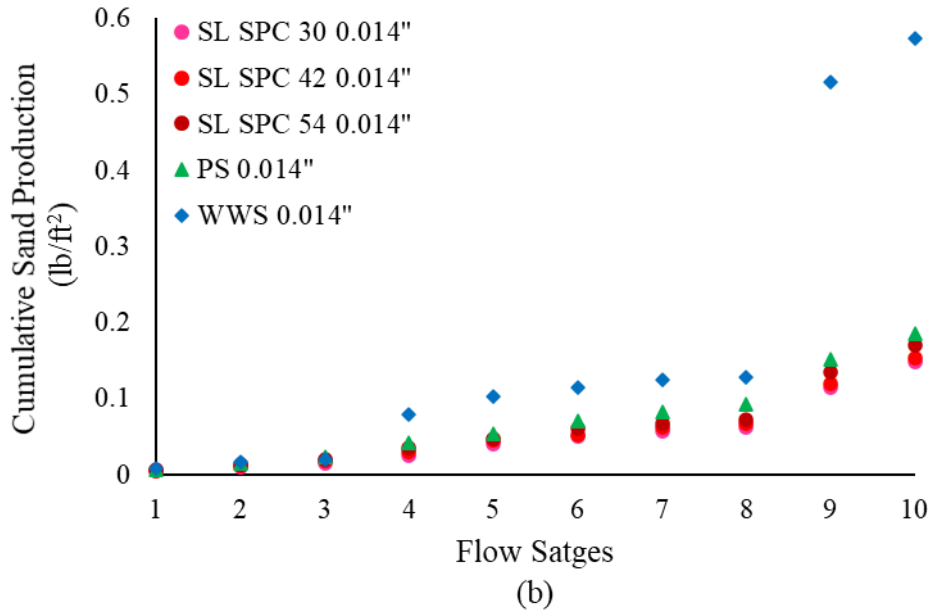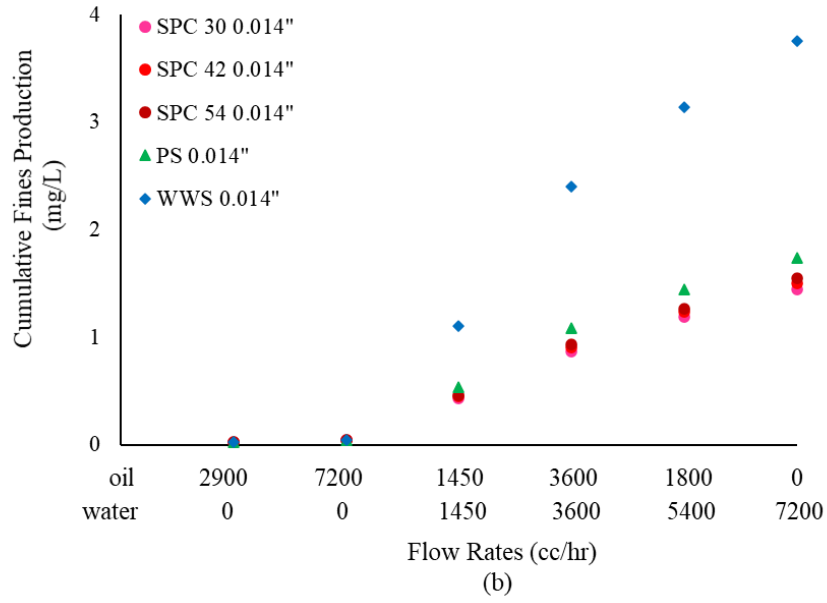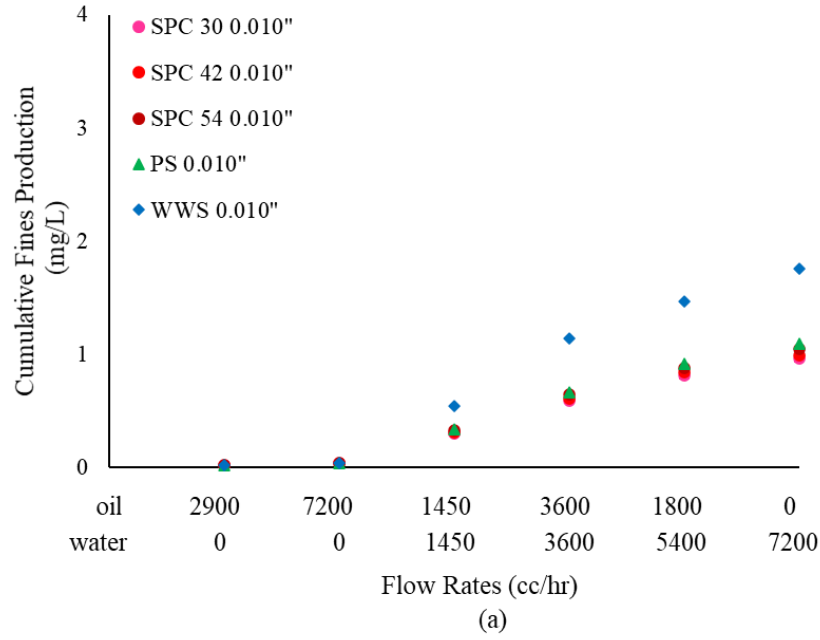Figure 8. 7 Fines production comparison results for DC-I, (a) 0.010'', (b) 0.014''
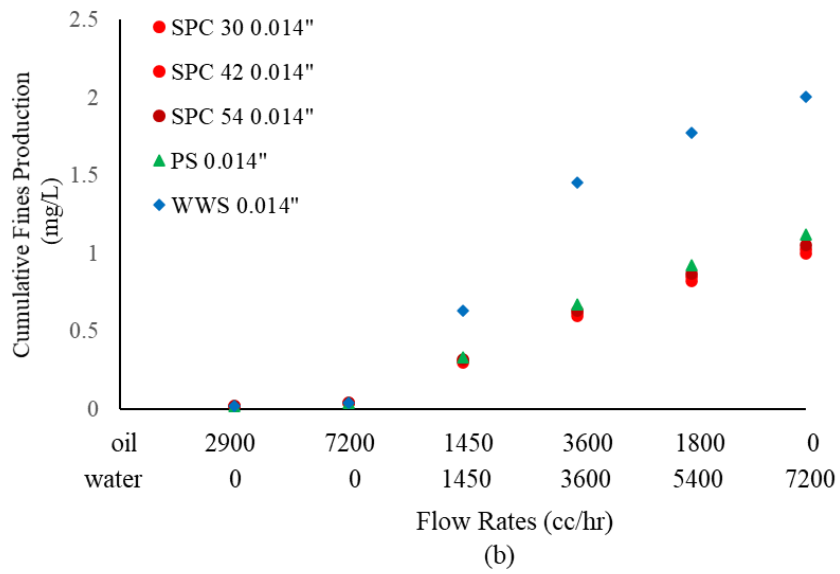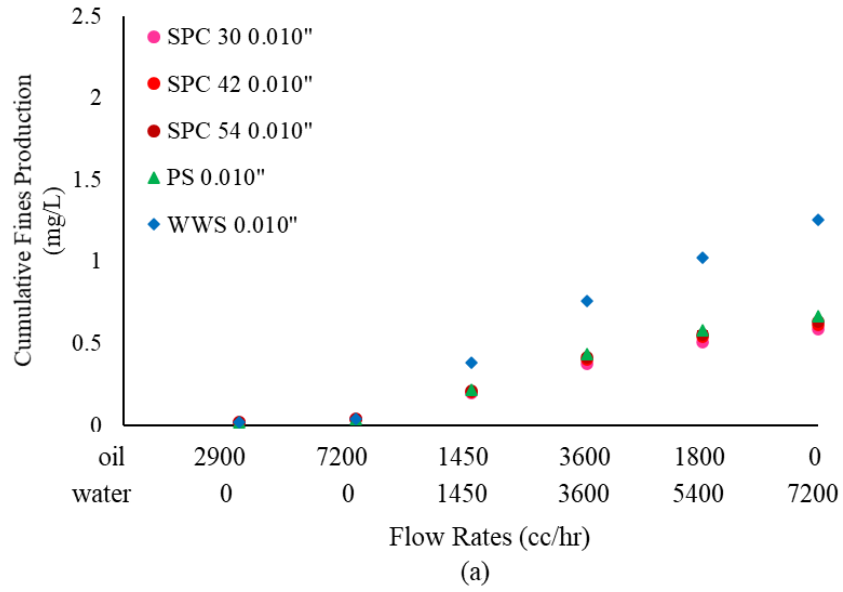
Figure 8. 8 Fines production comparison results for DC-II, (a) 0.010'', (b) 0.014''
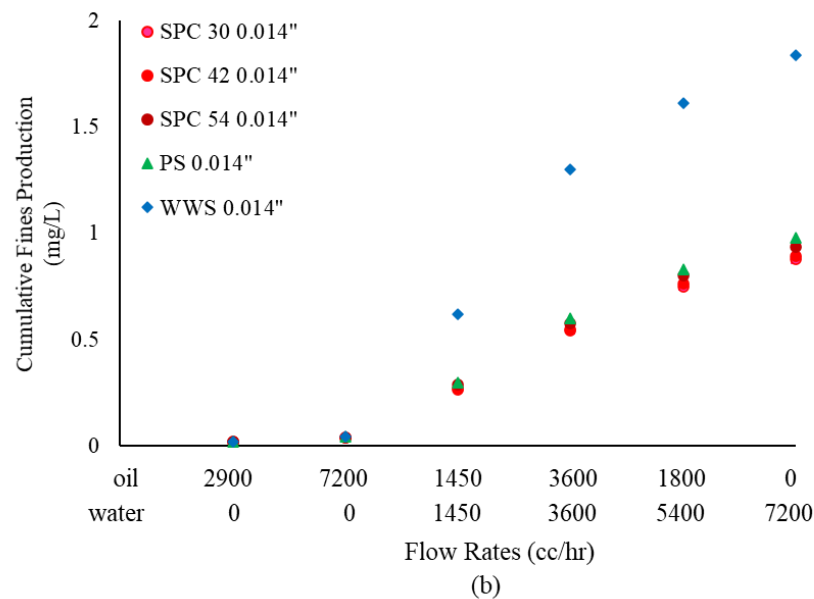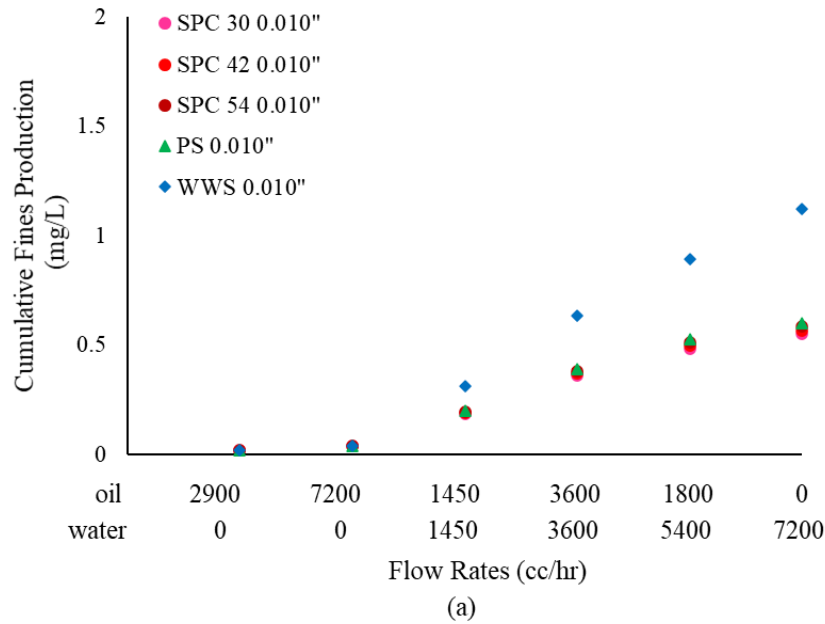
Figure 8. 9 Fines production comparison results for DC-III, (a) 0.010'' and (b) 0.014''

From the turbidity measurements, it is found that the WWS produces the most amount of fines during the liquid production compared to the PS and SL. The ability to produce fines of the PS is comparable to the SL. This is due to the higher OFA nature of the WWS, which provides more open space for fines production. The fines production comparison results also verify the retained permeability comparison results: the more fines production, the less formation damage, therefore,

the more retained permeability. Another notable finding is that the difference in the fines production becomes evident after the water breakthrough. During the oil injection stages, there is negligible fines migration, and minor fine particles are produced due to the water-wet properties of the fine particles. Thus, the difference between these screens is insignificant.

Statistical data of the comparative analyses are provided. In DC-I, the WWS produces 60% total amount of fines more than the PS for aperture size of 0.010''. The PS produces fines of 4% more than the SL with SPC 54. SL with SPC 54 increases the fines production by 8% of SPC 30 (Figure 8.7 (a)). For the aperture size of 0.014'', the WWS produces 116% of fines more than the PS. The PS produces fines of 12% more than the SL with SPC 54. SL with SPC 54 increases the fines production by 7% of SPC 30 (Figure 8.7 (b)).

In DC-II, for aperture size of 0.010'', the total fines production increases by 8% from SL SPC 30 to SPC 54. The PS allows 5% more fines production than SL SPC 54. However, it produces 89% fewer fines than the WWS (Figure 8.8 (a)). While for aperture size of 0.014'', the WWS produces 78% of fines more than the PS. The PS produces fines of 7% more than the SL with SPC 54. SL with SPC 54 increases the fines production by 5% of SPC 30 (Figure 8.8 (b)).

In DC-III, the WWS produces 87% total amount of fines more than the PS for aperture size of 0.010''. The PS produces fines of 3% more than the SL with SPC 54. SL with SPC 54 increases the fines production by 6% of SPC 30 (Figure 8.9 (a)). For the aperture size of 0.014'', the WWS produces 88% of fines more than the PS. The PS produces fines of 4% more than the SL with SPC 54. SL with SPC 54 increases the fines production by 7% of SPC 30 (Figure 8.9 (b)).

8.2.4 Fines Accumulation Comparison

Figures 8.10 through 8.12 show the comparison results of the fines concentration variation in the near-screen zone for DC-I, DC-II, and DC-III, respectively. The fines concentration data are obtained from the wet-sieve analyses.
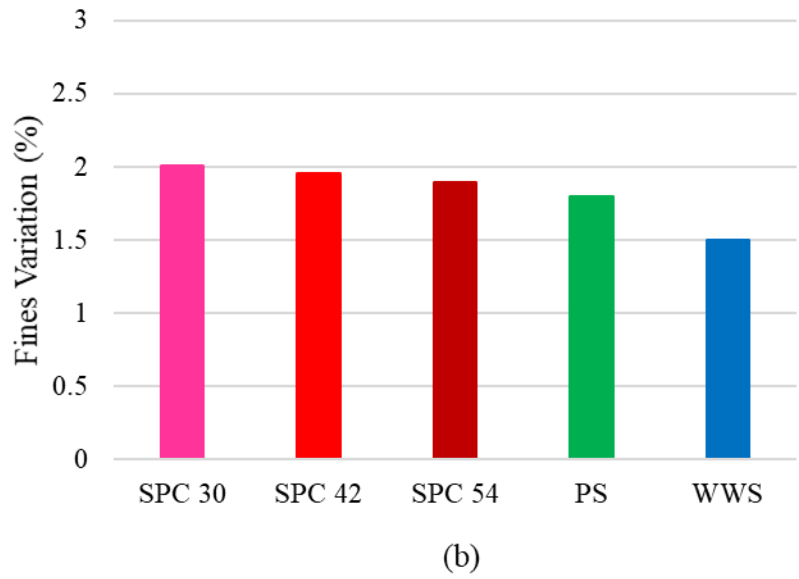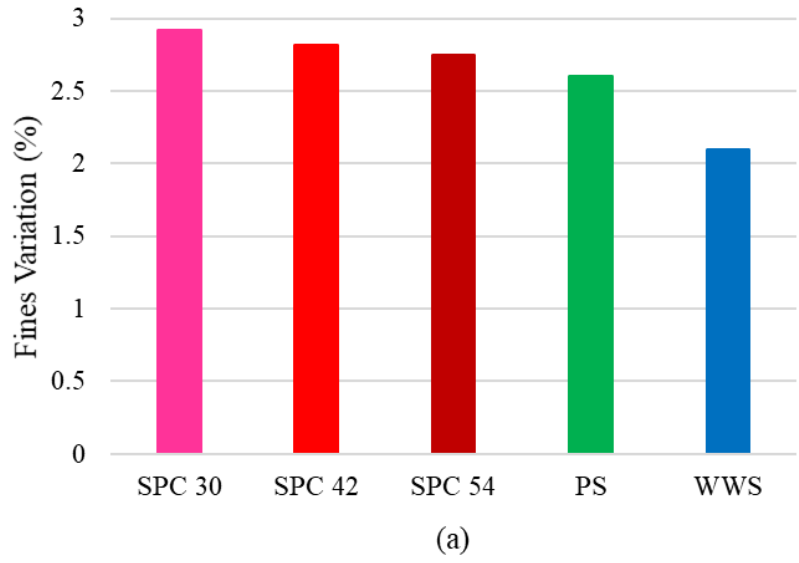
Figure 8. 10 Fines concentration variation for DC-I, (a) 0.010'' (b) 0.014''
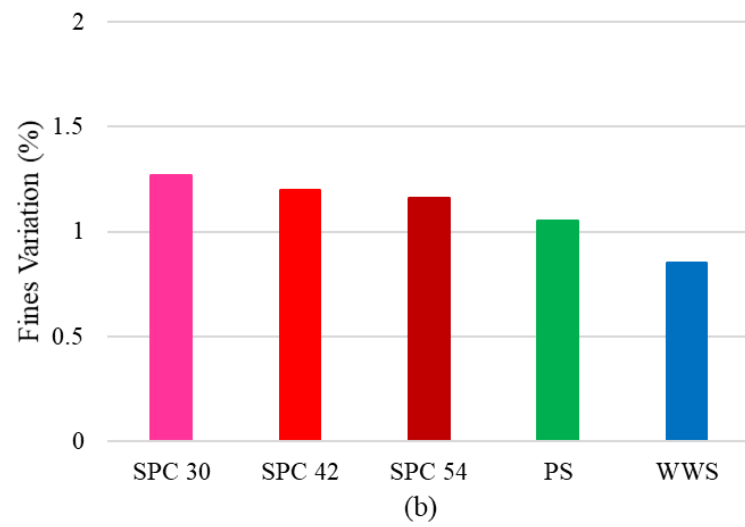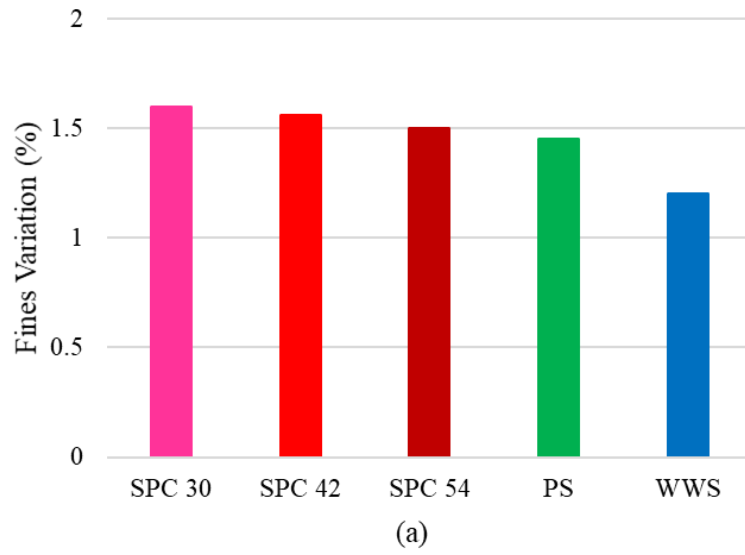
Figure 8. 11 Fines concentration variation for DC-II, (a) 0.010'', (b) 0.014''
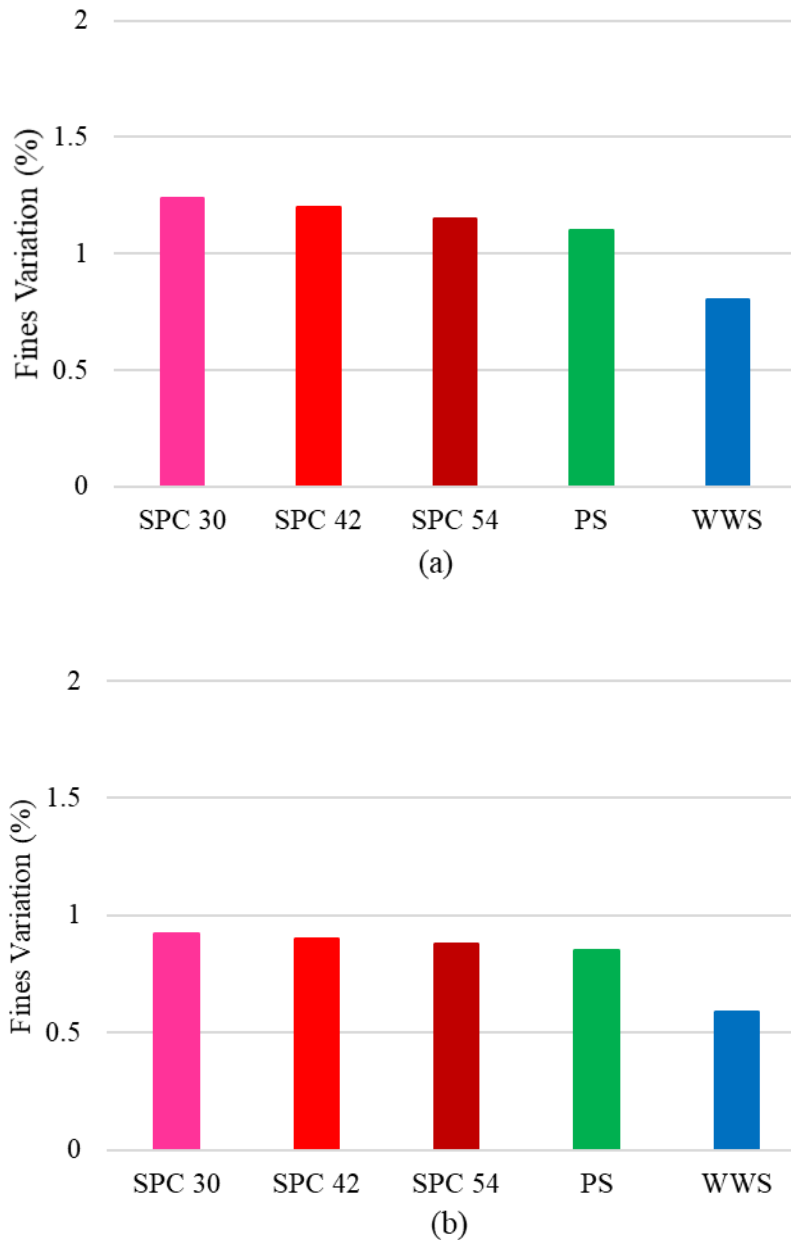
Figure 8. 12 Fines concentration variation for DC-III, (a) 0.010'', (b) 0.014''

Based on the comparison of the results, it is shown that the WWS has the least fines concentration increase in the near-screen zone. This is aligned with the fines production results. Since the WWS allows more fines production, fewer fines are captured and accumulated behind the slots. The PS accumulates more fines than the WWS. However, when compared to the SL, it shows fewer fines accumulation. Also, SL with higher slot density shows fewer fines accumulation. Moreover, aperture size 0.014'' retains fewer fines than aperture size of 0.010''.

In DC-I, the fines accumulation in the near-screen zone is between 2 to 3% and 1.5 to 2% for 0.010'' and 0.014'', respectively. For DC-II, the fines accumulation in the near-screen zone is between 1 to 2% and 0.5 to 1.5% for 0.010'' and 0.014'', respectively. And for DC-III, the fines accumulation in the near-screen zone is between 0.5 to 1.5% and 0.5 to 1% for 0.010'' and 0.014'', respectively. The decrease of the fines concentration from DC-I to DC-III is because of the total amount of original fines concentration decrease from DC-I to DC-III.

8.2.5 Design Criteria Comparison

Figures 8.13 through 18 present the TLS design criteria comparison. The design criteria are compared based on normal SAGD conditions and aggressive SAGD conditions.
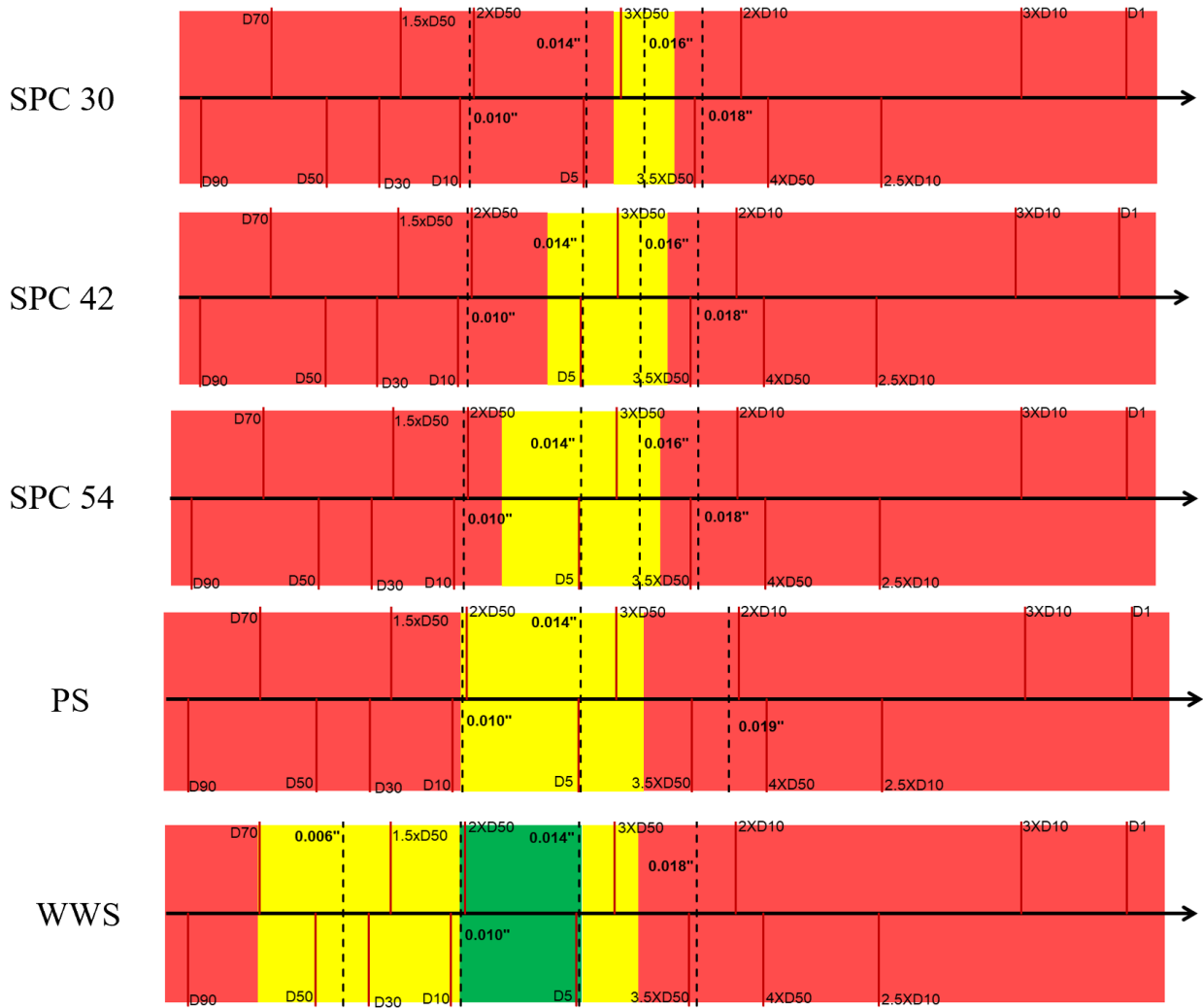
Figure 8. 13 Design criteria comparison of DC-I normal SAGD condition
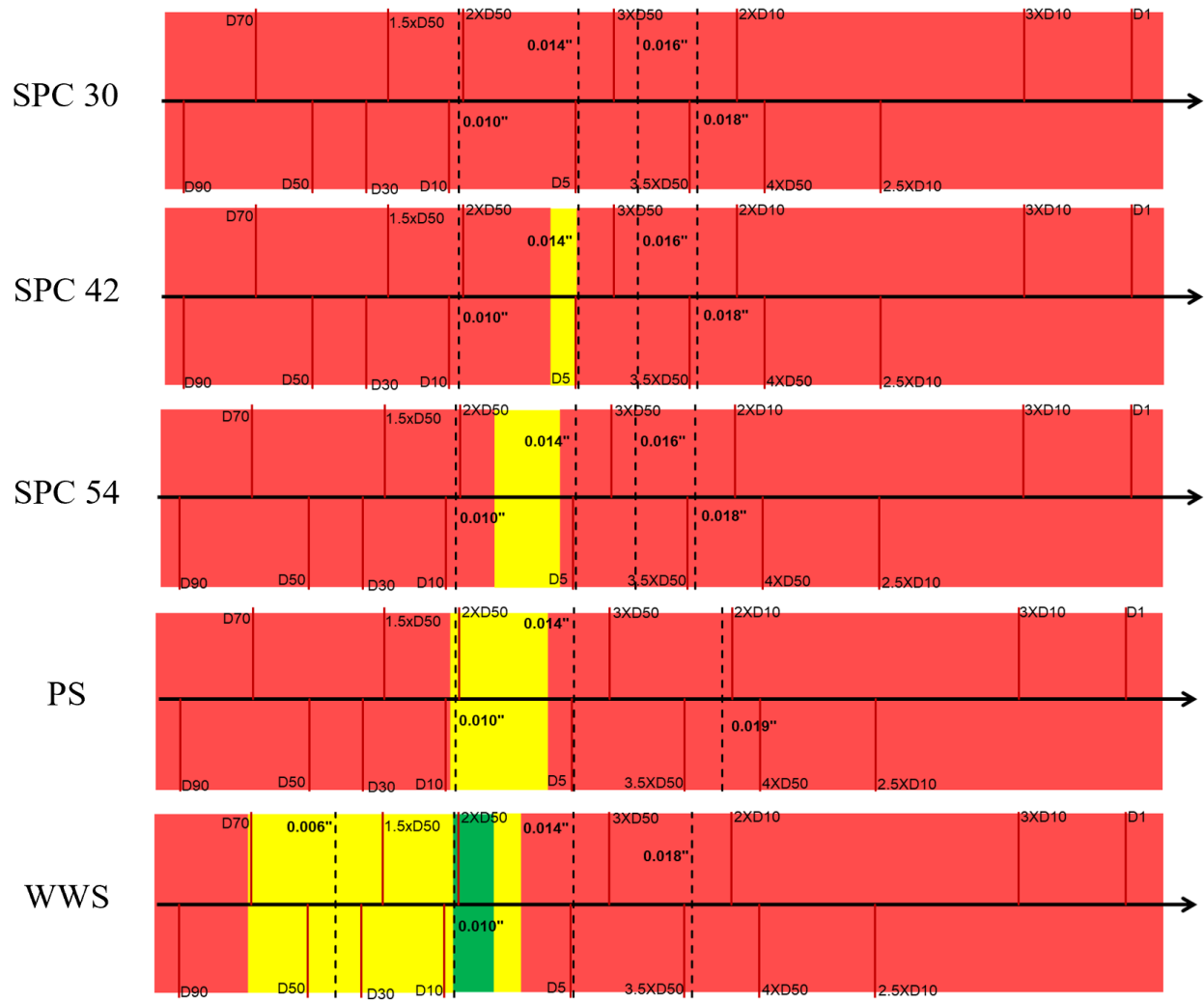
Figure 8. 14 Design criteria comparison of DC-I aggressive SAGD condition
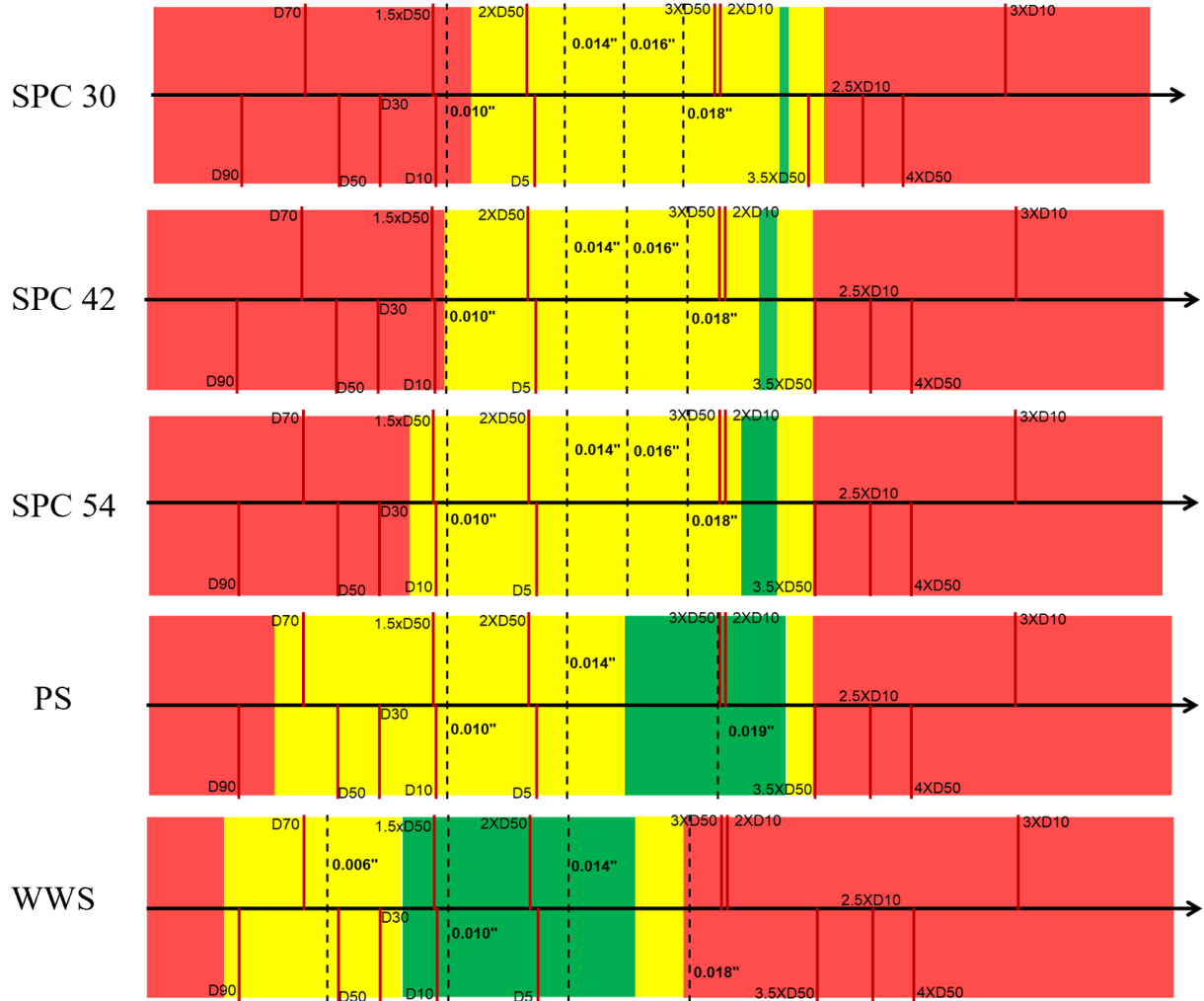
Figure 8. 15 Design criteria comparison of DC-II normal SAGD condition

159
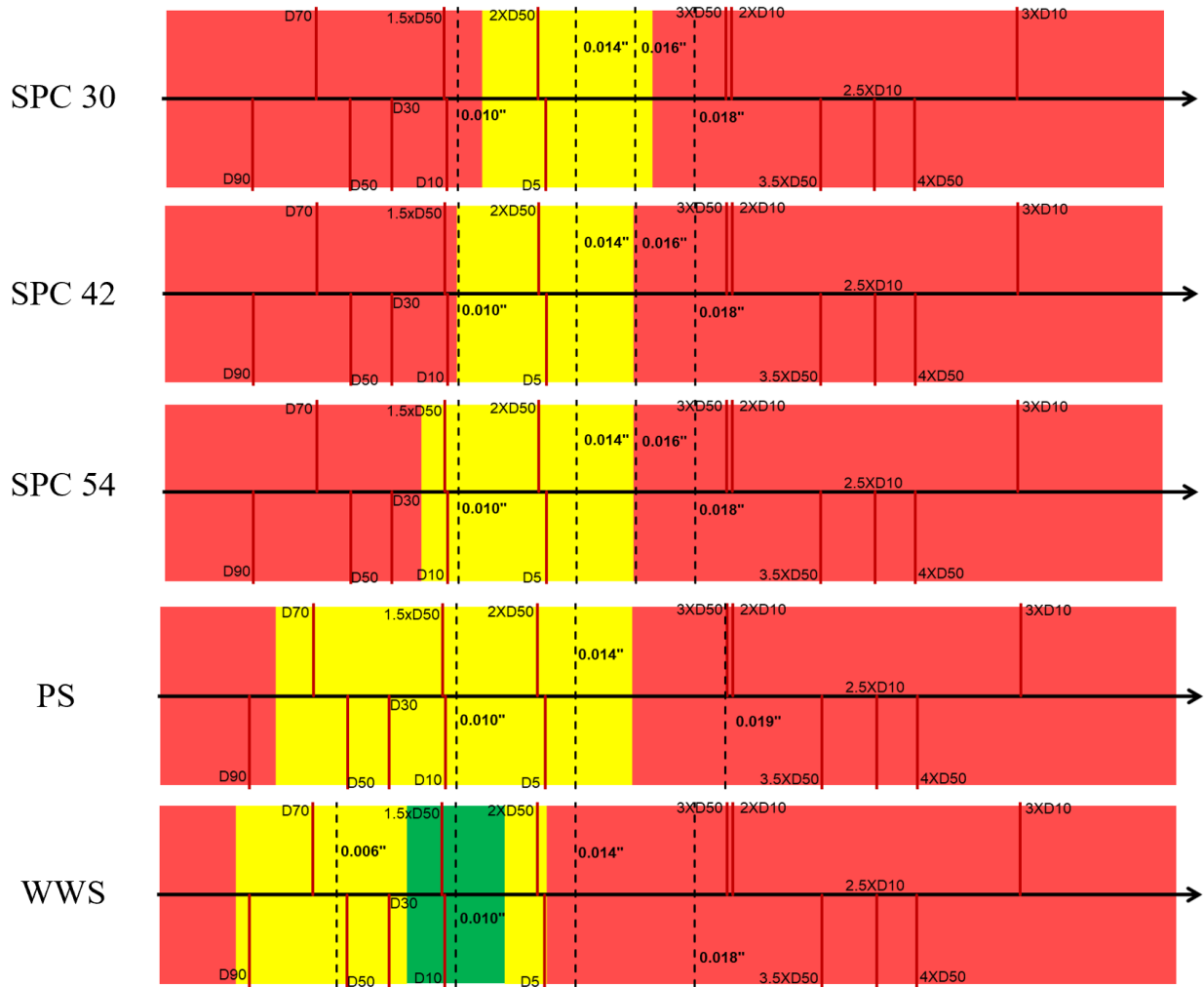
Figure 8. 16 Design criteria comparison of DC-II aggressive SAGD condition
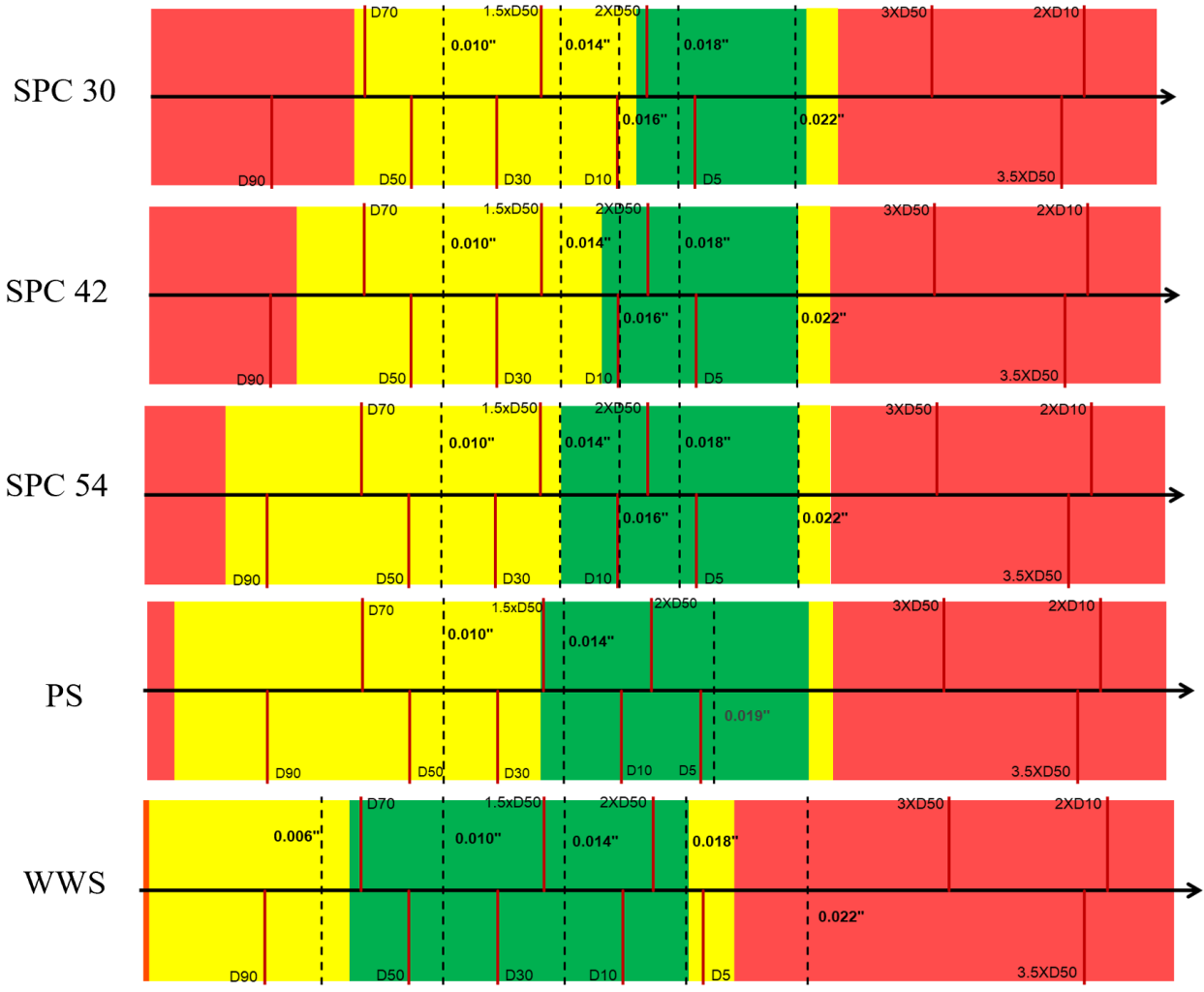
Figure 8. 17 Design criteria comparison of DC-III normal SAGD condition
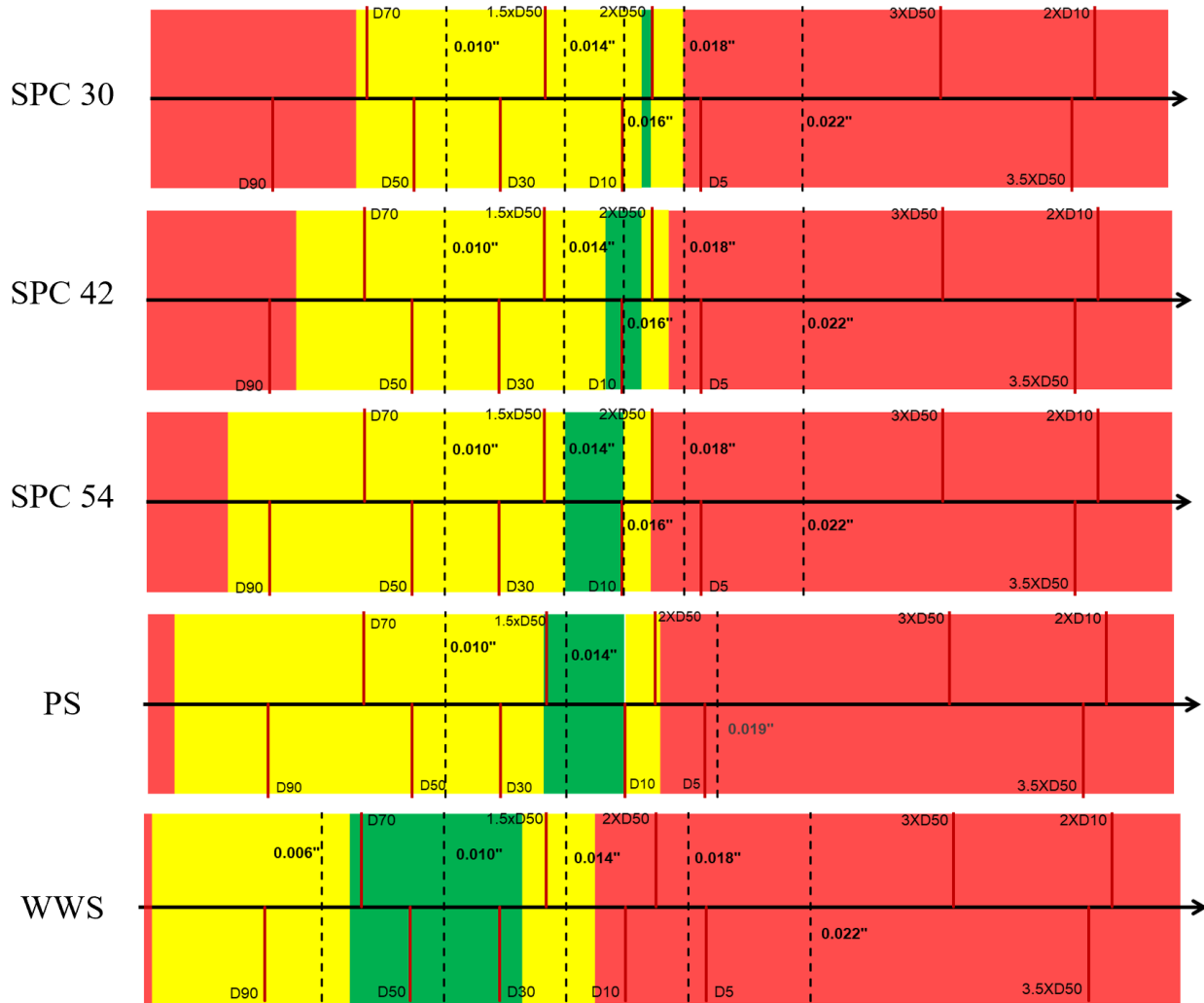
Figure 8. 18 Design criteria comparison of DC-III aggressive SAGD condition

Generally, it is found that for all three PSDs, the safe aperture windows (yellow plus green) shift towards the left with the screen type changing from the WWS to PS, then to the SL. This is mainly due to the increase of the OFA. The increase of the OFA leads to more sand production and higher retained permeability. Therefore, both the upper and lower boundaries move to the left to maintain the required sanding and flow performance. Similarly, the upper bound in the aggressive SAGD condition shifts towards the left compared to the normal SAGD condition to compensate for the additional sand production during the gas breakthrough.

Notably, in DC-I, only some narrow yellow zones exist for the PS and SL. Notably, there is no safe aperture window of the SL with SPC 30, which means no matter what slot size is used, the SL with SPC 30 could not provide the required performance. However, the WWS could still offer

162

a decent aperture window with green zones in normal and aggressive SAGD conditions. This is due to the high OFA nature of the WWS, which makes it provide desirable flow performance even with dirty formations.

In DC-II, the PS and SL could provide desirable flow performance under normal SAGD condition indicated by the existence of the narrow green zone in the TLS. Although the green zone vanishes under the aggressive SAGD condition, the PS and SL could still provide some broad yellow zones with the WWS. Also, the range of safe aperture windows is comparable.

When it comes to DC-III, with the fines concentration substantially reduced, it is found that all three screens can provide comparable performance. The widths of the safe aperture windows are comparable for all three screens. Also, the green zones exist in all screens under both normal and aggressive SAGD conditions. This is due to the limited amount of the fines content in the DC-III, which yields a lower plugging tendency. Even though the SL and PS have limited OFA compared to the WWS, they can still maintain excellent flow performance in DC-III.

8.3 Screen Selection Protocols

The TLS design criteria indicate that the WWS can provide superior sanding and flow performance for DC-I, which cannot be provided by the PS and SL. However, the performance of these screens is comparable in DC-II and DC-III. Thus, considering the economy and cost, it is recommended to apply the WWS in formations with a more considerable amount of plugging materials (dirty formations) to guarantee the desired performance of the completion work. The PS and SL, which are relatively cheaper than the WWS, are suggested to be implemented in formations with low plugging tendency (clean formations). They can provide comparable performance to the WWS at a relatively low cost. Also, when using SL, the SL with higher SPC is recommended as it can provide better flow performance.

8.4 Conclusions

This chapter compares the performance of the SL, PS, and WWS based on the experimental testing and numerical simulation results. Sand production, retained permeability, fines production, fines accumulation, and TLS design criteria are used to assess the comparison comprehensively. It is found that the WWS produces more sand production and has higher retained permeability values compared to the PS and SL for the same aperture size. Also, the WWS allows more fines production and retains fewer fines behind the screen. The design criteria comparison indicates that

the WWS has the superior overall performance in all three PSDs. The PS shows an intermediate overall performance, while the SL shows the worst overall performance. However, the overall performance is comparable in DC-II and DC-III due to the limited amount of plugging materials.

Finally, a screen selection protocol is generated based on the performance comparison assessment that the WWS is recommended for using in dirty formations, like DC-I. Regarding the PS and SL, it is suggested to be implemented in clean formations to reduce cost.

Chapter 9: Conclusions and Future Work

9.1 Main Results and Contribution

This research assesses the performance of stand-alone screens, including the SL, WWS, and PS, by experimental and numerical techniques. The experimental study uses the large-scale pre-packed SRT facility to analyze the sand production, retained permeability, and fines production of the screens. The tests use screen coupons and are designed to incorporate all necessary influential factors, such as aperture size, slot density, flow velocity, fluid-phase change, and PSD. Synthetic sand-pack samples are used in the testing. Design criteria are generated based on the testing results by applying the sanding and flow performance limits. The design criteria are presented graphically by using the TLS method. Empirical correlations are also built to predict the safe aperture window mathematically. The validated equations can predict the safe aperture window for any PSDs. The numerical method uses CFD to assess formation damage in the near-screen zone. Damage due to the flow convergence and fines migration are characterized individually. Finally, the experimental and numerical results are compared between all three stand-alone screens to develop the optimal screen selection protocols.

- Massive sand production is observed during the gas breakthrough due to high fluid velocity and pressure gradient.
- Fine particles start mobilization and production after the flow of the wetting-phase fluid.
- Higher flow velocity and water cut enhance the fines migration process due to the higher drag force and exposure area.
- For the same specifications, the WWS produces the highest amount of sand production than the PS. Also, the PS produces more sand than the SL. SL with higher slot density causes more sand production than lower slot density.
- The WWS provides the best flow performance compared to the PS and SL. SL, with the lowest OFA nature, has the worst flow performance. The PS has an intermediate flow performance for the same specifications.
- Design criteria are generated for all three stand-alone screens using the TLS method. Proposed criteria can be used by SAGD operators in designing the screens for the McMurray Formation.

- Empirical correlations with dimensionless parameters are formulated to predict the safe aperture window mathematically.

- Design criteria results indicate only the WWS can provide desirable performance in DC-I. There is no safe aperture window for the SL with SPC 30 under aggressive SAGD conditions. However, all the screens can provide comparable performance in DC-II and III.

- The numerical CFD simulation shows that the flow streamlines in the near-screen zone of the SL are converged. Also, the flow direction is changed for the PS due to the unique geometry design. The flow streamlines show a linear pattern in the WWS.

- Most of the formation damage in the WWS is due to the fines migration. The formation damage due to the flow convergence is negligible.

- Both fines migration and flow convergence are critical to the formation damage for the SL and PS. However, in dirty formations, fines migration is the dominant parameter.

9.2 Recommendations for Future Work

The following aspects are proposed as potential future work.

- Investigate the impact of PSD on the sanding and flow performance of stand-alone screens. So far, three representative PSDs have been analyzed. More PSDs with different sorting parameter could help fully understand the impact of PSD.

- Investigate the impact of clay composition. Kaolinite, which is the non-swelling clay, is used in this research. Other clay materials, such as smectite, are swelling clays. The impact of swelling clay and the combination of swelling and non-swelling clays have not been assessed.

- Investigate the impact of emulsions on the screen performance. In this research, mineral oil is used in the testing. However, in real SAGD production wells, the produced liquid is in the form of a water-oil emulsion. Thus, understanding the impact of emulsion on the screen is significant.

- Investigate the impact of the radial flow regime. The pre-packed SRT facility establishes a linear flow regime. However, in the real SAGD well, the liquid pool around the horizontal screen causes a radial flow regime. Thus, it is essential to understand the screen behavior under radial flow conditions.

- Investigate the impact of corrosion and erosion on the liner performance. The current testing condition does not involve these two parameters. However, in the actual down-hole conditions, liner corrosion and erosion are common.

- Investigate the impact of in-situ stresses on the screen performance. The pre-packed SRT applied a limited amount of stress to the sand-pack. However, in the SAGD down-hole condition, the screen may undergo a stress build-up process due to thermal expansion. Thus, the impact of stress on the screen needs to be understood.

Bibliography

Abass, H., Nasr-El-Din, H., & BaTaweel, M. (2002). Sand Control: Sand Characterization, Failure Mechanisms, and Completion Methods. Paper presented at the SPE Annual Technical Conference and Exhibition.

Abrams, A. (1977). Mud design to minimize rock impairment due to particle invasion. *Journal of petroleum technology, 29*(05), 586-592.

AER. 2018. "ST98: Alberta's Energy Reserves & Supply/Demand Outlook." Government of Alberta

Agunloye, E., & Utunedi, E. (2014, August). Optimizing sand control design using sand screen retention testing. In *SPE Nigeria Annual International Conference and Exhibition*. Society of Petroleum Engineers.

Aksu, I., Bazilevskaya, E., Karpyn, Z.T., 2015. Swelling of clay minerals in unconsolidated porous media and its impact on permeability. GeoResJ. 7, 1-13.

Al-Awad, M. N., El-Sayed, A. and Desouky, S. (1999). Factors affecting sand production from unconsolidated sandstone Saudi oil and gas reservoir. *Journal of King Saud University, Engineering Sciences, 11*(1), 151-174.

Al-Bahlani, A. M., & Babadagli, T. (2009). SAGD Laboratory Experimental and Numerical Simulation Studies: A Review of Current Status and Future Issues. Journal of Petroleum Science and Engineering, 68(3), 135-150.

Anderson, M., 2017. SAGD sand control: large scale testing results. In: Paper Presented at the SPE Canada Heavy Oil Technical Conference, Calgary, Alberta, Canada, 15-16 February, SPE-185967-MS.

Ballard, T., and Beare, S. (2003). Media sizing for premium sand screens: Dutch twill weaves. Presented at the SPE European Formation Damage Conference, 13-14 May, The Hague, Netherlands. SPE 82244-MS.

Ballard, T. and Beare, S. P. (2006). *Sand retention testing: the more you do, the worse it gets.* Paper presented at the SPE International Symposium and Exhibition on Formation Damage Control.

Ballard, T. J. and Beare, S. P. (2012). *An investigation of sand retention testing with a view to developing better guidelines for screen selection.* Paper presented at the SPE International Symposium and Exhibition on Formation Damage Control.

Barkman, J. H., & Davidson, D. H. (1972). Measuring water quality and predicting well impairment. *Journal of Petroleum Technology*, *24*(07), 865-873.

Bedrikovetsky, P., Tran, P., Van den Broek, W. M. G. T., Marchesin, D., Rezende, E., Siqueira, A., Serra, A.L. & Shecaira, F. (2002, January). Damage characterization of deep bed filtration from pressure measurements. In *International Symposium and Exhibition on Formation Damage Control*. Society of Petroleum Engineers.

Bedrikovetsky, P. G., Vaz, A., Machado, F. A., Zeinijahromi, A., & Borazjani, S. (2011, January 1). Productivity Impairment Due to Fines Migration: Steady State Production Regime. Society of Petroleum Engineers. doi:10.2118/143744-MS.

Bennett, C., Gilchrist, J.M., Pitoni, E., Burton, R.C., Hodge, R.M., Troncoso, J., Ali, S.A., Dickerson, R., Price-Smith, C., Parlar, M., 2000. Design methodology for selection of horizontal open-hole sand control completions supported by field case histories. In: Paper Presented at the SPE European Petroleum Conference, Paris, France, 24-25 October. SPE-65140-MS.

Bennion, D. B., Ma, T., Thomas, F. B. et al. (2007). Laboratory Procedures for Optimizing the Recovery from High Temperature Thermal Heavy Oil and Bitumen Recovery Operations. Presented at the Canadian International Petroleum Conference, 12-14 June, Calgary, Alberta. PETSOC-2007-206.

Bennion, D., Gupta, S., Gittins, S. and Hollies, D. (2009). Protocols for slotted liner design for optimum SAGD operation. *Journal of Canadian Petroleum Technology, 48*(11), 21-26.

Beshry, M. A., Krawchuk, P., Brown, G. A. et al. (2006). Predicting the Flow Distribution on Total E&P Canada's Joslyn Project Horizontal SAGD Producing Wells Using Permanently Installed

Fiber-Optic Monitoring. Presented at the SPE Annual Technical Conference and Exhibition, 24-27 September, San Antonio, Texas, USA. SPE 102159-MS.

Birks, J., Fennell, J., Yi, Y., Gibson, J., & Moncur, M. (2017). Regional Geochemistry Study for the Southern Athabasca Oil Sands (SAOS) Area.

Bradshaw, A. S., & Baxter, C. D. P. (2007). Sample preparation of silts for liquefaction testing. Geotechnical Testing Journal, 30(4), 324-332.

Butler, R. and Stephens, D. (1981). The gravity drainage of steam-heated heavy oil to parallel horizontal wells. Journal of Canadian Petroleum Technology, 20(02).

Butler, R. (1985). A new approach to the modeling of steam-assisted gravity drainage. *Journal of Canadian Petroleum Technology, 24*(03), 42-51.

Butler, R. M. (2001, January 1). Some Recent Developments in SAGD. Petroleum Society of Canada. doi:10.2118/01-01-DAS.

Bybee, K. (2002, March 1). High-Temperature Acidization Prevents Fines Migration. Society of Petroleum Engineers. doi:10.2118/0302-0040-JPT.

Carlson, J., Gurley, D., King, G., Price-Smith, C. and Waters, F. (1992). Sand control: Why and how? *Oilfield Review*.

CAPP (2018) Canada Oil and Natural Gas. Canada's Energy Resources. Retrieved from: https://www.capp.ca/canadian-oil-and-natural-gas/canadas-petroleum-resources.

Changyin, D.O.N.G., ZHANG, Q., Kaige, G.A.O., Kangmin, Y.A.N.G., Xingwu, F.E.N.G. and Chong, Z.H.O.U., 2016. Screen sand retaining precision optimization experiment and a new empirical design model. Petroleum Exploration and Development, 43(6), pp.1082-1088.

Chanpura, R. A., Hodge, R. M., Andrews, J. S., Toffanin, E. P., Moen, T. and Parlar, M. (2011). A review of screen selection for standalone applications and a new methodology. *SPE Drilling & Completion, 26*(01), 84-95.

Chanpura, R. A., Mondal, S., Andrews, J. S., Mathisen, A. M., Ayoub, J. A., Parlar, M. and Sharma, M. M. (2012a). *Modeling of square mesh screens in slurry test conditions for standalone screen*

applications. Paper presented at the SPE International Symposium and Exhibition on Formation Damage Control.

Chanpura, R. A., Mondal, S., Sharma, M. M. et al. (2012b). Unraveling the Myths in Selection of Standalone Screens and a New Methodology for Sand Control Applications. Presented at the SPE Annual Technical Conference and Exhibition, 8-10 October, San Antonio, Texas, USA. SPE 158922-MS.

Chenault, R. L. (1938, January). Experiments on Fluid Capacity and Plugging of Oil-Well Screens. In *Drilling and Production Practice 1938*. American Petroleum Institute.

Civan, F. (2007). Reservoir Formation Damage: Fundamentals, Modeling. *Assessment and*, *339*.

Coberly, C., 1937. Selection of screen openings for unconsolidated sands. In: Paper Presented at the Drilling and Production Practice, New York, 1 January, API-37-189.

Constien, V. G., and Skidmore, V. (2006). Standalone Screen Selection Using Performance Mastercurves. Presented at the SPE International Symposium and Exhibition on Formation Damage Control, 15-17 February, Lafayette, Louisiana, USA. SPE-98363-MS.

Cowie, B. R., James, B., & Mayer, B. (2015). Distribution of total dissolved solids in McMurray Formation water in the Athabasca oil sands region, Alberta, Canada: Implications for regional hydrogeology and resource developmentDistribution of Total Dissolved Solids in McMurray Formation Water. *Aapg Bulletin*, *99*(1), 77-90.

Dang, C.T.Q., Nguyen, N.T.B., Bae, W., Nguyen, H.X., Tu, T., Chung, T., 2010. Investigation of SAGD recovery process in complex reservoir. In: Paper Presented at the SPE Asia Pacific Oil and Gas Conference and Exhibition, Brisbane, Queensland, Australia, 18-20 October, SPE-133849-MS.

Denney, D., 1998. Fines-migration control in high-water-cut Nigerian oil wells. Journal of Petroleum Technology. 50(03), 88-89.

Denney, D. (2008). Near-Wellbore Modeling: Sand-Production Issues. *Journal of Petroleum Technology, 60*(09), 106-111.

Devere-Bennett, N. (2015, November 23). Using Prepack Sand-Retention Tests (SRT's) to Narrow Down Liner/Screen Sizing in SAGD Wells. Society of Petroleum Engineers. doi:10.2118/178443-MS.

Dong, C., Li, Y., Zhang, Q., Feng, S., Zhang, L., 2014. Experimental study on sand-carrying mechanism and capacity evaluation in water-producing gas wells and its application in artificial lift optimization. In: Paper Presented at the SPE Middle East Artificial Lift Conference and Exhibition, Manama, Bahrain, 26-27 November, SPE-173700-MS.

Driscoll, F. G. (1986). Groundwater and wells. Second Edition: *St. Paul, Minnesota: Johnson Filtration Systems Inc*.

Fattahpour, V., Azadbakht, S., Mahmoudi, M. et al. (2016). Effect of Near Wellbore Effective Stress on the Performance of Slotted Liner Completions in SAGD Operations. Presented at the SPE Thermal Well Integrity and Design Symposium, 28 November-1 December, Banff, Alberta, Canada. SPE 182507-MS.

Fauré, M. H., Sardin, M., & Vitorge, P. (1997). Release of clay particles from an unconsolidated clay-sand core: experiments and modelling. *Journal of contaminant hydrology*, *26*(1-4), 169-178.

Fermaniuk, B. (2013). Sand Control in Steam Assisted Gravity Drainage (SAGD) Wellbores and Process of Slotted Liner Design and Process. *Master of Engineering thesis, University of Calgary*.

Fjar, E., Holt, R. M., Raaen, A. M., Risnes, R., & Horsrud, P. (2008). Petroleum Related Rock Mechanics (Vol. 53). Elsevier.

Firoozabadi, S., & Aziz, K. (1986). Stanford," Analysis and Correlation of Nitrogen and Lean-Gas Miscibility Pressure", SPE RES.

Furui, K., Zhu, D., Hill, A. D., Davis, E. R. and Buck, B. R. (2007). Optimization of horizontal well-completion design with cased/perforated or slotted liner completions. *SPE Production & Operations, 22*(02), 248-253.

Gabriel, G. A., & Inamdar, G. R. (1983). An experimental investigation of fines migration in porous media. Presented at SPE Annual Technical Conference and Exhibition, 5-8 October, San Francisco, California. SPE-12168-MS.

Gates, I.D., Kenny, J., Hernandez-Hdez, I.L., Bunio, G.L., 2005. Steam injection strategy and energetics of steam-assisted gravity drainage. SPE Reservoir Evaluation & Engineering. 10(01), 19-34.

Gates, I. D., Kenny, J., Hernandez, I. L. et al. (2007). Steam Injection Strategy and Energetics of Steam-Assisted Gravity Drainage. *SPE Reservoir Evaluation & Engineering*, **10** (1): 19-34. SPE-97742-PA.

Gillespie, G., Deem, C. K. and Malbrel, C. (2000). Screen selection for sand control based on laboratory tests. Paper presented at the SPE Asia Pacific Oil and Gas Conference and Exhibition.

Gray, D.H. and Rex, R.W. 1996. Formation Damage in Sandstones Caused by Clay Dispersion and Migration. Clays, Clay Minerals 14 (1): 355.

Guo, Y. (2018). Effect of Stress Build-up around SAGD Wellbores on the Slotted Liner Performance. Master of Science thesis, University of Alberta.

Guo, Y., Roostaei, M., Nouri, A. et al. (2018). Effect of stress build-up around standalone screens on the screen performance in SAGD wells. *Journal of Petroleum Science and Engineering*, 171, 325-339.

Guo, Y., Nouri, A., & Nejadi, S. (2020). Effect of Slot Width and Density on Slotted Liner Performance in SAGD Operations. *Energies*, *13*(1), 268.

Haavind, F., Bekkelund, S. S., Moen, A., Kotlar, H. K., Andrews, J. S., & Haland, T. S. (2008, January). Experience With Chemical Sand Consolidation as a Remedial Sand-Control Option on the Heidrun Field. In *SPE International Symposium and Exhibition on Formation Damage Control*. Society of Petroleum Engineers.

Han, D. H., Yao, Q., & Zhao, H. Z. (2007). Complex properties of heavy-oil sand. In *SEG Technical Program Expanded Abstracts 2007* (pp. 1609-1613). Society of Exploration Geophysicists.

Handfield, T. C., Nations, T., & Noonan, S. G. (2009). SAGD gas lift completions and optimization: a field case study at surmount. *Journal of Canadian Petroleum Technology*, *48*(11), 51-54.

Haftani, M., Kotb, O., Nguyen, P. H., Wang, C., Salimi, M., & Nouri, A. (2020). A Novel sand control testing facility to evaluate the impact of radial flow regime on screen performance and its verification. *Journal of Petroleum Science and Engineering*, 107903.

Hodge, R.M., Burton, R.C., Constien, V., Skidmore, V., 2002. An evaluation method for screen-only and gravel-pack completions. In: Paper Presented at the international Symposium and Exhibition on Formation Damage Control, Lafayette, Louisiana, 20-21 February, SPE-73772-MS.

Honarpour, M., & Mahmood, S. M. (1988, August 1). Relative-Permeability Measurements: An Overview. Society of Petroleum Engineers. doi:10.2118/18565-PA.

Imasuen, O.I., Tazaki, K., Fyfe, W.S., Kohyama, N., 1989. Experimental transformations of kaolinite to smectite. Applied clay science. 4(01), 27-41.

Irani, M. and Ghannadi, S. (2013). Understanding the heat-transfer mechanism in the steam-assisted gravity-drainage (SAGD) process and comparing the conduction and convection flux in bitumen reservoirs. *SPE Journal, 18*(01), 134-145.

Islam, M. and George, A. (1989). *Sand control in horizontal wells in heavy oil Reservoirs.* Paper presented at the SPE California Regional Meeting.

Ives, K. J. (1987). Filtration of clay suspensions through sand. *Clay Minerals*, *22*(1), 49-61.

Jimenez, J. (2008). The Field Performance of SAGD Projects in Canada. In International Petroleum Technology Conference. International Petroleum Technology Conference.

Jin, Y., Chen, J., Chen, M., Zhang, F., Lu, Y., & Ding, J. (2012). Experimental study on the performance of sand control screens for gas wells. *Journal of petroleum exploration and production technology*, *2*(1), 37-47.

Joseph, A., Ilozue, C.T., Osokogwu, U., Ajienka, J.A., 2011. Effect of water-cut on sandstone strength and its implications in sand production prediction. In: Paper Presented at the Nigeria Annual International Conference and Exhibition, Abuja, Nigeria, 30 July - 3 August. SPE-150758-MS.

Kaiser, T. M. V., Wilson, S., & Venning, L. A. (2002). Inflow analysis and optimization of slotted liners. *SPE drilling & completion*, *17*(04), 200-209.

Karazincir, O., Williams, W., Rijken, P., 2017. Prediction of fines migration through core testing. In: Paper Presented at the SPE Annual Technical Conference and Exhibition, San Antonio, Texas, USA, 9-11 October, SPE-187157-MS.

Khilar, K. C., & Fogler, H. S. (1984). The existence of a critical salt concentration for particle release. *Journal of colloid and interface science*, *101*(1), 214-224.

Khilar, K. C., & Fogler, H. S. (1998). *Migrations of fines in porous media* (Vol. 12). Springer Science & Business Media.

Kotylar, L.S., Sparks, B.D., Schutfe R., 1996. Effect of salt on the flocculation behavior of nano particles in oil sands fine tailings. Clays and Clay Minerals. 44(0l): 121-131.

Ladd, R. S. (1978). Preparing test specimens using undercompaction. Geotechnical testing journal, 1(1), 16-23.

Larsen, T., Lioliou, M. G., Josang, L. O., & Ostvold, T. (2006). Quasi Natural Consolidation of Poorly Consolidated Oil Field Reservoirs. In SPE International Oilfield Scale Symposium. Society of Petroleum Engineers.

Leone, J. A., & Scott, E. M. (1988). SPE Reservoir Eng.

Liu, X., Jiang, X., Liu, J., Li, J., & Li, W. (2017). The effect of the injection salinity and clay composition on aquifer permeability. *Applied Thermal Engineering*, *118*, 551-560.

Lunn, S. (2013). Water use in Canada's oil-sands industry: The facts. *SPE Economics & Management, 5*(01), 17-27.

Ma., C., Deng., J., Tan., Q., Li, C., Lin., H., Li, H., Liu., W. 2018. Development of a New Pre-Packed Sand-Retaining Cell. American Rock Mechanics Association.

Ma, C., Deng, J., Dong, X., Sun, D., Feng, Z., Yan, X., Hui, C. and Tian, D., 2019a. Comprehensive experimental study on the sand retention media of pre-filled sand control screens. Particulate Science and Technology, pp.1-10.

Ma, C., Deng, J., Dong, X., Sun, D., Feng, Z., Luo, C., Xiao, Q. and Chen, J., 2019b. A new laboratory protocol to study the plugging and sand control performance of sand control screens. Journal of Petroleum Science and Engineering, p.106548.

Mahmoudi, M., Fattahpour, V., Nouri, A., Yao, T., Baudet, B. A., Leitch, M., & Fermaniuk, B. (2016, November). New criteria for slotted liner design for heavy oil thermal production. In *SPE Thermal Well Integrity and Design Symposium*. Society of Petroleum Engineers.

Mahmoudi, M. (2017). *New Sand Control Design Criteria and Evaluation Testing for Steam Assisted Gravity Drainage (SAGD) Wellbores.* (Ph.D.), University of Alberta, Canada.

Mahmoudi, M., Nejadi, S., Roostaei, M., Olsen, J., Fattahpour, V., Lange, C. F., Zhu, D., Fermanuik, B. & Nouri, A. (2017, November). Design Optimization of Slotted Liner Completions in Horizontal Wells: An Analytical Skin Factor Model Verified by Computational Fluid Dynamics and Experimental Sand Retention Tests. In *SPE Thermal Well Integrity and Design Symposium*. Society of Petroleum Engineers.

Malbrel, C., Procyk, A., and Cameron, J. (1999). Screen sizing rules and running guidelines to maximize horizontal well productivity. In SPE European Formation Damage Conference. Society of Petroleum Engineers.

Markestad, P., Christie, O., Espedal, A. and Rørvik, O. (1996). Selection of screen slot width to prevent plugging and sand production. Paper presented at the SPE Formation Damage Control Symposium.

Martins, A. L., de Magalhaes, J. V. M., Ferreira, M. V. D., Calderon, A., & de Sa, A. N. (2009, January). Sand Control in Long Horizontal Section Wells. In *Offshore Technology Conference*. Offshore Technology Conference.

Matanovic, D., Cikes, M., and Moslavac, B. (2012). *Sand control in well construction and operation*. First Edition: Springer Science & Business Media.

Medina, M. (2010). SAGD: R&D for unlocking unconventional heavy-oil resources. *The Way Ahead, 6*(02), 6-9.

Minnich, K.R., Gamache, D.E. and Kus, J., Statoil Canada Ltd, Veolia Water Solutions and Technologies North America Inc, 2013. Process for solidifying organic and inorganic provisional constituents contained in produced water from heavy oil operations. U.S. Patent 8,506,467.

Miura, K., Maeda, K., & Toki, S. (1997). Method of measurement for the angle of repose of sands. *Soils and foundations*, *37*(2), 89-96.

Montero, J. D., Chissonde, S., Kotb, O. et al. (2018). A Critical Review of Sand Control Evaluation Testing for SAGD Applications. Presented at the SPE Canada Heavy Oil Technical Conference, 13-14 March, Calgary, Alberta, Canada. SPE 189773-MS.

Montero Pallares, J. D., Wang, C., Haftani, M., & Nouri, A. (2020). Experimental Correlations for the Performance and Aperture Selection of Wire-Wrapped Screens in Steam-Assisted Gravity Drainage Production Wells. *SPE Production & Operations*.

Morita, N., Whitfill, D. L., Massie, I., & Knudsen, T. W. (1989). Realistic Sand-production Prediction: Numerical Approach. SPE Production Engineering, 4(01), 15-24.

Morita, N., & Boyd, P. A. (1991). Typical Sand Production Problems Case Studies and Strategies for Sand Control. In SPE Annual Technical Conference and Exhibition. Society of Petroleum Engineers.

Muecke, T. W. (1979). Formation fines and factors controlling their movement in porous media. *Journal of petroleum technology*, *31*(02), 144-150.

Mungan, N. (1965). Permeability reduction through changes in pH and salinity. *Journal of Petroleum Technology*, *17*(12), 1-449.

Musharova, D., Mohamed, I.M., Nasr-El-Din, H.A., 2012. Detrimental effect of temperature on fines migration in sandstone formations. In: Paper Presented at the SPE International Symposium and Exhibition on Formation Damage Control, Lafayette, Louisiana, USA, 15-17 February, SPE-150953-MS.

Naganathan, S., Li, P. Y., Hong, L. H., & Sharara, A. M. (2006). Developing Heavy Oil Fields By Horizontal Well Placement-A Case Study. Paper presented at the International Oil & Gas Conference and Exhibition in China.

Nasr, T., Golbeck, H. and Pierce, G. (1998). SAGD operating strategies. Paper presented at the SPE international conference on horizontal well technology.

Noik, C., Dalmazzone, C. S. H., Goulay, C., & Glenat, P. (2005, January 1). Characterisation and Emulsion Behaviour of Athabasca Extra Heavy Oil Produced by SAGD. Society of Petroleum Engineers. doi:10.2118/97748-MS

O'Hara, M. (2015). Thermal Operations in the McMurray; an Approach to Sand Control. Presented at the SPE Thermal Well Integrity and Design Symposium, 23-25 November, Banff, Alberta, Canada. SPE 178446-MS.

Ohen, H.A., Civan, F., 1991. Predicting skin effects due to formation damage by fines migration. In: Paper Presented at the SPE Production Operations Symposium, Oklahoma City, Oklahoma, 7-9 April, SPE-21675-MS.

Ott, W. K., and Woods, J. D. (2003). *Modern sandface completion practices handbook*. Second Edition: World Oil Magazine.

Papamichos, E., & Malmanger, E. M. (1999, January). A sand erosion model for volumetric sand predictions in a North Sea reservoir. In *Latin american and caribbean petroleum engineering conference*. Society of Petroleum Engineers.

Penberthy, W. L., and Shaughnessy, C. M. (1992). *Sand control*. Henry L. Doherty Memorial Fund of AIME, Society of Petroleum Engineers.

Petrowiki (2017) Slotted liner and wire-wrapped screens. Retrieved from: https://petrowiki.org/Slotted_liners_and_wire_wrapped_screens.

Qiu, K., Gherryo, Y., Shatwan, M., Fuller, J., Martin, W., 2008. Fines migration evaluation in a mature field in Libya. In: Paper Presented at the SPE Asia Pacific Oil and Gas Conference and Exhibition, Perth, Australia, 20-22 October, SPE-116063-MS.

RGL Reservoir Management Inc, 2018 Retrieved from https://www.rglinc.com/solutions/sand-control/

Rodriguez, K., Araujo, M., 2006. Temperature and pressure effects on zeta potential values of reservoir minerals. J. Colloid Interface Sci. 300, 788–794.

Romanova, U. G., and Ma, T. (2013). An Investigation on the Plugging Mechanisms in a Slotted Liner from the Steam Assisted Gravity Operations. Presented at the SPE European Formation Damage Conference & Exhibition, 5-7 June, Noordwijk, The Netherlands. SPE 165111-MS.

Romanova, U. G., Gillespie, G., Sladic, J. et al. (2014). A Comparative Study of Wire Wrapped Screens vs. Slotted Liners for Steam Assisted Gravity Drainage Operations. Presented at the World Heavy Oil Congress, 5-7 March, New Orleans, USA. WHOC14-113.

Romanova, U. G., Ma, T., Piwowar, M. et al. (2015). Thermal Formation Damage and Relative Permeability of Oil Sands of the Lower Cretaceous Formations in Western Canada. Presented at the SPE Canada Heavy Oil Technical Conference, 9-11 June, Calgary, Alberta, Canada. SPE 174449-MS.

Romanova, U., Michel, D., Strom, R. and Stepic, J. (2017). *Understanding Sand Control for Thermal Heavy Oil and Bitumen Production Operations.* Paper presented at the SPE Thermal Well Integrity and Design Symposium.

Roostaei, M., Guo, Y., Velayati, A., Nouri, A., Fattahpour, V., Mahmoudi, M., 2018. How the design criteria for slotted liners in SAGD are affected by stress buildup around the liner. In: Paper Presented at the 52nd U.S. Rock Mechanics/Geomechanics Symposium, Seattle, Washington, 17-20 June, ARMA-2018-642.

Rose, W. D. (1985). *U.S. Patent No. 4,506,542.* Washington, DC: U.S. Patent and Trademark Office.

Rosenbrand, E., Kjoller, C., Riis, J.F., Haugwitz, C., Kets, F., Fabricius, I.L., 2015. Different effects of temperature and salinity on permeability reduction by fines migration in Berea Sandstone. Geothermics. 53, 225-235.

Roscoe, M. (1990). Roscoe Moss Company, handbook of ground water development (p. 493): New York: Wiley.

Russell, T., Pham, D., Neishaboor, M. T., Badalyan, A., Behr, A., Genolet, L., ... & Bedrikovetsky, P. (2017). Effects of kaolinite in rocks on fines migration. *Journal of Natural Gas Science and Engineering*, *45*, 243-255.

Russell, T., Chequer, L., Borazjani, S., You, Z., Zeinijahromi, A., & Bedrikovetsky, P. (2018). Formation damage by fines migration: Mathematical and laboratory modeling, field cases. In *Formation Damage During Improved Oil Recovery* (pp. 69-175). Gulf Professional Publishing.

Sacramento, R. N., Yang, Y., You, Z., Waldmann, A., Martins, A. L., Vaz, A. S., ... & Bedrikovetsky, P. (2015). Deep bed and cake filtration of two-size particle suspension in porous media. *Journal of Petroleum Science and Engineering*, *126*, 201-210.

Sanyal, T., Al-Hamad, K., Jain, A. K., Al-Haddad, A. A., Kholosy, S., Ali, M. A., & Abu Sennah, H. F. (2012, January). Laboratory challenges of sand production in unconsolidated cores. In *SPE Kuwait International Petroleum Conference and Exhibition*. Society of Petroleum Engineers.

Sharma, M.M., Yortsos, Y.C., 1986. Permeability impairment due to fines migration in sandstones. In: Paper Presented at the SPE Formation Damage Control Symposium, Lafayette, Louisiana, 26-27 February, SPE-14819-MS.

Simon, D. E., McDaniel, B. W., & Coon, R. M. (1976, January). Evaluation of fluid pH effects on low permeability sandstones. In *SPE Annual Fall Technical Conference and Exhibition*. Society of Petroleum Engineers.

Sivagnanam, M., Wang, J., & Gates, I. D. (2017). On the fluid mechanics of slotted liners in horizontal wells. *Chemical Engineering Science*, *164*, 23-33.

Sokolov, V. N., & Tchistiakov, A. A. (1999). Physico-chemical factors of clay particle stability and transport in sandstone porous media. In *Proceedings of the European Geothermal Conference* (pp. 199-209).

Spronk, E.M., Doan, L.T., Matsuno, Y., Harschnitz, B., 2015. SAGD liner evaluation and liner test design for JACOS Hangingstone SAGD development. In: Paper Presented at the SPE Canada Heavy Oil Technical Conference, Calgary, Alberta, Canada, 9-11 June, SPE-174503-MS.

Stone, T. W., and Bailey, W. J. (2014). Optimization of Subcool in SAGD Bitumen Processes. Presented at the World Heavy Oil Congress, 5-7 March, New Orleans, USA. WHOC14-271.

Suman, G., Ellis, R., and Snyder, R. (1985). *Sand Control Handbook*. Houston: Gulf publishing company.

Tausch, G. H., & Corley Jr, B. (1958, January). Sand exclusion in oil and gas wells. In *Drilling and Production Practice*. American Petroleum Institute.

Tiffin, D. L., King, G. E., Larese, R. E. et al. (1998). New Criteria for Gravel and Screen Selection for Sand Control. Presented at the SPE Formation Damage Control Conference, 18-19 February, Lafayette, Louisiana. SPE 39437-MS.

Underdown, D., Dickerson, R. and Vaughan, W. (2001). The nominal sand-control screen: A critical evaluation of screen performance. *SPE Drilling & Completion, 16*(04), 252-260.

Van Oort, E., van Velzen, G., and Leerlooijer, K. (1993). Impairment by Suspended Solids Invasion: Testing and Prediction. *SPE Prod & Fac*, 8(3): 178-184. SPE 23822-PA.

Valdes, J. R., & Santamarina, J. C. (2006). Particle clogging in radial flow: Microscale mechanisms. *SPE Journal*, *11*(02), 193-198.

Valdya, R. N., & Fogler, H. S. (1992). Fines migration and formation damage: influence of pH and ion exchange. *SPE production engineering*, *7*(04), 325-330.

Van Vliet, J., and Hughes, M. J. (2015). Comparison of Direct-Wrap and Slip-On Wire Wrap Screens for Thermal Well Applications. Presented at the SPE Thermal Well Integrity and Design Symposium, 23-25 November, Banff, Alberta, Canada. SPE 178462-MS.

Velayati, A., Roostaei, M., Fattahpour, V., Mahmoudi, M., Nouri, A., Alkouh, A., Fermanuik, B., & Kyanpour, M. (2018, December). Design Optimization of Slotted Liner Completions in Cased and Perforated Wells: A Numerical Skin Model. In *SPE International Heavy Oil Conference and Exhibition*. Society of Petroleum Engineers.

Velayati, A., Roostaei, M., Sharbatian, A., Fattahpour, V., Mahmoudi, M., Lange, C. F., & Nouri, A. (2019, August). On the Sanding and Flow Convergence Skin in Cased and Perforated Slotted Liner Vertical Production Wells. In *53rd US Rock Mechanics/Geomechanics Symposium*. American Rock Mechanics Association.

Wan, R. (2011). *Advanced well completion engineering*. Gulf professional publishing.

Wang, C., Pang, Y., Montero Pallares, J.D., Haftani, M., Fattahpour, V., Mahmoudi, M., Nouri, A., 2018. Impact of anisotropic stresses on the slotted liners performance in steam assisted gravity drainage process. In: Paper Presented at the SPE Thermal Well Integrity and Design Symposium, Banff, Alberta, Canada, 27-29 November, SPE-193347-MS.

Wang, C., Pang, Y., Mahmoudi, M., Haftani, M., Salimi, M., Fattahpour, V., & Nouri, A. (2020a). A set of graphical design criteria for slotted liners in steam assisted gravity drainage production wells. *Journal of Petroleum Science and Engineering*, *185*, 106608.

Wang, C., Pallares, J. D. M., Haftani, M., & Nouri, A. (2020b). Developing a methodology to characterize formation damage (pore plugging) due to fines migration in sand control tests. *Journal of Petroleum Science and Engineering*, *186*, 106793.

Wang, C., Pallares, J. D. M., Haftani, M., & Nouri, A. (2020c) Protocol for optimal size selection of punched screen in Steam Assisted Gravity Drainage operations. *Journal of Petroleum Science and Engineering*, *196*, 107689.

Williams, C. F., Richard, B. M. and Horner, D. (2006). A new sizing criterion for conformable and nonconformable sand screens based on uniform pore structures. Paper presented at the SPE International Symposium and Exhibition on Formation Damage Control.

Wilson, A. (2013). Review of Water Use at Canada's Oil Sands Points Toward Environmental Sustainability. *Journal of Petroleum Technology, 65*(08), 132-134.

Wu, B., Tan, C.P., Lu, N., 2006. Effect of water-cut on sand production - an experimental study. SPE Production & Operations. 21(03), 349-356.

Wu, B., Choi, S. K., Feng, Y. et al. (2016). Evaluating Sand Screen Performance Using Improved Sand Retention Test and Numerical Modelling. Presented at the Offshore Technology Conference Asia, 22-25 March, Kuala Lumpur, Malaysia. OTC-26434-MS.

Xie, J., 2015. Slotted liner design optimization for sand control in SAGD wells. In: Paper Presented at the SPE Thermal Well Integrity and Design Symposium, Banff, Alberta, Canada, 23-25 November, SPE-178457-MS.

Yang Y., Siqueira F.D., Vaz A., Badalyan A., You Z., Zeinijahromi A., Carageorgos T., Bedrikovetsky P., 2018. Part 1: fines migration in aquifers and oilfields: laboratory and mathematical modelling; flow and transport in subsurface environment. Springer.

Yi, X. (2002). Simulation of sand production in unconsolidated heavy oil reservoirs. *Journal of Canadian Petroleum Technology, 41*(03).

You, Z., Badalyan, A., Yang, Y., Bedrikovetsky, P., Hand, M., 2019. Fines migration in geothermal reservoirs: laboratory and mathematical modeling. Geothermics. 77, 344-367.

You, Z., Bedrikovetsky, P., 2018. Well productivity impairment due to fines migration. In: Paper Presented at the SPE International Conference and Exhibition on Formation Damage Control, Lafayette, Louisiana, USA, 7-9 February, SPE-189532-MS.

Zeinijahromi, A., Machado, F. A., Bedrikovetsky, P.G., 2011. Modified mathematical model for fines migration in oil fields. In: Paper Presented at the Brasil Offshore, Macaé, Brazil, 14-17 June, SPE-143742-MS.

Zhang, W., Youn, S. and Doan, Q. T. (2007). Understanding reservoir architectures and steam-chamber growth at Christina Lake, Alberta, by using 4D seismic and crosswell seismic imaging. *SPE Reservoir Evaluation & Engineering, 10*(05), 446-452.

Appendix A: Testing Repeatability

This section proves the repeatability of the testing. Additional pre-packed SRT tests are conducted with the same coupon specifications. Sand production and retained permeability are used to judge the repeatability. Slotted liner with the slot size of 0.014'' and slot density of SPC 54 and punched screen with the aperture size of 0.014'' are used in the repeatability analyses. The formation sand for the repeatability tests is DC-III.

Figure A.1 shows the sand production repeatability results for the slotted liner and punched screen, respectively. Table A-1 presents the retained permeability repeatability results. The results prove the repeatability of experimental testing.

(a)

(b)
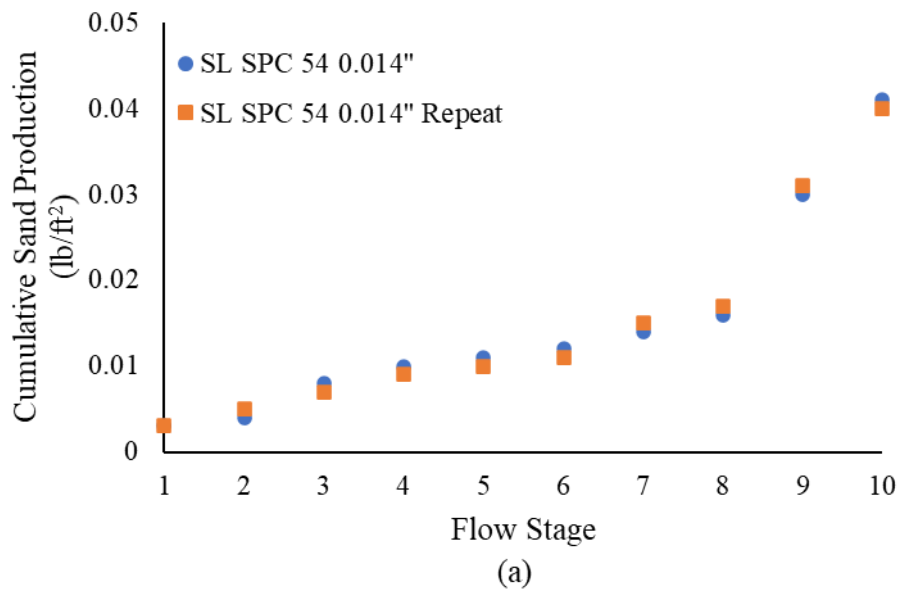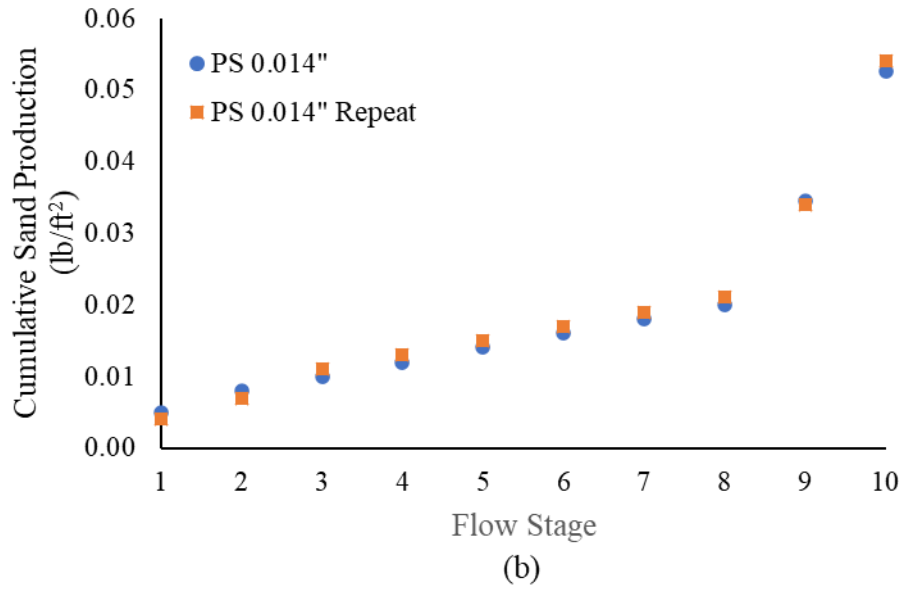
Figure A. 1 Sand production repeatability results, (a) slotted liner 0.014'', SPC 54, (b) punched screen 0.014''

Table A. 1 Retained permeability repeatability results

slotted liner (SPC54)		punched screen	
k_{ret} (%)		k_{ret} (%)	
0.014"	0.014" - repeat	0.014"	0.014" - repeat
70%	71%	71%	73%

Appendix B: Standard Operating Procedure (SOP) of Pre-packed SRT

B.1 Introduction

B.1.1 Policy

The Sand Retention Test (SRT) should be conducted in accordance with predetermined specifications to obtain the desired testing results. All the personnel involved in conducting the test should understand the testing procedure and ensure standard operating procedures follow every step.

B.1.2 Purpose

This SOP is prepared to present a consistent method for the sand retention test under three-phase flow conditions.

The objective of this SOP is to compare the performance of different Stand-along Screens (SASs). In this study, the slotted liner, wire-wrapped screen, and punched screen coupon will be used. Multi-phase flow using brine, oil, and nitrogen is used as the injection fluid to emulate the real reservoir fluid.

B.1.3 Scope

This procedure should be followed by all personnel involved in the handling and conducting of SRT.

B.1.4 Safety instructions

PPE should be on regardless of the task.

Installing/removing the cell head requires at least two people; all the ports should be open.

A face mask should be used if dealing with dry sand, "especially clay."

B.1.5 Covid-19 Prevention

Check your physical conditions before entering the lab. If you feel unwell, stay at home. Clean up facilities and workspace before running the test. Wear gloves and mask and keep social distancing with your co-workers. Avoid touching your face while running the test. Change the glove or mask whenever necessary. After finishing the test, clean up the facilities with alcohol and sanitize your hands.

B.2 Testing Procedures

B.2.1 Brine Preparation

1) Check pH and EC from the DI water supplier, pH should be neutral (≈7), and EC should be less than five μs/cm.

2) Prepare 40L brine for each test. The concentration of the brine is 0.04% (weight percent). For 100L water (100 kg, water density is 1Kg/L), 4g salt should be added. For 40L water, 16g NaCl salt should be added.

3) Mix the brine thoroughly to obtain a uniform mixture using the driller (no deposit at the bottom).

4) The pH should be checked and calibrated using a pH meter whenever brine is prepared. pH$^-$ or pH$^+$ (available in the lab) should be used to adjust the pH as required. The target pH is 7.9.

5) EC of brine should be measured using the EC meter and recorded in the test datasheet.

B.2.2 Oil Preparation

1) Prepare 40L H5 mineral oil for each test. The viscosity of H5 oil is around ten cp @ 20ºC.

B.2.3 Nitrogen Preparation

1) Before starting the test, check the nitrogen cylinder pressure through the pressure regulator gauge to ensure the pressure is in the green zone, which means there is enough pressure to operate. If the pressure dropped to a certain limit, for example, the red zone, it means the cylinder needs to be refilled soon. Make sure to close the valve as well as the regulator after each test.

B.2.4 Sand Pack Preparation

1) 12kg dry sand should be prepared for each test.

2) Commercial sand compositions to replicate the four representative McMurray Formation Oil Sands are listed in Table B.1. Example: Obtain a certain amount of each sand type based on the weight proportion of DC-II; Sil-1: 1584g, LM70: 9538g, Helmer Kaolinite: 888g.

3) Clay should be sieved (mesh size 160μm) in the geotechnical lab to remove large particles.

4) Thoroughly mix all the dry sands in the sandbox.

Table B. 1 Sand Composition

Sand Type	Ind 50	Sil-1	Sil-4	Sil-7	LM 70	LM 125	Helmer Kaolinite
DC-I	-	15.5%	-	-	-	70.0%	14.5%
DC-II	-	13.2%	-	-	79.4%	-	7.4%
DC-III	-	66.1%	-	2.9%	25.7%	-	5.4%
DC-IV	-	-	36.5%	47.1%	6.9%	5.4%	4.2%

5) Add 1.2 kg brine to reach 10% water contain (water contain= total weight of water added / total weight of dry sand).

6) Thoroughly mix all the dry sand and brine to have homogenous moisture.

7) Take a sample to define the PSD of the mixed sample.

B.2.5 Cell Assembly

1) Install the bottom sand trap and make sure there is no remaining sand in it. Use the Viton Gasket to prevent leakage during the test.

2) Clean the coupon with air; make sure no plugging inside the slots.

3) Mount the selected coupon (e.g., 0.008" WWS) onto the core holder assembly.

4) Put steel mesh into the inlet and outlet of the pressure port fittings.

5) Install the cell in its place on the testing plate. Put the Viton Gasket to prevent leakage during the test.

6) Tight the bottom sand trap and cell holder together

7) Add prepared sand, silt, and clay mixture (as specified) to the core holder space above the coupon using layer by layer moist tamping method. The weight of each layer of the sand sample is 1kg. Use the packing tool to compact each layer of sand sample to reach specific porosity. Measure the height of each layer of the sand pack in four positions and consider the average value to calculate the porosity and density. The height and porosity should be consistent for each layer. The error tolerance for porosity is 0.01. There are 13 layers in total. Use the spreadsheet on the lab computer for calculation; E:\SRT\Sand pack preparation.

   Once the height of a layer is less than expected one means that the layer is overpacked. In this situation, the last sand layer should be scratched and mixed, and then packed again to be consistent.

8) After packing, put the porous disk and install the top confining (injection end) piston in the apparatus (use oil to lubricate the piston) and apply the equivalent of 60 psi axial load. Apply vacuum grease on the O-ring and during the installation, make sure the O-ring stays in its groove.

9) Saturate the sand pack with brine (400ppm salinity) at 250 cc/hr (it is almost 11 on the screen of the converter). Record the mass balance reading before and after saturation is

done (so fluid rate during saturation can be estimated). Connect the lines for pressure readings and de-air the pressure transducer during the saturation stage.

10) Flow water from top to bottom at 1000cc/hr for 10mins to measure the absolute permeability (K_{abs}) and check if the K_{abs} values at the top and middle section are within acceptable difference (around 100 md).

11) Displace water to reach irreducible water saturation (S_{wir}) from top to bottom using oil at a low rate (1000 cc/hr).

12) Injection Phases: The injection scheme will consist of single-phase oil flow, two-phase flow (oil, water), and finally, three-phase flow (oil, water, and gas). Different flow rates are employed, accounting for various scenarios of effective flow (Figure B-1):

Single-phase flow by oil:

- Commence injection (top to bottom of the sand pack and out through slot) with oil phase at a rate of 2900 cc/hr. Flow until stable delta P is reached. Afterward, record pressure drops through the entire sand pack, on top of the slot, and at the base of the slot for 30 mins.

- Stop the fluid injection,

- Close the butterfly valve after 30mins flow and then open the sand trap. Collect the produced sand in the sand trap. Fill the sand trap with water and connect it back to the butterfly valve and open the valve for the next flow. This step should be repeated after each phase flow to collect the produced sand for each flow stage.

- Take samples in each flow stage to measure the produced fine. Open the valve slowly to take the sample.

- Commence injection (top to bottom of the sand pack and out through slot) with oil phase at a rate of 4300 cc/hr. Flow until stable delta P is reached. Record pressure drops through the entire sand pack, on top of the slot, and at the base of the slot. Inject the oil for 30 mins in this flow rate, and then stop the injection to take the samples as mentioned.

- Commence injection (top to bottom of the sand pack and out through slot) with oil phase at a rate of 7200 cc/hr. Flow until stable delta P is reached. Record pressure drops through the entire sand pack, on top of the slot, and at the base of the slot.

Inject the oil for 30 mins in this flow rate, and then stop the injection to take the samples as mentioned.

Two-phase flow by oil and water:

- Inject oil and water phase both at a rate of 1450 cc/hr, meaning 50% Water cut (W_{cut}) and total liquid rate of 2900 cc/hr. Flow until stable delta P is reached. Record pressure drops through the entire sand pack, on top of the slot, and at the base of the slot for 30 mins. Measure the weight of oil and water entering as well as leaving the sand pack to know the saturation of the sand pack for each flow stage. This procedure should be repeated for the rest of the two-phase flow stages to track the saturation change.

- Stop the flow injection.

- Take a sample for each flow stage to measure the produced fine. Each fluid sample shall be taken from the onset of the breakthrough for 20 mins.

- Initiate co-injection (top to bottom of the sand pack and out through slot) with oil phase at a rate of 2150 cc/hr and water phase at a rate of 2150 cc/hr. Again, 50% of W_{cut} is achieved. Flow until stable delta P is reached. Record pressure drops through the entire pack, on top of the slot, and at the base of the slot. Injected the fluids for 30 mins in this flow rate and follow the tests as abovementioned.

- Commence co-injection (top to bottom of the sand pack and out through slot), maintaining a 50% W_{cut} with oil phase at a rate of 3600 cc/hr and water phase at a rate of 3600 cc/hr. Flow until stable delta P is reached. Record pressure drops through the entire pack, on top of the slot, and at the base of the slot. Injected the fluids for 30 mins in this flow rates and follow the tests as abovementioned.

- Keeping the liquid injection rate constant, vary the W_{cut} from 50% to 75% by decreasing the oil rate to 1600 cc/hr and increasing the water rate to 4800 cc/hr. Flow until stable delta P is reached. Record pressure drops through the entire pack, on top of the slot, and at the base of the slot. Note any sand production. Injected the fluids for 30 mins in this flow rates and follow the tests as abovementioned.

- Stop oil injection and increase the water flow rate to 7200 cc/hr to have single-phase water injection (100% water cut). Injected the fluids for 30 mins in this flow rate and follow the tests as abovementioned.

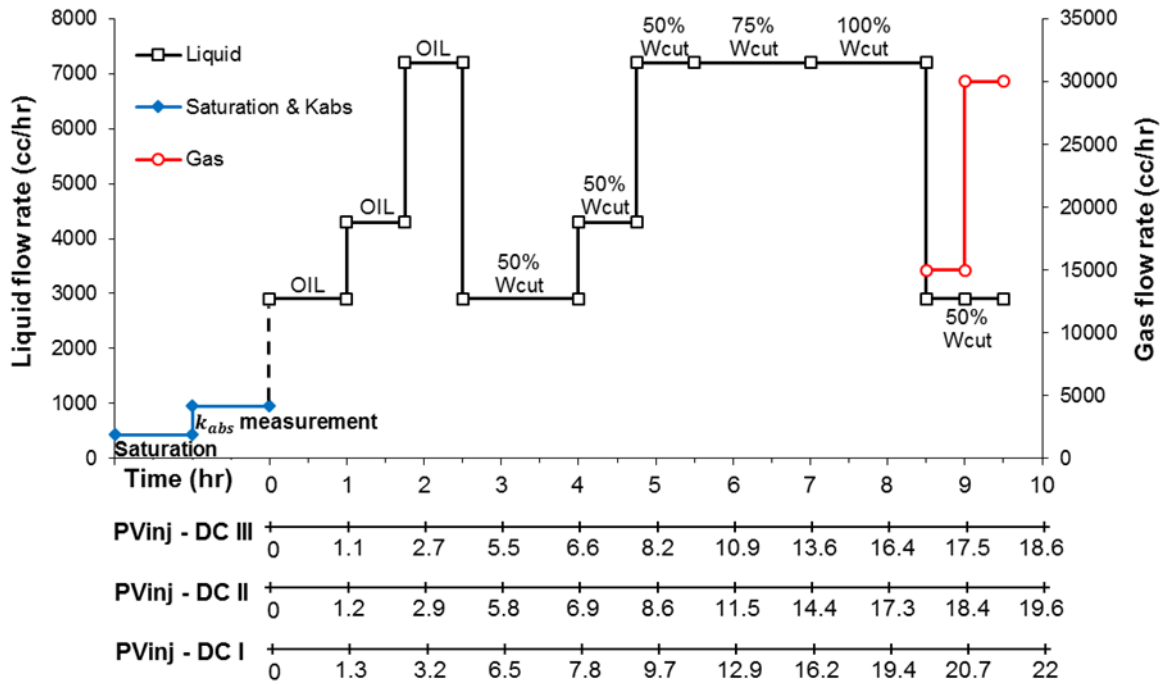- The liquid injection scheme will follow the pattern shown in the figure below.

**Figure B. 1 Different flow rates of oil-water in SRT**

Three-phase flow by oil, water, and gas:

- Commence simultaneous injection of the three phases (top to bottom of the sand pack and out through slot). Inject oil at the rate of 1450 cc/hr, water at the rate of 1450 cc/hr, and gas at the rate of 15000 cc/hr. Flow until stable delta P is reached. Record pressure drops through the entire pack, on top of the slot, and at the base of the slot.

- The gas injection will look like the trend presented in Figure B.1.

- Finalize with injection (top to bottom of the sand pack and out through slot) of oil phase at the rate of 1450 cc/hr, water phase at the rate of 1450 cc/hr, and gas phase at the rate of 30000 cc/hr. Flow until stable delta P is reached. Record pressure drops through the entire pack, on top of the slot, and at the base of the slot. Note any sand production.

B.2.6 Disassemble the Cell and Taking the Samples

1) Stop the pumps and the gas supply,
2) Close the pump intake valves,

191

3) Stop recording the data acquisition software and save the data,

4) Start to drain the back-pressure column,

5) Release the axial load,

6) Disconnect pump and gas lines and remove the top platen,

7) Disconnect the pressure transducer lines and clean them using water,

8) Take a core sample from the sand pack using the split core barrel. Take three large scale samples at i. Top, ii. Middle and iii. Bottom. Put all samples in the container and label them based on the labeling protocol. Figure B.5 shows the position of each core sample.
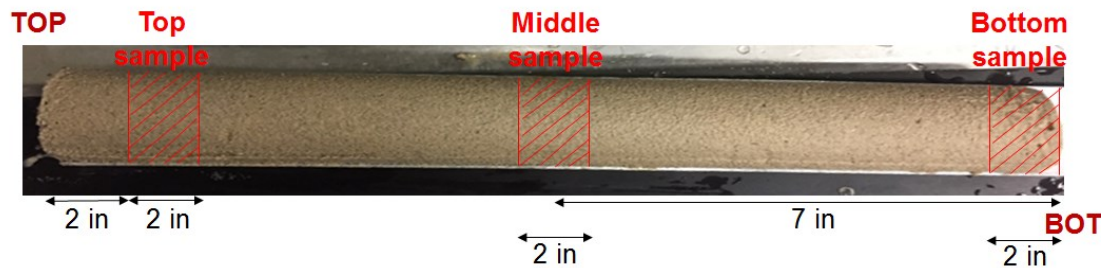
Figure B. 2 Core Sample Demonstration

9) Remove the sand pack slowly with shovels,

10) Open the nuts and take out the cell,

11) Clean the sand above the coupon with a vacuum.

12) Remove the coupon and wash the bottom surface of the coupon carefully into the bottom part (sand trap) to gather the produced sand or passed sand from the slots.

13) Collect the produced sand at the bottom part (sand trap).

14) Take a picture of the coupon with a flashlight at the back to check if there is any plugging inside the slots. In this regard, it is better to use a magnifier to check all slits for any plugging inside them.

15) Clean the coupon with compressed air, then put it into the oil to avoid rusting.

16) Clean the produced sand particles with soap and rinse with hot water to remove part of the oil attached to the grains. Additional heating in the oven can provide a good sample,

B.2.7 Analysis of Samples Taken from Sand Pack

1) Put sand samples (one sample from the mixture and three samples from the sand pack after the test) into the oven and cook under $100\,℃$ to vaporize the residual oil in the sand sample.

2) Record the weight of each part and also the weight of their containers. Record them in a table shown below (Table B.2).

3) Crash each part of the sample slowly by mortal and pastel (grinder) and mix with water. Use a blender to mix them thoroughly. Dump the mixture into the specially designed sieve (#325, 44 microns) to separate sand and fines.

4) Take some fluid sample (with washed fines) in small bottles, label the bottle based on the labeling protocol.

5) Wash sand out of sieve into a container and label the container based on the labeling protocol. Dry the sand in the oven (100°C) for at least 6 hours.

6) Weight the dry sand with the container and record the weight in Table B.2.

7) Then, easily calculate the weight of the clay content in each sample.

Table B. 2 Wet sieving data recording table.

Date:				
Sample Name	Weight of container (gr)	Weight of sand & clay (gr)	Weight of dry sand & container (gr)	Weight of washed clay (gr)

B.2.8 Analysis of Produced Sand

1) Use detergents to clean the produced sand and make sure there is no residual oil on the sand grain surface.

2) Dry the sand at room temperature.

3) Collect the dry sand in small cups and weigh them.

4) Record the weight of produced sand and label the container based on the labeling protocol.

B.2.9 Analysis of Produced fine

1) Put single-phase fluid samples into small bottles and put them into the turbidity meter chamber to measure the turbidity of each sample. Be sure to shake them before measuring.

Ps: Unit: NTU (Nephelometric Turbidity Unit)   Tap water: 0.32

2) For the two-phase fluid samples, evaporate the samples in the oven (100℃) and measure the remaining fines weight. It is essential to measure the volume of the fluid before putting it in the oven.

B.2.10 Labeling Protocols

The standard procedure should be followed for labeling the samples taken during and after the test, as given in Table B.3.

Table B. 3 Labeling table

Sand Control Testing Lab			
Operator and Test No.	CW-15-2	**Date**	2018.03.29
Test ID & Phases	SRT (O,W,G)	**PSD**	DC-III
Sample Type	PS	**Coupon**	Seamed, SPC30, 0.026"
Salinity (ppm)	400	**pH**	7.9
Remark	Control effect of flow rate		
Sample Name	CW12-2-180329-SRT-DCIII- PS –Seamed30,0.026		

Operator and Test No.: Initial of a person who is doing the test and number of the test and sample; for example, CW-15-2 is 2nd sample in the 15th test of Chenxi Wang.

Date: When the sample is taken.

Test ID and Phases: Define the type of the test, number of the flow phases and type of flow (B, O, and G for Brine, Oil, and Gas, respectively) applied in the test. For examples, SRT1 to SRT3 for single phase to three phases Sand Retention Test, respectively

PSD: Insert the type of sample or PSD used for the test.

Sample Type: Define what the sample is; such as Produced Sand (PS), Produced Clay (PC), Fine Particles and Stage (FP3), Sand -Top (S, T), Sand-Mid (S, M), Sand-Bot (S, B), Clay-Top (C, T), Clay-Mid (C, M), Clay-Bot (C, B), …

Coupon: Define the type of coupon and its specifications such as slot per column (SPC) and size of each slot, such as WWC, Single Slot, Multi-slot, …

Salinity (ppm): Insert salinity of brine.

pH: Insert pH of brine.

Remark: Briefly explain the aim of the test.

Sample Name: It is composed of abbreviations of the information mentioned above.

Appendix C: Hazard Assessment

C.1 Instructions:

Review the Hazard Description (column 3) of each Exposure Condition (column 2) and check the ones that are present (column 1). For every condition present, review the Examples of Engineering Controls and Personal Protective Equipment (column 4) and then complete the Specific Engineering Controls and PPE (column 5) that you intend to use to reduce or eliminate the hazard.

| Check if Present	Exposure Condition	Hazard Description	Examples of Engineering Controls and Personal Protective Equipment (PPE)	Specific Engineering Controls and Personal Protective Equipment (PPE)
		Biological Hazards		
☐	Nano-particles	Unknown health hazards due to small size	Containment, respirators	Mandatory use of a mask
Chemical Hazards				
☐	Chemicals, low hazard with low splash probability	Skin and eye irritation	Safety glasses, chemical resistant gloves, lab coat, closed shoe of good structure, long pants; Be aware of the nearest eyewash and shower	

Check if Present	Exposure Condition	Hazard Description	Examples of Engineering Controls and Personal Protective Equipment (PPE)	Specific Engineering Controls and Personal Protective Equipment (PPE)
☐	Compressed gases	Asphyxiation, accidental tip over, content release, and pinch points	Gas cylinder and line must be secured to stationary objects in a safe location away from danger or impact; Safety glasses and gloves	
☐	Washing glassware	Skin lacerations from broken glass	Safety glasses, rubber gloves, lab coat.	
Physical Hazards				
☐	Compression (pressure)	Injury from sudden release of energy from valves, compression chambers	Energy control, safety classes, shields if necessary, body position	
☐	Confined Spaces	Exposure, falls, dangerous atmospheres, asphyxiation, noise, vibration	Buddy system, lanyards, ventilation, monitoring	

Check if Present	Exposure Condition	Hazard Description	Examples of Engineering Controls and Personal Protective Equipment (PPE)	Specific Engineering Controls and Personal Protective Equipment (PPE)
☐	Sliding hammer	Pinch, crush, caught, pulled in, electrocution	Energy control, signage, guards, no jewelry, tie back long hair	
☐	Impact	Injury to head or body	Hard hat, impact resistant toed shoes, body position	
☐	Manipulation of large objects	Injury, death	Training, proper lifting equipment, procedures, inspections, buddy system	
☐	Material Handling	Physical injury, strains, sprains	Training, buddy system, gloves, standard operating procedures	
☐	Noise	Deafness, hearing damage, inability to communicate	Noise monitoring, hearing protection if necessary, training, and engineering controls (e.g., enclosures, baffles, mufflers)	

| Check if Present	Exposure Condition	Hazard Description	Examples of Engineering Controls and Personal Protective Equipment (PPE)	Specific Engineering Controls and Personal Protective Equipment (PPE)
☐	Penetration	Wounds	Training, padding of surfaces, signage, and body position, avoid use of sharp object	
☐	Respirable Dust	Lung damage	Local exhaust ventilation. Monitoring, respirator, access to vented room (soil preparation lab)	

Appendix D: Absolute Permeability of All Testing Samples

D.1 Absolute Permeability for Punched Screen Testing

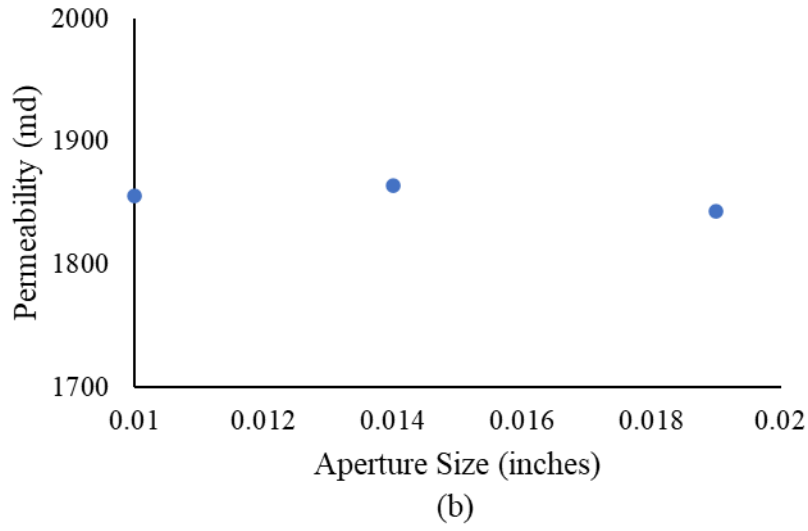*D.1.1 Absolute Permeability for DC-I*

(a)

(b)

(c)
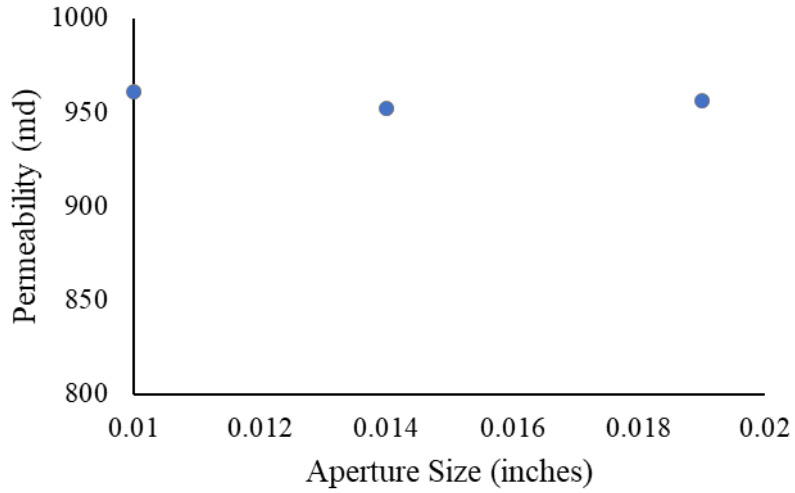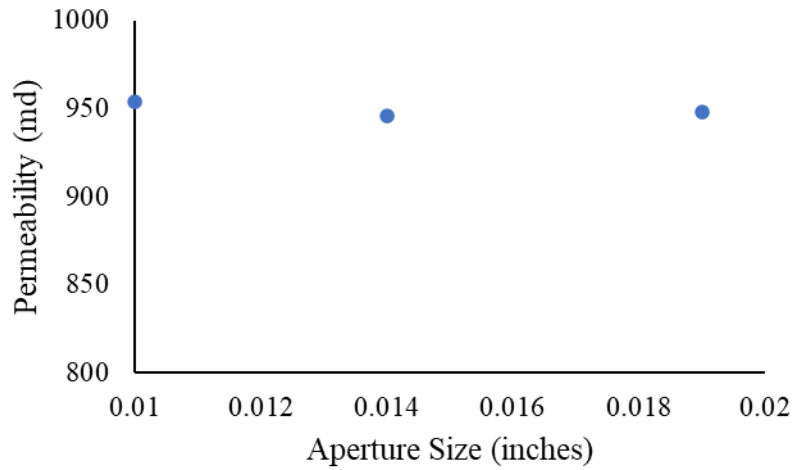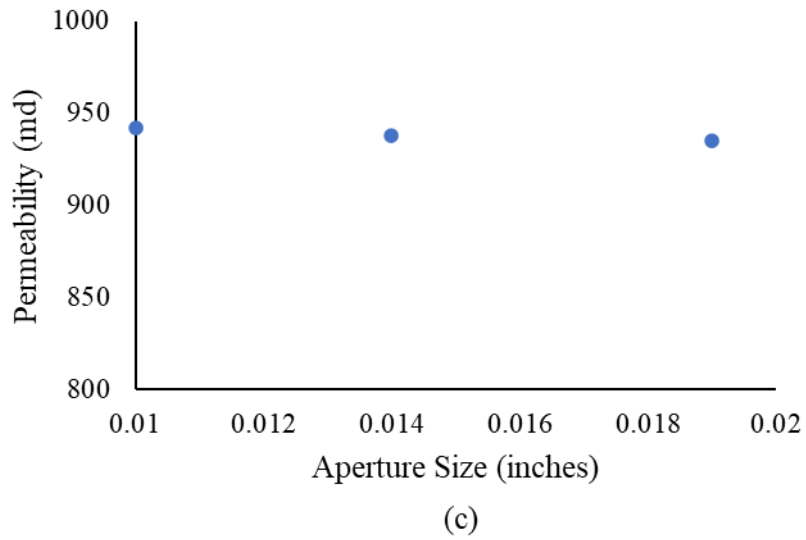
Figure D. 1 Absolute permeability of the punched screen tests, (a) top section, (b) middle section, and (c) bottom section

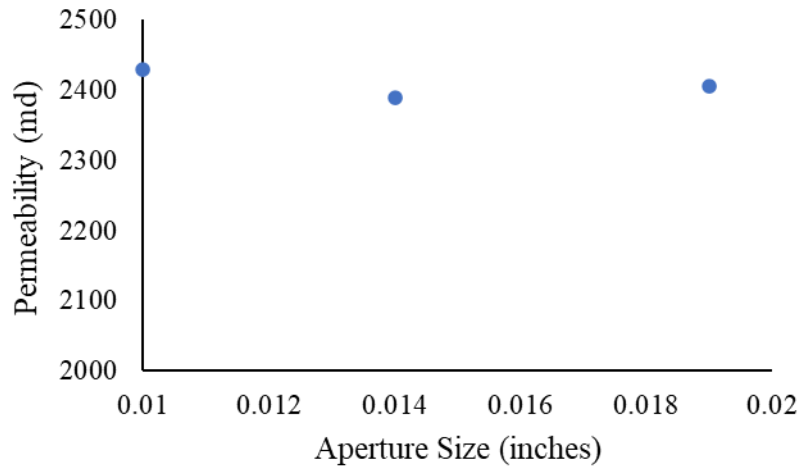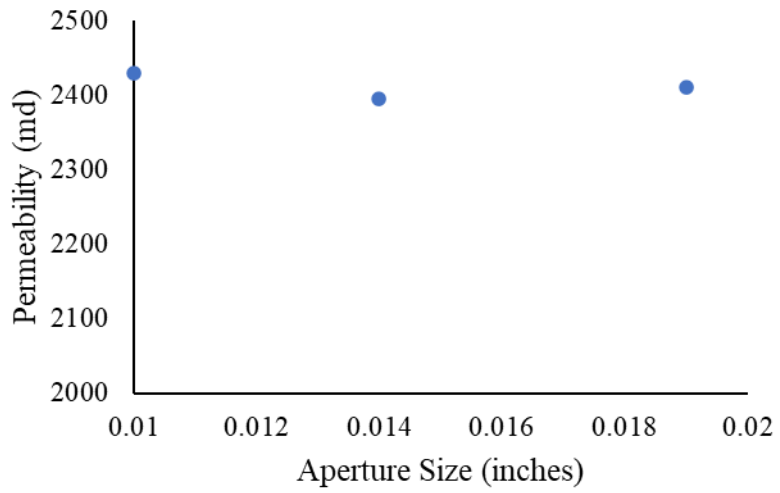*D.1.2 Absolute Permeability for DC-II*

(a)
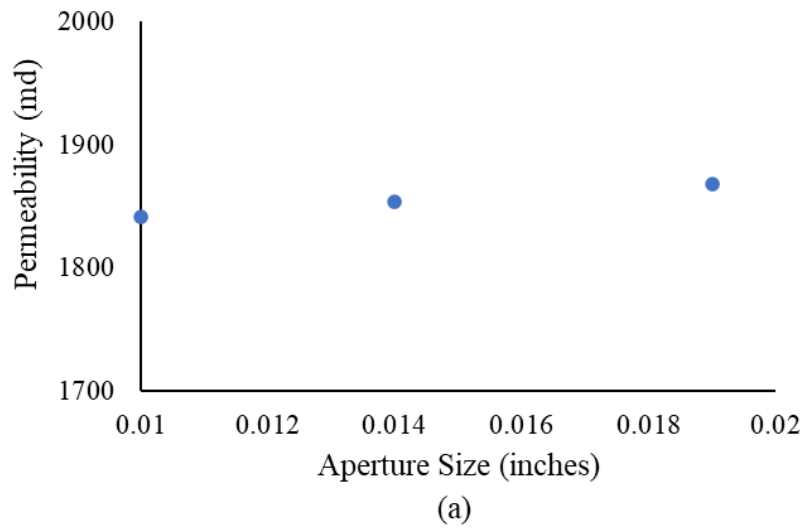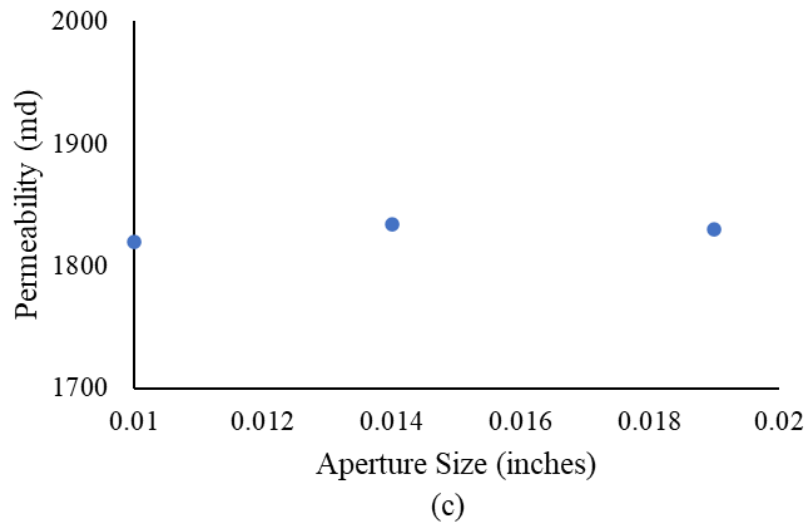
Figure D. 2 Absolute permeability of the punched screen tests, (a) top section, (b) middle section, and (c) bottom section

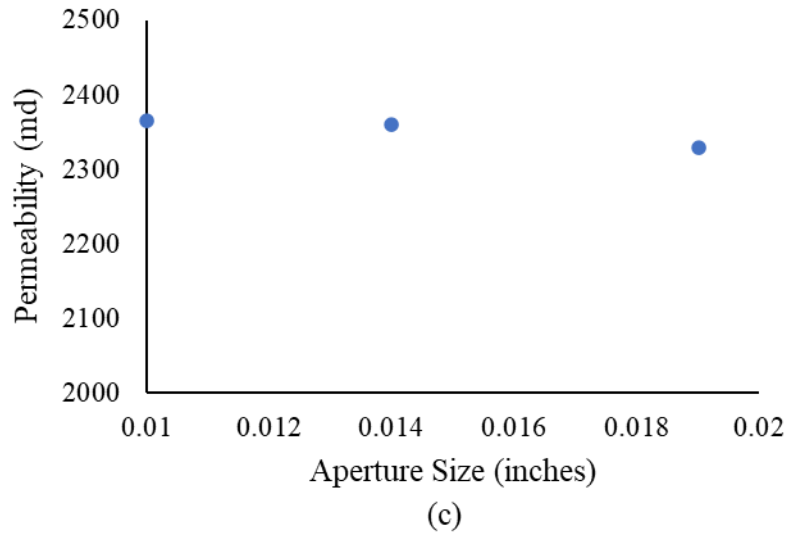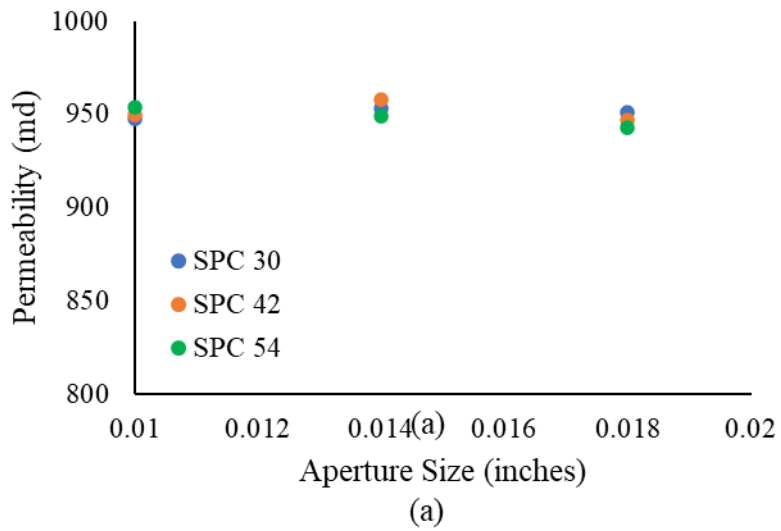*D.1.3 Absolute Permeability for DC-III*
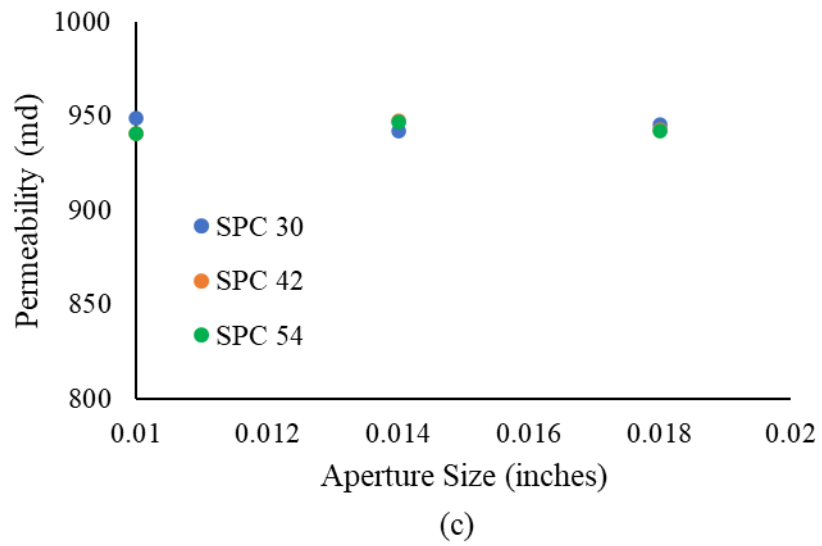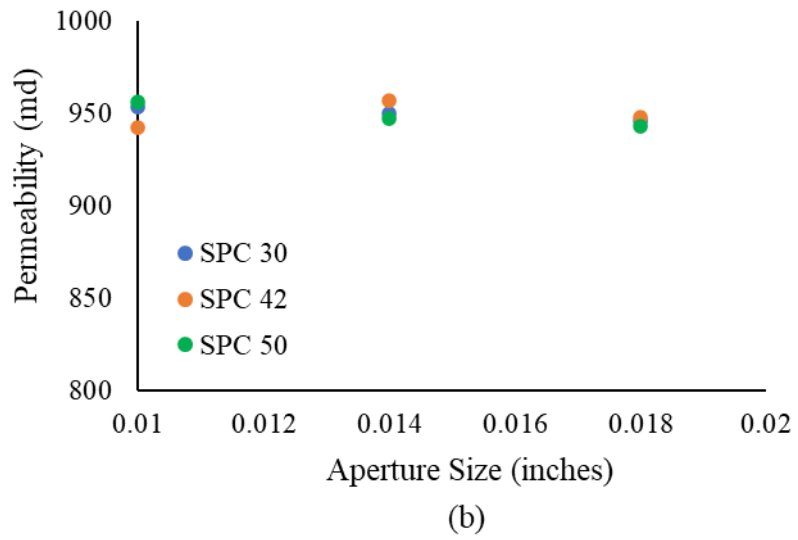

(a)

(b)

Figure D. 3 Absolute permeability of the punched screen tests, (a) top section, (b) middle section, and (c) bottom section

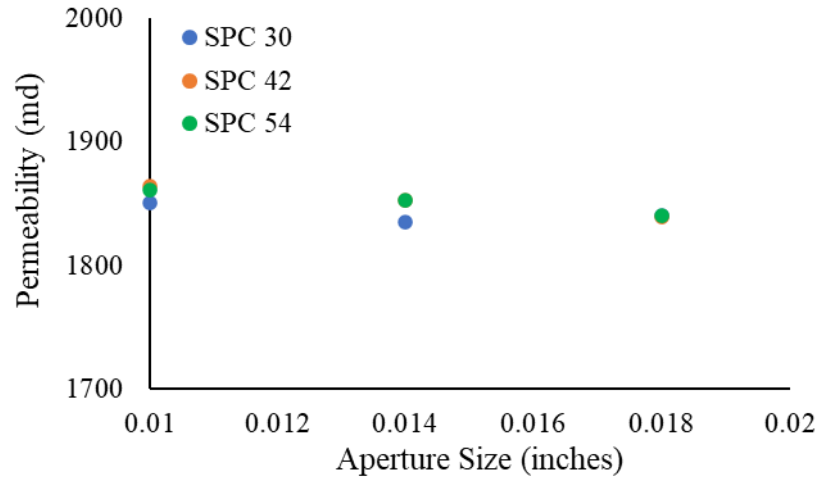## D.2 Absolute Permeability for Slotted Liner Testing

D.2.1 Absolute Permeability for DC-I

Figure D. 4 Absolute permeability of the slotted liner tests, (a) top section, (b) middle section, and (c) bottom section

D.2.2 Absolute Permeability for DC-II

(a)
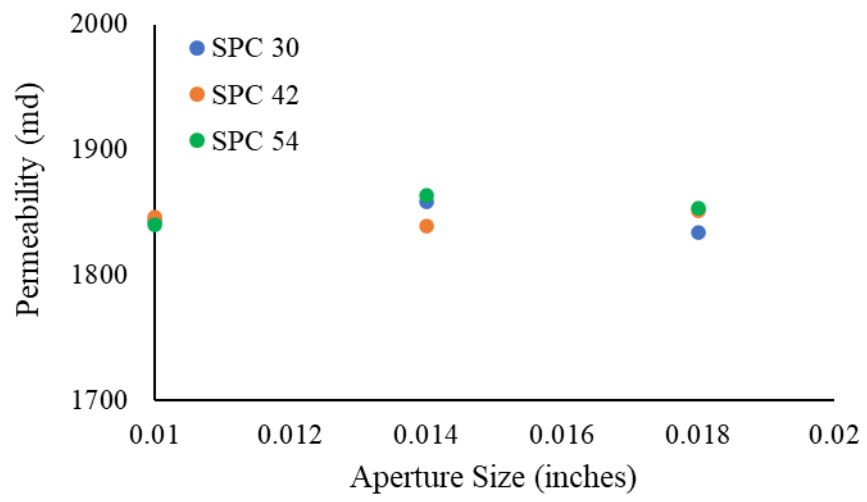

(b)

(c)

Figure D. 5 Absolute permeability of the slotted liner tests, (a) top section, (b) middle section, and (c) bottom section

D.2.3 Absolute Permeability for DC-III

(a)

Figure D. 6 Absolute permeability of the slotted liner tests, (a) top section, (b) middle section, and (c) bottom section
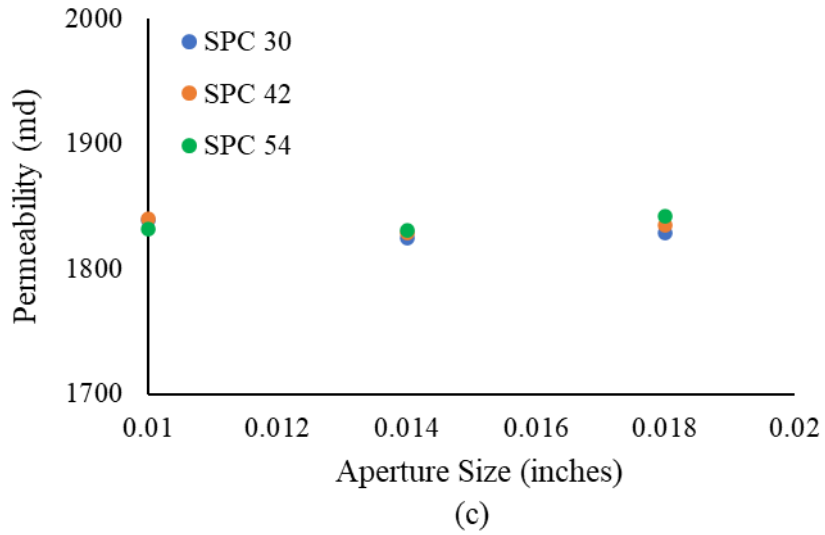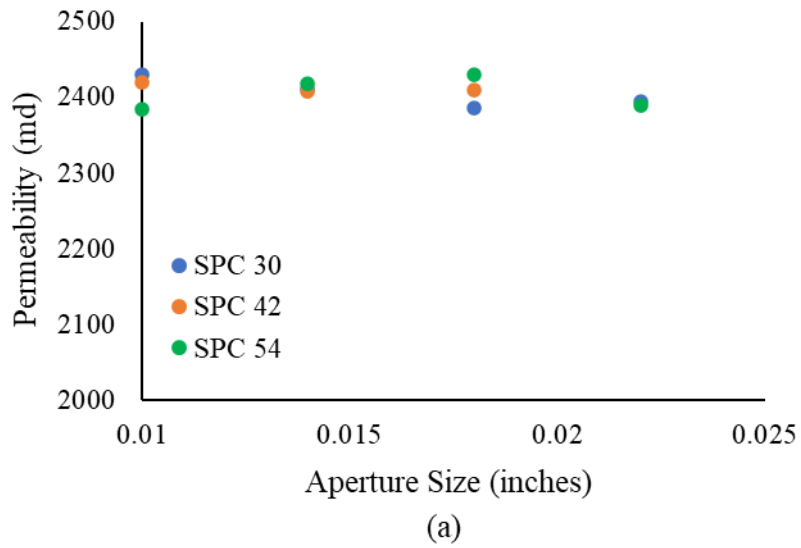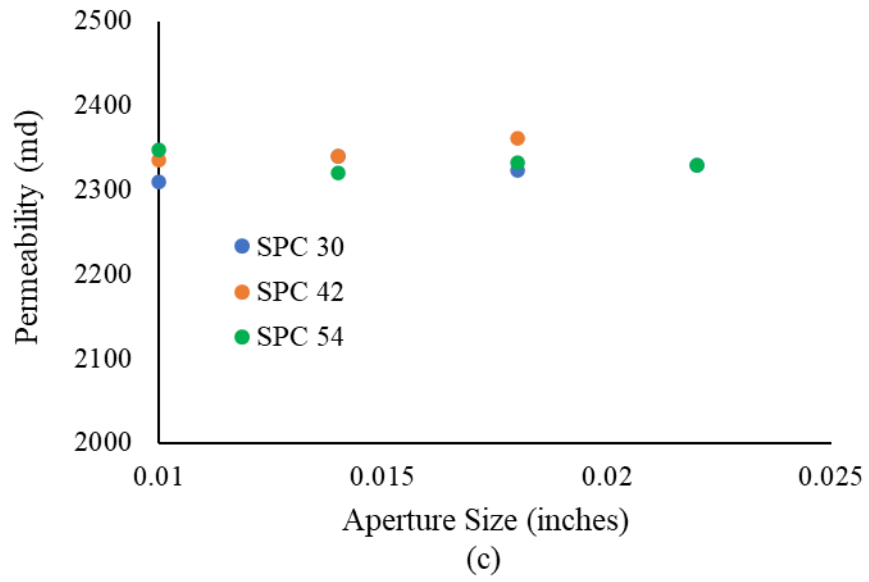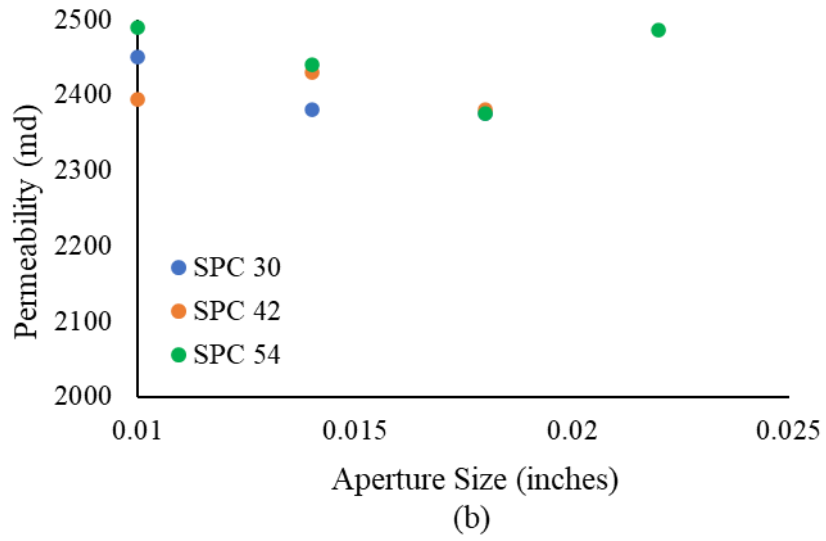
Appendix E: Empirical Correlations

E.1 Dimensionless Parameters

From the testing results, it is found the sand production is a function of drag force, resisting force, aperture size, and PSD, while the retained permeability is a function of fines concentration and aperture size.

E.1.1 Dimensionless Parameters for the Sand Production

A dimensionless factor of γ is formulated to correlate the drag force, resisting force, and PSD, as shown in Equation E.1. The PSD is dictated by using the D_{50}/D_{10} value. The drag force is proportional to the square of the velocity, and the resisting force is quantified using the shear strength of the sand-pack sample (τ'). The shear strength of the sand-pack sample is determined by Equation E.2. C_o is the cohesion of the sample. φ is the friction angle obtained through direct shear testing. σ'_a is the effective axial stress, which is around 393 kPa during the testing. It shall be mentioned that the resisting force includes not only the shear strength but also the capillary bonding force. However, the capillary bonding force measurement is complicated due to the large-scale sample and saturation variation during the tests. Thus, shear strength is applied here as the only resisting force.

$$\gamma = \frac{\rho \cdot D_{50} \cdot v}{\mu} \cdot \frac{v \cdot \mu}{D_{10} \cdot \tau'} = \frac{D_{50} \cdot \rho \cdot v^2}{D_{10} \cdot \tau'} \qquad Eq.(E.1)$$

$$\tau' = C_o + \sigma'_a \cdot tan\varphi \qquad Eq.(E.2)$$

δ is the dimensionless factor regarding the aperture size, as shown in Equation 6.3.

$$\delta = \frac{w}{D_{50}} \qquad Eq.(6.3)$$

E.1.2 Dimensionless Parameters for the Retained Permeability

θ is the fines concentration (%) of the sand-pack samples used in the retained permeability formulation.

E.2 Friction Angle and Cohesion

The direct shear testing results of the sand-pack samples (DC-I, II, and III) are obtained from Mahmoudi (2017) using the ASTM D3080 procedure. Following the same procedure, direct shear tests are conducted to measure the friction angle and cohesion of the two new PSDs.

E.2.1 Friction Angle Results

Table E.1 shows the friction angle (φ) of the sand-pack samples.

Table E. 1 Friction Angle of Sand-pack Samples

	DC-I	DC-II	DC-III	New-PSD I	New-PSD II
Friction Angle (°)	32.8	33.5	34.4	33	34.7

E.2.2 Cohesion Results

Figures E.1 and E.2 presents the direct shear testing results of the samples. The cohesion is obtained when the normal stress equals zero. Table E.2 shows the cohesion and effective shear strength of the sand-pack samples.
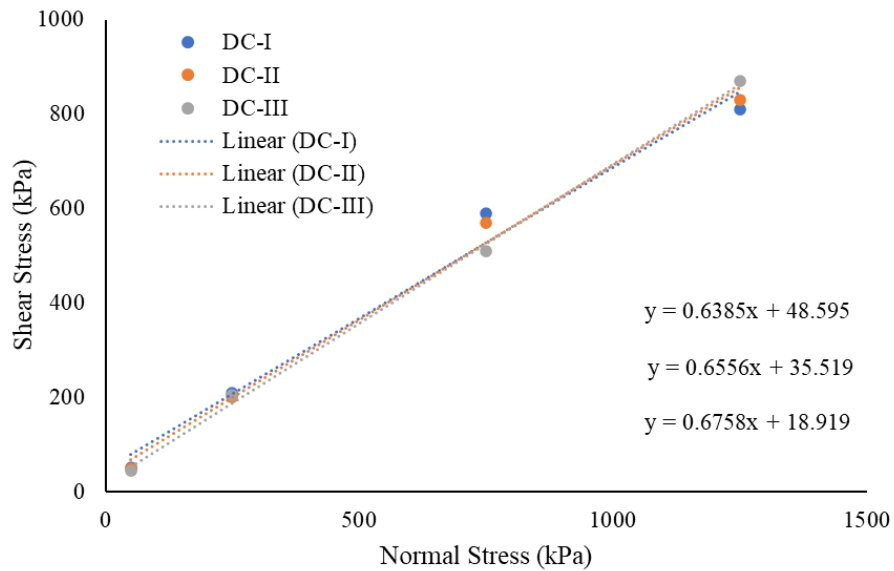
Figure E. 1 Direct Shear Testing Results of DC-I, DC-II, and DC-III

Plot with Shear Stress (kPa) on y-axis (0 to 400) and Normal Stress (kPa) on x-axis (0 to 400). Legend: NEW PSD-I, NEW PSD-II, Linear (NEW PSD-I), Linear (NEW PSD-II).

$y = 0.6896x + 10.957$

$y = 0.6485x + 39.652$
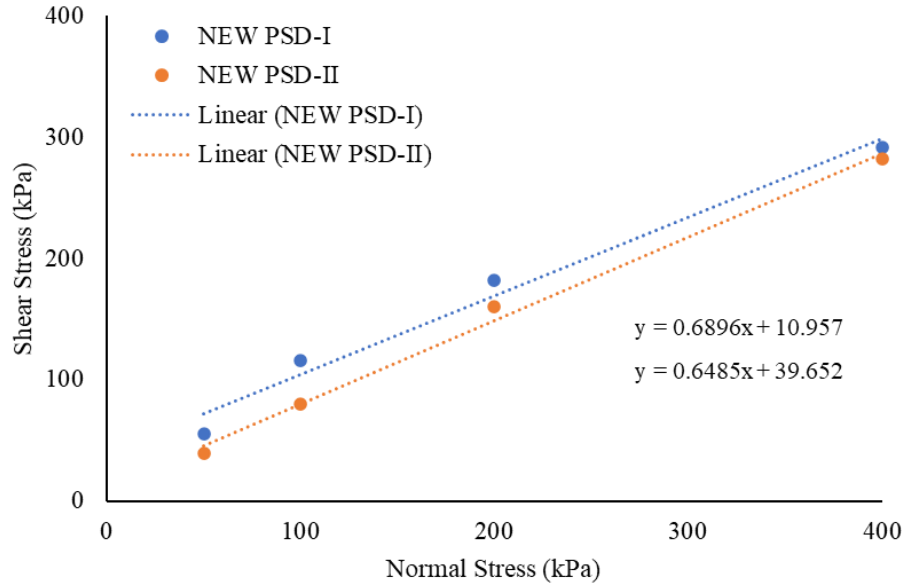
Figure E. 2 Direct Shear Testing Results of NEW PSD I and II

Table E. 2 Cohesion Results

	Cohesion (kPa)	τ' (kPa)
DC-I	48.6	300
DC-II	35.5	292
DC-III	18.9	284
NEW-PSD I	40	295
NEW-PSD II	11	280

E.3 Sand Production and Retained Permeability Correlations

E.3.1 Sand Production Correlation

The sand production correlation is obtained by dimensionless parameters of $\gamma_o, \gamma_w, \gamma_g, \delta$, and SPC, where $\gamma_o, \gamma_w, \gamma_g$ are the dimensionless factors for the oil, water, and gas phase, respectively. After examining the relationship between each parameter and the sand production, three compact and straightforward function structures are built, as shown in Equations E.4 to E. 6 for the SL, WWS, and PS, respectively. The coefficients through Equations E.4 to E.6 (a, b, c, d, e) are obtained through the curve fitting with testing data. The curve fitting procedure uses the Generalized

Reduced Gradient non-linear regression method to minimize the Mean Absolute Error (MAE) between the correlation data and experimental results.

$$P_{sand} = a \cdot SPC \cdot (b \cdot \gamma_w + c \cdot \gamma_o + d \cdot \gamma_g)^{e \cdot \delta} \qquad Eq.(E.4)$$

$$P_{sand} = a \cdot (b \cdot \gamma_w + c \cdot \gamma_o + d \cdot \gamma_g)^{e \cdot \delta} \qquad Eq.(E.5)$$

$$P_{sand} = a \cdot (b \cdot \gamma_w + c \cdot \gamma_o + d \cdot \gamma_g)^{e \cdot \delta} \qquad Eq.(E.6)$$

E.3.2 Retained Permeability Correlation

The retained permeability correlation is obtained by dimensionless parameters of δ, θ, and SPC. Equations E.7 to E.9 shows the proposed correlation structure of the retained permeability for the SL, WWS, and PS, respectively.

$$k_{ret} = a + b \cdot SPC + c \cdot \delta - d \cdot \theta \qquad Eq.(E.7)$$

$$k_{ret} = a + b \cdot \delta - c \cdot \theta \qquad Eq.(E.8)$$

$$k_{ret} = a + b \cdot \delta - c \cdot \theta \qquad Eq.(E.9)$$